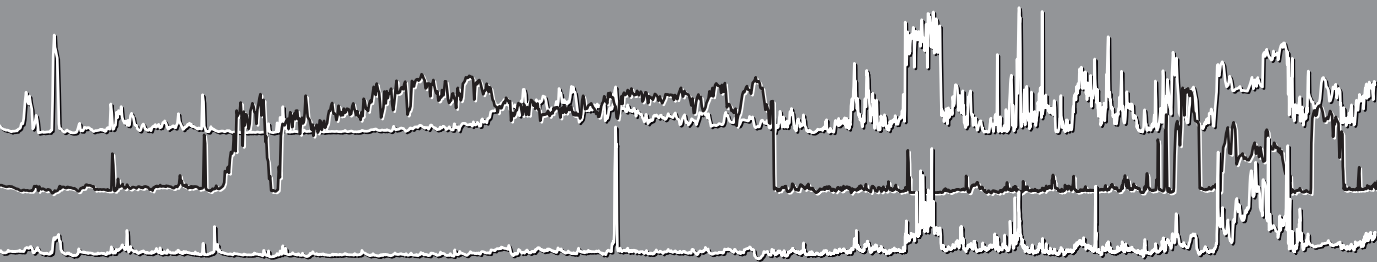


**Climate and environmental change in southern Europe -  
The paleoecological record of Padul, Sierra Nevada  
(western Mediterranean, southern Iberian Peninsula)**



**Jon Camuera Bidaurreta  
PhD Thesis  
Granada, 2019**



**UNIVERSIDAD  
DE GRANADA**



**UNIVERSIDAD  
DE GRANADA**

**Facultad de Ciencias  
Departamento de Estratigrafía y Paleontología**

**Climate and environmental change in southern Europe –  
The paleoecological record of Padul, Sierra Nevada  
(western Mediterranean, southern Iberian Peninsula)**

**Cambio climático y ambiental en el sur de Europa –  
El registro paleoecológico de Padul, Sierra Nevada  
(Mediterráneo occidental, sur de la Península Ibérica)**

**Jon Camuera Bidaurreta**

**PhD Thesis / Tesis Doctoral  
Granada, 2019**



**Programa Doctorado  
Ciencias de la Tierra**

Editor: Universidad de Granada. Tesis Doctorales  
Autor: Jon Camuera Bidaurreta  
ISBN: 978-84-1306-287-7  
URI: <http://hdl.handle.net/10481/56799>



**UNIVERSIDAD  
DE GRANADA**

**Facultad de Ciencias  
Departamento de Estratigrafía y Paleontología**

**Climate and environmental change in southern Europe –  
The paleoecological record of Padul, Sierra Nevada  
(western Mediterranean, southern Iberian Peninsula)**

**Cambio climático y ambiental en el sur de Europa –  
El registro paleoecológico de Padul, Sierra Nevada  
(Mediterráneo occidental, sur de la Península Ibérica)**

**Jon Camuera Bidaurreta  
PhD Thesis / Tesis Doctoral**

**Director:  
Gonzalo Jiménez Moreno**



**Programa Doctorado  
Ciencias de la Tierra**





## Agradecimientos

En primer lugar, me gustaría agradecer a las instituciones que mediante su financiación han permitido la realización de la presente Tesis Doctoral:

- Secretaría de Estado de Investigación, Desarrollo e Innovación del Ministerio de Economía y Competitividad del Gobierno de España, dentro del marco de ayudas para contratos predoctorales para la formación de doctores (convocatoria 2014) contempladas en el Programa Estatal de Promoción del Talento y su Empleabilidad del Plan Estatal de Investigación Científica y Técnica y de Innovación 2013-2016. En concreto, el contrato predoctoral BES-2014-069117 dentro del proyecto CGL2013-47038-R titulado “Cambio ambiental y climático en el sur de Europa: el registro paleoecológico de Padul, Sierra Nevada”.
- Secretaría de Estado de Investigación, Desarrollo e Innovación del Ministerio de Economía y Competitividad del Gobierno de España por la financiación de la estancia internacional (Geographical and Earth Sciences, University of Glasgow) dentro del marco de ayudas a la movilidad predoctoral para la realización de estancias breves en centro de I+D (convocatoria 2015).
- Al grupo de investigación de Análisis de Cuencas (RNM190) de la Universidad de Granada por la ayuda en la financiación de determinados análisis.

Por otra parte, me gustaría dar las gracias a mi director de tesis Gonzalo por su gran dedicación, conocimiento, fantástica dirección y su visión pragmática mediante la cual la finalización de la tesis ha sido muchísimo más fácil.

Gracias a Nono su permanente disposición, su ayuda durante la estancia en Glasgow y sus incansables revisiones. También agradecer a Francis, Scott, Jaime y toda esa gente con la que he tenido el placer de trabajar.

Mil gracias a todas las personas con las que he tenido la suerte de compartir despacho (Wero, Elena, Samu, Vedra, Santiago, Cristian...). En especial a María José y Paola, con las que he compartido la gran mayoría de los buenos ratos y gracias a las cuales estos años se han pasado volando. También agradecer a Bob por esas discusiones de mediodía alimentadas por unos cuantos “cafés fríos” y a Raef por hacer con sus comentarios unas charlas muchísimo más amenas. A toda la gente del Departamento de Estratigrafía y Paleontología que directa o indirectamente me han ayudado durante todo este tiempo.

Gracias también a esa gente con la que me he cruzado en Granada tanto dentro como fuera de la Universidad (Mertxe, Jotake, Mada, Alvarito, Manu, Gersan...), y sobre todo a esa cuadrilla de Bilbao (Aritz, Borja, Aldekoa, Iker, Iñigo, Asier, Julen, Diego, Cristian...) que a pesar de la distancia, siempre estaremos juntos. Y por supuesto a Natalia por su inestimable compañía durante estos años.

No hay palabras para agradecer el amor y constante apoyo vuestro: aita, ama, Jani, amama, Nahia, Edu, tíos, tías y primos. El saber que siempre estaréis ahí para lo que sea da una tranquilidad inmensa. Finalmente, esta tesis va especialmente dedicada a mi aítite, cuya honradez, honestidad, integridad e infinito conocimiento siempre fue el ejemplo a seguir.



## **TABLE OF CONTENTS**

<b>EXTENDED ABSTRACT</b>	<b>1</b>
<b>RESUMEN EXTENDIDO</b>	<b>3</b>
<b>LAYOUT</b>	<b>7</b>
<b>CHAPTER 1: INTRODUCTION</b>	<b>11</b>
1. Background	11
2. Orbital-scale climate variability: Milankovitch cycles	12
3. Suborbital-scale climate variability: Bond cycles, Dansgaard-Oeschger and Heinrich variability	13
4. Terrestrial Mediterranean climate reconstruction	15
5. Objectives	17
6. Regional and local settings: geography, geology and climate	18
7. Materials and methods	21
7.1. Padul-15-05 core	21
7.2. Paleoclimatic multiproxy study	24
<b>CHAPTER 2: ORBITAL-SCALE ENVIRONMENTAL AND CLIMATIC CHANGES RECORDED IN A NEW ~200,000-YEAR-LONG MULTIPROXY SEDIMENTARY RECORD FROM PADUL, SOUTHERN IBERIAN PENINSULA</b>	<b>37</b>
Abstract	38
1. Introduction	38
2. Geographical and geological setting	42
2.1. Sierra Nevada range	42
2.2. Padul basin and wetland: geography, geology and climate	42
3. Materials and methods	44
3.1. Padul-15-05 core: drilling and sampling	44
3.2. Dating and age-depth model	44
3.3. Lithology and color	49
3.4. Magnetic susceptibility	49
3.5. Mineralogy	49
3.6. Inorganic geochemistry	49
3.7. Organic geochemistry	55
3.8. Palynological analysis	55
3.9. Principal Component Analysis (PCA)	55
3.10. Spectral analysis	56
4. Results	58
4.1. Chronology and sediment accumulation rates (SAR)	58
4.2. Principal component analysis	60
4.3. Lithology and sedimentary facies	60
4.4. Pollen results	64
4.5. Spectral analysis	64
5. Discussion	64

5.1.	New age control for the Padul sedimentary sequence	64
5.2.	Facies, environment, climate and lake level reconstruction	65
5.3.	An idealized orbital cyclic pattern in Padul (from MIS 6 to MIS 1): integrating orbital variability, vegetation, facies and lake level	70
5.4.	Padul and other Mediterranean lake level records	74
6.	Conclusion	77
	Supplementary Information	79

**CHAPTER 3: VEGETATION AND CLIMATE CHANGES DURING THE LAST TWO GLACIAL-INTERGLACIAL CYCLES IN THE WESTERN MEDITERRANEAN: A NEW LONG POLLEN RECORD FROM PADUL (SOUTHERN IBERIAN PENINSULA) 83**

	Abstract	84
1.	Introduction	84
2.	Regional and local settings	85
2.1.	Sierra Nevada Range: geography, climate and vegetation	85
2.2.	Padul basin and wetland: geography, climate and vegetatio	87
3.	Materials and methods	89
3.1.	Padul-15-05 core: drilling and sampling	89
3.2.	Chronology and age-depth model	89
3.3.	Palynological analysis	90
3.4.	Pollen Climate Index (PCI)	91
3.5.	Principal Component Analysis (PCA)	91
3.6.	Spectral analysis	92
4.	Results	92
4.1.	Palynological results	92
4.2.	Principal Component Analysis (PCA)	98
4.3.	Spectral analysis	98
5.	Discussion	99
5.1.	Vegetation and climate reconstruction: from MIS 6 to MIS 1	99
5.2.	Orbital forcing: regional climate and local environmental changes	106
5.3.	Comparison with previous palynological records from Padul	108
5.4.	Padul and other Mediterranean pollen records	111
6.	Conclusions	114
	Supplementary Information	116

**CHAPTER 4: ORGANIC BIOMARKERS (N-ALKANES, DIOLS, FATTY ACIDS) AS A PROXY FOR ENVIRONMENTAL CHANGES IN THE PADUL WETLAND AND SOUTHERN IBERIAN PENINSULA 119**

1.	Introduction	119
2.	Methodology	120
3.	Results and discussion	121
4.	Conclusions	124

**CHAPTER 5: MILLENNIAL- AND CENTENNIAL-SCALE CLIMATE VARIABILITY DURING THE LAST 65 KYR BP IN THE SOUTHERN IBERIAN PENINSULA 127**

1.	Introduction	127
----	--------------	-----

2.	Methodology	128
3.	Results and discussion	128
3.1.	Environmental and climatic response to HSs and D-O variability in the western Mediterranean	128
4.	Conclusions	131

**CHAPTER 6: EARLY RECORD OF HEINRICH STADIAL 1 IN SOUTHERN EUROPE AND THE MEDITERRANEAN REGION** **135**

	Abstract	136
	Plain language summary	136
1.	Introduction	136
2.	Material and methods	137
2.1.	Padul-15-05 paleoclimatic record of HS1	137
2.2.	Synthetic HS1 age-range boundaries for southern Europe and the Mediterranean region	139
3.	Results and discussion	140
3.1.	Early beginning of HS1 in southern Europe and the Mediterranean area	141
3.2.	Early end of HS1 in southern Europe and the Mediterranean area	142
3.3.	HS1 age discrepancies between continental and marine environments	144
4.	Conclusions	144
	Supplementary Information	146

**CHAPTER 7: CLIMATIC SUBDIVISION OF HEINRICH STADIAL 1 BASED ON CENTENNIAL-SCALE PALEOENVIRONMENTAL CHANGES OBSERVED IN WESTERN MEDITERRANEAN AREA** **157**

	Abstract	158
1.	Introduction	158
2.	Materials and methods	159
3.	Results and discussion	159
3.1.	Heinrich Stadial 1 (HS1)	159
3.2.	Bølling-Allerød (BA) and Younger Dryas (YD)	162
3.3.	Climate variability and solar forcing in the Iberian Peninsula	162
4.	Conclusion	164
	Supplementary Information	166

**CHAPTER 8: HOLOCENE GEOCHEMICAL FOOTPRINT FROM SEMI-ARID ALPINE WETLANDS IN SOUTHERN SPAIN** **173**

	Abstract	174
1.	Background and summary	174
2.	Methods	178
2.1.	Sampling methods and sediment core and age models	179
2.2.	Organic geochemistry	181
2.3.	Inorganic geochemistry	182
2.4.	Code availability	183
3.	Data records	184
4.	Technical validation	185
4.1.	Organic geochemistry	185
4.2.	Inorganic geochemistry	186

Data citations	187
<b>CHAPTER 9: CONCLUSIONS AND FUTURE PERSPECTIVES</b>	<b>191</b>
Conclusions	191
Future perspectives	194
<b>REFERENCES</b>	<b>195</b>

## Extended abstract

There are large gaps in our understanding of natural climate variability and how the water cycle and ecosystems will respond to global climate warming. Several scientific reports show that in the near future the southern Iberian Peninsula and other Mediterranean areas will be affected by increased drought frequency. This will generate very important economic and social problems in this region, characterized by scarce water resources. However, climate prediction is still a challenge, due to lack of long databases with quantitative measurements (especially for precipitation and temperature) and studies of how the environment reacted to climate change before the historical record. To solve this problem we need long continuous paleoclimatic records that will allow us to predict ecosystem response to climate change at short and long term. The present PhD Thesis focuses on the paleoenvironmental reconstruction of the last two glacial-interglacial cycles (the last ~200,000 years) in southern Iberian Peninsula through the study of the Padul-15-05 core, a 42.64 m-long continuous continental record that was retrieved from the Padul wetland. This sediment core was studied using high-resolution multiproxy analyses, including lithology/sedimentology, physical properties, mineralogy, inorganic and organic geochemistry, paleontological analysis and chronological analysis. These multiproxy analyses have provided with high-quality data that can be used for local (Padul wetland) and regional (southern Iberian Peninsula) paleoenvironmental and paleoclimatic reconstructions. The obtained data allowed identifying environmental variability due to orbital- and sub-orbital scale climate changes, improving the comprehension of factors and patterns influencing the environment caused by past climate changes in this region.

In this study, the age-depth model of the Padul sedimentary sequence was improved with respect to previously published studies from this site. This was done using high-resolution accelerator mass spectrometry (AMS) radiocarbon dating, amino acid racemization (AAR) dating and sediment accumulation rates (SAR). This allowed constructing a robust age-depth model that permitted a good understanding of the time frame for paleoenvironmental reconstructions from the Padul wetland and the southern Iberian Peninsula for the last two glacial-interglacial cycles.

The detailed palynological analysis from the Padul-15-05 sediment core has provided with one of the longest and most exhaustive past vegetation record from the Mediterranean region. The expansion and contraction of the forest cover and vegetation changes in the study area were strongly related with changes in insolation at this latitude, which was forced by the orbital-scale precession and eccentricity parameters. In general, the evolution of the vegetation in Padul in the last two glacial-interglacial cycles agree with other continental pollen records from the Mediterranean region, but some differences can also be recognized. The abundance of temperate humid forest taxa together with Mediterranean forest in the Padul pollen record during the last interglacial period (MIS 5e) shows the highest moisture conditions of the last ~200,000 years in the study area. Mediterranean forest taxa are the main components of the forest cover during the Holocene and the MIS 5a. Thus, the recent Holocene interglacial period in Padul seems to be climatically more similar to the MIS 5a interstadial than to the last interglacial period.



Lithological and sedimentological features of the Padul record were mostly related to lake level oscillations, which were dependent on the precipitation/evapotranspiration balance. Two lake level reconstructions carried out using different multiproxy data (i.e., compilation of inorganic and organic geochemistry and magnetic susceptibility data for the first reconstruction and palynological data for the second) presented very high correlation, indicating that both methods are good proxies for the lake level interpretation and useful for future water level reconstructions in other similar lakes and wetlands. Generally, warm interglacial/interstadial phases were characterized by negative precipitation/evapotranspiration balance, and therefore, low lake levels, while during cold glacial/stadial periods the absence of evapotranspiration resulted in a higher lake water level. Moreover, higher siliciclastic/detrital input in the lake/wetland occurred during cold/arid periods and minima in insolation, as result of increased soil erosion during periods of low forest cover. Therefore, insolation also seems to be the main factor controlling local and regional environmental changes in Padul and in the southern Iberian Peninsula. The organic biomarkers from the last 36 kyr BP provide information about local environmental changes in Padul with a close relationship with regional variability displayed by the pollen data, and therefore, also suggesting insolation as the main factor conditioning both paleoenvironmental signals.

The high-resolution pollen analysis of the last 65 kyr BP from the Padul-15-05 sedimentary record show millennial- and centennial-scale vegetation and environmental changes in the southern Iberian Peninsula most-likely related to Heinrich Stadials (HSs) and Dangaard-Oeschger (D-O) variability. The Padul-15-05 record shows covariation with other paleoclimatic records from the western Mediterranean, pointing into a same millennial- and centennial-scale climatic control affecting environments in this climatically sensitive region. In addition, the amplitude of the observed short-scale climate variability (e.g., D-O cycles) was conditioned by insolation, presenting high-amplitude D-O interstadials during insolation maxima (e.g., D-O interstadials 17-14 and 8-5) and a buffered variability during insolation minima (e.g., D-O interstadial 13-12 and 4-2).

The compilation of several marine and continental paleoclimatic records from southern Europe and the Mediterranean region reveal an early record of Heinrich Stadial 1 (HS1 between 17,780 and 15,080 cal yr BP) in the study area with respect to the correspondent Greenland Stadial 2.1a from Greenland ice core records (GS-2.1a; 17,480 – 14,692 cal yr BP). Moreover, high-resolution pollen analysis allowed identifying three main climatic phases during HS1 in the Padul record, i.e., HS1a (18,400 – 17,200 cal yr BP), HS1b (17,200 – 16,700 cal yr BP) and HS1c (16,700 – 15,600 cal yr BP), showing an overall arid(cold) – humid(cool) – arid(cold) trend. In addition, for the first time, seven centennial-scale sub-phases within HS1 (i.e., HS1a.1, HS1a.2, HS1a.3, HS1b, HS1c.1, HS1c.2 and HS1c.3) have been described, which seem to be related with solar activity.

## Resumen extendido

Existen grandes lagunas cuando se trata de comprender la variabilidad climática natural y cómo el ciclo del agua y los ecosistemas en su conjunto reaccionarán frente al calentamiento global. Varios informes científicos muestran que en un futuro cercano el sur de la Península Ibérica y diferentes zonas del Mediterráneo se verán afectadas por un aumento en la frecuencia de las sequías. Esto generará importantes problemas económicos y sociales en esta región, caracterizada por los escasos recursos hídricos. Sin embargo, las predicciones climáticas presentan todavía un desafío para los investigadores debido a la falta de bases de datos con medidas cuantitativas (especialmente de temperatura y precipitación), así como de estudios que reflejen como reaccionaron los medio ambientes a los cambios climáticos previos a registro histórico. Para resolver este problema se requiere de registros paleoclimáticos largos y continuos que permitan predecir las respuestas de los ecosistemas frente a los cambios climáticos a corto y largo plazo. La actual Tesis Doctoral se centra en la reconstrucción ambiental de los dos últimos ciclos glaciares-interglaciares (últimos ~200.000 años) en el sur de la Península Ibérica mediante el estudio de sondeo Padul-15-05, el cual presenta un registro sedimentario continuo de 42.64 m de profundidad obtenido del margen de la laguna de Padul. Este sondeo ha sido estudiado mediante análisis multiproxy, en el que se incluyen análisis litológico/sedimentológico, propiedades físicas, mineralogía, geoquímica orgánica e inorgánica, paleontología y análisis cronológico. Estos análisis multiproxy han proporcionado datos de alta calidad que han permitido reconstrucciones paleoambientales y paleoclimáticas locales (Laguna de Padul) y regionales (sur de la Península Ibérica). Los datos obtenidos permiten la identificación de la variabilidad ambiental como consecuencia de los cambios climáticos orbitales y sub-orbitales, mejorando la comprensión de los factores y patrones que influyen los cambios medio ambientales y climáticos en esta región.

En este estudio, el modelo de edad-profundidad de la secuencia sedimentaria de Padul se mejoró con respecto a estudios previos realizados en la propia laguna, utilizando dataciones de radiocarbono por espectrometría de masas con acelerador (AMS en inglés), dataciones por racemización de aminoácidos (AAR en inglés) y tasas de acumulación sedimentaria. Esto permitió generar un modelo de edad robusto que facilitó una mejor y más precisa comprensión temporal de los cambios paleoambientales ocurridos en el humedal de Padul y en el sur de la Península Ibérica durante los dos últimos ciclos glaciares-interglaciares.

El análisis palinológico detallado del sondeo Padul-15-05 ha proporcionado uno de los registros de vegetación pasados más largos y detallados de la región Mediterránea. La expansión y contracción de la cubierta forestal y los cambios de vegetación en el área de estudio estuvieron estrechamente relacionados con los cambios en la insolación en esta latitud, que está a su vez condicionado por los cambios en los parámetros de precesión y excentricidad. En general, la evolución de la vegetación en Padul durante los dos últimos ciclos glaciares-interglaciares presenta una buena correlación con respecto a otros registros de vegetación Mediterráneos, aunque también se observan ciertas diferencias. La abundancia de taxones de vegetación característicos de bosques templados y húmedos junto con la presencia de bosque Mediterráneo en Padul durante el último periodo interglaciar (MIS 5e) muestra las condiciones de mayor

humedad de los últimos ~200.000 años esta área de estudio. Las especies de bosque Mediterráneo son el principal componente de la cubierta forestal durante el Holoceno y el MIS 5a. Esto demuestra que el periodo interglaciar Holoceno en Padul parece ser climáticamente más similar a el interestadío MIS 5a que con el último periodo interglaciar.

Las características litológicas y sedimentológicas del registro de Padul están principalmente relacionadas con las oscilaciones en el nivel del lago, que a su vez dependen del balance entre la precipitación de lluvia y la evapotranspiración en la laguna. Las dos reconstrucciones del nivel del lago obtenidas mediante diferentes datos multiproxy (la primera reconstrucción basada en datos de geoquímica orgánica e inorgánica y susceptibilidad magnética y la segunda reconstrucción basada en datos palinológicos) presentaron una muy alta correlación, indicando que ambas metodologías dan lugar a buenas reconstrucciones del nivel del lago, y que son a su vez útiles para reconstrucciones paleoambientales locales en lagunas y humedales similares a Padul. En general, los interglaciares/interestadíos cálidos en esta zona de estudio se caracterizan por un balance de precipitación/evapotranspiración negativo, y por lo tanto, niveles del lago bajos, mientras que durante periodos glaciares/estadíos fríos la ausencia de evapotranspiración da como resultado niveles del lago más altos. Además, el alto aporte siliciclástico/detrítico a la laguna se da principalmente durante épocas frías/áridas y mínimos de insolación como consecuencia de una mayor erosión del suelo durante periodos de menor cubierta forestal. Por lo tanto, la insolación parece ser el principal factor que controla los cambios ambientales locales y regionales en Padul y en el sur de la Península Ibérica. Los biomarcadores orgánicos durante los últimos 36 ka AP también proporcionan información sobre los cambios ambientales locales en Padul, estrechamente relacionados con la variabilidad regional registrada por los datos de polen, y en definitiva, sugiriendo que ambas señales ambientales (local y regional) están fuertemente condicionadas por el factor de insolación.

El análisis de polen de alta resolución de los últimos 65 ka AP del humedal de Padul muestra cambios en la vegetación y en el medioambiente a escala de milenios y centurias en el sur de la Península Ibérica, principalmente asociados a Estadíos Heinrich (HSs en inglés) y variabilidad Dangaard-Oeschger (D-O). El registro Padul-15-05 también muestra una buena correlación con otros registros del Mediterráneo occidental a escala milenial, lo que sugiere que el medio ambiente es muy sensible y se ve afectado por un mismo control climático en esta región. Además, la amplitud de la señal ambiental de esta variabilidad climática de escala corta (p.e., ciclos D-O) está condicionada por la insolación, presentando una amplitud de la señal ambiental muy marcada durante los interestadíos D-O coincidentes con los máximos de insolación (p.e., interestadíos D-O 17-14 y 8-5), mientras que los interestadíos ocurridos durante mínimos de insolación presentan una señal ambiental amortiguada (p.e., interestadíos D-O 13-12 y 4-2).

La recopilación de varios registros paleoclimáticos marinos y continentales del sur de Europa y de la región Mediterránea han revelado un registro temprano del Estadío Heinrich 1 (HS1 entre 17.780 y 15.080 años cal AP) en el área de estudio con respecto al correspondiente Estadío Greenland 2.1a registrado en los sondeos de hielo de Groenlandia (GS-2.1a; 17.480 – 14.692 años cal AP). Además, el análisis de polen de alta resolución permitió identificar tres fases climáticas principales durante el HS1 en Padul, en concreto, HS1a (18.400 – 17.200 años cal AP), HS1b (17.200 – 16.700 años cal AP) and HS1c (16.700 – 15.600 años cal AP), las

cuales muestras una tendencia climática general árida(fría) – húmeda(fresca) – árida(fría). Además, se han descrito por primera vez siete sub-fases a escala de centurias durante el propio HS1 (en concreto, HS1a.1, HS1a.2, HS1a.3, HS1b, HS1c.1, HS1c.2 and HS1c.3) que parecen estar relacionadas con la actividad solar.



## Layout

The results of the present PhD Thesis have been published as research papers in scientific journals, all of them included in the Science Citation Index. As it is mandatory, the chapters related to the published papers have the same content than the original source. Thus, the present PhD Thesis is divided as follow:

**Chapter 1:** Divided in 7 main points. (1) A background for this study. (2) An introduction to orbital- and (3) suborbital-scale Earth's forcing and (4) the importance of Padul and the Mediterranean region for climate reconstructions. (5) The main objective of this PhD Thesis. (6) The regional setting of Sierra Nevada and Padul. (7) Materials and methods used in the Padul-15-05 record for paleoenvironmental reconstructions.

**Chapter 2:** Research paper title: *Orbital-scale environmental and climatic changes recorded in a new ~200,000-year-long multiproxy sedimentary record from Padul, southern Iberian Peninsula*. Quaternary Science Reviews, 2018, v. 198, p. 91-114.

**Chapter 3:** Research paper title: *Vegetation and climate changes during the last two glacial-interglacial cycles in the western Mediterranean: a new long pollen record from Padul (southern Iberian Peninsula)*. Quaternary Science Reviews, 2019, v. 205, p. 86-105.

**Chapter 4:** *Organic biomarker (n-alkanes, diols, fatty acids) as a proxy for environmental changes in the Padul wetland and southern Iberian Peninsula*.

**Chapter 5:** *Millennial- and centennial-scale climate variability during the last 65 kyr BP in the southern Iberian Peninsula*.

**Chapter 6:** Research paper title: *Early record of Heinrich Stadial 1 in southern Europe and the Mediterranean region*. Under review, Geophysical Research Letters.

**Chapter 7:** Research paper title: *Climate subdivision of Heinrich Stadial 1 based on centennial-scale paleoenvironmental changes observed in western Mediterranean area*. Under review, Geology.

**Chapter 8:** Research paper title: *Holocene geochemical footprint from semi-arid alpine wetlands in southern Spain*. Scientific Data, 2018, v. 5, n. 180024.

**Chapter 9:** Conclusions and future perspectives.



# *Chapter 1*

*Introduction*





## ***Chapter 1: Introduction***

### **1. Background**

In the last decades a significant effort has been put into studying past climate changes, trying to understand past global climate variations and how they affected environments, also with the goal of deducing factors implied in recent global warming and how it will affect our society (Parmesan, 2006; Bindoff et al., 2013). Climate predictions for the next decades for southern Europe and the Iberian Peninsula estimate higher temperatures and lower precipitations associated to an augmentation in the drought frequency and intensity (Kirtman et al., 2013). This will result in strong changes in the environment, crop productivity, water availability and societies (IPCC, 2013). In this regard, there is a necessity of paleoenvironmental and paleoclimatic archives that are deeper in time than instrumental and historical data for future prediction and mitigation. Therefore, the study of past environmental changes are essential for: (1) identifying patterns, ranges and causes of the natural climate variability, (2) identifying causes of catastrophic environmental events (e.g., droughts), and (3) generating a long database that will help differentiating between natural and anthropogenic climate changes (Overpeck, 1995).

Past climate research projects focusing on high-resolution ice and marine records, such as the *Climate: Long-Range Investigation, Mapping and Prediction (CLIMAP)*, *Greenland Ice Sheet Project (GISP)*, *Greenland Ice Core Project (GRIP)*, *North-Greenland Ice Core Project (NGRIP)* and *Integrated Ocean Drilling Program (IODP)* have generated very accurate and valuable information about environmental and climate change in marine and high-latitude areas. However, terrestrial records are also needed to provide with comparable information about climatic variability that occurred in continental mid-latitudes, as result of similar external forcings (e.g., changes in Earth's orbit and/or Sun's activity) and their interactions in the climate system (Fig. 1.1) (Ruddiman, 2001). In this respect, the continental Mediterranean region and, in particular the southern Iberian Peninsula, could provide with an ideal location for a multidisciplinary investigation of past climate conditions, justified by the high sensitivity of this area to climate changes consequence of its location between north humid and south arid zones (Kottek et al., 2006).

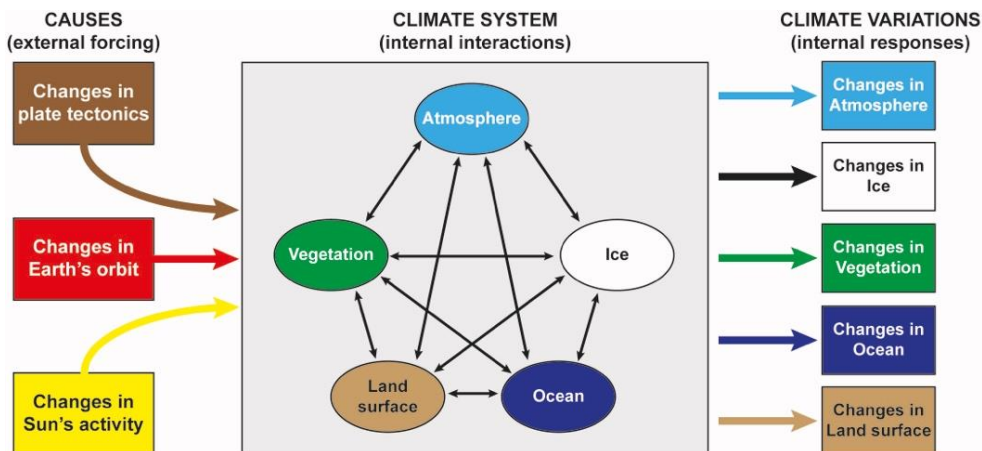


**Figure 1.1.** Interactions between the components of the climate system, external causes affecting them and implications in climate variations (modified from Ruddiman, 2001).

## 2. Orbital-scale climate variability: Milankovitch cycles

Insolation is one of the main factors affecting the Earth's long-term cyclic climate during the Quaternary (Imbrie et al., 1992), which is conditioned by variations in the Earth's orbit around the Sun (Berger, 1980; Berger, 1988). The past record of climate oscillations of the last ~900,000 years show that glacial-interglacial cycles are linked to the highest amplitude orbital parameter (eccentricity, with periodicities of about 100,000 years) (Berger and Jansen, 1994), also conditioned by the lower amplitude and higher frequency oscillations (i.e., obliquity and precession, with periodicities of around 41,000 and 23,000 years, respectively) (Fig. 1.2). These three parameters, discovered by Milankovitch (1920), are responsible of the amount of insolation, which is the main regulator of the Earth's climate system at hundreds and tens of thousands year-scales. Quaternary glacial-interglacial climatic cycles were named as Marine Isotope Stages (MISs) by Emiliani (1955), based on oxygen isotopic analyses on foraminifera from deep marine sediment cores, which is a good proxy for ice volume and thus global climate.

The climate system evolution during the Quaternary reflected an asymmetric pattern due to changes in the intensity of the different orbital parameters involved. From the Early Pleistocene until the Middle Pleistocene transition (2.5 – 0.7 Ma), climate variability was mainly controlled by the obliquity orbital parameter, being progressively replaced by the eccentricity, which is the principal factor controlling glacial-interglacial cycles since the Middle Pleistocene transition to present (Lisiecki and Raymo, 2005).

Insolation changes in the Mediterranean region, highly controlled by eccentricity and precession parameters (obliquity seems to control climate seasonality at higher latitudes), resulted in well-defined glacial-interglacial cycles in this area. This climate variability affected terrestrial and marine environments and is recorded in sedimentary archives using very different paleoclimate proxies, such as pollen analysis,  $\delta^{18}\text{O}$  from foraminifera, alkenone-deduced sea surface temperature (SST) or Saharan dust, among others (Wijmstra, 1969; Lourens et al., 1996;

Kroon et al., 1998; Larrasoana et al., 2003; Tzedakis et al., 2006; Tzedakis, 2007) (see also *Chapter 2*). However, climate changes are not always perfectly responding to orbital parameters and insolation. Discrepancies between astronomical forcing and ice, marine and terrestrial records could be explained by the interaction of other variables in the climate system, such as greenhouse gasses and/or the albedo (Shackleton and Pisias, 1985; Ruddiman, 2003).

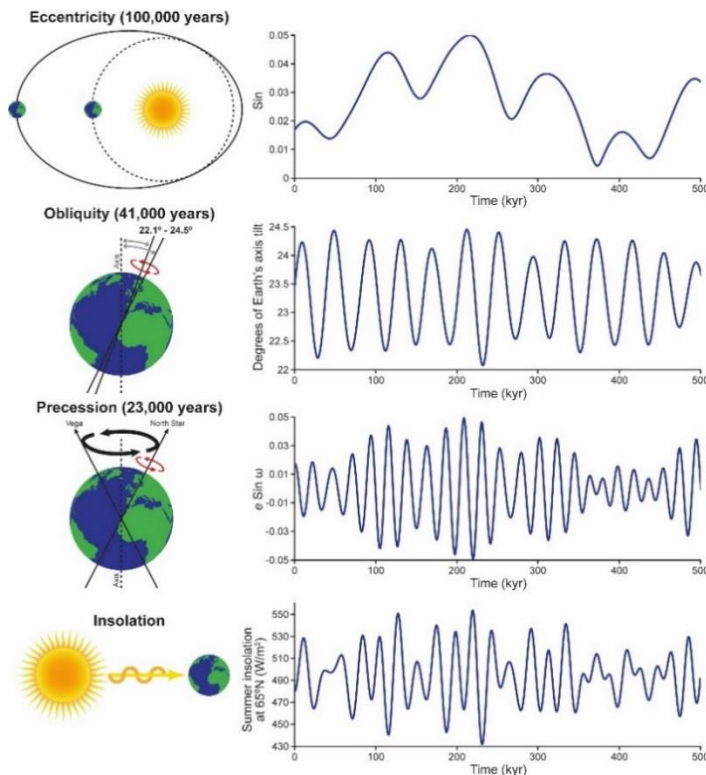


**Figure 1.2.** Left: Scheme of the three orbital parameters (eccentricity, obliquity and precession) and insolation. Right: Periodic record of each parameter along with summer insolation values at 65°N for the last 500 kyr, based on Laskar et al. (2004) and obtained from the Analyseries 2.0 software (Paillard et al., 1996).

### 3. Suborbital-scale climate variability: Bond cycles, Dansgaard-Oeschger and Heinrich variability

Besides orbital-scale climate changes, climate is characterized by higher frequency millennial-scale climatic variability (Shackleton and Opdyke, 1973; Imbrie et al., 1984). This is deduced by several ice, marine and terrestrial paleoclimatic studies that also evidenced high frequency cycles not related to the orbital parameters predicted by Milankovitch. Ice and marine sedimentary studies have revealed important air and ocean water temperature oscillations at millennial (under 10,000 years) time-scales, such as Dansgaard-Oeschger (D-O) (common periodicity = 1,500 years; less common periodicities = 3,000 and 4,500 years) (Dansgaard et al.,

1984; Alley et al., 2001; Ganopolski and Rahmstorf, 2001) and Heinrich events (periodicity = 5,000 – 10,000 years) (Heinrich, 1988). Bond et al. (1992, 1993) showed that various D-O events were grouped in larger scale cycles (subsequently called Bond cycles) that present a progressive cooling and culminates in the coldest conditions represented in the marine records from the North Atlantic by Heinrich events (Fig. 1.3). Heinrich events, discovered by Heinrich (1988) in deep-sea sediment cores from the Northeast Atlantic Ocean, represent sedimentation of ice-rafted debris (IRD) attributed to periods of large iceberg surges during especially cold phases of the last glacial period (Broecker et al., 1992). These abrupt cooling episodes occurred in the North Hemisphere and have been explained as a consequence of the fusion of the Laurentide, Fennoscandian and Greenland ice-sheets and of the large postglacial lakes, producing significant meltwater inputs in the North Atlantic, the collapse of the thermohaline circulation and sudden cold conditions, as suggested for the well-known Younger Dryas event (Ganopolski and Rahmstorf, 2001; Clark et al., 2002; Kageyama et al., 2010). Even if suborbital climate events have been described worldwide, implying strong climate teleconnections between Northern and Southern Hemispheres (Ahn and Brook, 2008), the origin of this variability is not completely understood. Some authors suggested centennial-scale oscillations in the orbital parameters of the Earth (Broecker and Denton, 1989), or the internal dynamics and instability of continental ice masses, showing that even modest ice sheets could produce significant impact on the ocean circulation and on climate system (Peck et al., 2006; Hodell et al., 2017). Many other studies have also shown that solar activity cycles could have also been causing the millennial- and centennial-scale climate variability observed in different paleoclimatic proxy records (Stuiver et al., 1995), as shown by the  $^{10}\text{Be}$  and  $^{14}\text{C}$  values recorded by Van Geel et al. (1999), Hughen et al. (2000), Renssen et al. (2000) and Bond et al. (2001).

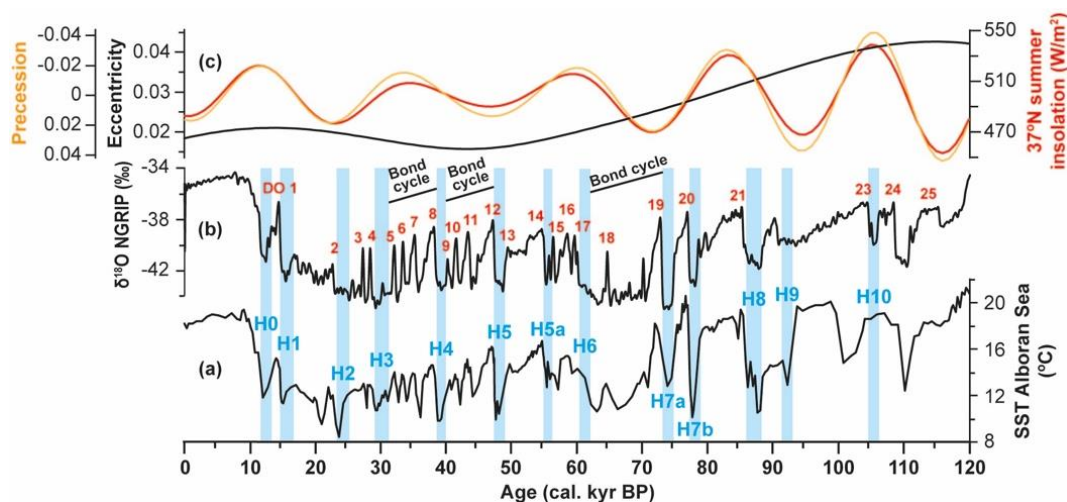


**Figure 1.3.** Comparison of: a) alkenone sea surface temperature (SST) record from Alboran Sea ( $^{\circ}\text{C}$ ) (Martrat et al., 2004), b)  $\delta^{18}\text{O}$  record from NGRIP ( $\text{‰ VSMOW}$ ) (NGRIP-Members, 2004), and c) precession (orange), eccentricity (black) and summer insolation at  $37^{\circ}\text{N}$  ( $\text{W}/\text{m}^2$ ) (red) during the last 120 kyr (based on Laskar et al., 2004). Red numbers indicate Dansgaard-Oeschger events, and blue numbers with vertical bands show Heinrich events. The largest Bond cycles have been marked.

Further shorter-scale atmospheric climatic oscillation that characterizes the study area is the North Atlantic Oscillation (NAO). NAO is strongly controlled by the intensity of the Azores high-pressure system generating anticyclonic ocean surface circulation, and the Iceland low-pressure system that generates westerly wind activity and the responsible of the North Atlantic subpolar oceanic gyre (Barry and Chorley, 2009). During high pressure differences between the Azores (high) and Icelandic (low) systems (positive NAO index), the Mediterranean area is predominated by dry and cold conditions whereas the northern Europe is characterized by wetter and warmer climate. In contrast, low pressure difference (negative NAO index) generates a southward displacement of the winter storm track activity and moisture/warm conditions over the Mediterranean and dry/cold climate over northern Europe (Visbeck et al., 2001). Even though the NAO is a climate variability at very short interannual and decadal time scales (Hurrell, 1995), it also seems to condition climate at centennial- and even millennial-scales (Trouet et al., 2009). In this respect, especially humid periods in southern Iberian Peninsula, such as the Iberian-Roman Humid Period, have been associated with negative NAO conditions, whereas arid conditions (e.g., MCA) have been related with positive NAO (Martín-Puertas et al., 2009). This is supported by a multi-decadal NAO reconstruction, which shows centennial-scale climate variability and persistent positive NAO phase during the Medieval Climate Anomaly and a change to negative NAO conditions during the Little Ice Age (Trouet et al., 2009).

The Atlantic Meridional Overturning Circulation (AMOC) is also essential in the global climate system regulation in the study area. Changes in the composition of this water current (salinity/freshwater balance) implies drastic climate changes, and therefore, variability in marine and continental environments (Repschläger et al., 2015 and references therein). For example, the polar conditions of Heinrich event 1 and Younger Dryas periods affected by phases of meltwater input and the warm climate during the Bølling-Allerød in the western Mediterranean were associated with alternating weak and strong AMOC states, respectively (Jiménez-Amat and Zahn, 2015). In addition, the mid-latitude westerlies, likely in relation with the latitudinal migration of the Intertropical Convergence Zone (ITCZ), have also been related with the variations in the AMOC strength, which seems to have affected past climate over Europe (Srokosz et al., 2012; Baldini et al., 2015; Bazzicalupo et al., 2018).

The continental Mediterranean region and the southern Iberian Peninsula has been shown to be an ideal location for the identification of millennial- and centennial-scale oscillations, displaying strong correlation between vegetation from pollen analysis from this area and the  $\delta^{18}\text{O}$  data from ice-cores, alkenone sea surface temperature records and NAO index reconstructions (Cacho et al., 1999; Fletcher and Sánchez Goñi, 2008; Ramos-Román et al., 2018a).

#### **4. Terrestrial Mediterranean climate reconstruction**

Wetland sedimentary sequences are great recording past climate conditions in the continent through the analysis of regional-scale environmental changes as well as local variability within

the wetland. However, very few terrestrial sedimentary cores have been retrieved containing more than 100 kyr of climate history in the Mediterranean area. Long-lived lake sites, characterized by specific geographical, geological and environmental conditions, bearing long and continuous sedimentary sequences, are rare in the semiarid subtropical Mediterranean area. Sites from southern Europe and the Mediterranean region recording more than 100 kyr of climate history are: Cañizar/Villarquemado (Spain) (González-Sampériz et al., 2013; García-Prieto, 2015), Fuentillejo maar lake (Spain) (Ortiz et al., 2013), Lago Grande di Monticchio (Italy) (Watts et al., 1996; Allen et al., 1999, 2009; Brauer et al., 2007), Valle di Castiglione (Italy) (Follieri et al., 1989; Magri, 1989), Tenaghi Philippon (Greece) (Wijmstra, 1969; Mommersteeg et al., 1995; Tzedakis et al., 2006; Pross et al., 2015), Lake Ioannina (Greece) (Tzedakis et al., 2002; Roucoux et al., 2008, 2011), Lake Ohrid (Albania/FYROM) (Lézine et al., 2010; Sadori et al., 2016; Wagner et al., 2017), Lake Van (Turkey) (Litt et al., 2014; Pickarski and Litt, 2017) and Yammoûneh (Libanon) (Develle et al., 2011). These continental records reveal the high sensitivity of this region to regional and global scale environmental and climate oscillations at long- and short-term. In addition, comparison between terrestrial sites with marine and ice core records are indispensable to understand terrestrial-ocean-atmospheric teleconnections in the past, which are key for predicting future climate scenarios.

The Padul wetland is one of the rare sites in the Iberian Peninsula that contains a long and continuous Quaternary sedimentary record, with more than 100 m of peat and lacustrine sediments deposited over the last ca. 0.8 – 1 Ma (Ortiz et al., 2004a, 2010). Padul is then a very interesting site for studying glacial/interglacial as well as stadial/interstadial oscillations related to orbital- and suborbital-scale climate changes.

Various paleoenvironmental reconstructions have been carried out in the last decades in Padul, mainly based on palynological and geochemical analyses. The first palynological studies were published by Menéndez-Amor and Florschütz (1962, 1964) and later on by Florschütz et al. (1971), Pons and Reille (1988) and Valle-Hernández et al. (2003), whereas the organic geochemical and lithological analyses were published by Ortiz et al. (2004a, 2010). These studies revealed climatically induced regional and local changes in the Padul environment. However, noticeable discrepancies in the interpretation and correlation of climatic events between the different records as result of the poor chronological control and age uncertainties demanded a further investigation. In particular, Florschütz et al. (1971) revealed that the Eemian interglacial (MIS 5e, ~115 – 130 kyr BP) was reached at 24 m depth in the Padul sedimentary sequence, and that their record extended back to the Holstein interglacial (MIS 11, ~350 – 400 kyr BP) at the base of the core at 70 m depth. On the contrary, the subsequent palynological study from Pons and Reille (1988) interpreted that a warm period observed at the base of their core at 24 m depth represented the first Prewürm interstadial (i.e., MIS 5c), not showing any other interglacial period apart from the Holocene for the uppermost 24 m of the sedimentary sequence. These different correlations of the vegetation changes to climatic events are mostly consequence of the poor chronological control of the previously studied records. Specifically, Florschütz et al. (1971) reconstructed the vegetation and climate changes of the last ~400 kyr using the age control of the nearby sediment core from Menendez-Amor and Florschütz (1964), which was only based on 14 radiocarbon dates with a maximum age of ~54 kyr BP. In addition,

they assumed the same sediment accumulation rates for both cores, not recommended for records retrieved in the Padul basin due to the presence of small faults that generated differential block subsidence and resulted in different sedimentation thickness (Domingo García et al., 1983). With respect to the study from Pons and Reille (1988), the vegetation results and interpretation of the last ~100 kyr was only based on 17 radiocarbon dates with a maximum age of  $29.3 \pm 0.6$  kyr BP. A more recent core obtaining a 100 m-long sedimentary sequence (Nestares and Torres, 1998) was studied by Ortiz et al. (2004a, 2010) focusing on organic geochemistry and lithology. The age control of the upper part of this core was based on 9 radiocarbon dates with a maximum age of  $17.3 \pm 0.5$  kyr BP, whereas the older part was dated using a combination of amino acid racemization (AAR), U/Th and paleomagnetic data. The AAR dating was based using the D/L ratios of amino acids from several locations of southern Spain and not specifically from Padul, whereas the U/Th results should be taken carefully, as they are not usually reliable due to the problematic behavior of the U-series in open wetland and lake systems (Sierralta et al., 2017). Finally, the paleomagnetic results are not provided in those publications, being difficult to prove the identification of the Matuyama-Brunhes magnetozone boundary in their sedimentary record. The low-resolution analysis from previous studies along with the previously-mentioned poor chronological control did not allow for an accurate interpretation of past climate conditions in this area.

In this PhD Thesis, a multidisciplinary study from a new sediment core from Padul, Padul-15-05, is presented. This was done with the goals of obtaining new paleoenvironmental information under a more robust age control and higher resolution data, integrating up-to-date lithological/sedimentological and facies, physical properties, inorganic and organic geochemical, mineralogical, paleontological and chronological data that were lacking on the previous studies from the study site. The comparison of these high-resolution multiproxy results with respect to other paleoclimatic records (including continental and marine records from southern Europe and the Mediterranean region as well as high-latitude ice-core records) is essential for understanding local and regional environmental changes (e.g., lake level, sedimentation, vegetation) of this semiarid and climate sensitive area to orbital and sub-orbital climate oscillations.

## 5. Objectives

The main goal of this PhD Thesis is to increase the knowledge about orbital- and suborbital-scale paleoenvironmental and paleoclimatic changes in the southern Iberian Peninsula and the Mediterranean region during the Middle and Late Pleistocene. This study is based on a multiproxy analysis on the ~200-kyr Padul-15-05 sedimentary record that provide with information about local and regional paleoenvironmental and paleoclimatic signals. Below are more specific aims that need to also be accomplished to reach the main goal:

- To refine the chronology of the Padul-15-05 core and Padul sedimentary sequence, using different accurate dating methodologies.



- To obtain higher resolution paleoenvironmental information, integrating up-to-date geological, paleontological and geochemical data, including new proxies that were lacking from previous studies.
- To identify orbital- and suborbital-scale climate changes in the Mediterranean region during the last glacial-interglacial cycles based on multiproxy analysis, with special attention to the regional paleovegetation signal provided by the palynological data.
- To interpret and correlate the past regional climate from southern Iberian Peninsula and the local signals recorded in Padul, reconstructing the paleoenvironmental conditions of the western Mediterranean and its influence in the wetland.
- To compare the new paleoenvironmental multiproxy record from the Padul wetland with other long paleoclimatic data (e.g., insolation values,  $\delta^{18}\text{O}$  from Greenland ice-cores, pollen data from Mediterranean records, SST from Alboran Sea, etc.) in order to understand the climatic factors affecting environmental responses in the western Mediterranean.
- To compare paleoenvironmental conditions of the last interglacial and present interglacial (Holocene) periods, focusing on differences/similarities between our record and other continental Mediterranean records.
- To compare the Heinrich Stadials (HS)- and Dansgaard-Oeschger (D-O)-like millennial-scale variability of the last 65 kyr (including from Heinrich Stadial 6 to Younger Dryas) from Padul with respect to other high-resolution paleoclimatic records from the Mediterranean region and ice-core records from Greenland for observing similarities/differences, leads/lags between the records and climate conditions during the different millennial- and centennial-scale HSs and D-O events.
- To specify the chronology and climate changes related to suborbital-scale variability (millennial to centennial-scale) from Heinrich Stadial 1, Bølling-Allerød and Younger Dryas events at mid latitudes, understanding patterns and possible triggers.

## 6. Regional and local settings: geography, geology and climate

The Sierra Nevada is an E-W aligned mountain range (~900 – 3479 m a.s.l.) located in southern Iberian Peninsula and in the Internal Zone of the Betic Range (Fig. 1.4). It is composed by three metamorphic complexes: 1) the Alpujarride Complex occurring at lowest elevations is mainly formed by Triassic limestones and dolostones; 2) the Nevado-Filábride Complex from highest elevations is characterized by Paleozoic siliceous metamorphic rocks (e.g., mica-schists); 3) the Maláguide Complex restricted to small areas is principally composed by limestones and quartzites (González Donoso et al., 1978; Sáenz de Galdeano et al., 1998).

This PhD research project focused on a 42.64 m-long continuous sedimentary record from the Padul-15-05 sediment core, retrieved in the lakeshore of the present-day Padul lake (37°00'39"N, 3°36'14"W). The Padul wetland (726 m a.s.l.) is located in the western margin of the Sierra Nevada mountain range, specifically in the Padul-Nigüelas basin (20 km south from Granada city, Spain), and covers an area of approximately 4 km<sup>2</sup> (Fig. 1.4). This basin started to form during the Alpine orogeny due to the NW-SE normal faulting activity (still active today)

that generated an endorheic and extensional-asymmetric basin. The higher displacement of the NE Padul-Nigüelas fault resulted in a deeper sedimentary infill in this margin of the basin, allowing a deposition of more than 100 m of Upper Miocene conglomerates, calcarenites and marls, and Pliocene and Quaternary alluvial, lacustrine and peat deposits (Domingo García et al., 1983; Nestares and Torres, 1998).

Climate in the Sierra Nevada has been recorded by the intensive monitoring weather stations, showing the meteorological data every hour since 2008. The mean annual temperature (MAT) at 1735 m a.s.l. (Robledal de Cañar station) is 11°C and at 3097 m a.s.l. (Veleta station) is 2.5°C (Pérez-Luque et al., 2012) ([http://wiki.obsnev.es/index.php/Estaciones\\_Monitoreo\\_Intensivo](http://wiki.obsnev.es/index.php/Estaciones_Monitoreo_Intensivo)). According to other discontinuous records between 1965 and 1993, the MAT at ~2500 m a.s.l. is ~4.4°C with a mean annual precipitation of ~750 mm/yr (García-Alix et al., 2018) (<http://linaria.obsnev.es>). Precipitation at the highest altitudes of the Sierra Nevada (> 2500 m a.s.l.) occurs mostly as snow and is concentrated between October and April (Oliva et al., 2009).

The lower altitude Padul-Nigüelas basin is characterized by a Mediterranean climate with strong continental influence. The mean annual precipitation in Padul is around 445 mm/yr. July and August are the driest months (2 mm/month) and December and January are the most humid months (68 mm/month). The mean annual temperature in the area is 14.4°C; the warmest months are July and August (mean of 24.2°C) and the coldest month is January (mean of 6.4°C) (data from [agroclimap.aemet.es](http://agroclimap.aemet.es) based on meteorological data recorded between 1971 and 2000).

The basin was drained for agricultural purpose in the late XVIII century (Villegas Molina, 1967), and more recently for peat exploitation. The first palynological studies during the 60s along with the discovery of the southernmost European remains of two mammoths from the last glacial period during the 70s and 80s, presented Padul as an important paleontological and paleobiogeographical site for diverse scientific projects (Florschütz et al., 1971; Pons and Reille, 1988; Álvarez-Lao et al., 2009). At present, the Padul wetland, included within the Sierra Nevada Natural Park since 1989, is protected and included in the international Ramsar list for the conservation and sustainable use of wetlands, and in the Special Protection Area (SPA, in Spanish ZEPA) created in the European Union for safeguard the habitats of migratory birds and certain threatened birds.

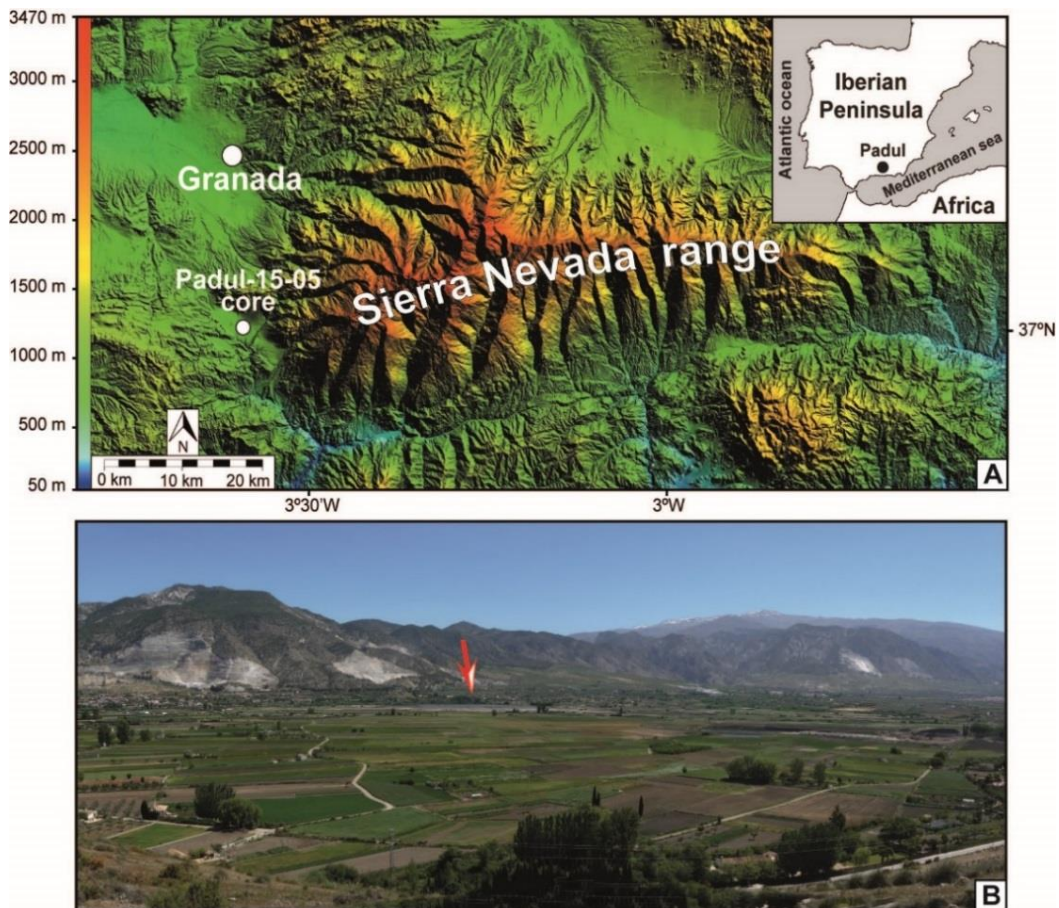


**Figure 1.4.** (A) Geographical location of the Padul-15-05 core in southern Iberian Peninsula, western margin of the Sierra Nevada and south of Granada city; (B) Panoramic photography (view from west to east) of the Padul-Nigüelas basin, Padul wetland (arrow) and the Sierra Nevada at the back.

Vegetation in the Sierra Nevada area is bioclimatically characterized by five vegetation belts (thermomediterranean, mesomediterranean, supramediterranean, oromediterranean and crioromediterranean vegetation belts). This characterization can be done due to the diversity of temperature and precipitation parameters conditioned by the large elevation gradient in the area. The thermomediterranean belt (~0-600 m a.s.l.) is composed by *Quercus coccifera*, *Pistacia lentiscus*, *Ceratonia siliqua*, *Osyris quadripartite*, *Pinus halepensis* and *P. pinea* as the most characteristic taxa. The mesomediterranean vegetation belt (~600-1400 m a.s.l.) presents *Quercus rotundifolia*, *Juniperus oxycedrus*, *Retama sphaerocarpa*, *Ulex parviflorus*, *Genista umbellata*, *Cistus albidus* and *C. laurifolius* as principal taxa, whereas the supramediterranean belt (~1400-1900 m a.s.l.) is characterized by *Quercus pyrenaica*, *Q. faginea*, *Q. rotundifolia*, *Acer opalus* subsp. *granatense*, *Fraxinus angustifolia*, *Sorbus torminalis*, *Adenocarpus decorticans*, *Helleborus foetidus* and *Artemisia glutinosa*. The oromediterranean belt (~1900-2800 m a.s.l.) presents *Pinus sylvestris*, *P. nigra*, *Juniperus hemisphaerica*, *J. sabina*, *J.*

*communis* subs. *nana*, *Genista versicolor*, *Cytisus oromediterraneus*, *Hormathophylla spinosa*, *Prunus prostrata*, *Deschampsia iberica* and *Astragalus sempervirens* subsp. *nevadensis* as most characteristic taxa. Finally, the highest elevation crioromediterranean vegetation belt (>2800 m a.s.l.) is characterized by *Festuca clementei*, *Hormathophylla purpurea*, *Erigeron frigidus*, *Saxifraga nevadensis*, *Viola crassiuscula*, *Linaria glacialis* and *Artemisia granatensis* (El Aallali et al., 1998; Blanca et al., 2002; Valle, 2003). This diversity in elevation makes Sierra Nevada one of the most important area of floral biodiversity in the western Mediterranean, presenting almost the 30% of the vascular plants of the Iberian Peninsula and characterized by high number of endemisms (Blanca et al., 2002), and therefore, included in the UNESCO Biosphere Reserve in 1986, Natural Park in 1989 and National Park in 1999.

## 7. Materials and methods

### 7.1. Padul-15-05 core

The paleoenvironmental and paleoclimatic study from Padul has been done using different analyses. In July 2015, a 42.64 m-long Padul-15-05 core was taken in the lakeshore of the Padul wetland (37°00'39''N, 3°36'14''W) using a Rolatec RL-48-L hydraulic percussion coring machine from the Centre for Scientific Instrumentation of the University of Granada (Fig. 1.5). Padul-15-05 core drilling stopped at 42.64 m depth due to the hard lithology mainly composed by conglomerates found at this depth. The coring machine retrieved a 42.64 m-long core, however, the peat deposits suffered a slight expansion in the laboratory and the total final length of the core was 43.94 m. Peat deposits represent more than the 70.2% of the total sedimentary record.



**Figure 1.5.** Panoramic photography of the coring during July 2015 in the southern edge of the Padul wetland.

The core was sampled and stored in a cooler at 4°C in the Stratigraphy and Paleontology Department of the Faculty of Science from the University of Granada. Thereafter, the core was analyzed using different non-destructive and destructive analysis. The non-destructive analyses carried out are: lithology/sedimentology and facies analysis, scanning photography and color analysis, magnetic susceptibility (MS) and continuous X-ray fluorescence (XRF). In contrast,

## *Introduction*

the destructive analyses done in this study are: elemental analysis (including total organic carbon, nitrogen, hydrogen and sulfur), organic biomarkers (including n-alkanes, alkenones/ketones, diols and fatty acids), X-ray diffraction (XRD), palynological analysis, accelerator mass spectrometry (AMS) radiocarbon dating (including dating on specific compounds) and amino acid racemization (AAR) dating. Other collaborators have also done the analysis of ostracods, gastropods, charophytes and charcoal. All proxies and analyses done on the Padul-15-05 core have been schematized in Figure 1.6.

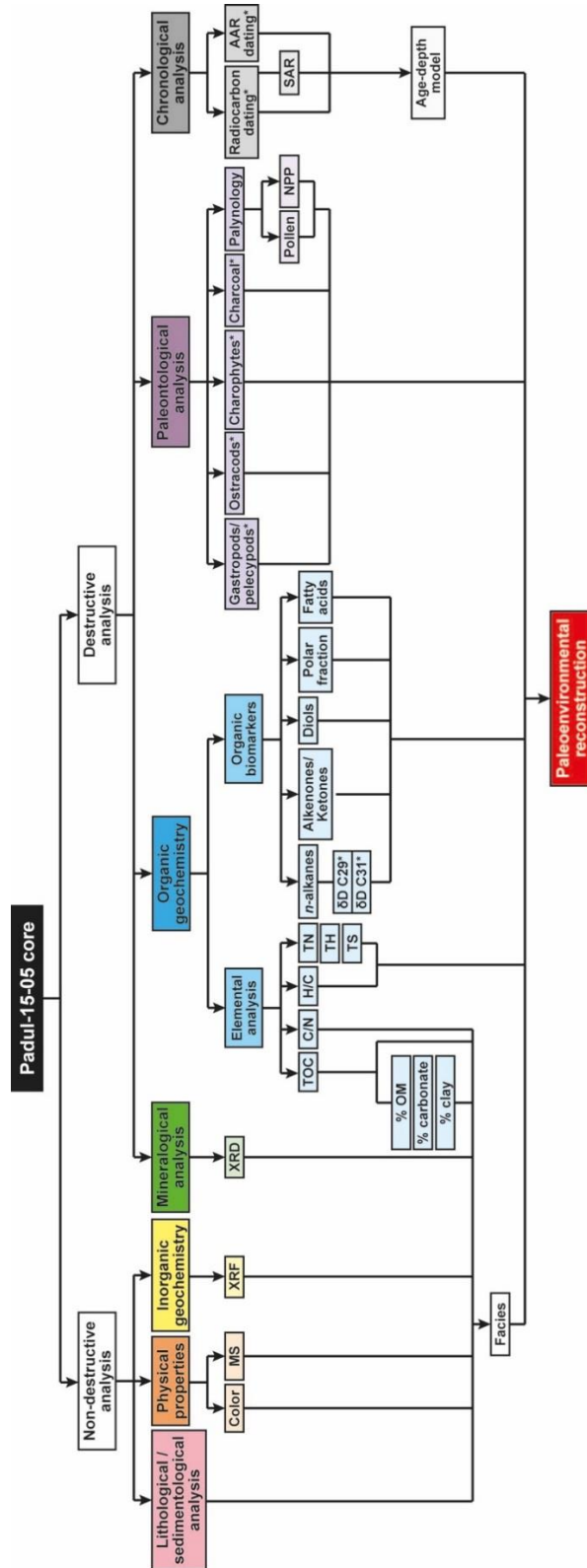


**Figure 1.6.** Scheme of all the analyses developed during this PhD Thesis in the Padul-15-05 core. Asterisks mark the analysis carried out by collaborators, including δD C29 and C31 values of n-alkanes, the quantitative analysis of gastropods/pelecypods, ostracods, charophytes and charcoals (not included in the Thesis), the radiocarbon dating on specific compounds and the amino acid racemization dating (AAR).

## 7.2. Paleoclimatic multiproxy study

A multiproxy study using different local and regional signals is essential in order to carry out a precise paleoenvironmental and paleoclimatic reconstruction. The comparison of the different proxy data provides with information about changes in the local Padul wetland conditions (e.g., lake level, sedimentation) as well as regional climate variations (e.g., vegetation, precipitation conditions). An introduction to every analysis and its use in this study has been described below:

### 7.2.1. Lithological, sedimentological and facies analyses

Lithological and sedimentological features of the entire core were described in the laboratory of the Stratigraphy and Paleontology Department (Faculty of Science, University of Granada). Thereafter, facies were classified based on the lithological/sedimentological description and on the analytical data obtained from other analyses, such as magnetic susceptibility, X-ray fluorescence or elemental analysis. Lithology and facies description are essential in order to determinate sedimentation in the lake/wetland related to variations in lake conditions (lake level changes, weathering/erosion processes in the area, etc.).

### 7.2.2. Physical properties

#### 7.2.2.1. High-resolution scanning photography and color data

High-resolution photography and color data were obtained using an Avaatech core scanner from the CORELAB laboratory at the University of Barcelona (Fig. 1.7). High-resolution photographs are essential when comparing the lithology with data from other analysis, helping in the identification of environmental and climate changes and its relation with the lithological/sedimentological features. Color results including lightness, RGB and the CIELAB color space, were recovered under a resolution of 0.073 mm. Color analysis was the highest resolution data from all the methodologies used in this study.

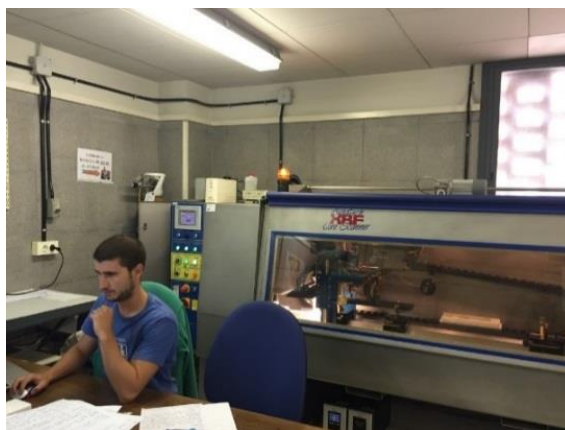


**Figure 1.7.** High-resolution scanning photography, color and X-ray fluorescence analyses of the Padul-15-05 core carried out using an Avaatech core scanner (University of Barcelona) in September 2015.



### 7.2.2.2. Magnetic susceptibility (MS)

The magnetic susceptibility of the core was measured with a Bartington MS3 meter operating with a MS2E manual sensor in the Stratigraphy and Paleontology Department at the University of Granada (Fig. 1.8). The maximum resolution of the MS3 meter was  $2 \times 10^{-6}$  SI and the operating frequency of the MS2E manual sensor was 2 kHz. The magnetic susceptibility data was recorded using the Bartsoft software (version 4.2.1.1) installed in a laptop computer. This analysis was done at 0.5 cm resolution and a measuring time period of 10 s. MS provides information about detrital input rich in magnetics (e.g., Fe, Ti) (Pérez-Sanz et al., 2013) in the lake/wetland associated with oscillations in the erosion of materials from the Sierra Nevada linked to changes in climate conditions.



**Figure 1.8.** Analysis of magnetic susceptibility measured using a Bartington MS3 meter operating with a MS2E manual sensor and connected to a laptop (University of Granada).

### 7.2.3. Inorganic geochemistry

#### 7.2.3.1. X-ray fluorescence (XRF)

The inorganic geochemical composition of the Padul-15-05 sediment core was obtained using a continuous XRF Avaatech core scanner from the CORELAB laboratory (University of Barcelona; Fig. 1.7). A total of 34 inorganic elements were measured at 1 cm resolution and with two different working conditions: (1) 10 s count time, 650mA of X-ray current and 10 kV of X-ray voltage for the measurement of Al, Si, P, S, Cl, Ar, K, Ca, Ti, V, Cr, Mn, Fe, Rh and Ag. (2) 35 s count time, 1700mA of X-ray current and 30 kV of X-ray voltage for the measurement of Ni, Cu, Zn, Ga, Ge, As, Se, Br, Rb, Sr, Y, Zr, Nb, Au, Hg, Pb, Bi, Th and U. Results were expressed in counts per second. The most representative elements (mainly Al, Si, S, K, Ca, Fe, Br, Rb, Sr and Zr) have been used for the identification of sedimentation changes in the lake/wetland linked to variations in environmental and climatic conditions, resulting in lake level oscillations, changes in detritic input and/or changes in the oxygen availability (oxic/anoxic conditions) (Corella et al., 2012; Francke et al., 2016).



## 7.2.4. Organic geochemistry

### 7.2.4.1. Elemental analysis

Elemental analysis on the Padul-15-05 core, including results of total carbon, nitrogen, hydrogen and sulfur, was done using the CHNS Elemental Analyzer Thermo Scientific Flash 2000 from the Centre for Scientific Instrumentation of the University of Granada. Four hundred and seventy-four samples with a mean resolution of ~9 cm (~37 cm resolution from 42.64 m to 7 m depth and ~2 cm resolution from 7 m depth to core top) were decalcified with 1:1 HCl before measuring. The total organic carbon (TOC), total nitrogen (TN), total hydrogen (TH), total sulfur (TS), and the atomic C/N and H/C ratios were obtained based on the analyzed data. TOC percentage was calculated from the percentage of carbon (%C) yielded by the elemental analyzed and recalculated by the weight of the sample before and after decalcification (also obtaining the total percentage of carbonate). Thereafter, the organic matter (OM) from every sample was estimated multiplying TOC by 1.724 of Van Bemmelen factor (Nelson and Sommers, 1982). Finally, clay content is the remnant, and can be calculated as follows: %Clay = 100 – %OM – %Carbonate. These data provide with information about organic productivity in the lake/wetland, the relation between continental vs aquatic signal, oxic/anoxic conditions and/or the water supply (Hedges et al., 1986; Barreiro-Lostres et al., 2015).

### 7.2.4.2. Organic biomarkers

Analysis on organic biomarkers, including n-alkanes, alkenones/ketones, diols, polar fraction and fatty acids, were carried out in the BECS (Biomarker for Environmental and Climate Science) laboratory at the School of Geographical and Earth Science of the University of Glasgow. Seventy samples between 3.13 m and 6.75 m depth (mean resolution of 5 cm) were decalcified with 1:1 HCl for eliminate the carbonate fraction. Thereafter, samples were pre-weighted, homogenized and freeze-dried, the Total Lipid Extract (TLE) was obtained with a Thermo Scientific Dionex ASE 350 Accelerated Solvent Extractor system using dichloromethane (DCM, CH<sub>2</sub>Cl<sub>2</sub>):methanol (MeOH) (3:1). Once the TLE was obtained, the Total Neutral Fraction (TNF) and the Total Acid Fraction (TAF) were separated by means of aminopropyl-silica gel chromatography using a solution of DCM:isopropanol (1:1) and a solution of 4% acetic acid, respectively. Thereafter, from the 4 different neutral fractions (N1 to N4), the organic content and the compounds of interest were extracted using the following solvents:

Fraction	Solvent	Organic content	Compound of interest
N1	Hexane	Aliphatic hydrocarbons	<i>n</i> -alkanes
N2	DCM	Ketone/Ester/Aromatics	Alkenones
N3	Ethyl acetate:hexane (25:75)	Alcohols	Diols
N4	Methanol	Polar	GDGTs

To check the reproducibility of measurements and to quantify the *n*-alkane content from N1, an external standard with a mixture of *n*-alkanes (C<sub>16</sub>, C<sub>18</sub>, C<sub>19</sub>, C<sub>20</sub>, C<sub>23</sub>, C<sub>25</sub>, C<sub>26</sub>, C<sub>28</sub>, C<sub>30</sub>, C<sub>32</sub>, C<sub>37</sub>) was measured every five samples. The *n*-alkanes were measured using a Gas Chromatography-Flame Ionization Detector (GC-FID) for quantification and a Gas Chromatography-Mass Spectrometry (GC-MS) (Shimadzu QP2010-Plus Mass Spectrometer interfaced with a Shimadzu 2010 GC) for the identification of several compounds from the most complicated samples.  $\delta D$  values of *n*-alkanes were measured using a Thermo Trace GC coupled via a pyrolysis reactor to a Thermo Fisher MAT 253 Isotope Ratio-Mass Spectrometer (GC/IR-MS).  $\delta D$  values were calibrated to external H<sub>2</sub> reference gas. For the Last Glacial Maximum and Heinrich Stadial 1, we have corrected the  $\delta D_{\text{wax}}$  values due to the effect of global-ice volume changes on meteoric water  $\delta D$  values (Collins et al., 2013a and references therein).

Diols were obtained in the third neutral fraction (alcohol fraction, N3), which was derivatized by bis-(trimethylsilyl) trifluoroacetamide (BSTFA). 30 $\mu$ l of BSTFA and 40 $\mu$ l of pyridine were added to the N3 fraction before heated at 80°C for 2 h and running the analysis. Samples were diluted in DCM and measured in the GC-FID to get an idea of the proper concentration to measure them by means of GC-MS under a Selected-Ion Monitoring (SIM) mode. We selected the masses (*m/z*) that are characteristic of the fragment ions from the most important long chain diols: 299, 313, 327, 341 and 355. Ion fragments of masses 313 and 341 were quantified using their relative intensities in the mass spectra for obtaining fractional abundances of the C<sub>28</sub> 1,13-diol, C<sub>30</sub> 1,13-diol, C<sub>30</sub> 1,15-diol, and C<sub>32</sub> 1,15-diol. The Long Chain Diols Index (LDI), used for interpreting the potential diol source (e.g., specific algae group), was calculated using fractional abundances of C<sub>28</sub> 1,13-diol, C<sub>30</sub> 1,13-diol, C<sub>30</sub> 1,15-diol as:  $LDI = FC_{30\ 1,15\text{-diol}} / (FC_{28\ 1,13\text{-diol}} + FC_{30\ 1,13\text{-diol}} + FC_{30\ 1,15\text{-diol}})$  (Rampen et al., 2012).

Fatty acids from the TAF were also obtained from samples derivatizing before eluting the chromatography column with hexane and DCM. The DCM fraction was transferred to 2ml GC-vials and dried under N<sub>2</sub>. Finally, samples were weighted and the mass of the TAF recorded before running the GC-FID and GC-MS.

The analysis on organic biomarkers have been shown to be good proxies for the biological source, the preservation of the organic matter, temperature reconstructions, precipitation changes and/or the aquatic/submerged plants portion of the organic compounds with respect to the terrestrial plants, among others (Shimokawara et al., 2010; Rampen et al., 2012; Fang et al., 2014; Ponton et al., 2014).

### 7.2.5. Mineralogical analysis

#### 7.2.5.1. X-ray diffraction (XRD)

The mineralogical composition of sediments from the Padul-15-05 core was obtained from the X-ray diffractograms using a PANalytical X'Pert PRO diffractometer with an X'celerator detector (under Cu-K $\alpha$  radiation) from the Instituto Andaluz de Ciencias de la Tierra (Granada). The analysis of 36 samples was run from 4° to 70° 2 $\theta$  and the estimations of semi-quantitative mineral abundance were obtained using the Xpovder software (Martin, 2004). This analysis

allowed us to interpret the different lithologies and facies from the core, providing information about the origin of sediments deposited in the lake/wetland and the related processes that have generated the deposition of these minerals in Padul, such as changes in the weathering/erosion of the surrounding materials from the Sierra Nevada or precipitation/evapotranspiration processes in the wetland. XRD analysis have been previously shown to be useful in the identification of weathering [e.g., in the Yammou'enh basin (Lebanon) (Develle et al., 2011)], and for precipitation and evaporation processes [e.g., in saline lakes from Central Ebro Basin (NE Spain) (González-Sampérez et al., 2008) and in Laguna de la Fuente de Piedra (S Spain) (Höbig et al., 2016)].

#### 7.2.6. Paleontological analysis

In this study a qualitative (not quantitative) analysis of gastropods, pelecypods and charophytes was carried out during the lithological and sedimentological description. A more detailed and complete study focused on palynological analysis, which is explained below.

##### 7.2.6.1. Palynology

The palynological analysis of this PhD research project was carried out in the Stratigraphy and Paleontology Department at the University of Granada studying 301 samples between 3.13 m and 42.64 m depth. The pollen extraction followed a modified methodology of Faegri and Iversen (1989) due to the high amount of organic matter presented in the Padul-15-05 core. The sample processing started adding *Lycopodium* spores to 1 cm<sup>3</sup>/sample of sediment and treated with HCl, HF and NaOH for removing carbonates, silicates and humic acid, respectively. The residue was sieved at 250 µm previous to the acetolysis procedure used for removing organic matter. This pretreatment finished with sieving at 10 µm. The final pollen residue, together with glycerin, was mounted in slides and counted using a Zeiss transmitted light microscope at 400 magnifications (Fig. 1.9). A minimum of 300 pollen grains were counted in most of the samples. However, at specific depths pollen concentration was lower, resulting on an average terrestrial pollen count of 256 grains (including all samples). Pollen counts were transformed to pollen percentages based on the terrestrial pollen sum and excluding aquatics. Pollen grains from trees and shrubs, herbs and grasses, aquatic plants and non-pollen palynomorphs (NPP) were identified (Fig. 1.10 and 1.11) using the pollen atlas book from Beug (2004).



**Figure 1.9.** Zeiss Transmitted light microscope used for the palynological analysis at the Paleontology and Stratigraphy Department of the University of Granada.

The palynological analysis is really useful for observing local oscillations in the wetland (e.g., algal and aquatic plant changes pointing to lake level variations) as well as detecting regional vegetation changes (e.g., variations in the forest abundance and composition), which allow reconstructing climate conditions in southern Iberian Peninsula (Fletcher et al., 2007; Anderson et al., 2011; Jiménez-Moreno et al., 2013; Ramos-Román et al., 2018b; Schröder et al., 2018). In particular, the Mediterranean forest taxa composed by *Quercus* total, *Olea*, *Phillyrea* and *Pistacia* have been used as good indicator of climate changes in the Mediterranean region, as they display a wide expansion during interglacial/interstadial periods and contractions during glacial/stadial periods due to colder and more arid climate conditions (Tzedakis, 2007; Sánchez Goñi et al., 2008; Fletcher et al., 2010a). The xerophytes pollen group includes *Artemisia*, *Amaranthaceae* and *Ephedra*. They are a good proxy for regional aridity and they are abundant during glacial/stadials due to their good adaptability under arid climate scenarios (Carrión et al., 2001; Moreno et al., 2012b). The Pollen Climate Index (PCI) proposed by Joannin et al. (2011) and based on the relation between mesothermic elements (interglacial conditions) and steppe elements (glacial conditions) exposed by Combourieu Nebout et al. (1999) was calculated for discriminating between glacial/stadial and interglacial/interstadial conditions. This index in the Padul-15-05 record has been developed dividing the main warm/humid vegetation species (sum of *Quercus* total, *Olea*, *Fraxinus*, *Phillyrea*, *Acer*, *Betula*, *Alnus*, *Ulmus*, *Taxus*, *Salix*, *Pistacia*, *Corylus* and *Carpinus*) by the principal cold/arid taxa (sum of *Artemisia*, *Ephedra*, *Hippophaë* and *Amaranthaceae*). The lake level in the Padul wetland has also been reconstructed with the palynological data, using algae (sum of *Pediastrum*, *Botryococcus*, *Mougeotia* and *Zygnema* type total), hygrophytes (sum of *Cyperaceae* and *Typha*) and *Poaceae*. Algae in the Padul wetland, principally represented by *Pediastrum* and *Botryococcus*, are floating planktonic organisms, associated to oxygenated and open lake waters (Whiteside, 1965; Guy-Ohlson, 1992). Hygrophytes in Padul, such as *Typha domingensis*, are attached to the wet and submerged substrate and usually growing along the lake shore with relatively shallow water depth (Mitchell, 1969; White and Ganf, 1998), suggesting lower lake levels with respect to algae. Finally, *Phragmites australis*, which is one of the main *Poaceae* species in Padul, are linked to emergent lake zones and seems to be well-adapted to the drawdown of the shoreline and low water availability (Whyte et al., 2008), suggesting the lowest lake levels. Therefore, the

reconstruction of the lake level in the Padul wetland as being done as following: Lake level = Algae / (Algae + Hygrophytes + Poaceae).

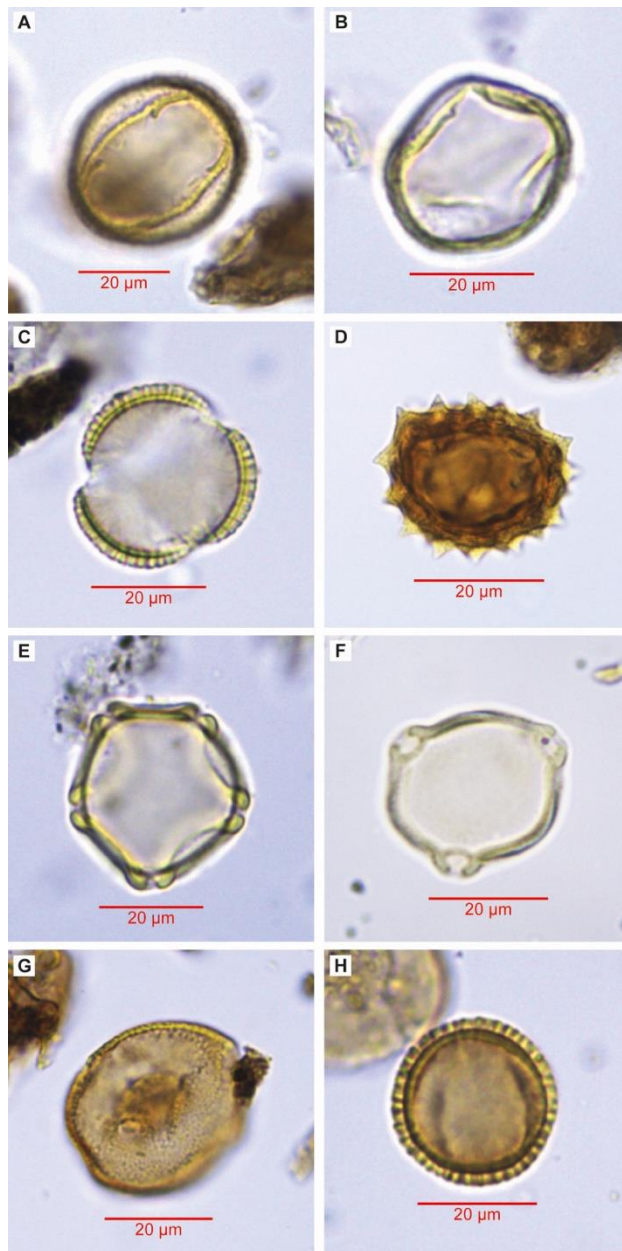


**Figure 1.10.** Pollen photographs of the main pollen species from the Padul-15-05 record. (A) *Quercus* deciduous (Drive 49, 20-21cm; 25.16m depth), (B) *Quercus* evergreen (Dr. 30, 40-41cm; 15.47m depth), (C) *Artemisia* (Dr. 9, 43-44cm; 4.58m depth), (D) Asteraceae Asteroideae (Dr. 11, 35-36cm; 5.54m depth), (E) *Alnus* (Dr. 47, 30-31cm; 24.22m depth), (F) *Betula* (Dr. 55, 28-29cm; 28.36m depth), (G) *Pistacia* (Dr. 7, 27-28cm; 3.37m depth) and, (H) *Olea europaea* (Dr. 8, 29-30cm; 3.91m depth).

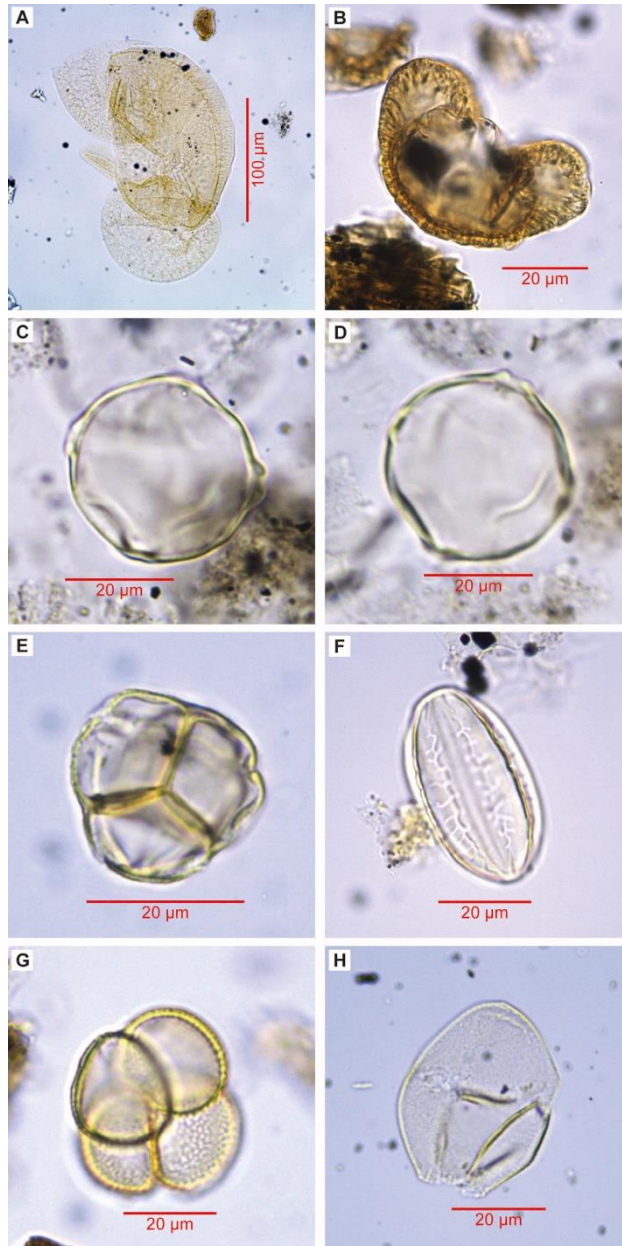


**Figure 1.11.** Pollen photographs of the main pollen species from the Padul-15-05 record. (A) *Abies* (Drive 53, 30-31cm; 27.34m depth), (B) *Cedrus* (Dr. 60, 42-43m depth), (C – D; the same pollen grain) *Carpinus betulus* (Dr. 49, 20-21cm; 25.16m depth), (E) Ericaceae (Dr. 10, 50-51cm; 5.19m depth), (F) *Ephedra distachya* (Dr. 51, 30-31cm; 26.29cm depth), (G) *Typha* (Dr. 71, 20-21cm; 36.59m depth) and, (H) Cyperaceae (Dr. 64, 30-31cm; 33.05m depth).

### 7.2.7. Chronological analysis

#### 7.2.7.1. Radiocarbon dating (including specific compounds)

A total of 67 samples were analyzed for AMS radiocarbon dating between the core-surface and 9.85 m depth, including 30 samples from plant remains, 20 samples from organic bulk sediment, 6 from organic residues, 5 from pollen residue, 3 from gastropods and 3 from specific compounds (fatty acids). From the total of 67 samples, 21 were excluded (a 31%) due to reservoir effects, vertical roots from upper layers or apparently too old/young dates. The plant remains were directly taken from the core. The bulk sediment samples were taken from depths where plant remains were absent. The organic residue consisted in samples that were pretreated with HCl and HF. The pollen residue was based on samples pretreated with HCl, HF and NaOH, obtaining the residue that remained after centrifuging. Gastropods were directly taken from the core and cleaned with milli-Q water. All these samples were indistinctly sent for dating to BETA Analytic radiocarbon dating laboratory or to Poznan radiocarbon laboratory.

The specific compound radiocarbon dating on fatty acids was carried out on 3 samples at 1.22 m, 4.52 m and 5.59 cm depth using the methodology from Yamane et al. (2014). Briefly, the sediment was extracted using DCM/MeOH (7:3) and the extract was saponified with KOH/MeOH. After removal of neutral components, the saponified solution was acidified with HCl, extracted with DCM and esterified with HCl/MeOH. Separation of the fatty acid methyl esters (FAMES) was conducted by silica gel column chromatography with *n*-hexane/DCM (2:1). Isolation of individual (C<sub>16</sub>-C<sub>30</sub>) FAMES was conducted using reversed-phase high-performance liquid chromatography (HPLC) with three columns (Develosil C30-UG-5, 4.6 x 250 mm, 5.5 µm particle size, Nomura Chemical) connected in series. The mobile phase was MeCN/MeOH (1:2) with 0-5% pyridine. The column temperature was increased in steps of 15°C from 0 to 35 min, ramped up at 2°C/min from 35 to 52.5 min, and held at 50°C until 80 min. The HPLC system consist of a binary pump (Agilent G1312A), on-line degasser (Agilent G1379B), autosampler (Agilent G1313A), total temperature controller (Polaratherm Series 9000), evaporative light scattering detector (ELSD; Polymer Laboratories PL-ELS 2100), and fraction collector (Agilent G1364C). The flow rate of the mobile phase was 1 ml/min. The isolated fraction was then subjected to silica gel column chromatography to remove impurities introduced during HPLC. After the isolated FAMES were collected and converted to graphite, radiocarbon measurement was conducted at the accelerator mass spectrometry facility from the University of Tokyo (Yokoyama et al., 2010). All <sup>14</sup>C values were corrected for the contribution of methyl carbon obtained from MeOH ( $\Delta^{14}\text{C} = -991\text{‰}$ ) during the esterification by isotope mass balance (Ohkouchi et al., 2003).

#### 7.2.7.2. Amino acid racemization (AAR) dating

The AAR dating was carried out taking 83 individual mollusc shells from 14 levels in the core, including gastropods and pelecypods. Samples were cleaned by sonication, soaked in 3% H<sub>2</sub>O<sub>2</sub> for 2 h, rinsed with purified H<sub>2</sub>O and dried under laminar flow. Individual shells were

placed in separate sterilized vials and dissolved in 6M HCl. Vial were sealed under N<sub>2</sub> and heated at 110°C for 22 h to recover the total hydrolysable amino acid population. Hydrolysate solutions were evaporated and rehydrated in 0.01M HCl with 1.5mM sodium azide. The chromatographic instrumentation and procedure used to separate amino acid enantiomers are presented in Kaufman and Manley (1998). Briefly, the derivatization using o-phthaldialdehyde together with the chiral thiol, N-isobutyryl-L-cysteine yielded fluorescent diastereomeric derivates of chiral primary amino acids. The derivatization was performed on-line prior to each injection using the auto-injector of an integrated Agilent HP1100 liquid chromatograph. Separation was by a reverse-phase column packed with a C<sub>18</sub> stationary phase using a linear gradient of aqueous sodium acetate, methanol and acetonitrile, and the detection was by fluorescence.

### 7.2.7.3. Age-depth model

The age control of the Padul-15-05 core was developed using accelerator mass spectrometry (AMS)-standard radiocarbon dating (including specific compound radiocarbon dating on fatty acids), amino acid racemization (AAR) dating and sediment accumulation rates (SAR). The age-depth model for the radiocarbon and AAR dated part (from surface to 23.27 m depth) was built using R-code package “Clam 2.2” software (Blaauw, 2010), using the IntCal13.14C calibration curve (Reimer et al., 2013) with a locally weighted spline age-depth model at 95% confidence level. Finally, for the lower part of the core between 42.64 and 23.27 m depth, the age model was built using a linear extrapolation based on the sediment accumulation rates (SAR) calculated from the average peat and carbonate/marl lithologies from the well-dated top part of the core.

### 7.2.8. Statistical analysis

#### 7.2.8.1. Principal component analysis (PCA) and correlation coefficients

A principal component analysis (PCA) was run on the most representative elements from the inorganic geochemistry obtained with the XRF (Ca, Sr, Si, Al, Fe, S and Br), elemental analysis from the organic geochemistry (TOC and C/N), magnetic susceptibility (MS) (*Chapter 2*), and pollen data from the Padul-15-05 core (*Chapter 3*). PCA was carried out using the PAST 3.19 software (Hammer et al., 2001). A previous resampling using linear interpolation was conducted on XRF, elemental analysis and MS data to achieve equivalent resolution among different proxies before normalize as:  $X = (x - \text{mean})/\text{standard deviation}$  (see *Chapter 2*). The most representative pollen taxa (*Quercus* evergreen, *Quercus* deciduous, *Olea*, *Pistacia*, *Pinus* total, Cupressaceae, *Artemisia*, Amaranthaceae, *Ephedra*, Ericaceae, Poaceae, Cyperaceae, *Botryococcus* and *Pediastrum*) were also normalized (see *Chapter 3*). All the resampled and normalized data were further analyzed to determinate the percentage of variance, scores, scatter plot and correlation loading plot.

In addition to the PCA, correlation coefficients were also computed as analytical approach on XRF, elemental analysis, MS and pollen data. This analysis was also run with the PAST 3.19 software.



### *7.2.8.2. Spectral analysis*

Spectral analyses were conducted on Si, MS, TOC, Mediterranean forest, xerophytes and Pollen Climate Index (PCI) data from the Padul-15-05 core. Spectral analyses on different proxy data time series were used for obtaining periodicities linked to local and regional environmental oscillations in Padul and in southern Iberian Peninsula in relation with orbital and sub-orbital scale climate changes. Statistically significant cyclicities were obtained using the PAST software under a Redfit spectral analysis type and based on a rectangular window function with the standard value of 2 for both segments and oversample parameters.

# *Chapter* 2

*Orbital-scale environmental and climatic changes recorded in a  
new ~200,000-year-long multiproxy sedimentary record from  
Padul, southern Iberian Peninsula*



## Chapter 2: Orbital-scale environmental and climatic changes recorded in a new ~200,000-year-long multiproxy sedimentary record from Padul, southern Iberian Peninsula

Jon Camuera<sup>1</sup>, Gonzalo Jiménez-Moreno<sup>1</sup>, María J. Ramos-Román<sup>1</sup>, Antonio García-Alix<sup>1</sup>, Jaime L. Toney<sup>2</sup>, R. Scott Anderson<sup>3</sup>, Francisco Jiménez-Espejo<sup>4</sup>, Darrell Kaufman<sup>3</sup>, Jordon Bright<sup>5</sup>, Cole Webster<sup>3</sup>, Yurena Yanes<sup>6</sup>, José S. Carrión<sup>7</sup>, Naohiko Ohkouchi<sup>4</sup>, Hisami Suga<sup>4</sup>, Masako Yamame<sup>8</sup>, Yusuke Yokoyama<sup>9</sup>, Francisca Martínez-Ruiz<sup>10</sup>

<sup>1</sup> Departamento de Estratigrafía y Paleontología, Universidad de Granada, Spain

<sup>2</sup> School of Geographical and Earth Sciences, University of Glasgow, UK

<sup>3</sup> School of Earth and Sustainability, Northern Arizona University, USA

<sup>4</sup> Department of Biogeochemistry, Japan Agency for Marine-Earth Science and Technology (JAMSTEC), Japan  
7351 E. Speedway Blvd, 30C, Tucson AZ, USA

<sup>6</sup> Department of Geology, University of Cincinnati, USA

<sup>7</sup> Departamento de Biología Vegetal, Facultad de Biología, Universidad de Murcia, Spain

<sup>8</sup> Institute for Space-Earth Environmental Research, Nagoya University, Japan

<sup>9</sup> Atmosphere and Ocean Research Institute, University of Tokyo, Kashiwanoha, Chiba, Japan

<sup>10</sup> Instituto Andaluz de Ciencias de la Tierra (IACT), Consejo Superior de Investigaciones Científicas-Universidad de Granada (CSIC-UGR), Granada, Spain


### Published in:

Quaternary Science Reviews, v. 198, p. 91-114 (2018)

Doi: 10.1016/j.quascirev.2018.08.014

Impact factor: 4.334


Quaternary Science Reviews 198 (2018) 91–114



Contents lists available at ScienceDirect

## Quaternary Science Reviews

journal homepage: [www.elsevier.com/locate/quascirev](http://www.elsevier.com/locate/quascirev)




---

**Orbital-scale environmental and climatic changes recorded in a new ~200,000-year-long multiproxy sedimentary record from Padul, southern Iberian Peninsula**

Jon Camuera <sup>a, \*</sup>, Gonzalo Jiménez-Moreno <sup>a</sup>, María J. Ramos-Román <sup>a</sup>, Antonio García-Alix <sup>a</sup>, Jaime L. Toney <sup>b</sup>, R. Scott Anderson <sup>c</sup>, Francisco Jiménez-Espejo <sup>d</sup>, Darrell Kaufman <sup>c</sup>, Jordon Bright <sup>e</sup>, Cole Webster <sup>c</sup>, Yurena Yanes <sup>f</sup>, José S. Carrión <sup>g</sup>, Naohiko Ohkouchi <sup>d</sup>, Hisami Suga <sup>d</sup>, Masako Yamame <sup>h</sup>, Yusuke Yokoyama <sup>i</sup>, Francisca Martínez-Ruiz <sup>j</sup>

<sup>a</sup> Departamento de Estratigrafía y Paleontología, Universidad de Granada, Spain  
<sup>b</sup> School of Geographical and Earth Sciences, University of Glasgow, UK  
<sup>c</sup> School of Earth and Sustainability, Northern Arizona University, USA  
<sup>d</sup> Department of Biogeochemistry, Japan Agency for Marine-Earth Science and Technology (JAMSTEC), Japan  
<sup>e</sup> 7351 E. Speedway Blvd, 30C, Tucson, AZ, USA  
<sup>f</sup> Department of Geology, University of Cincinnati, USA  
<sup>g</sup> Departamento de Biología Vegetal, Facultad de Biología, Universidad de Murcia, Spain  
<sup>h</sup> Institute for Space-Earth Environmental Research, Nagoya University, Japan  
<sup>i</sup> Atmosphere and Ocean Research Institute, University of Tokyo, Kashiwanoha, Chiba, Japan  
<sup>j</sup> Instituto Andaluz de Ciencias de la Tierra (IACT), Consejo Superior de Investigaciones Científicas-Universidad de Granada (CSIC-UGR), Granada, Spain



## **Abstract**

Padul is one of the few wetland sites in southern Europe and the Mediterranean region that exhibits an unusually large temporal span (>100 kyr) and continuous Quaternary sedimentary record. Previous core-based studies from Padul yielded paleoecological datasets (i.e., pollen and organic geochemistry), but with a poor age control that resulted in rather arbitrary climate inferences. Therefore, precise age control and a multidisciplinary approach is necessary to understand long-term regional environmental and climate change and the associated local response of the Padul wetland environment. Here we present a new long sediment record (Padul-15-05) from this wetland in the southern Iberian Peninsula with the aim of improving the age control of the sedimentary sequence and carrying out up-to-date high-resolution multiproxy analyses. In this study the age control is based on 61 AMS radiocarbon dates for the last ca. 50 kyr BP and on the extent of amino acid racemization (AAR) in mollusc shells extending back ~118 kyr BP. No numerical ages are available for the bottom part of the core but the sediment accumulation rates (SAR) and the cyclostratigraphic analysis of the multiproxy data suggest that the core preserves a continuous record of the last ~197 kyr (from late MIS 7 to present) with millennial-scale time resolution. Sedimentological (lithology, magnetic susceptibility, XRD, color), geochemical (XRF, TOC, C/N, % carbonate content) and paleontological (pollen, charophytes, gastropods) data show co-varying cyclical paleoenvironmental changes linked to orbital-scale climatic variability. Silicon, magnetic susceptibility (MS) and total organic carbon (TOC) data show periodicities between ~26.2 – 19.6 kyr linked to insolation, which is strongly dominated by precession cycles at this latitude. High values of Si and MS data have been related to high siliciclastic/detrital input from Sierra Nevada range during minima in insolation due to enhanced soil weathering/erosion during regional aridity and lower forest cover recorded by the arboreal pollen, which could also be favored by a minor biogenic productivity. In addition, warm climate conditions during maxima in insolation mostly resulted in negative precipitation/evapotranspiration balance and low lake levels, while cold glacial and stadial periods were mainly characterized by positive precipitation/evapotranspiration balance, and therefore, high lake levels. The improved chronology of the Padul sedimentary sequence along with a multiproxy study permitted us to better relate environmental and vegetation changes to climatic events and to demonstrate how both local (i.e., lake level, sedimentation) and regional (i.e., vegetation) environments responded to orbital-scale climate changes.

**Keywords:** Pleistocene; Holocene; Climate; Environmental changes; Facies; Lake level; Padul

## **1. Introduction**

Climate during the Quaternary has oscillated between glacial and interglacial conditions in response to Earth's orbital cycles. Long paleoenvironmental records are necessary to investigate recurrent climatic or paleoenvironmental changes occurring with a certain periodicity (e.g., glacial-interglacial cycles). Over the last few decades, a significant effort has been made to understand climate and environmental variability during the Quaternary in southern Europe and the Mediterranean region. A handful of continuous long terrestrial sedimentary sequences

recording more than 100 kyr have been studied in the Mediterranean region, including well-known sites such as Lago Grande di Monticchio (Italy) (Watts et al., 1996; Allen et al., 1999; 2000), Ioannina lake (Greece) (Tzedakis et al., 2002; Tzedakis et al., 2003a), Tenaghi Philippon (Greece) (Wijmstra, 1969; Tzedakis et al., 2003b; Tzedakis et al., 2006; Pross et al., 2015), Lake Ohrid (Macedonia/Albania) (Wagner et al., 2014; Francke et al., 2016; Wagner et al., 2017), Lake Van (Turkey) (Litt et al., 2014) and Yammoûneh (Lebanon) (Develle et al., 2011). These studies, together with other high-resolution multiproxy studies in long marine sedimentary cores from the nearby Alboran Sea (Combourieu Nebout et al., 2002; Martrat et al., 2004; Fletcher and Sánchez Goñi, 2008), reveal the high sensitivity of this region for recording orbital and millennial-scale climate variability. These multiproxy studies offer a plethora of paleoclimate and paleoenvironmental data to assess ocean-atmosphere linkages and examine local, regional and global climate patterns. However, in the Iberian Peninsula a limited number of long (>100 kyr) and continuous terrestrial sedimentary records have been described, including Villarquemado (González-Sampéris et al., 2013; García-Prieto, 2015), Carihuela Cave (Fernández et al., 2007), Fuentillejo maar lake (Ortiz et al., 2013) and Padul (Florschütz et al., 1971; Nestares and Torres, 1998).

The Padul wetland in southern Iberian Peninsula (Fig. 2.1) is an indispensable site for understanding past glacial/interglacial climate variability in the Mediterranean region due to its sensitive location between temperate and humid climate to the north and the subtropical and arid climate to the south. The Padul wetland has one of the longest and most continuous sediment records of southern Europe, with more than 100 m of peat and lacustrine sediments deposited over the last ~1 Ma (Ortiz et al., 2004a, 2010). Previous palynological studies from the Padul wetland (Menéndez-Amor and Florschütz, 1962, 1964; Florschütz et al., 1971; Pons and Reille, 1988) revealed a climatically induced regional vegetation changes during the late Quaternary, although noticeable discrepancies in the interpretation of the pollen data due to age control uncertainties demands further investigation. Florschütz et al. (1971), based on pollen data, suggested that sediment from the Eemian interglacial (MIS 5e, ~115 – 130 kyr BP) was reached at 24 m depth and that sequence extended back to the Holsteinian interglacial (MIS 11, ~350 – 400 kyr BP) at the base of their core at 70 m depth. On the contrary, Pons and Reille (1988), with very similar pollen data, interpreted the base of their core at 24 m depth as representing the first Prewürm interstadial (i.e., MIS 5c), not showing any other interglacial period apart from the Holocene for the upper 24 m. These different correlations of the vegetation changes to climatic events are mostly a consequence of the poor chronologic control of the different sediment cores. In particular, Florschütz et al. (1971) used the age control of a nearby sediment core from Menéndez-Amor and Florschütz (1964) that was based on only 14 radiocarbon dates (with a maximum age of 54 kyr BP), assuming the same sediment accumulation rates for both cores. Using age information based only on radiocarbon dating, they tried to reconstruct the vegetation of the last ~400 kyr. With respect to the study from Pons and Reille (1988), the vegetation results and interpretation of the last ~100 kyr is based only on 17 radiocarbon dates with a maximum age of  $29,300 \pm 600$  years BP. A more recent core retrieving a 100 m-long sedimentary sequence was taken in Padul in 1997 (Nestares and Torres, 1998), from which (Ortiz et al., 2004a, 2010) studied the organic geochemistry and lithology. In this core, the age control

for the upper part of the core was based only on 9 radiocarbon dates with a maximum age of  $17,300 \pm 500$  years BP. The older part of the core was dated using a combination of AAR, U/Th and paleomagnetic information. However, the AAR dating was based on the D/L ratios of several amino acids from different locations of southern Spain and not from the specific Padul wetland (Ortiz et al., 2004a, b). Moreover, the U/Th results used for the older ages have to be taken carefully due to the problematic behavior of the U-series in open peatland and lake systems as recently outlined by Sierralta et al. (2017). Finally, (Ortiz et al., 2004a, b) did not provide the paleomagnetic results from the Padul record, so the boundary between the Matuyama and Brunhes magnetozones is difficult to identify. In addition, their results were interpreted as local paleoenvironmental and paleohydrological changes at moderate to low temporal resolution, and the lack of additional multiproxy data limited their interpretation and linkages to global climate changes.

Therefore, improving the age control using higher resolution (61 radiocarbon dates) updated dating methodologies (AMS radiocarbon dating, including compound-specific radiocarbon dating, and AAR dating based on gastropods from Padul) and increasing the resolution of multiproxy analyses (i.e., lithology/facies, mineralogy, inorganic/organic geochemistry, magnetic susceptibility, palynological analysis) from the Padul sedimentary sequence were necessary to solve previous inconsistencies, facilitating the investigation of the response of the environment to rapid events and allowing more accurate correlations between millennial-scale paleoenvironmental changes with orbital- and suborbital-scale climate variability. In addition, a principal component analysis involving different multiproxy datasets (i.e., inorganic and organic geochemistry and magnetic susceptibility) under a well-constrained chronology was still imperative in order to obtain more accurate lake level estimations.

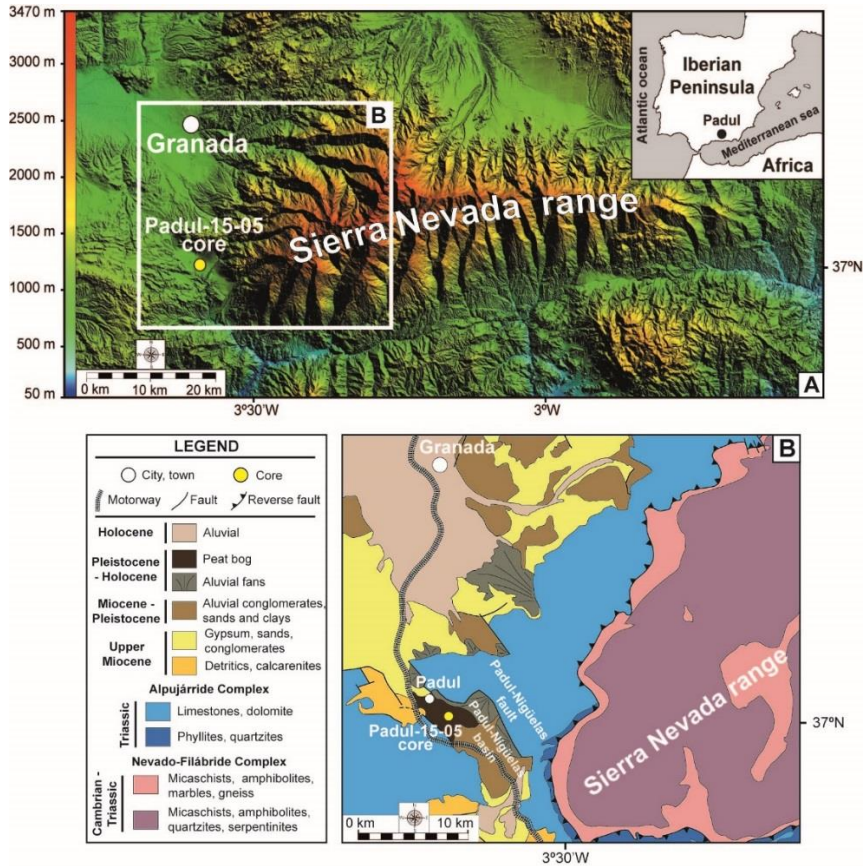


**Figure 2.1.** (A) Geographical location of the Padul wetland in western Sierra Nevada range (southern Iberian Peninsula, western Mediterranean region) and the Padul-15-05 core, and (B) simplified geological map of the area surrounding Padul.

In this study we present a high-resolution multiproxy record from a new ~43 m-long core, Padul-15-05, taken from the Padul wetland. This study complements a previously published high-resolution paleoenvironmental and paleoclimatic record of the uppermost 3.67 m Holocene section of the Padul-15-05 core (Ramos-Román et al. 2018a, b). This new core was studied with the goals of (1) generating a highly resolved and robust age control and (2) obtaining new paleoenvironmental information at higher sampling resolution, integrating up-to-date geological, biological and geochemical proxies that were lacking from previous studies. Here we also investigated (3) a detailed sedimentary facies analysis and its paleoenvironmental interpretation, which have been overlooked in previous studies. Finally, the new chronological and paleoenvironmental results presented here are (4) compared and discussed with respect to previous local and regional studies from Padul and the Mediterranean area and with insolation and ice volume records, sea surface temperatures from the western Mediterranean, and atmospheric temperatures from Greenland. This was done with the aim of understanding the environmental (i.e., lake levels, vegetation, sedimentation) response of this semiarid and climate sensitive region to orbital and suborbital climate variability.



## **2. Geographical and geological setting**

### *2.1. Sierra Nevada range*

The Padul wetland is located at the foothills of the Sierra Nevada range, which is an 85 km long and E-W aligned alpine mountain chain located in the Internal Zone of the Betic Cordillera (southern Spain) (Fig. 2.1A). Elevation in Sierra Nevada ranges between ca. 900 to 3479 m a.s.l., including three of the five highest peaks on the Iberian Peninsula. Sierra Nevada was one of the southernmost European areas to be glaciated during cold phases of the Late Pleistocene (Schulte, 2002). Late Pleistocene valley glaciers occurred at higher elevation in Sierra Nevada than in other mountain ranges of the Iberian Peninsula due to its southernmost location and the nearby Mediterranean Sea influence (Gómez Ortiz et al., 2005). Valley glaciers extended down to ca. 2300-2400 m on north-facing slopes and to ca. 2400-2500 m on south-facing slopes during the Late Pleistocene (Palacios et al., 2016). Erosion by Pleistocene valley and cirque glaciers allowed the formation of numerous small lakes and wetlands in high-elevation alpine environments after deglaciation (Castillo Martín, 2009).

The Sierra Nevada range is formed by 3 main tectonic complexes according to different metamorphic facies: 1) Alpujárride, 2) Nevado-Filábride, and 3) Maláguide. Sierra Nevada is mainly formed by the Alpujárride Complex (mostly limestones and dolomites) and the Nevado-Filábride Complex (mostly mica schists), while the Maláguide Complex (mostly limestones and quartzites) is restricted to a small area in the north of Sierra Nevada and NE of the city of Granada (González Donoso et al., 1978) (Fig. 2.1B).

### *2.2. Padul basin and wetland: geography, geology and climate*

The Padul wetland is located 20 km south of Granada city (Andalusia, Spain) (Fig. 2.1B), in the western foothills of the Sierra Nevada and in the Internal Zone of Betic Cordillera. It occurs at 726 m a.s.l., in the NW-SE elongated Padul-Nigüelas extensional endorheic basin (12 km long, 4 km wide and total area of 45 km<sup>2</sup>). This endorheic basin formed during the Alpine orogeny as a result of the extensional activity of the main Padul-Nigüelas normal fault, which is delimiting the NE edge of the basin with more than 250 m of vertical throw (Santanach et al., 1980), while the fault delineating the SW edge of the basin is antithetic to the Padul-Nigüelas fault and with less throw (Delgado et al., 2002). The different displacement of these two faults generated an asymmetric basin, causing deeper sedimentation and the formation of the Padul wetland at the NE edge of the basin (Domingo García et al., 1983). Previous cores taken from the Padul wetland (Menéndez-Amor and Florschütz, 1964; Florschütz et al., 1971; Pons and Reille, 1988; Ortiz et al., 2004a) show different sediment thickness and sedimentation rates according to their proximity to the depocenter of the basin located nearby the main Padul-Nigüelas fault. Therefore, correlations with previous cores should not be done based on depth but with respect to lithology/facies and other proxy data (e.g., pollen). The Padul wetland likely exhibits a maximum sedimentary sequence depth greater than 100 m (Ortiz et al., 2004a). The

presence of smaller faults in the basin that generated differential block subsidence could also result in different sedimentation thickness (Domingo García et al., 1983).

The catchment of the Padul wetland comprises principally Triassic limestones and dolostones from the Alpujárride Complex and silicate-rich schists from the Nevado-Filábride Complex, whereas basin fill sediments are comprised of Upper Miocene conglomerates and calcarenites and Pliocene and Quaternary alluvial sediments and lacustrine deposits (González Donoso et al., 1978; Domingo García et al., 1983; Delgado et al., 2002). Therefore, the potential sedimentary input in the Padul-Nigüelas basin and in the Padul depression and wetland are Paleozoic-Triassic metamorphic and Triassic carbonate rocks eroded and carried by fluvial activity from the western side of Sierra Nevada and fluvial, alluvial, lacustrine and marine deposits from the Miocene and Pliocene basin fill (González Donoso et al., 1978) (Fig. 2.1B).

This area is characterized by a semiarid Mediterranean climate (summer drought) with strong continental influence, with mean annual rainfall of 445 mm and mean annual temperature of 14.4°C (agroclimap.aemet.es). The warmest month in Padul is July, with an average air temperature of 24.2°C, whilst January is the coldest month, with temperatures averaging 6.4°C. Most of the precipitation in this area occurs in December, averaging 68 mm (agroclimap.aemet.es). Due to its geographical situation, precipitation variability in this region is mostly controlled by the North Atlantic Oscillation, characterized by atmospheric pressure fluctuations between the Icelandic Low (cyclone) and Azores High (anticyclone) (Rodó et al., 1997; Lionello and Sanna, 2005). Groundwater flow from the aquifer of the dolomitic Trevenque Unit (one of the three units of the Alpujárride Complex described above) is the primary water source in the Padul wetland (Castillo Martín and Fernández-Rubio, 1984). Hydrogeological studies show that total water input is around 25 hm<sup>3</sup>/yr, with 24 hm<sup>3</sup>/yr corresponding to groundwater from the carbonate aquifer (Beas, 1990). Consequently, changes in the level of the water table in the Padul are directly controlled by water infiltration from the surrounding mountains into the aquifer, which occurs mainly during the snow melting season (Ortiz et al., 2004a). The Padul wetland was drained for the first time in 1779 for agricultural purposes and more recently in 1943 for peat mining (Carrasco Duarte, 1998). The closure of one of the mines and the special environmental protection from the government since early 2000s allowed the regeneration and natural expansion of the wetland.

Local vegetation at Padul is mainly composed by wetland communities (*Phragmites australis*, *Chara vulgaris*...) while the regional vegetation is mainly composed of taxa belonging to mesomediterranean vegetation belt (*Quercus rotundifolia*, *Q. faginea*, *Q. coccifera*, *Pistacia terebinthus*, *Celtis australis*...). For further information about vegetation in Sierra Nevada range see El Aallali et al. (1998), Valle (2003) and Jiménez-Moreno et al. (2013) whereas for vegetation around Padul wetland see Pérez Raya and López Nieto (1991) and Ramos-Román et al. (2018a).

### **3. Materials and methods**

#### *3.1. Padul-15-05 core: drilling and sampling*

The Padul-15-05 core was drilled at the present-day lakeshore during July, 2015, 50 m from the current edge of the Padul wetland (37°00′39″N, 3°36′14″W). The continuous 42.64 meters-long core was retrieved using a Rolatec RL-48-L hydraulic percussion coring machine from the Centre for Scientific Instrumentation of the University of Granada. Drilling ended at 42.64 m depth where the drill was unable to penetrate the hard lithology (conglomerates). The core was stored in a cooler at the Paleontology and Stratigraphy Department, University of Granada, where it was split into two halves and examined for lithology, and scanned for color analysis, continuous X-ray fluorescence (XRF) and magnetic susceptibility (MS). The core was sampled for different analyses, including accelerator mass spectrometry (AMS) radiocarbon dating, amino acid racemization (AAR) in molluscs, X-ray diffraction (XRD), organic geochemistry (Total Organic Carbon and C/N) and pollen analyses.

#### *3.2. Dating and age-depth model*

The age model for the Padul-15-05 core was developed using AMS-standard radiocarbon dating, specific compound radiocarbon dating on fatty acids, and by measuring the extent of AAR in mollusc shells (Fig. 2.2). The age for the lower part of the core, beyond where <sup>14</sup>C and AAR samples were taken, was constrained by extrapolating sedimentary rates from the <sup>14</sup>C-dated top part of the core as explained below (Fig. 2.2).

A total of 61 samples from different depths were analyzed for AMS radiocarbon dating, including plant remains (30 samples), organic bulk sediment (20 samples), pollen residues (5 samples), gastropod shells (3 samples) and specific compounds (3 samples) (Table 2.1 and 2.2). Bulk sediment samples and pollen residues were used for dating due to absence of plant remains at some depths. All samples were dried and weighed before submission. Pollen residue samples were previously treated with hydrochloric acid (HCl) and hydrofluoric acid (HF) with the purpose of separating the organic material from detritals in the sediments.

Compound-specific radiocarbon analysis was conducted using the protocols of Yamane et al. (2014). Briefly, the sediment was extracted using dichloromethane/methanol (CH<sub>2</sub>Cl<sub>2</sub>/MeOH, 7:3, v/v), and the total extract was saponified with KOH/MeOH. After removal of neutral components, the saponified solution was acidified with HCl and extracted with CH<sub>2</sub>Cl<sub>2</sub>. This fraction was then esterified with HCl/MeOH. Separation of the fatty acid methyl esters (FAMES) was conducted by silica gel column chromatography with *n*-hexane/CH<sub>2</sub>Cl<sub>2</sub> (2:1, v/v). Isolation of individual (C<sub>16</sub>–C<sub>30</sub>) FAMES was conducted using reversed-phase high-performance liquid chromatography (HPLC), with (Develosil C30-UG-5, 4.6 × 250 mm, 5.5 mm particle size). The mobile phase was MeCN/MeOH (1:2, v/v) with 0.5% pyridine. The column temperature was increased in steps of 15°C from 0 to 35 min, ramped up at 2°C/min from 35 to 52.5 min and finally held at 50°C. The HPLC system consists of a binary pump, on-line degasser, autosampler, temperature controller (Polaratherm Series 9000), evaporative light scattering

detector (ELSD; Polymer Laboratories PL-ELS 2100), and fraction collector. The flow rate of the mobile phase was 1 mL/min. The isolated fraction was then subjected to silica gel column to remove impurities. After the isolated FAMES were collected and converted to graphite, radiocarbon measurement was conducted at the accelerator mass spectrometry facility at the University of Tokyo (Yokoyama et al., 2010). All radiocarbon values were corrected for the contribution of methyl carbon obtained from MeOH ( $\delta^{14}\text{C} = -991\text{‰}$ ) during the esterification by isotope mass balance.

For amino acid racemization (AAR) (Figs. 2.2 and 2.3; Table 2.3), molluscs were cleaned by brief sonication, then soaked in 3%  $\text{H}_2\text{O}_2$  for 2 hours, rinsed with purified  $\text{H}_2\text{O}$ , then air dried under laminar flow. Single individual shells were placed in separate sterilized, conical bottomed micro-reaction vials and dissolved in 7  $\mu\text{L}$  of 6 M HCl. Vials were sealed under  $\text{N}_2$  and heated at  $110^\circ\text{C}$  for 22 hours to recover the total hydrolysable amino acid population. Hydrolysate solutions were evaporated to dryness *in vacuo*, then rehydrated in 4  $\mu\text{L}$  of 0.01 M HCl with 1.5 mM sodium azide. The chromatographic instrumentation and procedure used to separate amino acid enantiomers is presented by Kaufman and Manley (1998). Briefly, derivatization using *o*-phthalaldehyde together with the chiral thiol, N-isobutyryl-L-cysteine yielded fluorescent diastereomeric derivatives of chiral primary amino acids. The derivatization was performed on-line prior to each injection using the auto-injector of an integrated Agilent HP1100 liquid chromatograph. Separation was by a reverse-phase column packed with a  $\text{C}_{18}$  stationary phase using a linear gradient of aqueous sodium acetate, methanol and acetonitrile. Detection was by fluorescence.

The age model for the upper part of the core, from surface to 23.27 m depth, was created with the R-code package “Clam 2.2” (Blaauw, 2010), using the IntCal13.14C calibration curve (Reimer et al., 2013) and locally weighted spline age-depth model at 95% confidence range. For the lower part of the core, from 23.27 m to 42.64 m depth, the age model was created using linear extrapolation with two different sediment accumulation rates (SAR) calculated on the average peat and carbonate/marl lithology from the top part of the core.

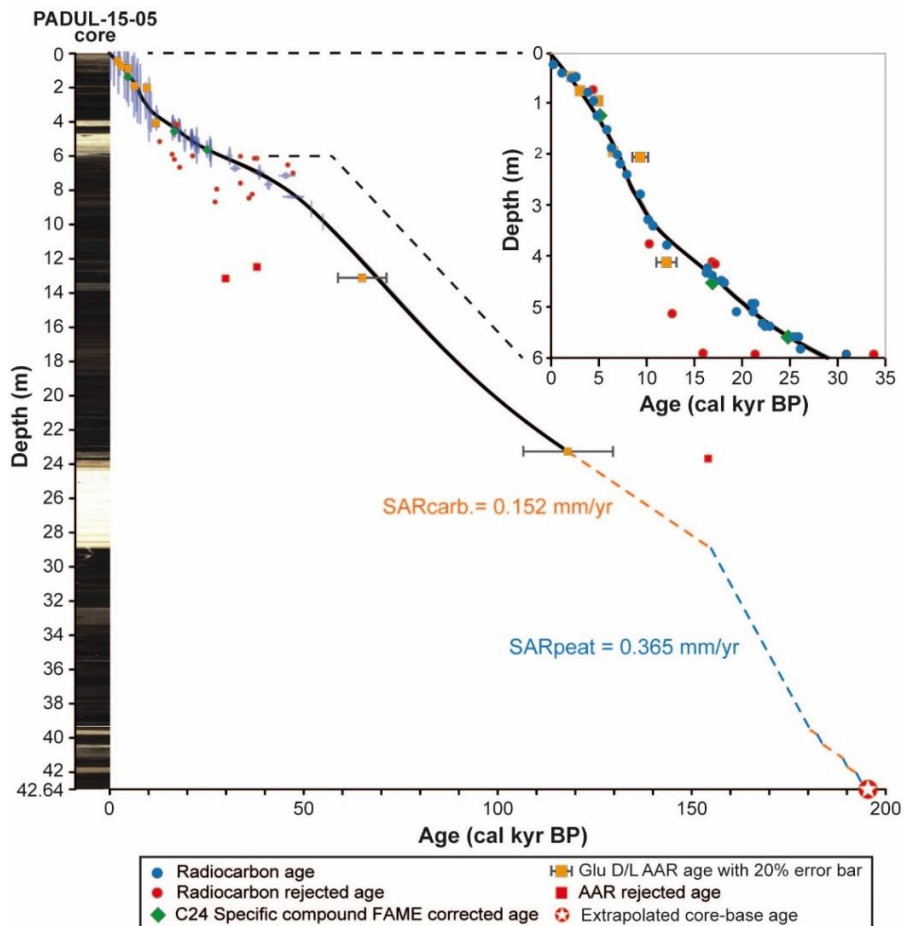


**Figure 2.2.** Scanner photograph of the Padul-15-05 core along with the age-depth model. Sedimentary accumulation rates for peat and carbonate/marl lithologies (SARpeat and SARcarb, respectively) are marked. The right panel shows the detailed age-depth model of the top 6 m of the core.

	Material	Depth (cm)	$\delta^{13}\text{C}$ (‰)	Age ( $^{14}\text{C}$ yr BP $\pm 1\sigma$ )	Calibrated age (cal yr BP) 95% confidence interval	Median age (cal yr BP)
Reference age		0		2015 CE	-65	-65
D-AMS 008531	Plant remains	21.67	-11.3	103 $\pm$ 24	23 - 264	127
Poz-77568	Org. bulk sed.	38.46	-31	1205 $\pm$ 30	1014 - 1239	1130
BETA-437233	Plant remains	46.04	-24.3	2480 $\pm$ 30	2385 - 2722	2577
Poz-77569	Org. bulk sed.	48.21	-29.2	2255 $\pm$ 30	2158 - 2344	2251
BETA-415830	Gastropods	71.36	-10.1	3910 $\pm$ 30	4248 - 4421	4343
BETA- 437234	Plant remains	76.34	-28	3550 $\pm$ 30	3722 - 3956	3838
BETA-415831	Org. bulk sed.	92.94	-26.7	3960 $\pm$ 30	4297 - 4519	4431
Poz-74344	Plant remains	122.96	-26.4	4295 $\pm$ 35	4827 - 4959	4871
BETA-415832	Plant remains	150.04	-26.8	5050 $\pm$ 30	5728 - 5900	5814
Poz-77571	Plant remains	186.08	-29.2	5530 $\pm$ 40	6281 - 6402	6341
Poz-74345	Plant remains	199.33	-29.7	6080 $\pm$ 40	6797 - 7154	6935
BETA-415833	Org. bulk sed.	217.36	-26.8	6270 $\pm$ 30	7162 - 7262	7212
Poz-77572	Org. bulk sed.	238.68	-29.6	7080 $\pm$ 50	7797 - 7999	7910
Poz-74347	Plant remains	277.24	-29.6	8290 $\pm$ 40	9138 - 9426	9293
BETA-415834	Plant remains	327.29	-26.4	8960 $\pm$ 30	9932 - 10221	10107
Poz-77573	Plant remains	340.04	-29.8	9420 $\pm$ 50	10514 - 10766	10640
Poz-74348	Plant remains	375.62	-26.7	9120 $\pm$ 50	10199 - 10412	10305
Poz-79815	Org. bulk sed.	377.83	-28.6	10310 $\pm$ 50	11847 - 12388	12144
Poz-79817	Gastropods	411.02	-7.2	13910 $\pm$ 60	16588 - 17088	16838
Poz-79818	Gastropods	414.89	-6.8	14130 $\pm$ 50	17001 - 17419	17210
Poz-77574	Org. bulk sed.	423.65	-27.2	13580 $\pm$ 80	16113 - 16654	16384
Poz-79819	Org. bulk sed.	432.82	-31.3	13500 $\pm$ 60	16047 - 16494	16270
Poz-19821	Org. bulk sed.	437.92	-29.7	13910 $\pm$ 70	16570 - 17113	16841
Poz-79822	Org. bulk sed.	448.12	-29.7	14640 $\pm$ 70	17618 - 18011	17814
Poz-77575	Org. bulk sed.	452.2	-28.6	14890 $\pm$ 80	17898 - 18325	18111
Poz-79837	Org. bulk sed.	493.43	-28.7	17580 $\pm$ 80	20966 - 21527	21246
Poz-79838	Pollen residue	493.43	-32	17450 $\pm$ 80	20813 - 21352	21082
Poz-79839	Org. bulk sed.	509.26	-28.2	17510 $\pm$ 80	20885 - 21429	21157
Poz-79843	Pollen residue	509.26	-29.8	16060 $\pm$ 70	19173 - 19587	19380
Poz-74349	Plant remains (vertical roots)	513.22	-26.9	10740 $\pm$ 60	12582 - 12737	12659
Poz-79841	Pollen residue	532.24	-31.9	18210 $\pm$ 90	21836 - 22329	22082
Poz-77576	Org. bulk sed.	537.84	-27.5	19010 $\pm$ 120	22538 - 23255	22896
Poz-79842	Pollen residue	537.84	-26.5	18570 $\pm$ 80	22280 - 22628	22454
Poz-77820	Org. bulk sed.	559.25	-30.5	21650 $\pm$ 130	25691 - 26132	25911
Poz-79844	Pollen residue	559.76	-27.6	20790 $\pm$ 90	24660 - 25378	25019
BETA-437235	Plant remains	582.92	-15.7	21900 $\pm$ 80	25916 - 26331	26123
Poz-77577	Plant remains (vertical roots)	590.72	-29.8	13240 $\pm$ 70	15695 - 16142	15918
BETA-437236	Plant remains	598.52	-26.8	17650 $\pm$ 60	21075 - 21592	21333
Poz-77578	Org. bulk sed.	599.56	-31.9	26750 $\pm$ 240	30594 - 31221	30907
Poz-79845	Org. bulk sed.	601.64	-27.6	29930 $\pm$ 210	33678 - 34419	34048
Poz-79846	Org. bulk sed.	613.08	-26	33700 $\pm$ 310	37056 - 38796	37926
Poz-77579	Org. bulk sed.	614.12	-31.4	33400 $\pm$ 500	36400 - 38768	37584
Poz-74350	Plant remains (vertical roots)	617.76	-30.1	13680 $\pm$ 70	16254 - 16794	16524
Poz-77581	Org. bulk sed.	652.04	-29.5	43000 $\pm$ 1500	44397 - 49512	46954
BETA-437237	Plant remains	667.33	-25.5	14720 $\pm$ 50	17731 - 18075	17903
Poz-74351	Plant remains	672.94	-29.4	28550 $\pm$ 270	31700 - 33352	32526
BETA-437238	Plant remains	694.5	-27.4	34150 $\pm$ 200	38263 - 39106	38684
Poz-74352	Plant remains	701	-29.2	45000 $\pm$ 2000	45915 - 50000	47957
BETA-437239	Plant remains	714.5	-24.4	42030 $\pm$ 570	44453 - 46418	45435
BETA-415837	Plant remains	760.24	-27.1	29840 $\pm$ 160	33666 - 34240	33953
BETA-437240	Plant remains	765.96	-26.6	36300 $\pm$ 210	40434 - 41434	40934
Poz-74409	Plant remains	798.2	-29	23510 $\pm$ 130	27450 - 27861	27655
BETA-437241	Plant remains	826.28	-27.2	33000 $\pm$ 170	36461 - 37802	37131
Poz-74411	Plant remains	838.12	-29.1	44000 $\pm$ 1000	45675 - 49488	47581
BETA-437242	Plant remains	850.86	-27.6	32310 $\pm$ 180	35766 - 36604	36185
BETA-437243	Plant remains	871.25	-25.5	22820 $\pm$ 100	26908 - 27448	27178
Poz-74412	Plant remains	909.48	-29.7	> 52000		52000
Poz-74413	Plant remains	984.95	-27.4	> 55000		55000

**Table 2.1.** AMS-standard radiocarbon ages from the Padul-15-05 sedimentary record ( $^{14}\text{C}$  ages for specific compounds have been included separately in Table 2.2). All radiocarbon ages were calibrated using R-code package “Clam 2.2” IntCal13.14C calibration curve at 95% confidence range. Rejected samples are marked in red.



Orbital-scale environmental and climatic changes recorded in a new ~200,000-year-long multiproxy sedimentary record from Padul, southern Iberian Peninsula

Laboratory number (YAUT)	Depth (cm)	Specific compound	Sample amount (µgC)	Sample amount (µgC) (estimated by gas press.)	δ <sup>13</sup> C	Δ <sup>14</sup> C	pMC	<sup>14</sup> C age (yr BP)	FAME corrected Δ <sup>14</sup> C	FAME corrected pMC	FAME corrected <sup>14</sup> C age (yr BP)	Age ranges (cal yr BP)	Median age (cal yr BP)
28335		C16 + C18	48	62.4	-37.7 ± 1.22	-458.28 ± 4.39	54.61 ± 0.44	4859 ± 65	-427.23 ± 4.64	57.74 ± 0.47	4411 ± 65	4854 - 5285	5017
28308		C20	201	196.1	-30.84 ± 3.90	-465.25 ± 3.92	53.91 ± 0.40	4963 ± 59	-440.78 ± 4.10	56.38 ± 0.41	4604 ± 59	5052 - 5570	5322
28334	122.96	C24	59	62.6	-25.92 ± 8.90	-448.33 ± 6.47	55.62 ± 0.65	4713 ± 94	-425.40 ± 6.74	57.93 ± 0.68	4386 ± 94	4826 - 5304	5008
28309		C26	185	151.2	-22.31 ± 3.48	-455.10 ± 4.15	54.93 ± 0.42	4812 ± 61	-435.74 ± 4.29	56.89 ± 0.43	4532 ± 61	4973 - 5443	5168
35722		C18	19	21.2	-32.38 ± 1.45	-739.79 ± 4.73	26.24 ± 0.48	10750 ± 145	-725.39 ± 4.99	27.69 ± 0.50	10315 ± 145	11410 - 12577	12112
35606		C20	166	152.8	-26.02 ± 2.54	-822.87 ± 1.39	17.86 ± 0.14	13840 ± 65	-814.06 ± 1.46	18.75 ± 0.15	13450 ± 65	15951 - 16419	16184
35615		C22	140	100.1	-40.82 ± 6.66	-820.35 ± 2.08	18.11 ± 0.21	13725 ± 95	-812.23 ± 2.17	18.93 ± 0.22	13370 ± 95	15780 - 16350	16085
35713	452.2	C23	37	34.5	-33.59 ± 1.08	-791.87 ± 2.79	20.98 ± 0.28	12540 ± 110	-782.87 ± 2.91	21.89 ± 0.29	12200 ± 110	13765 - 14620	14110
35614		C24	140	104.6	-38.37 ± 4.37	-832.09 ± 1.69	16.93 ± 0.17	14265 ± 80	-825.13 ± 1.76	17.63 ± 0.18	13940 ± 80	16579 - 17186	16995
35607		C26	167	144.0	-38.86 ± 2.92	-825.62 ± 1.42	17.58 ± 0.14	13965 ± 65	-818.95 ± 1.48	18.25 ± 0.15	13660 ± 65	16234 - 16756	16470
35719		C18	22	26.1	-23.15 ± 2.62	-876.08 ± 2.75	12.49 ± 0.28	16710 ± 180	-869.25 ± 2.90	13.18 ± 0.29	16275 ± 180	19171 - 20009	19647
35706		C20	44	61.4	-26.59 ± 0.55	-881.97 ± 1.54	11.90 ± 0.16	17100 ± 105	-876.12 ± 1.62	12.49 ± 0.16	16710 ± 105	19883 - 20467	20165
35707		C22	50	53.5	-34.91 ± 1.37	-896.37 ± 1.63	10.45 ± 0.16	18145 ± 125	-891.70 ± 1.70	10.92 ± 0.17	17790 ± 125	21140 - 21884	21541
35617	559.25	C24	103	107.9	-34.02 ± 3.90	-926.83 ± 1.00	7.38 ± 0.10	20940 ± 110	-923.82 ± 1.05	7.68 ± 0.11	20615 ± 110	24458 - 25206	24826
35618		C26	143	97.6	-42.51 ± 5.82	-907.00 ± 1.29	9.38 ± 0.13	19015 ± 110	-903.46 ± 1.34	9.73 ± 0.13	18715 ± 110	22370 - 22875	22581
35610		C28	130	117.9	-34.66 ± 3.88	-899.70 ± 1.09	10.11 ± 0.11	18405 ± 85	-896.16 ± 1.13	10.47 ± 0.11	18130 ± 85	21724 - 22269	21979

**Table 2.2.** Age data from specific compound radiocarbon dating from Padul-15-05. Ages were calibrated using IntCal13.14C calibration curve at 95% confidence range. The selected C<sub>24</sub> specific compound ages used for the age-depth model are marked in green.

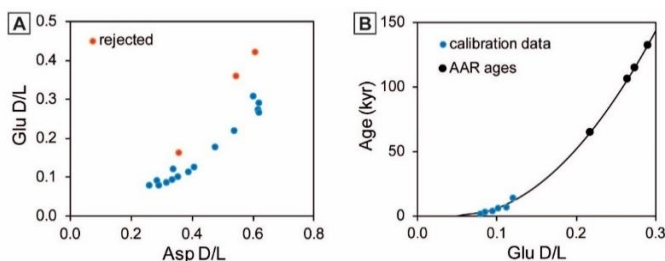


**Figure 2.3.** Amino acid racemization results from the Padul-15-05 record. (A) Sample mean D/L values for aspartic acid (Asp) and glutamic acid (Glu); rejected samples fall of the trend defined by others. (B) Simple parabolic kinetic model fit through independently dated samples (blue circles) used to estimate the ages of four gastropod samples (black circles). Data are listed in Table 2.3.

UAL	depth (m)	n <sup>a</sup>	rej <sup>b</sup>	material	mean Asp D/L	stdev	mean Glu D/L	stdev	<sup>14</sup> C age (kyr) <sup>c</sup>	Glu D/L age (kyr)
14978	0.46	4	1	gastropod	0.292	0.024	0.079	0.011	2.0	2.1
15605	0.48	5	0	bivalve	0.261	0.009	0.079	0.003		
14979	0.75	3	2	gastropod	0.317	0.023	0.085	0.003	3.7	3.0
14980	0.92	4	0	gastropod	0.335	0.043	0.095	0.011	4.3	4.8
15606	0.92	3	1	bivalve - dirty	0.285	0.072	0.090	0.012		
14981	1.93	5	0	gastropod	0.354	0.032	0.102	0.008	6.6	6.4
14982	2.04	3	2	gastropod	0.388	0.037	0.113	0.008	6.9	9.3
15608	4.11	3	1	gastropod	0.339	0.054	0.121	0.009	14.3	11.8
15607	4.11	5	0	bivalve	0.406	0.013	0.127	0.010		
15444 <sup>d</sup>	12.45	2	1	gastropod	0.477	0.055	0.178	0.031		38
15445	13.13	3	2	gastropod	0.538	0.032	0.218	0.017		65
15609 <sup>e</sup>	13.13	5	0	bivalve - dirty	0.358	0.049	0.162	0.040		30
15446	22.98	4	1	gastropod	0.619	0.034	0.290	0.051		133
15447	23.37	4	1	gastropod	0.616	0.021	0.274	0.013		116
15448	23.42	4	1	gastropod	0.622	0.032	0.265	0.027		107
15611 <sup>f</sup>	23.57	5	0	bivalve	0.543	0.050	0.359	0.043		222
15449 <sup>g</sup>	23.57	2	1	gastropod	0.602	0.033	0.309	0.085		154
15610 <sup>h</sup>	28.77	5	0	bivalve	0.608	0.009	0.421	0.020		320

<sup>a</sup> n = number of separate analyses used to calculate mean D/L, one individual per analysis  
<sup>b</sup> rej = number of analyses rejected due to obvious signs of contamination by young amino acids  
<sup>c</sup> independent age used to calibrate the rate of racemization  
<sup>d</sup> sample rejected because too few individual analyses (n = 2)  
<sup>e</sup> sample rejected because covariance between Asp D/L and Glu D/L falls off trend

**Table 2.3.** Summary of amino acid racemization results from Padul-15-05. Rejected samples are marked in red.

### *3.3. Lithology and color*

Lithology for the Padul-15-05 core was described in the laboratory of Paleontology and Stratigraphy at the University of Granada. The core was scanned for high-resolution photography and color data using the Avaatech core scanner from the CORELAB laboratory at the University of Barcelona (Spain). Numerical color results, such as lightness, RGB and CIELAB color space ( $b^*$ ) were obtained (Fig. 2.4). Color data resolution was 0.073 mm so a resampling with a linear regular interpolation using the PAST 3.19 software (Hammer et al., 2001) was applied in order to obtain lower resolution results (0.5 mm resolution) comparable to other proxies.

### *3.4. Magnetic susceptibility*

Magnetic susceptibility was measured to infer detrital input to the lake in relation with environmental and climate conditions. It was measured with a Bartington MS3 magnetic susceptibility meter operating with a MS2E sensor under stable temperature conditions in the Department of Stratigraphy and Paleontology, University of Granada (Spain). The maximum resolution of the MS3 meter was  $2 \times 10^{-6}$  SI and the operating frequency of the MS2E sensor was 2 kHz. Magnetic susceptibility was measured every 0.5 cm with a measuring time period of 10 sec. Data are represented in Figure 2.4.

### *3.5. Mineralogy*

Thirty-six bulk sediment samples from different lithologies throughout the core were selected for X-ray diffraction (XRD) analyses in order to identify the mineralogical compositions of the different sedimentary facies and to provide accurate information about the relation between sedimentation, lake level and climate conditions. X-ray diffractograms were obtained using a PANalytical X'Pert PRO diffractometer with Cu-K $\alpha$  radiation and automatic slit. Scans were run from 4° to 70° 2 $\theta$  and semi-quantitative estimations of mineral abundance were obtained by using Xpoflower software (Martin, 2004). The mineral components in the different facies are shown in Figures 2.5 and 2.6 and Table 2.5.

### *3.6. Inorganic geochemistry*

Inorganic geochemical composition of the sediments was obtained using a continuous XRF Avaatech core scanner from the CORELAB at the University of Barcelona (Spain). Measurements were taken at a resolution of 1 cm and under two different working conditions: (a) 10 sec count time, 650uA of X-ray current and 10kV of X-ray voltage for the measurement of Al, Si, P, S, Cl, Ar, K, Ca, Ti, V, Cr, Mn, Fe, Rh and Ag; and (b) 35 sec count time, 1700uA of X-ray current and 30kV of X-ray voltage for the measurement of Ni, Cu, Zn, Ga, Ge, As, Se, Br, Rb, Sr, Y, Zr, Nb, Au, Hg, Pb, Bi, Th and U. All results were expressed in counts per second (cps) and only values over 1000 counts were considered significant results. The most characteristic selected elements used as proxies for paleoenvironmental reconstruction (Al, Si,



S, K, Ca, Fe, Br, Sr and Zr) have been represented in counts per second (cps) and as normalized data. Normalization was done dividing each element by the total counts including Si, K, Ca, Ti, Fe, Br, Sr and Zr. A Rb/Sr ratio was also calculated (Fig. 2.4). For the paleoclimate reconstruction of the entire Padul-15-05 record, non-normalized element data have been used due to their better correlation with other proxies (e.g., pollen) and providing better results in the statistical analyses (i.e., principal component analysis and spectral analysis, explained below).

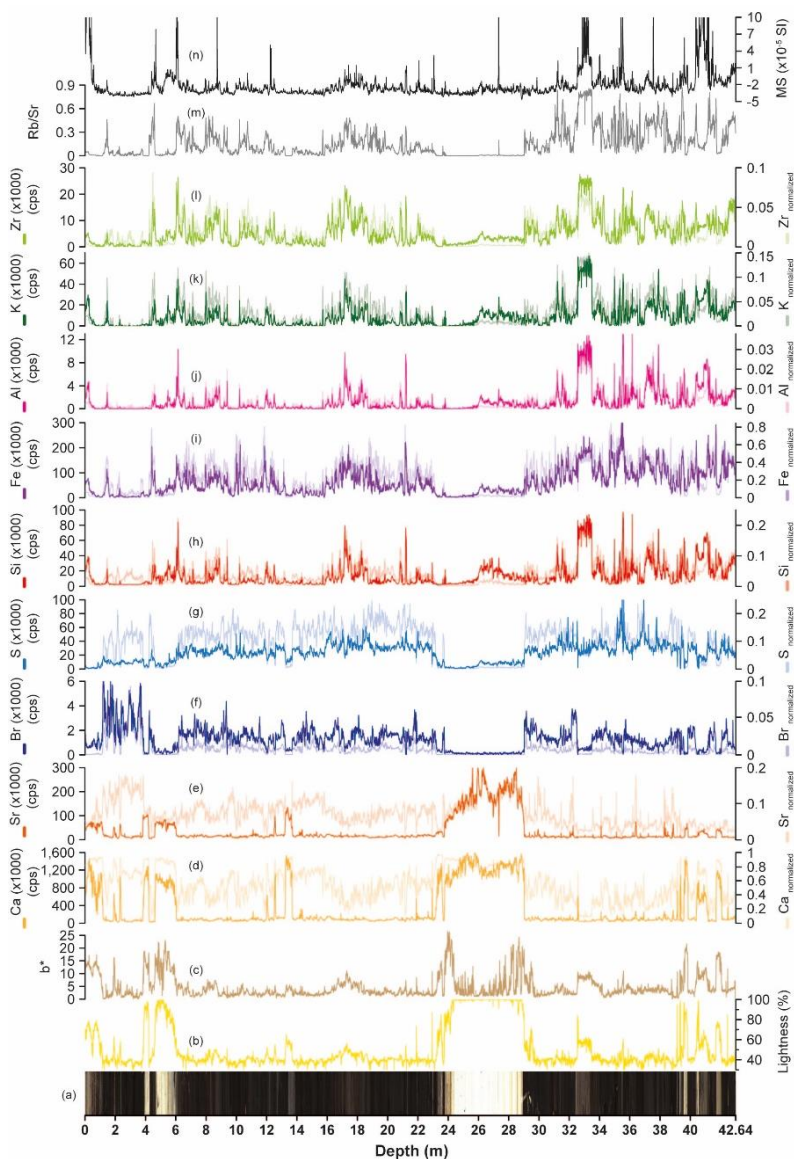


**Figure 2.4.** Padul-15-05 core photo and physical and chemical data. From bottom to top: (a) scanner photograph of Padul-15-05 core, (b) lightness, (c)  $b^*$  values, (d) Ca, (e) Sr, (f) Br, (g) S, (h) Si, (i) Fe, (j) Al, (k) K, (l) Zr, (m) Rb/Sr ratio, and (n) magnetic susceptibility (MS). XRF data have been represented in cps (dark line) and normalized (light line).



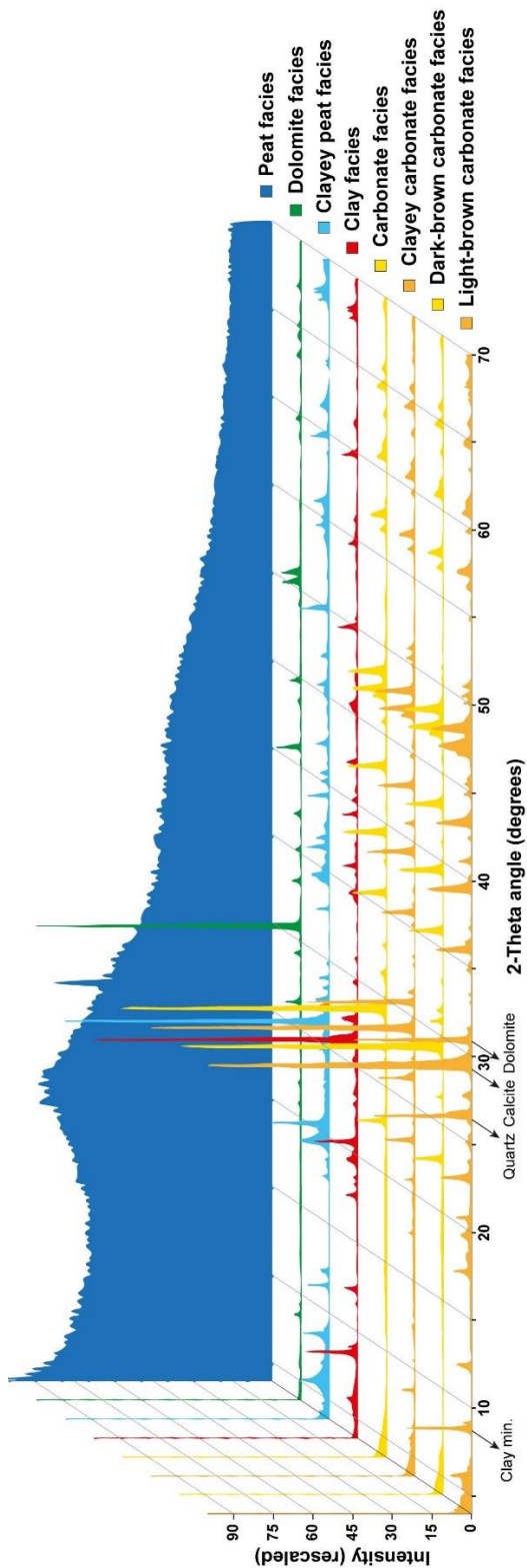









**Figure 2.6.** Representation of the most characteristic diffractograms for every facies. The most representative peaks of clay minerals, quartz, calcite and dolomite have been marked.

	Ca	Sr	Si	Al	MS	Fe	S	Br	TOC	C/N
Ca		0	1.90E-01	8.17E-11	3.14E-04	3.76E-174	0	0	0	3.95E-323
Sr	0.8592		4.17E-02	7.55E-13	2.02E-05	1.17E-126	0	1.68E-278	0	1.12E-265
Si	-0.0201	-0.0312		0	6.91E-323	0	6.66E-16	2.84E-129	6.32E-115	2.82E-36
Al	-0.0993	-0.1095	0.9774		2.86E-299	0	5.12E-25	2.91E-90	5.30E-69	5.01E-14
MS	0.0551	-0.0652	0.5410	0.5238		7.25E-144	9.64E-01	2.96E-47	2.39E-71	4.09E-40
Fe	-0.4117	-0.3547	0.6461	0.6562	0.3767		0	1.04E-09	8.83E-01	1.74E-18
S	-0.6587	-0.5427	0.1232	0.1573	-0.0007	0.6356		1.14E-54	4.83E-242	1.61E-267
Br	-0.6083	-0.5079	-0.3582	-0.3014	-0.2185	-0.0933	0.2352		0	8.49E-48
TOC	-0.7697	-0.6463	-0.3399	-0.2651	-0.2695	0.0023	0.4793	0.6448		0
C/N	-0.5429	-0.4993	-0.1916	-0.1154	-0.2018	0.1343	0.5008	0.2206	0.7192	

**Table 2.4.** Correlation coefficients between the most representative XRF data (Ca, Sr, Si, Al, Fe, S, Br), magnetic susceptibility (MS), TOC and C/N from Padul-15-05. Positive correlations are marked in green while negative correlations are in red.



RESULTS				INTERPRETATION		
Facies	Core-scan images	Sedimentological features	Mineralogy	Most representative inorganic/organic geochemistry and magnetic susceptibility*	Depositional subenvironment	Relative lake level (0 to 5)
Peat facies		Black massive peat with high amount of organic matter and vegetative roots	Low quartz	Ca = 20,000 - 100,000 cps S = 10,000 - 75,000 cps TOC = 30 - 60 % C/N = 35 - 60	Very shallow palustrine environment with high amount of littoral vegetation and organic matter	1
Clayey peat facies		Organic clayey peat. Vegetal remains are common	Quartz, illite	Ca = 20,000 - 100,000 cps S = 10,000 - 75,000 cps TOC = 20 - 40 % C/N = 25 - 40	Shallow palustrine environment with detritic input from Sierra Nevada due to low forest cover during cold climate periods	1 - 2
Clayey carbonate facies		Yellowish carbonate with clayey layers. Frequent gastropods and pelecypods	Calcite, dolomite, low quartz	Ca = > 800,000 cps S = 5,000 - 25,000 cps TOC = 0 - 3 % C/N = 20 - 30	Opened high lake level stages. Clay/detritic input is related to cold periods with low forest cover	4 - 5
Carbonate facies		Light yellowish charophyte carbonate. Full of gastropods and pelecypods	Calcite	Ca = > 800,000 cps S = 0 - 6,000 cps TOC = 0 - 3 % C/N = 15 - 25	Opened high lake level phases that allowed the proliferation of organisms	4 - 5
Light-brown carbonate facies and Dark-brown carbonate facies		Light-brown carbonate facies: Light brown carbonate. Higher Si and MS than in Dark-brown carbonate facies Dark-brown carbonate facies: Dark brown carbonate. Gastropods, pelecypods and charophytes more abundant	Calcite, dolomite, quartz, illite	Ca = > 200,000 cps S = 0 - 8,000 cps TOC = 0 - 10 % C/N = 0 - 25	Light-brown carbonate facies: Exposed lake stage with important detritic presence Dark-brown carbonate facies: Shallow opened lake with proliferation of organisms	0 2 - 3
Clay facies		Brown clay organic bands. Presence of vegetal remains. Mottling and mixed sediment textures	Quartz, illite	Ca = 30,000 - 100,000 cps S = 20,000 - 45,000 cps TOC = 0 - 10 % C/N = 15 - 30	Low water depth. Detritic input from Sierra Nevada is due to low forest cover linked to cold climate periods	1 - 2
Dolomite facies		Grayish white dolomitic layers	Dolomite, low quartz	Ca = > 700,000 cps S = 0 - 5,000 cps TOC = 0 - 1 % C/N = 20 - 25	Episodes of high runoff during tectonic pulses and/or biogenically induced dolomite precipitation	1 - 2

\* Values for every analysis are classified with colors as Very low, Low, Medium, High and Very high for a better comprehension. Maximum values of the more relevant data from the PADUL-15-05 core: Ca = 1,800,000 cps, Si = 95,000 cps, S = 130,000 cps, MS = 40 x 10<sup>5</sup> SI, TOC = 60%, C/N = 60%

**Table 2.5.** Schematic table showing a short description of the results and interpretations of different facies presented in the Padul-15-05 core. Relative values from different analyses have been colored for a better comprehension: very low (blue), low (green), medium (yellow), high (orange) and very high (red).

### 3.7. Organic geochemistry

A total of 474 samples (mean sampling interval of ~37 cm from 42.64 m to 7 m depth and at ~2 cm resolution from 7 m depth to core top) were analyzed by means of a CHNS Elemental Analyzer Thermo Scientific Flash 2000 from the Centre for Scientific Instrumentation of the University of Granada (Spain). Samples were decalcified with 1:1 HCl before measuring. Atomic C/N ratio were calculated from the obtained TOC and TN (total nitrogen). TOC percentage was calculated from the percentage of carbon (%C) yielded by the elemental analyzer and recalculated by the weight of the sample before and after decalcification (also obtaining the total % of carbonate). Then, the organic matter (OM) in the sediment was estimated multiplying TOC by 1.724 of Van Bemmelen factor (Nelson and Sommers, 1982). Clay content in the samples is the remnant and could be calculated as follows (% Clay = 100 - % OM - % Carbonate). Data are represented in Figure 2.9.

### 3.8. Palynological analysis

A total of 414 samples were analyzed for pollen analysis: 176 samples between 0 – 3.67 m (Ramos-Román et al., 2018b) and 238 samples between 3.67 – 42.64 m depth (Fig. 2.9). Pollen extraction followed a modified Faegri and Iversen (1989) methodology. *Lycopodium* spores were added to 1 cm<sup>3</sup>/sample of sediment for pollen concentration calculations. Hydrochloric acid (HCl), hydrofluoric acid (HF), sodium hydroxide (NaOH) and acetolysis were used to remove carbonates, silicates, humic acids, and cellulosic organic matter, respectively. The residue was sieved at 250 µm to remove very coarse vegetal and detrital remains prior to the NaOH and acetolysis treatments. Thereafter, the residue was sieved at 10 µm and subsequently mixed with glycerin for slide preparation and counting. A minimum of 300 terrestrial pollen grains per sample were identified using a Zeiss transmitted light microscope at 400 magnifications. A detailed pollen study and reconstruction of the vegetation is in Camuera et al. (2019) and here we only show the abundance of Arboreal Pollen (AP) (sum of *Quercus* total, *Olea*, *Phillyrea*, *Fraxinus*, *Pistacia*, *Acer*, *Castanea*, *Corylus*, *Juglans*, *Betula*, *Alnus*, *Ulmus*, *Abies*, *Populus*, *Salix*, *Celtis*, *Carpinus*, *Cedrus*, *Taxus*, *Buxus*, *Tamarix*, *Hippophaë* and *Rhamnus*), which was calculated with respect to the total terrestrial pollen sum without *Pinus*, which is sometimes overrepresented. Cyperaceae and *Typha* were not included in the total pollen sum, also because they are overrepresented in the local aquatic environment.

### 3.9. Principal Component Analysis (PCA)

PCA was run on the most representative inorganic geochemistry (Ca, Sr, Si, Al, Fe, S and Br), organic geochemistry (TOC and C/N) and magnetic susceptibility (MS) data using the PAST 3.19 software (Hammer et al., 2001) (Fig. 2.7). A previous resampling using linear interpolation was conducted to achieve equivalent resolution among different proxies. Moreover, all data were normalized using the formula  $X = (x - \text{mean}) / \text{standard deviation}$ . Resampled and normalized data were further analyzed to determine the percentage of variance,

scores, scatter plot and correlation loading plot. In addition to the PCA, a table with correlation coefficients was also computed as analytical approach (Table 2.4). Correlation coefficient was also calculated for Si (in counts per second) with respect to the Arboreal Pollen percentages, taking into account the specific depths that have been analyzed for the palynological analysis.

### *3.10. Spectral analysis*

Spectral analysis using the REDFIT procedure of Schulz and Mudelsee (2002) was performed on Si, MS and TOC in order to identify cyclical periodicities using the PAST 3.19 software. This analysis focused on frequencies below 0.00025 (4000 years) for a better identification of the highest amplitude orbital-scale cycles (Fig. 2.8).

**Figure 2.7.** The Principal Component Analysis (PCA) from Ca, Sr, Si, Al, Fe, S, Br, MS, TOC and C/N data from Padul-15-05 showing: (A) the scatter plot with PC1 and PC2 axis variations, and (B) PC1 and (C) PC2 variations on loading plots.

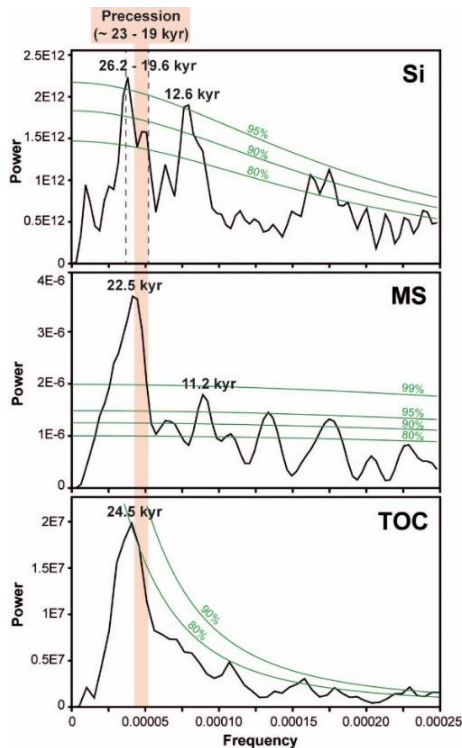
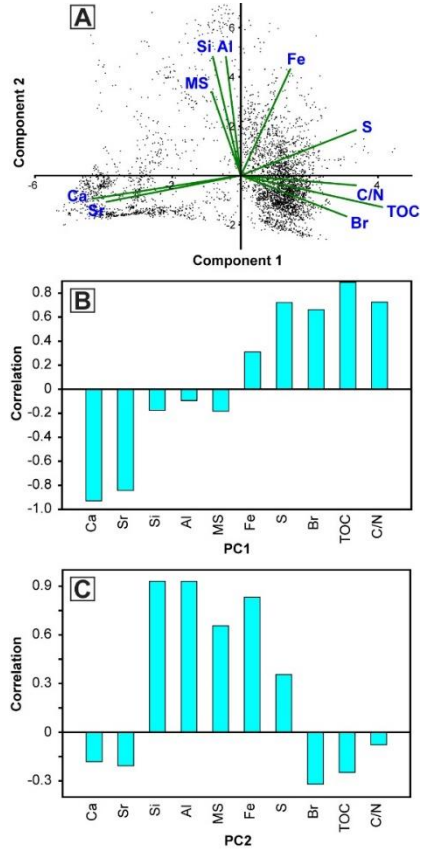


**Figure 2.8.** Spectral analysis results performed on Si, MS and TOC data from Padul-15-05. Main periodicities as well as confidence intervals (green line) are shown. Dashed lines mark the age range of a same period. The age range of the precession cycle (~23 – 19 kyr) has also been marked.



## **4. Results**

### *4.1. Chronology and sediment accumulation rates (SAR)*

#### *4.1.1. AMS-standard radiocarbon dating*

From the total of 61 radiocarbon dates (including 3 specific compound dates), 19 were excluded for the age model due to: reservoir effect (3 gastropod samples), vertical macrophyte roots from upper layers (3 plant remain samples), and seemingly too young dates (8 samples from plant remains) and too old dates (4 samples from bulk organic sediment and 1 sample from plant remains). The age-depth model for the last ~30,000 cal yrs BP (~6 m depth) of the Padul-15-05 core is quite robust and only 7 out of 42 AMS radiocarbon samples (including specific compound dates) were rejected (Tables 2.1 and 2.2). The  $\delta^{13}\text{C}$  values in the analyzed samples mainly ranged from -24 to -32‰ (Table 2.1), pointing into terrestrial plants that use the C3 photosynthetic pathway (Deines, 1980). As for the three radiocarbon dates on FAMEs (at 122.96 cm, 452.2 cm and 559.25 cm depth), the C<sub>24</sub> fatty acid was chosen for the age model because it derives from emerged plants (Ficken et al., 2000) in the studied context (i.e., Juncaceae, *Phragmites* or *Typha*). These plants display an in-situ growth, avoiding external inputs in the wetland system from longer chain fatty acids (terrestrial input) from the catchment basin (Table 2.2).

Several AMS radiocarbon dates older than ~30,000 cal yrs BP were not used in the age model, in particular: 1 root sample (at 617.7 cm depth) that yielded a younger age probably contaminated from younger sediments, 4 organic bulk sediment samples (from 601.6 cm to 652 cm depth) too old with respect to previous/older ages and that would imply an excessively high SAR for the corresponding peat lithology, and 7 plant remain samples (from 667.3 cm to 871.2 cm depth) of which 6 yielded anomalously young ages interpreted as contamination from younger sediments.

#### *4.1.2. AAR dating*

A total of 83 individual shells were analyzed separately for AAR dating from 14 levels in the core (Table 2.3), including gastropods (hydrobiid *Milesiana schuelei*) from 12 levels and pelecypods (*Pisidium* sp.) from 6 levels; both gastropods and pelecypods were analyzed from 4 levels. Five individual shells, each prepared separately, were analyzed from most levels. A total of 14 analyses (17%) were rejected because of obvious signs of contamination by young amino acids. The rejection rate was higher for gastropods than for pelecypods, which is common for AAR analyses.

Of the eight amino acids routinely separated by reverse phase HPLC, aspartic acid (Asp) and glutamic acid (Glu) are present in the highest concentrations (therefore better detected in the tiny specimens) and are resolved best by the chromatography (therefore highest precision). With few exceptions, D/L values increase down core (Table 2.3). The results for two of the gastropod samples (12.45 and 23.57 m depth) were rejected because they were based on only two

individuals, which is insufficient to confidently determine a mean D/L value for the sample. The D/L values for one of the pelecypod samples (13.13 m depth) were unexpectedly low. Although a full suite of five individuals was analyzed for this sample, the result was rejected because the shells were heavily encrusted in carbonate and difficult to clean. For this sample and two others (23.57 and 28.77 m depth), the covariance between D/L Asp and D/L Glu fell off of the expected trend as defined by the other samples and these were rejected (Fig. 2.3). Because the rate of racemization differs between pelecypods and gastropods, and because the AAR data from the three pelecypod samples beyond the range of  $^{14}\text{C}$  dating were rejected, we focused on the results from the gastropods.

The rate of racemization (calibrated age equation) was quantified using the mean D/L values for six independently dated samples ( $^{14}\text{C}$ -based age-depth model), ranging in age from 2.0 to 14.3 kyr (Table 2.3). The rate of racemization was calibrated using a simple parabolic kinetic model ( $\text{D/L} = \text{age}^{0.5}$ ) (Mitterer and Kriausakul, 1989). We focused on Glu because it has been shown to be well suited for older (middle Pleistocene) molluscs, whereas the apparent rate of racemization for Asp typically plateaus (Laabs and Kaufman, 2003).

Using least-squares regression to fit the sample-mean Glu D/L value to the square root of time yields the AAR age equation:  $t = (1507.5 \cdot \text{D/L} - 73.715)^2$ , where  $t$  is age in years and D/L is the mean Glu D/L value for gastropods (Fig. 2.3). The parabolic function fits the D/L versus age data well ( $r^2 = 0.89$ ,  $n = 6$ ). No attempt was made to formally quantify the age uncertainty. At a minimum, the uncertainty includes the intra-sample variability in Glu D/L values, which averages 11% for these samples. More important is the uncertainty derived from extrapolating ages beyond the calibration data (beyond 14 kyr), which is significant for this core (Fig. 2.3). The age model is highly sensitive to the choice of mathematical function used to infer the rate of racemization beyond the calibration. A rough estimate of the age uncertainty is at least  $\pm 20\%$ .

Given the above assumptions, the AAR data can be used to estimate the age of four undated samples (at 13.13 m, 22.98 m, 23.37 m and 23.42 m depth) (Fig. 2.3 and Table 2.3). The three AAR ages on gastropods from 23.42 to 22.98 m depth range from 107 to 133 kyr, but are in reversed stratigraphic order. We consider the three ages to be within errors of one another and take the mean age (118 kyr) to represent the mean sample depth (23.26 m).

#### 4.1.3. *Sediment accumulation rates (SAR)*

The age-depth model from 23.27 m to 42.64 m depth was made using linear extrapolation with calculated sedimentation rates from the radiocarbon-dated part of the Padul-15-05 core because of the lack of age control points below 23.27 m. The sedimentation rate of the peat lithology (SAR<sub>peat</sub>) was calculated according to the well dated Holocene interval (from 1.23 m to 3.65 m depth) while the carbonate/marl SAR (SAR<sub>carb</sub>) was calculated based on the well dated carbonate/marl intervals from the last glacial period and deglaciation (from 3.85 m to 5.82 m depth). Therefore, the obtained peat SAR was 0.365 mm/yr whereas carbonate/marl SAR was 0.152 mm/yr (Fig. 2.2). SAR<sub>carb</sub> was used from 23.27 m to 28.78 m depth in accordance with the carbonate-rich sediments that dominate this interval. Age control through three small carbonate/marl intervals at 39.26 – 39.53 m, 40.10 – 40.82 m and 41.39 – 41.72 m depth was

extrapolated using SARcarb as well. SARpeat was used from 28.78 m down to the bottom (42.64 m), in accordance with the peat-rich sediments that dominate this interval. Following this method, the base of the Padul-15-05 core would have an age of ~197 kyr BP (Fig. 2.2).

#### *4.2. Principal component analysis*

The Principal Component 1 (PC1) obtained from the PCA accounts for 40.1% of the total variance with positive correlation between S, Br, TOC and C/N, and negative correlation to Ca and Sr. The Component 2 (PC2) accounts for 32.3% of the total variance and is mainly controlled by Si, Al, Fe and MS. The rest of the Principal Components were not included because they represent low percentages of the total variance (<9%). Scatter and loading plots are represented in Figure 2.7 while PC1 and PC2 scores for the entire core are given in Figure 2.9.

#### *4.3. Lithology and sedimentary facies*

The lithology of the Padul-15-05 core begins with peat sediment at the bottom (42.64 m depth) until 28.78 m depth, with 3 thin marl layers at 41.71 – 41.38 m, 40.81 – 40.24 m and 39.52 – 39.33 m depth and a thin clay layer at 33.22 – 32.35 m depth. From 28.78 m to 25.44 m depth marls are predominant, transitioning to carbonate sediments until 23.57 m depth. From 23.57 m to 5.98 m depth lithology is mainly composed of peat, but a clay layer is present at 17.43 – 17 m depth and a carbonate layer is present at 13.58 – 13.13 m depth. Marls occur again between 5.98 m and 4.57 m depth, followed by a thin peat layer from 4.57 m to 4.19 m depth, which is then followed by a thin carbonate layer at 4.19 m – 3.82 m depth. Peat sediments are again deposited from 3.82 m to 1.15 m depth. The topmost 1.15 m of the core is characterized by brown carbonates and marls (Fig. 2.9).

Lithological features as well as the most representative inorganic geochemistry data (Ca, Si, S), magnetic susceptibility, TOC (wt %), C/N, color lightness and the PCA results were used for the facies classification of the core (Table 2.5). According to their presence in the core, we distinguished four main facies (*Peat facies*, *Clayey peat facies*, *Clayey carbonate facies* and *Carbonate facies*) and four secondary facies (*Dark-brown carbonate facies*, *Light-brown carbonate facies*, *Clay facies* and *Dolomite facies*). Every secondary facies represents less than the 5% of the total depth of the core. Note that Ca shows very similar trends compared to Sr, lightness and b\* values, while Si covaries with Fe, Al, K, Zr, Rb/Sr and MS. Finally, S shows a good correlation with Br, TOC and C/N (Figs. 2.4 and 2.9). Correlation coefficients of the different proxies are also shown in Table 2.4. Data from different facies described below are presented in Figure 2.9 and in Table 2.5.

##### *4.3.1. Clayey carbonate facies*

Yellowish carbonates with internal cm- to dm-clayey layers, occur between ~42 – 39 m (~194 – 182 kyr BP), at ~29 – 25.5 m (~154 – 133kyr BP) and at ~6 – 4.6 m depth (~29 – 18 kyr BP). Charophytes, gastropods and pelecypods are very frequent, while plant remains are not

common. Mineralogy is composed of calcite, dolomite and quartz. Inorganic geochemistry yields high relative values in Ca (>800,000 cps), medium values in Si (15,000 – 30,000 cps) and low values in S (5,000 – 25,000 cps). Magnetic susceptibility ( $< 1 \times 10^{-5}$  SI), C/N (20 – 30) and TOC (0 – 3%) is low. Lightness is high (70 – 100%). PC1 is characterized by low values and PC2 by medium values.

#### 4.3.2. *Carbonate facies*

This facies is characterized by light yellowish carbonate mainly composed of calcified remains of charophytes, and occurs at ~25.5 – 23 m (~133 – 117 kyr BP), 13.58 – 13.13 m (~71 – 69 kyr BP) and at 4.19 – 3.82 m depth (15.5 – 12.6 kyr BP). There are also high occurrences of gastropods and pelecypods, while plant remains are rare. Calcite is the principal mineral. According to inorganic geochemistry, Ca shows high relative values (>800,000 cps) while Si (0 – 10,000 cps) and S values (0 – 6,000 cps) are low. Magnetic susceptibility ( $< 2 \times 10^{-5}$  SI), TOC (0 – 3%) and C/N (15 – 25) are also low, while lightness is high (70 – 100%). Values for PC1 and PC2 are low.

#### 4.3.3. *Peat facies*

Black massive peat with high amounts of organic matter and plant remains occurs in different sections throughout the core. There are no gastropods, pelecypods or charophytes in this facies. Mineralogical analysis shows very flat diffractograms, with very occasional rare quartz. According to inorganic geochemistry, this facies characterized by high relative S values (10,000 – 75,000 cps), and low Ca (20,000 – 100,000 cps) and Si (0 – 4,000 cps) values. Magnetic susceptibility ( $< 3 \times 10^{-5}$  SI) and lightness (25 – 40%) are also low. Both TOC (30 – 60%) and C/N (35 – 60) values are high. PCA analysis yields positive PC1 and negative PC2 values.

#### 4.3.4. *Clayey peat facies*

Clayey organic peat with some plant roots is normally intercalated with the *Peat facies*. As in the *Peat facies*, there are no gastropods, pelecypods or charophytes. Quartz and illite are the main minerals in the diffractograms. Inorganic geochemistry shows high relative Si (10,000 – 85,000 cps) and S values (10,000 – 75,000 cps) and low Ca (20,000 – 100,000 cps) values. Magnetic susceptibility has medium relative values ( $< 3 \times 10^{-5}$  SI), whereas TOC (20 – 40%) and C/N (25 – 40) are high. Lightness (25 – 50%) is low. This facies is characterized by positive PC1 and relatively high PC2 values. The *Clayey peat facies* and the previous *Peat facies* make up approximately a 73% of the total facies in the core. The intercalation between these two facies is common.

#### *4.3.5. Dark-brown carbonate and Light-brown carbonate facies*

These two secondary facies are characterized by light to dark carbonates that occur in the topmost part of the core (1.15 to 0 m, 4.7 – 0 kyr BP). Inorganic geochemistry for both facies yield high relative Ca values (>200,000 cps), medium Si (0 – 40,000 cps) values and low S (0 – 8,000 cps) values. Magnetic susceptibility varies from low to high (from  $-4 \times 10^{-5}$  to  $30 \times 10^{-5}$  SI). Both TOC (0 – 10%) and C/N (0 – 25) values are low, while color lightness is high (40 – 80%). Specifically, the *Dark-brown carbonate facies* (1.15 – 0.4 m depth) is principally composed of calcite without detrital sediments (no dolomite, quartz, illite, and low values of Si and MS). Charophytes, gastropods and pelecypods are more abundant than in the *Light-brown carbonate facies* (0.4 – 0 m depth). PCA yields low values for PC1 and PC2. On the contrary, the *Light-brown carbonate facies* presented calcite, dolomite, quartz and illite. Silicon, MS and PC2 values in this facies are higher, while PC1 is also low.

#### *4.3.6. Clay facies*

This secondary facies consists of brown organic clayey layers with occasional mottling and mixed sediment textures that occur at ~33.2 – 32.3 m (~166 – 164 kyr BP) and ~17.4 – 17 m depth (~87 – 81 kyr BP). Other thin layers (<10 cm thick) appear at ~35.3 m (~172 kyr BP), ~21 m (~104 kyr BP) and ~6 m depth (~29 kyr BP). There is occasional presence of plant roots. Mineralogy is mainly composed of quartz and illite. Inorganic geochemistry yields high relative values of Si (20,000 – 95,000 cps), medium values of S (20,000 – 45,000 cps) and low values in Ca (30,000 – 100,000 cps). Magnetic susceptibility varies from low to high (from  $-2 \times 10^{-5}$  to  $15 \times 10^{-5}$  SI). Both TOC (0 – 10%) and C/N (15 – 30) are low, while lightness is medium (45 – 60%). PCA yields relatively low PC1 but high PC2 values.

#### *4.3.7. Dolomite facies*

This secondary facies is formed by ten grayish-whitish dolomitic sediment layers (maximum thickness of 7 cm) randomly distributed in the lower half of the core between 40.2 – 38.8 m (~187 – 181 kyr BP), at 32.3 m (~164 kyr BP) and between 23.5 – 21.7 m depth (~120 – 108 kyr BP). Mineralogy is mainly dolomitic, with occasional quartz. Inorganic geochemistry yields high relative Ca (>700,000 cps), high Si (20,000 – 60,000 cps) and low S (0 – 5,000 cps) values. Magnetic susceptibility ( $< -1 \times 10^{-5}$  SI), TOC (0 – 1%) and C/N (20 – 25) values are all low. This facies is characterized by the absence of plant remains, charophytes, gastropods and pelecypods. Lightness is high (95 – 100%). PCA is characterized by low PC1 and PC2 values.

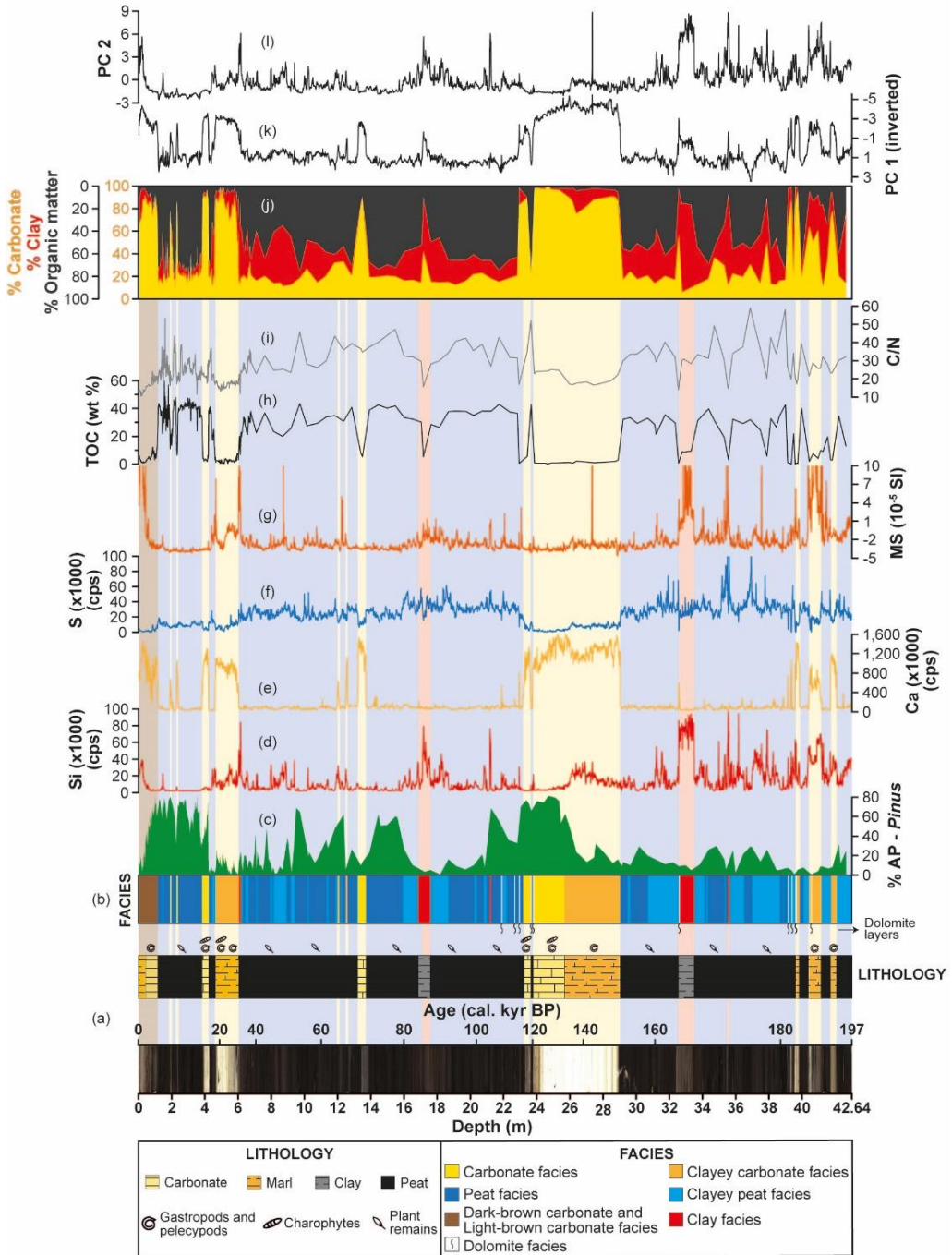


**Figure 2.9.** Multiproxy data comparison with respect to depth from the Padul-15-05 sedimentary record. From bottom to top: (a) scanner photography with the correspondent lithology and organisms (gastropods, pelecypods, charophytes and plant remains); (b) facies also showing the occurrence of thin dolomite facies/layers; (c) Arboreal Pollen percentages (AP) with *Pinus* excluded from the total terrestrial pollen sum; (d) Si data in cps; (e) Ca data in cps; (f) S data in cps; (g) magnetic susceptibility in SI; (h) TOC in weight percent; (i) C/N; (j) carbonate, clay and organic matter percentages; (k) PC1 values (inverted) and (l) PC2 values.

#### *4.4. Pollen results*

The Arboreal Pollen (AP) percentage (excluding *Pinus*), shows important abundance variations throughout the Padul-15-05 core. Values are relatively low (average value of ~17%) at the bottom of the core between 42.64 m to ~26 m depth (~196 – 135 kyr BP). At ~26 m depth (~135 kyr BP) AP begin to develop, reaching its maxima at ~24.5 m depth (~126 kyr BP) with ~82% of the pollen assemblage. A decrease in AP values occur between ~22.5 – 22 m depth (~115 – 111 kyr BP) before another increase until ~21 m depth (~105 kyr BP). Between ~21 m to ~16 m depth (~105 – 80 kyr BP), average AP values are around 13%, with highest peaks never exceeding a 27%. Thereafter, relatively high percentages occur (maxima of ~60%) between ~16 m to ~13.5 m depth (~80 – 73 kyr BP), as well as between ~12 – 9.5 m depth (~65 – 53 kyr BP), with maximum values at ~65 kyr (maxima of ~62%) and ~53 kyr BP (maxima of ~69%). During the last glacial period (~9.5 – 4.19 m depth, ~53 – 15.5 kyr BP), AP percentages decline to average values of ~12%. Finally, from 4.19 m to the core top (from 15.5 kyr to the present), AP increases with an average value of ~50% and a maximum peak of ~81% (Figs. 2.9 and 2.10).

#### *4.5. Spectral analysis*

Statistically significant spectral cyclicities at ~26.2 kyr (>95% CI) and ~19.6 kyr (>80% CI) are present in Si, which are probably pointing into the same cycle. A ~24.5 kyr cycle (>80% CI) is present in the TOC while in MS occur at ~22.5 kyr (>99% CI). A cycle of ~12.6 kyr (>95% CI) in Si and ~11.2 kyr (>95% CI) in MS are most likely the harmonics of the ~26.2 – 19.6 kyr and 22.5 kyr cycles, respectively. We focused on the highest amplitude cycles so smaller scale periodicities have not been described. Note that the spectral analysis on Si was developed using Si data in counts per second (cps) due to its better results and representation with respect to normalized Si. However, both Si data time-series present very similar trends with a correlation coefficient of 0.807.

## **5. Discussion**

### *5.1. New age control for the Padul sedimentary sequence*

This study has improved the age control of the Padul sedimentary sequence compared with previous works through a large number of AMS radiocarbon ages (a total of 61 samples analyzed), specific-compound radiocarbon dating and amino acid racemization (AAR) in gastropods from the Padul wetland. The lack of tephras in this part of the western Mediterranean region (Satow, 2012), the lack of siliciclastic-rich sands/clays that could be used for optically stimulated luminescence (OSL), and issues related to U/Th ages in an open wetland system that preclude obtaining accurate U/Th dates (Sierralta et al., 2017), led us to the AAR dating method for dating sediment older than the radiocarbon limit. In absence of independent numerical ages for the bottom part of the core, we decided to use the sediment accumulation rates (SAR) of the two main lithologies (peat and carbonate/marl) from the well-dated top part of the core, with the

purpose of creating a relatively objective age-depth model for the entire Padul-15-05 core. Tuning was avoided in order to elude circular reasoning (Blaauw, 2012). A spectral analysis in the depth domain of the silicon data and a subsequent filtering based on the obtained frequency ( $f = 0.0018762$ ) was also developed to identify the periodicity of the lithological changes and to compare with insolation cycles. This cyclostratigraphic exercise supports the age model for the Padul-15-05 record, agreeing with the total number of cycles that occurred in the last ~197 kyr obtained in the age-depth model and related with insolation (Supplementary Fig. 2.S1).

### 5.2. Facies, environment, climate and lake level reconstruction

Depositional environments and lake level reconstruction at Padul were determined based on the different previously described proxies and facies. Sedimentary facies changed through time due to paleoenvironmental changes depending on climate changes and lake level response (Figs. 2.10 and 2.11; Table 2.5). Lake level of the Padul-15-05 core was reconstructed using the smoothed PC1 score that included the most representative multiproxy data (Ca, Sr, Si, Al, Fe, S, Br, TOC, C/N and MS). Negative PC1 scores with positive correlation between Ca and Sr and opposite to S, Br, TOC and C/N (Figs. 2.7 and 2.9) suggest high lake level related to carbonate/marl precipitation (*Clayey carbonate facies* and *Carbonate facies*). In contrast, positive PC1 scores could be indicative of low lake level during peat formation (*Peat facies* and *Clayey peat facies*) with high amount of organic matter and abundant littoral emerged vegetation. Below we give a more extended interpretation of the different identified facies in terms of environmental conditions:

*Clayey carbonate facies* is interpreted here as being deposited during highest lake level stages with frequent occurrences of gastropods and pelecypods. Detrital input characteristic from this facies occurred during increasing regional aridity, resulting in less forest cover/barrier in the nearby Sierra Nevada and the Padul area (see low AP in Fig. 2.10) and intensifying the erosion during the coldest and most arid climate conditions. As also occurred in Lake Ohrid explained by Francke et al. (2016), enhanced physical weathering and erosion could be due to an intensification of glacial and/or periglacial activity. The PC2 in the PCA shows positive correlation of Si, Al, Fe and MS, also pointing towards predominant detrital deposition, likely linked to higher clastic input from Sierra Nevada (Figs. 2.7, 2.9 and 2.11A) and/or minor biogenic productivity in the lake. This *Clayey carbonate facies* mainly occurred during minima in summer insolation and low eccentricity during MIS 6b and 6a (~29 – 25.5 m) and again during MIS 2 (~6 – 4.6 m) (see Figs. 2.9 and 2.10), indicating that this is the coldest-related facies in the core. The three clayey carbonate facies bands between ~195 – 182 kyr BP also largely correspond to a period of minimum insolation, suggesting cold and arid phases, even if eccentricity was not at the lowest values. Vaks et al. (2003) and Hodge et al. (2008) show that during glacial periods, Mean Temperature of the Warmest Month (MTWA) and Mean Annual Temperature (TANN) in the Mediterranean region reduced while Effective Annual Precipitation (EAP) (precipitation/evapotranspiration balance) increased. Therefore, strong cold conditions and absence of evapotranspiration would result in high lake level at Padul (Fig. 2.11A). The occurrence of glaciers at higher elevations in Sierra Nevada during glacial periods could also be



an important source of water to lower elevation areas, through increased aquifer discharge during slightly warmer summers, and therefore, could also contribute to a high water table at Padul.

*Carbonate facies* is also interpreted here as indicative of relatively high lake level, which would enable the proliferation of organisms, such as charophytes, gastropods and pelecypods, organisms that would increase carbonate sedimentation. The maximum lake level should not have been excessively high, because charophytes typically grow in water depths of only a few meters (<4 m) (Cohen, 2003; Pelechaty et al., 2013). Even if the water contained abundant dissolved carbonate and was supersaturated in these elements, a triggering mechanism is needed in order to precipitate carbonate, such as an increase in CO<sub>2</sub> degassing (Jones and Renaut, 2010) or the activity of calcifying charophytes (Pentecost, 2005). Negative PC1 values, with a strong correlation between Ca and Sr (opposite to S, Br, TOC and C/N), are characteristic of this facies (Figs. 2.7 and 2.9). The absence of detrital input from Sierra Nevada also indicate less weathering and erosion, perhaps pointing to warmer conditions and/or probably higher biogenic deposition. Several previous works (Ortiz et al., 2004a; Magny et al., 2007) also interpreted this facies as deposited in relatively deep lake waters. This facies typically started right after minima in insolation, and thus, during warming transitions, such as Termination II after the penultimate glacial period or Termination I after the last glacial period (Figs. 2.10 and 2.11B). A high water table in Padul at these times would be closely related to the melting of snow/ice that accumulated in Sierra Nevada during the preceding cold phases (as explained above in *Clayey carbonate facies*), suggesting a delay in the response of the lake system during increasing summer insolation after glaciations. Thereafter, lake level remained relatively high for a period of time (~3,000 years for the last deglaciation; ~15.5 – 12.6 kyr BP) until glaciers disappeared, aquifer discharge diminished, and lake level decreased due to evapotranspiration. However, *Carbonate facies* should have not only be related to water input from glacier melting, but also rainwater supply during high moisture climate conditions greatly exceeding evapotranspiration in the lake resulting in positive EAP, as occurred during the MIS 5e (see *Section 5.3.2*). A similar carbonate layer occurred between 13.13 – 13.58 m depth (~71 – 69 kyr BP; early MIS 4), but this interval has a different color, with lower lightness, yields much lower AP values (<12%), slightly higher TOC percentages and higher C/N ratio (Figs. 2.4 and 2.9), not representing either a deglaciation nor an interglacial period. High C/N ratio would indicate low presence of nitrogen from algae and aquatic plants (Meyers, 1994), so the lake level was also probably lower. A similar facies layer occurred in the Holocene part of the core at 7.5 kyr BP, which might signify shallow lake environments but under cold and arid climate conditions (Ramos-Román, 2018).

*Peat facies* can be interpreted as deposited in very shallow palustrine environments with littoral vegetation and large accumulation of organic matter promoting anoxic conditions in the sediment during degradation. This is confirmed by the PCA, showing a positive PC1 with very good correlations between S, Br, TOC and C/N (Figs. 2.7 and 2.9). This correlation between Br and TOC has also been observed in a sedimentary records from the Gulf of Cadiz in the southwest Iberian Peninsula (Bahr et al., 2014). C/N ratios greater than 20 are characteristic of cellulose-rich vascular land plants, while mixture of vascular and algal plants shows values between 12 and 17 (Ertel and Hedges, 1985; Meyers, 1994). High C/N values in this facies indicate that the organic matter originated from vascular plants. Pollen data, along with the

absence of siliciclastics in this facies show that the forest cover was relatively high around Padul and Sierra Nevada, and consequently, the weathering/erosion in the catchment basin was low and/or the biogenic productivity in the lake probably higher. Therefore, *Peat facies* is interpreted here as developed during high summer insolation under relatively warm and regionally humid periods as shown by the Arboreal Pollen data (e.g., MIS 5a and Holocene) (Fig. 2.10), and similar to that recorded in Lake Accessa during the Holocene by Magny et al. (2007). High summer insolation would have triggered enhanced land-sea temperature contrast, producing more cyclonic activity and fall-winter precipitation in the area. Climate during peat formation was then characterized by strong seasonality with maximum summer drought and high winter precipitation, but evapotranspiration mainly during summer due to maxima in summer insolation greatly exceeded aqueous input (low effective precipitation), resulting in very low lake level (Figs. 2.10 and 2.11C). This would agree with several previous works, such as Ortiz et al. (2004a) at Padul, Magny et al. (2007) at Lake Accessa or García-Prieto (2015) at El Cañizar Lake, who also interpreted peat sedimentation as being produced during episodes of low water depth. Shallow wetland environments would favor abundant emerged vegetation that could trigger anoxia during periods of high productivity and high water temperature (Cohen, 2003).

*Clayey peat facies* results from the combination of peat formation and detrital input. This facies is interpreted as deposited during low lake level, but when water levels were slightly higher than during the sedimentation of *Peat facies*. Therefore, this facies is transitional between peat (interglacial/interstadial) and clayey carbonate (fully glacial) facies. *Clayey peat facies* is interpreted as typically occurring during the transition between insolation maxima and minima, and during arid and cool stadials. The detrital component (shown by positive PC2 values with good correlations between Si, Al, Fe and MS), generally interpreted as fluvial sediments carried into Padul from Sierra Nevada and/or lower biogenic productivity, could be due to enhanced erosion during these climate conditions. Relatively low summer insolation might produce colder and/or drier conditions that would have prevented the expansion of forest cover/barrier, and therefore, would have resulted in increased siliciclastic input to the lake from Sierra Nevada, as occurred for example during the MIS 3 (in particular between ~30 – 50 kyr BP) (Figs. 2.10 and 2.11D). High rates of sediment transport linked to open landscape vegetation can be observed in the alluvial fan systems from Lahontan and Mojave (USA) (Harvey et al., 1999) and in the lacustrine record of El Cañizar Lake (Spain) (García-Prieto, 2015).

*Clay facies* is characterized by important detrital content (Si, Al, Fe, K, Zr, Ti, Rb/Sr, MS and positive PC2 values of the PCA) (Figs. 2.4, 2.7 and 2.9). Similar to *Clayey peat facies* explained above, it occurred during insolation minima and thus could be interpreted as occurring during cold-arid abrupt stages, when erosion increased because of the low forest cover, such as during MIS 5b (~5,000 years delay probably due to dating uncertainties) (Fig. 2.10). This facies shows that lake level should not have been very high due the presence of mottling textures that are associated with ephemeral lake margin environments and that are indicative of oxidizing-reducing conditions (Buurman, 1980; Wells, 1983; Alonso Zarza et al., 1992).

*Dolomite facies* is defined by several centimeters-thick dolomite laminae with some quartz (Fig. 2.6; Table 2.5), which could be related to episodes of high runoff or fast tectonic pulses resulting in dolomite sedimentation carried from the Triassic dolomitic complex from Sierra

Nevada. However, we cannot rule out dolomite precipitation due to cyanobacterial degradation during evaporation/desiccation stages as recorded in shallow ephemeral lakes from Coorong region in Australia (Wright, 1999), or the authigenic precipitation linked to sulfate reducing bacteria under anoxic conditions as occur in modern hypersaline lakes from Spain (Corzo et al., 2005).

*Dark-brown carbonate facies* and *Light-brown carbonate facies* occur in the topmost part of the core (the last ~4.5 kyr BP) and could be interpreted as deposited in a shallow and a seasonal lake environment, respectively (Fig. 2.9; Table 2.5). *Dark-brown carbonate facies* (~4.5 – 1.5 kyr BP) probably corresponded to shallow lake phases, allowing the presence of carbonate-shell organisms such as gastropods, pelecypods and charophytes to produce carbonate sediments. *Light-brown carbonate facies* (the last ~1.5 kyr) would correspond to ephemeral/dried lake stages preventing both very shallow palustrine sedimentation (peat formation) and deeper lake signals (carbonate with gastropods, pelecypods or charophytes). For a more detailed interpretation of lithology and facies of the last ~4,700 years from the Padul-15-05 core, see Ramos-Román et al. (2018a).

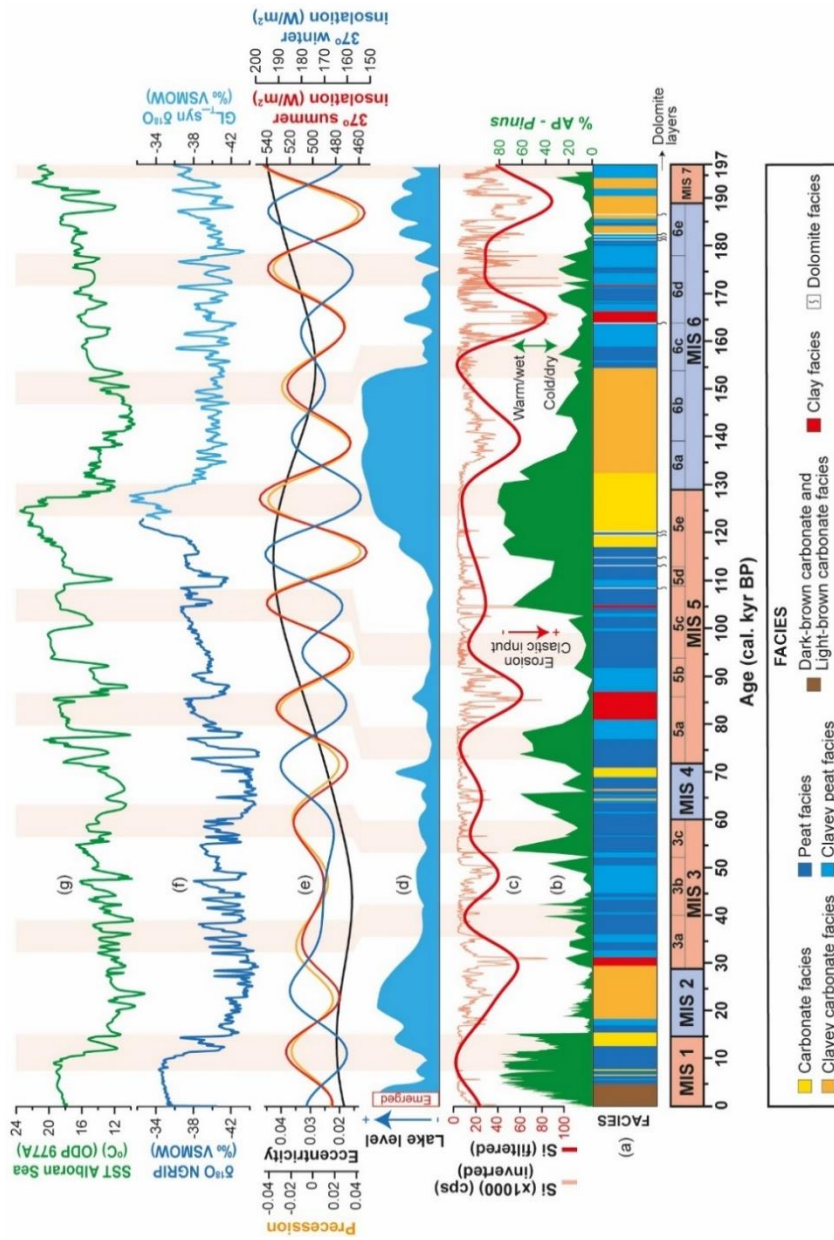


**Figure 2.10.** Representation and interpretation of different proxies from Padul-15-05 with respect to age showing: (a) facies with the presence of thin dolomite layers; (b) Arboreal Pollen (AP) percentages with *Pinus* excluded from the terrestrial pollen sum, indicating warm/wet or cold/dry climate; (c) Si values in cps (light red) (inverted) and filtered Si data (red) indicative of erosion and clastic input and/or biogenic dilution; (d) lake level reconstruction based on smoothed PC1 data; (e) summer insolation at 37°N (red), precession (orange) and eccentricity (black); (f)  $\delta^{18}\text{O}$  values from NGRIP and GL\_syn  $\delta^{18}\text{O}$  records (% VSMOW) and (g) Sea Surface Temperature (SST) record from Alboran Sea (°C). Light red vertical bands show correlation between minima in Si and maxima in summer insolation. Marine Isotope Stage (MIS) 6 and substages have been ascribed following the Table 2.1 from Sun and An (2005). MIS 5 and substages are based on the SST from Martrat et al. (2004) and vegetation data from Milner et al. (2016). Finally, MIS 4, 3, 2 and 1 have been delimited according to vegetation changes from Fletcher et al. (2010a).

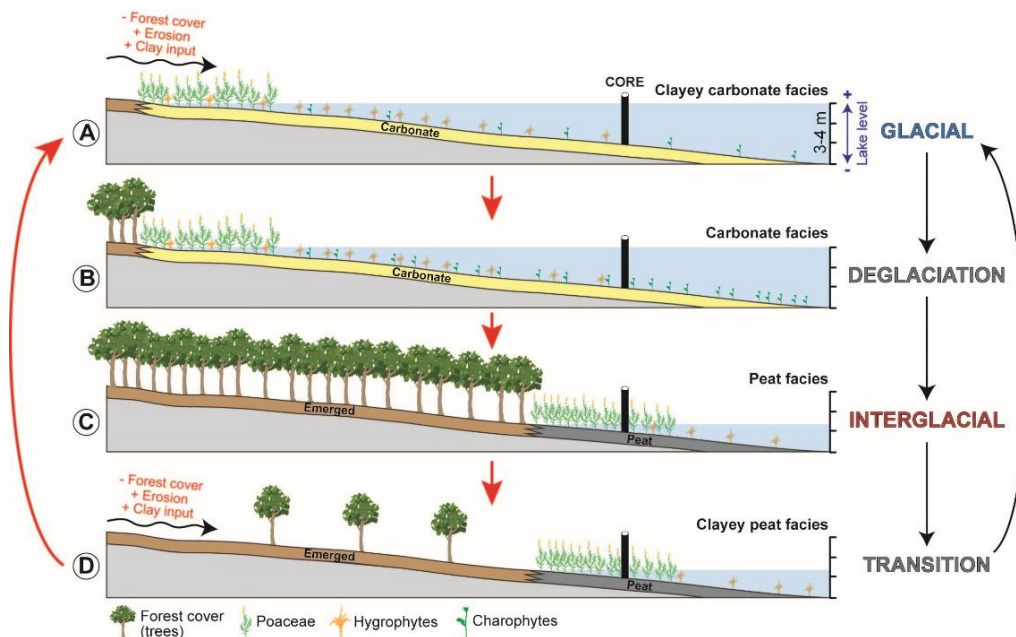


**Figure 2.11.** Schematic representation of different glacial, deglaciation, interglacial and transition phases with respect to *Clayey carbonate*, *Carbonate*, *Peat* and *Clayey peat* facies, respectively, from Padul-15-05 record. Each climatic period shows different sedimentation, lake level and vegetation.

### 5.3. An idealized orbital cyclic pattern in Padul (from MIS 6 to MIS 1): integrating orbital variability, vegetation, facies and lake level

Glacial/interglacial oscillations had an influence on lake levels at Padul, and thus, on the sedimentation (i.e., facies). This is deduced by the studied proxies at Padul, which show similar patterns with respect to paleoclimate variations (i.e., insolation), allowing us to reconstruct an idealized climate-vegetation-lake level-sedimentation cyclic pattern, based on and modified from previously published climate-vegetation cycles from Turner and West (1968), Combourieu-Nebout (1993), Bertini (2001) and Tzedakis (2007) (Fig. 2.12). The idealized cyclic patterns represented in Figure 2.12 summarize different facies deposition along with their respective lake level, climate and specific vegetation (Camuera et al., 2019) for the last glacial-Holocene interglacial cycle and for the penultimate glacial-last interglacial cycle. Both idealized cyclic patterns start from Phase 1 (*Clayey carbonate facies*; number 1 in Fig. 2.12) during the glacial period, passing through the Phase/number 2 (*Carbonate facies*) during deglaciations and in the case of the last interglacial cycle also during the interglacial maxima. Phase/number 3 (*Peat facies*) occurred during the Holocene interglacial maxima and mainly during interstadials in both cycles. The alternation between Phases/numbers 3 and 4 (*Peat facies* and *Clayey peat facies*) suggest fluctuations in insolation during interglacial-glacial transitions, representing maxima and minima in insolation, respectively.

Spectral analyses on different proxy time series (Si, MS and TOC) show statistically significant periodicities between  $\sim 26.2 - 19.6$  kyr, which are concordant with the orbital precession cycle ( $\sim 23 - 19$  kyr) (Milankovitch, 1920; Imbrie and Imbrie, 1980; Berger et al., 1998) (Fig. 2.8). Silicon was filtered based on the average frequency from the 26.2 kyr and 19.6 kyr cycles ( $4.4497E-05$ ) using the Analyseries 2.0 software (Paillard et al., 1996) and compared with insolation (Fig. 2.10). This data are most likely indicating that siliciclastic deposition in the lake was enhanced during minima in summer insolation due to intensified weathering and/or erosion, favored by less forest cover in Sierra Nevada and around Padul during cold and arid climate conditions (Fig. 2.11A and 2.11D). This is supported in Padul by the pollen analysis, where the lowest arboreal pollen values coincide with Si maxima and insolation minima (Fig. 2.10), as also indicate the negative correlation coefficient of  $-0.53$  ( $p = 3.5763E-31$ ) between Si and the Arboreal Pollen data.

High-resolution multiproxy analyses in the Padul-15-05 record show strong similarities with Marine Isotope Stages (MISs), as well as with Alboran Sea Surface Temperature (Martrat et al., 2004),  $GL_T\_syn$   $\delta^{18}O$  synthetic isotope record (from the base of the Padul core -197 kyr- to 123 kyr) (Barker et al., 2011) and  $\delta^{18}O$  record from North Greenland (from 123 kyr to the present) (NGRIP-Members, 2004) at orbital glacial/interglacial and sub-orbital stadial/interstadial time scales (Fig. 2.10). Below is a description of the main paleoenvironmental (lake level and facies) and paleoclimate oscillations observed in Padul-15-05 record with respect to global climate oscillations (i.e., MIS oscillations).

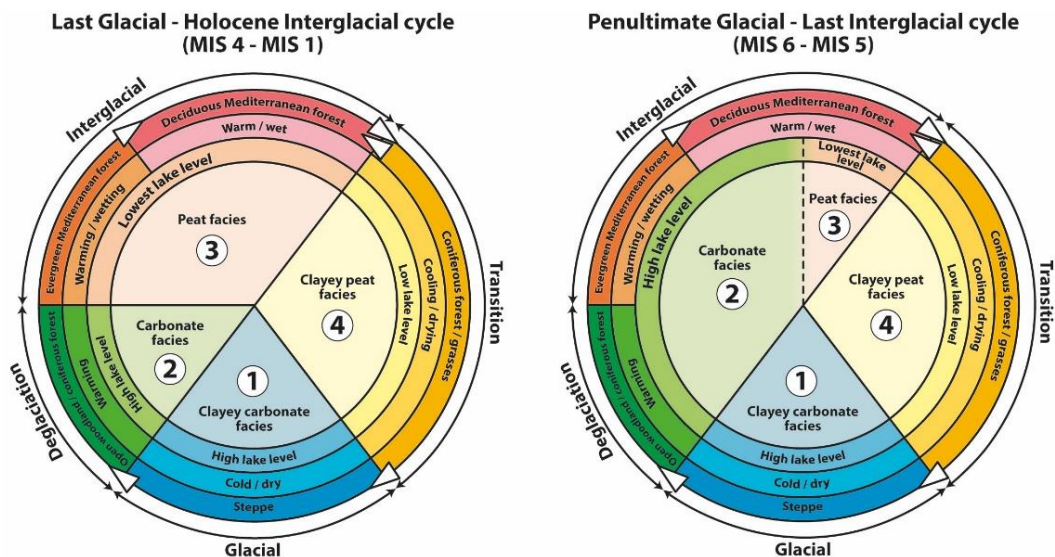


**Figure 2.12.** Idealized Facies-Lake level-Climate-Vegetation patterns for the Last Glacial-Holocene Interglacial cycle (left) and Penultimate Glacial-Last Interglacial cycle (right). White arrows in the external part show the direction of the change.

### *5.3.1. Glacial and cold stadial periods*

The coldest and driest glacial conditions in the Padul-15-05 record are characterized by *Clayey carbonate facies*, occurring during MIS 6b and 6a at ~155 – 132 kyr (~29 – 25.5 m depth) and during MIS 2 at ~29 – 18 kyr BP (~6 – 4.6 m depth) (Figs. 2.9 and 2.10). High lake levels occurring at those times in Padul, were most likely due to low evaporation, and thus, high Effective Annual Precipitation (EAP). This seems to agree with General Circulation Models from Kutzbach and Guetter (1986) and COHMAP-Members (1988) and corroborated by the study of Harrison and Digerfeldt (1993) about lake level responses during glacial periods. They suggest that colder Sea Surface Temperature (SST) and the development of a fixed anticyclone over the North European ice sheets during glaciations generated a cold/dry storm track from the western Atlantic into the Mediterranean region that produced cloudy summers (with no precipitation) and also brought cold/dry air masses from the North European glacial anticyclone into the Padul area during winter times. Besides, Prentice et al. (1992) also suggested cool and dry summer climate for the Last Glacial Maximum (LGM) (which could be extrapolated to other glacial periods), even if winter precipitation models were not completely clear. Therefore, cold conditions during both seasons and a reduction in evaporation rates during cloudy summer times resulted in positive precipitation-evapotranspiration balance and high EAP (even with low winter precipitation), and high lake level. Moreno et al. (2012a) in Villarquemado paleolake (central Spain) also suggested high lake level conditions for carbonate lake environments as a consequence of cold and relatively humid climate during the LGM, while Vegas et al. (2010) in Fuentillejo maar (central Spain) showed low lake levels during arid climates. It should also be noted that even if glaciers at high elevations of Sierra Nevada were not the main water sources at Padul, they could have also provided some water supply to lower areas (i.e., Padul lake) due to partial melting during slightly warmer summer times.

The lower Si content during the early MIS 6b (~155 – 144 kyr BP) with a slight increase in AP at ~145 kyr compared to the late MIS 6b and early MIS 6a (~144 – 137 kyr BP), could be related to a more temperate and humid climate, resulting from higher summer insolation but still under lowest eccentricity, as shown in the Ioannina pollen record from Northern Greece at 150 kyr (Tzedakis et al., 2003a). In addition, a slight more humid climate under overall cold climate conditions could have allowed higher EAP than previously in the Sierra Nevada area, and therefore, the beginning of high lake level clayey carbonate formation during MIS 6b at around 155 kyr ago. The coldest and most arid conditions of the last part of the penultimate glacial period occurred between ~145 – 137 kyr (~27.3 – 26.2 m depth), with *Clayey carbonate facies* with high siliciclastic input due to low lacustrine productivity and/or high weathering/erosion favored by low forest cover during minimum summer insolation just after minimum eccentricity (Figs. 2.10 and 2.11A), agreeing with coldest conditions recorded by SST in Alboran Sea (Martrat et al., 2004).

*Clayey peat facies* characterized by relatively low AP and high Si content also interpreted as relatively cold and arid regional conditions occurred mainly during MIS 6d, 6c, 5b, 5a, 3b and 3a. The low forest cover indicated by the low AP percentages and subsequent high siliciclastic input in the lake fit well with minima in summer insolation. High Si values in Padul



during MIS 6e through 6c at ~190 – 155 kyr BP (~42 – 29 m depth) suggest cold/arid climate and *Clayey peat facies* deposition with low EAP between ~180 – 155 kyr, agree well with stable isotope-based paleoclimatic records from Gitana Cave ( $\delta^{13}\text{C}$ ) in the southern Iberian Peninsula (Hodge et al., 2008) and from Soreq Cave ( $\delta^{13}\text{C}$ ,  $\delta^{18}\text{O}$ ) in the eastern Mediterranean (Bar-Matthews et al., 2003). With respect to the MIS 5b stadial, is characterized by low summer insolation with low AP development and high siliciclastic input (*Clay facies* and *Clayey peat facies*), suggesting cooler and drier climate. This would be a result of low summer and high winter insolation that could lead to lower summer evaporation, and therefore, lower winter precipitation, similar to that explained by Berger et al. (2007) for the Post-temperate transition at 115 kyr BP. Nevertheless, it should be mentioned that maximum Si data and *Clay facies* at ~87 – 81 kyr BP present a delay with respect to minimum summer insolation at ~92 kyr BP, probably due to lack of age control samples at this depth. Finally, note that the alternation between *Clayey peat facies* and *Peat facies* was very frequent throughout the Padul-15-05 core probably due to smaller millennial climate oscillations (i.e., D-O and Heinrich-like variability).

### 5.3.2. Interglacial and warm interstadial periods

Interglacial and interstadial periods in the Padul-15-05 record are mainly characterized *Peat facies* with lack of siliciclastic input and high AP percentages (Figs. 2.9 and 2.10). The early and middle Holocene (12.6 – 4.5 kyr BP) as well as interstadials are characterized by this lithology, suggesting climate warming that enhanced evapotranspiration in the lake, exceeding rain/groundwater input and decreasing the EAP and lake level. This is in agreement with other Mediterranean records such as Lake Accesa in north-central Italy, which also shows peat lithology during the early and middle Holocene (Magny et al., 2007). In addition, low lake levels during maximum summer insolation have also been described in different records from the Iberian Peninsula, such as in Villarquemado paleolake (Aranbarri et al., 2014), Lake Estanya (González-Sampériz et al., 2017) and Lake Banyoles (Valero-Garcés et al., 1998), and summarized in Morellón et al. (2018). Nevertheless, almost the entire MIS 5e (~132 – 117 kyr BP) in Padul is characterized by *Carbonate facies*, suggesting different environmental conditions during the last interglacial in the Padul area. *Carbonate facies* could have been related to prolonged glacier melt-water supply to this area, as occurred during the deglaciation after the last glacial period (15.5 – 12.6 kyr BP). However, sedimentation of the ~15,000 year-long carbonate deposits during the MIS 5e could have also been related to a wetter climate. Temperature reconstructions by Kaspar et al. (2005) based on 48 European pollen and plant microfossil records indicate higher summer temperature during the last interglacial (at 125 kyr) compared to the Holocene, associated with higher summer insolation. These data are supported by SST from the Alboran Sea, which show the highest temperatures of the last 130 kyr at ~127 – 118 kyr (~20-23 °C) (Martrat et al., 2004), while SST from two records in the Iberian Margin show highest temperatures between ~128 – 123 kyr (~18-20 °C) and ~126 – 118 kyr (~19-22 °C) (Pailler and Bard, 2002). As explained above, the enhanced temperature contrast between land and ocean masses due to maxima in summer insolation could have favored humid wind transport from both Mediterranean Sea and North Atlantic Ocean triggering higher fall-winter



precipitation at those times. This would agree with climatic interpretations pointing to increasing precipitation under summer aridity from several previous studies on vegetation changes, isotopic composition and sapropel 5 deposition during the last interglacial period in the Iberian Peninsula, Italy and Greece (Sánchez Goñi et al., 1999; Tzedakis et al., 2003a; Brauer et al., 2007; Ziegler et al., 2010). Milner et al. (2012) using pollen, macrofossil and mineralogical data, showed that the higher summer insolation and summer warming during the MIS 5e generated a more extreme seasonal moisture than during present and the early Holocene. Moreover, the lowest  $\delta^{18}\text{O}$  values during the MIS 5e from Soreq Cave also suggest higher rainfall with respect to the Holocene (Bar-Matthews et al., 2003). Abundant precipitation at that time most likely exceeded evapotranspiration in the lake and resulted in positive EAP, triggering higher lake level during the MIS 5e than in other warm periods such as the Holocene or interstadials, resulting in *Carbonate facies* sedimentation instead of *Peat facies*.

#### *5.4. Padul and other Mediterranean lake level records*

Very few lake level reconstructions from long cores (>100 kyr) exist in the Mediterranean region, being an important parameter to use with other proxies to understand regional climatic changes and the response of local wetland environments. The Padul-15-05 record shows the highest lake levels mainly during the coldest and most arid glacial periods at MIS 6b and 6a and MIS 2 (~155 – 132 and ~29 – 18 kyr BP, respectively) and during MIS 5e and the most part of the Younger Dryas/Bølling-Allerød (~132 – 117 kyr and 15.5 – 12.6 kyr BP, respectively). Previous studies have also shown this apparent contradiction between regional (i.e., pollen) paleoclimate evidence, showing aridity during the last glaciation, and geomorphological evidence for high lake levels in the northern Mediterranean area (Prentice et al., 1992; Harrison and Digerfeldt, 1993; Harrison et al., 1996).

A previous lake level reconstruction from Padul from Ortiz et al. (2004a), based on the organic geochemistry of the core (EQUIP borehole) from Nestares and Torres (1998), shows similar trends with respect to our Padul-15-05 record (Fig. 2.13). Nevertheless, the age control between our study and the previous work presents discrepancies at ages older than ca. 40 kyr BP. Ortiz et al. (2004a, 2010) indicated the highest lake levels at ~185 – 170 kyr BP, while our study suggests highest water depth during glacial periods MIS 6a and 6b, and MIS 5e (~155 – 117 kyr BP), as explained above.

According to the INTIMATE network, the age of the LGM was defined as occurring between 23 – 19 kyr BP (Mix et al., 2001). Tzedakis (2007) summarized that maximum lake levels during the LGM in the eastern Mediterranean region were reached ~27 – 24 kyr ago, based on different lake level reconstructions from the Dead Sea (Israel, Jordan, Palestine) (Bartov et al., 2002), Lake Kinneret (Israel) (Hazan et al., 2005) and Konya Basin (Turkey) (Roberts, 1983; Roberts et al., 1999). In the central Mediterranean region, different Greek lakes also reached their highest lake levels during the LGM. For example, high lake level in Ioannina occurred ~30 – 14 kyr ago with the maximum between ~25 – 14 kyr BP (Harrison and Digerfeldt, 1993) while Xinias lake reached its highest level ~30 – 24 kyr ago, before slightly decreasing until ~16 kyr BP (Digerfeldt et al., 2000) (Fig. 2.13). In the western Mediterranean, lake level of Padul was

reconstructed in a previous study by Harrison and Digerfeldt (1993), who found maximum water depths occurred ~22 – 15 kyr ago, with the highest values between ~19 – 15 kyr BP. The Fuentillejo maar lake level reconstruction from central Spain (Vegas et al., 2010) also recorded highest lake levels during the glacial period but with a decrease between 24 – 20 kyr BP. In addition, they showed low lake levels between 18 – 15 kyr ago, similar to that recorded in our study from Padul (Fig. 2.13).

The high lake level reconstruction for the most part of the Younger Dryas/Bølling-Allerød (15.5 – 12.6 kyr BP) in the Padul-15-05 core is similar to the reconstructions from Konya Basin (Turkey) (Roberts, 1983). Our Holocene lake level reconstruction from Padul-15-05 presents similar trends with respect to Ortiz et al. (2004a, 2010), which showed that from 10 kyr to 4.5 kyr BP C<sub>27</sub>, C<sub>29</sub> and C<sub>31</sub> *n*-alkanes occurred along with vascular plants, macrophytes and high amounts of organic matter, indicative of palustrine conditions and low lake levels (Ortiz et al., 2010). The Accesa Lake (Magny et al., 2007) also presented lower lake level during the early-middle Holocene (~10 – 5 kyr BP) compared with the last 5,000 years BP, in which lake level increased similar to that occurred in Padul-15-05, even if Padul wetland recorded an ephemeral/emerged phase during the last 1,500 years, as explained by Ramos-Román et al. (2018a). On the contrary, our Holocene reconstruction disagrees with other Mediterranean lake level reconstructions, including the previous reconstructions from Padul (Harrison and Digerfeldt, 1993), Lake Xinias (Digerfeldt et al., 2000) and Ioannina (Harrison and Digerfeldt, 1993), showing higher water depth during early and middle Holocene and a decrease during the late Holocene (Fig. 2.13). The suggested contrary trend from Harrison and Digerfeldt (1993) at Padul, could be related to lake level interpretations only based on lithological aspects.

Finally, lake level reconstructions for alpine environments from Sierra Nevada (Laguna de Río Seco lake; 3020 m) showed the highest lake levels during the early Holocene (Anderson et al., 2011; Jiménez-Espejo et al., 2014). This contrasts with our lake level reconstruction from Padul at lower elevation, showing lowest lake levels at that time. This could be explained by the differences in elevation and contrasting precipitation/evapotranspiration balances between the two sites. A greater seasonal insolation difference during the early Holocene may have produced higher snowpack in alpine lakes in Sierra Nevada, in contrast to low elevation areas where high evapotranspiration rates prevailed (Anderson et al., 2011). Therefore, even if regional climate data (i.e., arboreal pollen) pointed into same climatic conditions, lake level could have responded differently depending on the altitude and/or latitude.

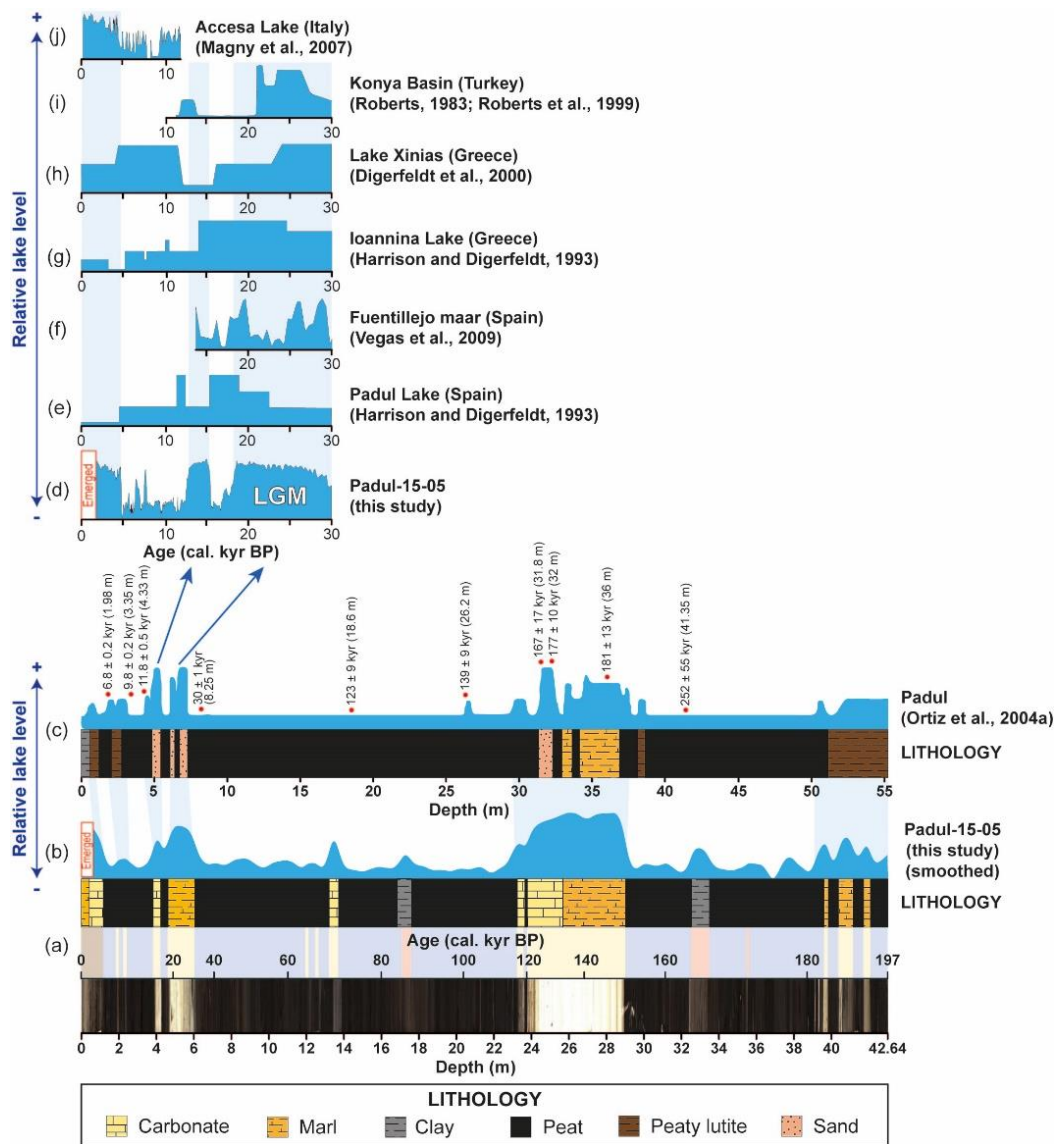


**Figure 2.13.** Comparison of different Mediterranean lake level reconstructions. From a to c: (a) scanner photograph of the Padul-15-05 core and lithology with (b) the correspondent lake level reconstruction based on smoothed PC1 data and (c) the correlation with the lake level and lithology from Ortiz et al. (2004a) (plotted with respect to depth). From d to j: comparison of the last 30 kyr lake level reconstructions of (d) Padul-15-05 core from this study, (e) Padul from Harrison and Digerfeldt (1993), (f) Fuentillejo maar from Vegas et al. (2010), (g) Ioannina lake from Harrison and Digerfeldt (1993), (h) lake Xinias from Digerfeldt et al. (2000), (i) Konya basin from Roberts (1983) and Roberts et al. (1999), and (j) lake Accessa from Magny et al. (2007).  $^{14}\text{C}$  ages from Lake Xinias and Konya Basin have been calibrated in order to plot lake level in the same cal. kyr BP scale as the rest of the records.

## 6. Conclusion

The high-resolution multiproxy analyses from the new Padul-15-05 sediment record shows:

1. The Padul wetland is confirmed as an extraordinary and unique paleoenvironmental and paleoclimatic site in the Iberian Peninsula, containing one of the few long and continuous sedimentary record (>100 kyr) from the southwestern Europe and Mediterranean region.

2. An improvement of the age-depth model for the Padul sedimentary sequence due to (1) a higher radiocarbon dating resolution for the last ~55 kyr (61 AMS radiocarbon samples), (2) the combination of different and updated dating techniques (AMS radiocarbon dating, specific-compound radiocarbon dating, AAR dating) and (3) the use of the SAR of peat and carbonate/marl lithologies from the well-dated top part of the core, which allowed a more objective estimation of the age control and climate reconstruction of the Padul sedimentary sequence for the last ~197 kyr.

3. Insolation, dominated by orbital-scale precession and to a lesser extent, eccentricity, at this latitude, was the most important factor controlling climatic changes in the Padul area, forcing regional (vegetation) and local (sedimentation, lake level) environmental changes.

4. Lithology/facies representing the local sedimentation were controlled by insolation. High siliciclastic input in the Padul wetland transported from Sierra Nevada mainly occurred during low summer insolation, triggering enhanced arid climate conditions, lower forest cover and higher soil weathering/erosion and/or low biogenic deposition.

5. Lake level variations, reconstructed using statistical analysis from inorganic geochemistry, organic geochemistry and magnetic susceptibility data, were triggered by the precipitation/evapotranspiration balance (EAP). Lake level at Padul, which also controlled lithology/facies sedimentation, showed the highest levels during minima in insolation (cold stadials and glacial periods) and deglaciations, while low water level occurred during warmer interstadials and interglacials (except for MIS 5e). Therefore, cold climate conditions with low evapotranspiration lead to positive EAP and high lake levels (and carbonate/marl precipitation), while high evapotranspiration rates exceeding rainfall during most of the warm periods resulted in negative EAP and low lake levels (and peat sedimentation).

6. The different lithological features, facies and lake levels occurring between the last interglacial and the Holocene interglacial periods are the result of distinct seasonality and temperature/precipitation patterns, driven by different orbital parameters and insolation values. Consequently, during the MIS 5e carbonate lithology predominated due to the positive EAP, in which precipitation exceeded evapotranspiration, in contrast to the period of peat accumulation during the Holocene, characterized by high evapotranspiration rates that exceeded rainfall.

7. Multiproxy analysis of sedimentary sequences, including statistical data processing, is necessary to produce a more comprehensive picture of the environmental and climatic changes affecting the local and regional environments in a wetland area.

## **Acknowledgments**

This work was supported by the projects CGL2013-47038-R and CGL-2017-85415-R funded by Ministerio de Economía y Competitividad of the Spanish Government and the research group RNM0190 (Junta de Andalucía). Jon Camuera acknowledges the PhD funding (BES-2014-069117) provided by the Ministerio de Economía y Competitividad of the Spanish Government under the project CGL2013-47038-R. María J. Ramos-Román also acknowledges the PhD and post-PhD fellowship from the Conserjería de Economía, Innovación, Ciencia y Empleo of the Junta de Andalucía (P11-RNM-7332). Antonio García-Alix was also supported by a Marie Curie Intra-European Fellowship of the 7<sup>th</sup> Framework Programme for Research, Technological Development and Demonstration of the European Commission (NAOSIPUK. Grant Number: PIEF-GA-2012-623027) and by a Ramón y Cajal Fellowship RYC-2015-18966 of the Spanish Government (Ministerio de Economía y Competitividad). Thanks also to Javier Jaimez (CIC-UGR) for helping with the drilling equipment and coring, Katherine Whitacre (Nau Amino Acid Laboratory) for the AAR analyses and Jaime Frigola (UB) for his help with the XRF scanning of the core. The authors thank the editor Neil Roberts, Mario Morellón and one anonymous reviewer for the very constructive revision of a previous version of this manuscript.

## Supplementary Information

### **Orbital-scale environmental and climatic changes recorded in a new ~200,000-year-long multiproxy sedimentary record from Padul, southern Iberian Peninsula**

Jon Camuera<sup>1</sup>, Gonzalo Jiménez-Moreno<sup>1</sup>, María J. Ramos-Román<sup>1</sup>, Antonio García-Alix<sup>1</sup>, Jaime L. Toney<sup>2</sup>, R. Scott Anderson<sup>3</sup>, Francisco Jiménez-Espejo<sup>4</sup>, Darrell Kaufman<sup>3</sup>, Jordon Bright<sup>5</sup>, Cole Webster<sup>3</sup>, Yurena Yanes<sup>6</sup>, José S. Carrión<sup>7</sup>, Naohiko Ohkouchi<sup>4</sup>, Hisami Suga<sup>4</sup>, Masako Yamame<sup>8</sup>, Yusuke Yokoyama<sup>9</sup>, Francisca Martínez-Ruiz<sup>10</sup>

<sup>1</sup> *Departamento de Estratigrafía y Paleontología, Universidad de Granada, Spain*

<sup>2</sup> *School of Geographical and Earth Sciences, University of Glasgow, UK*

<sup>3</sup> *School of Earth and Sustainability, Northern Arizona University, USA*

<sup>4</sup> *Department of Biogeochemistry, Japan Agency for Marine-Earth Science and Technology (JAMSTEC), Japan*

<sup>5</sup> *7351 E. Speedway Blvd, 30C, Tucson AZ, USA*

<sup>6</sup> *Department of Geology, University of Cincinnati, USA*

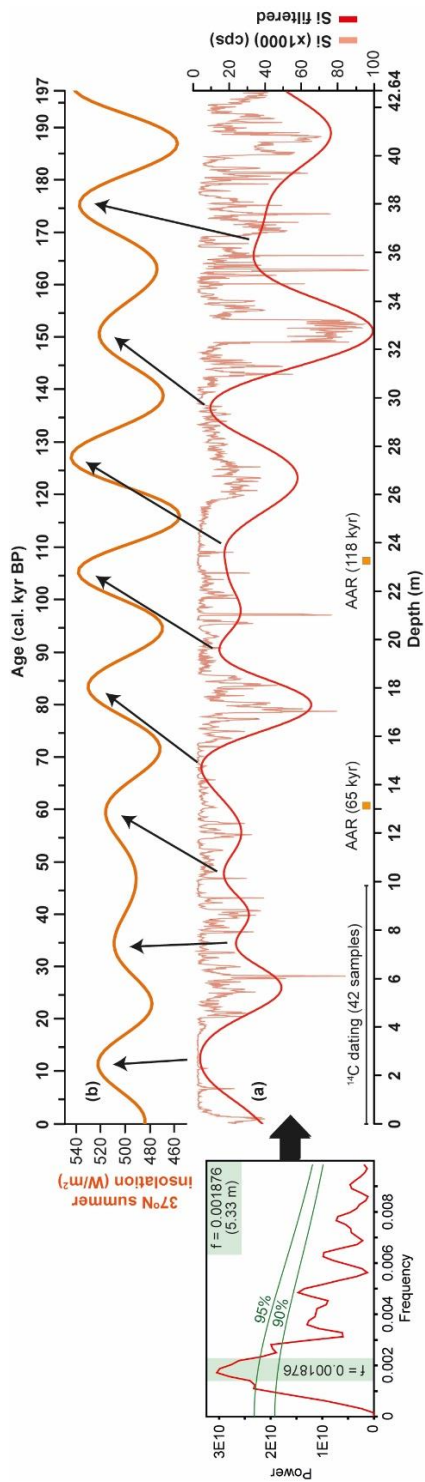
<sup>7</sup> *Departamento de Biología Vegetal, Facultad de Biología, Universidad de Murcia, Spain*

<sup>8</sup> *Institute for Space-Earth Environmental Research, Nagoya University, Japan*

<sup>9</sup> *Atmosphere and Ocean Research Institute, University of Tokyo, Kashiwanoha, Chiba, Japan*

<sup>10</sup> *Instituto Andaluz de Ciencias de la Tierra (IACT), Consejo Superior de Investigaciones Científicas-Universidad de Granada (CSIC-UGR), Granada, Spain*

Supplementary Figure



**Supplementary Figure 2.S1.** The cyclostratigraphic analysis showing the spectral analysis of the Si data (left panel) and (a) Si data (in cps) and filtered curve based on the obtained frequency ( $f = 0.0018762$ ), in comparison with (b) insolation cycles for the last 197 kyr (Laskar et al., 2004).

# *Chapter* 3

*Vegetation and climate changes during the last two glacial-interglacial cycles in the western Mediterranean: a new long pollen record from Padul (southern Iberian Peninsula)*





## Chapter 3: Vegetation and climate changes during the last two glacial-interglacial cycles in the western Mediterranean: a new long pollen record from Padul (southern Iberian Peninsula)

Jon Camuera<sup>1</sup>, Gonzalo Jiménez-Moreno<sup>1</sup>, María J. Ramos-Román<sup>1</sup>, Antonio García-Alix<sup>1, 2</sup>, Jaime L. Toney<sup>3</sup>, R. Scott Anderson<sup>4</sup>, Francisco Jiménez-Espejo<sup>2, 5</sup>, Jordon Bright<sup>6</sup>, Cole Webster<sup>4</sup>, Yurena Yanes<sup>7</sup>, José S. Carrión<sup>8</sup>

<sup>1</sup> Departamento de Estratigrafía y Paleontología, Universidad de Granada, Spain

<sup>2</sup> Instituto Andaluz de Ciencias de la Tierra (IACT), Consejo Superior de Investigaciones Científicas-Universidad de Granada (CSIC-UGR), Granada, Spain

<sup>3</sup> School of Geographical and Earth Sciences, University of Glasgow, UK

<sup>4</sup> School of Earth Sciences and Environmental Sustainability, Northern Arizona University, USA

<sup>5</sup> Department of Biogeochemistry, Japan Agency for Marine-Earth Science and Technology (JAMSTEC), Japan

<sup>6</sup> 7351 E. Speedway Blvd, 30C, Tucson AZ, USA

<sup>7</sup> Department of Geology, University of Cincinnati, USA

<sup>8</sup> Departamento de Biología Vegetal, Facultad de Biología, Universidad de Murcia, Spain


### Published in:

Quaternary Science Reviews, v. 205, p. 86-105 (2019)

Doi: 10.1016/j.quascirev.2018.12.013

Impact factor: 4.334


Quaternary Science Reviews 205 (2019) 86–105



Contents lists available at [ScienceDirect](#)


## Quaternary Science Reviews

journal homepage: [www.elsevier.com/locate/quascirev](http://www.elsevier.com/locate/quascirev)



---

Vegetation and climate changes during the last two glacial-interglacial cycles in the western Mediterranean: A new long pollen record from Padul (southern Iberian Peninsula)



Jon Camuera <sup>a,\*</sup>, Gonzalo Jiménez-Moreno <sup>a</sup>, María J. Ramos-Román <sup>a</sup>, Antonio García-Alix <sup>a,b</sup>, Jaime L. Toney <sup>c</sup>, R. Scott Anderson <sup>d</sup>, Francisco Jiménez-Espejo <sup>b,e</sup>, Jordon Bright <sup>f</sup>, Cole Webster <sup>d</sup>, Yurena Yanes <sup>g</sup>, José S. Carrión <sup>h</sup>

<sup>a</sup> Departamento de Estratigrafía y Paleontología, Universidad de Granada, Spain  
<sup>b</sup> Instituto Andaluz de Ciencias de la Tierra (IACT), Consejo Superior de Investigaciones Científicas-Universidad de Granada (CSIC-UGR), Granada, Spain  
<sup>c</sup> School of Geographical and Earth Sciences, University of Glasgow, UK  
<sup>d</sup> School of Earth Sciences and Environmental Sustainability, Northern Arizona University, USA  
<sup>e</sup> Department of Biogeochemistry, Japan Agency for Marine-Earth Science and Technology (JAMSTEC), Japan  
<sup>f</sup> 7351 E. Speedway Blvd, 30C, Tucson, AZ, USA  
<sup>g</sup> Department of Geology, University of Cincinnati, USA  
<sup>h</sup> Departamento de Biología Vegetal, Facultad de Biología, Universidad de Murcia, Spain

## **Abstract**

A new sediment core from Padul, Padul-15-05, provides a long and continuous sedimentary and paleoenvironmental record of the last ~200 kyr. Here we present a detailed palynological study from this sedimentary sequence with new vegetation and paleoenvironmental data and a climatic interpretation for the last two climatic cycles from the southern Iberian Peninsula in the western Mediterranean region. Pollen analysis from this core shows orbital-scale vegetation oscillations (mainly forced by precession and eccentricity) pointing into insolation as the principal factor controlling vegetation changes at this latitude. The last two glacial-interglacial cycles (from MIS 6 to the present) as well as stadial and interstadial phases are well represented and characterized by significant oscillations in Mediterranean forest in the area, but several differences with respect to other Mediterranean long pollen records can be recognized. Some of these disparities between regions seem to be more related to different precipitation rates linked to the specific geographical features (e.g. strong topographic relief) than to latitudinal differences between the sites. In addition, a lake level reconstruction based on palynological data was developed and compared with the previous reconstruction from this record, representing local environmental changes in the Padul wetland that seems to be related to precipitation/evapotranspiration balance, and therefore, to changes in regional climate conditions. During glacial/stadial conditions recorded by maxima in xerophytes, the p/e increased due to very low evapotranspiration, resulting in high lake levels, while during warmer interglacial/interstadial phases (except for the MIS 5e), mainly represented in this record by maxima in the Mediterranean forest, water level decreased as a result of high evapotranspiration exceeding precipitation input. The comparison of the new Padul-15-05 pollen record with the two previous palynological studies from Padul shows significant differences mainly due to disagreements in the age control of the sequences. This study shows that an accurate age-depth model becomes essential when interpreting long paleoenvironmental and paleoclimate records.

**Keywords:** Glacial-interglacial cycles; vegetation; climate; environmental changes; lake level; Padul

## **1. Introduction**

The Mediterranean region is very interesting for paleoclimatic studies as its climate is strongly influenced by interrelationships between the climatic pattern of Europe, by close atmospheric and oceanic linkages to the North Atlantic region, and those of the adjacent areas of North Africa and Asia (i.e. African and Asian monsoons) (Lionello et al., 2006). This is also a very sensitive area for reflecting environmental changes due to its location between arid (south) and humid (north) regions. Several previous palynological studies using long cores showing high-frequency vegetation changes have been documented in lakes from southern Europe and the Mediterranean region, such as in Tenaghi Philippon (Wijmstra, 1969), Lago Grande di Monticchio (Watts et al., 1996; Brauer et al., 2007), Lago di Vico (Magri and Sadori, 1999), Lake Ioannina (Tzedakis et al., 2002), Lake Ohrid (Lézine et al., 2010) or Lake Van (Litt et al.,

2014). However, very few long continental pollen records older than 100 kyr are documented in the Iberian Peninsula. Therefore, Padul, containing one of the longest (ca. 0.8 – 1 Ma) (Ortiz et al., 2004a) and continuous sedimentary records, plays an important role if we want to understand long- and short-term climate variability.

During the second half of the 20th century and the beginning of the 21st century, the Padul wetland became the focus of several palynological studies (Menéndez-Amor and Florschütz, 1962, 1964; Florschütz et al., 1971; Pons and Reille, 1988; Valle-Hernández et al., 2003). Florschütz et al. (1971) published the low resolution palynological analyses of the entire Padul-IV (24 m depth) and Padul-IVa (70 m depth) cores. Seventeen years later, Pons and Reille (1988) published the palynology of the Padul 3 (8 m depth) and Padul 2 (14.8 m depth) cores, representing approximately the sedimentation of the upper 24 meters. Nevertheless, the long pollen records from different authors presented big discrepancies due to poor chronological control and, therefore, different vegetation and climate interpretations were made. Florschütz et al. (1971) indicated that the Early Weichselian (Early Glacial, ~70 – 115 kyr BP) and the Eemian (MIS 5e, ~115 – 130 kyr BP) were represented from ~12 m to 24 m depth, reaching the Saalian glaciation (MIS 6 – MIS 10, ~130 – 350 kyr BP) and even a part of the Holsteinian interglacial (MIS 11, ~350 – 400 kyr BP) at 70 meters depth. On the contrary, Pons and Reille (1988) interpreted the base of Padul 2 (at ~14.8 m depth on Padul 2 and at ~24 m depth in the composite record of Padul 3 and Padul 2) as the first Prewürm interstadial (i.e., MIS 5c) instead of the Eemian interglacial (as previously interpreted by Florschütz's team), not having any other interglacial period represented in the sedimentary sequence apart from the Holocene. Therefore, a better chronological control of the sedimentary sequence and a higher-resolution pollen analysis were necessary on the Padul record to improve our understanding of the environmental changes through time in this area.

This study aims to reconstruct the environmental and climatic signal of the last ~197 kyr from the southern Iberian Peninsula using a new 42.64 m-long record (Padul-15-05 core) from the Padul wetland site. This new study is based on palynological analysis under a robust age control based on high-resolution AMS radiocarbon dating (61 radiocarbon dates) and other different methodologies (specific-compound radiocarbon dating, amino acid racemization dating and sedimentary accumulation rates) developed in Camuera et al. (2018). The comparison of this precisely dated pollen record with other long paleoclimatic records (i.e., insolation, SST Alboran Sea) and other Mediterranean continental pollen archives will improve the understanding environmental factors affecting the environment, flora and vegetation in the southwestern Mediterranean during the last two glacial-interglacial cycles.

## **2. Regional and local settings**

### *2.1. Sierra Nevada Range: geography, climate and vegetation*

The Sierra Nevada is an approximately 85 km long E-W aligned mountain range, located in southern Spain and presenting the highest peaks of the Iberian Peninsula (Mulhacén, 3479 m a.s.l.) (Fig. 3.1). It is one of the southernmost European areas to be glaciated (Schulte, 2002)

and, as a consequence of its southern latitude, Late Pleistocene snowlines were higher in the Sierra Nevada than in other Iberian mountain ranges (2300-2500 m) (Messerli, 1965; Gómez Ortiz et al., 2005).

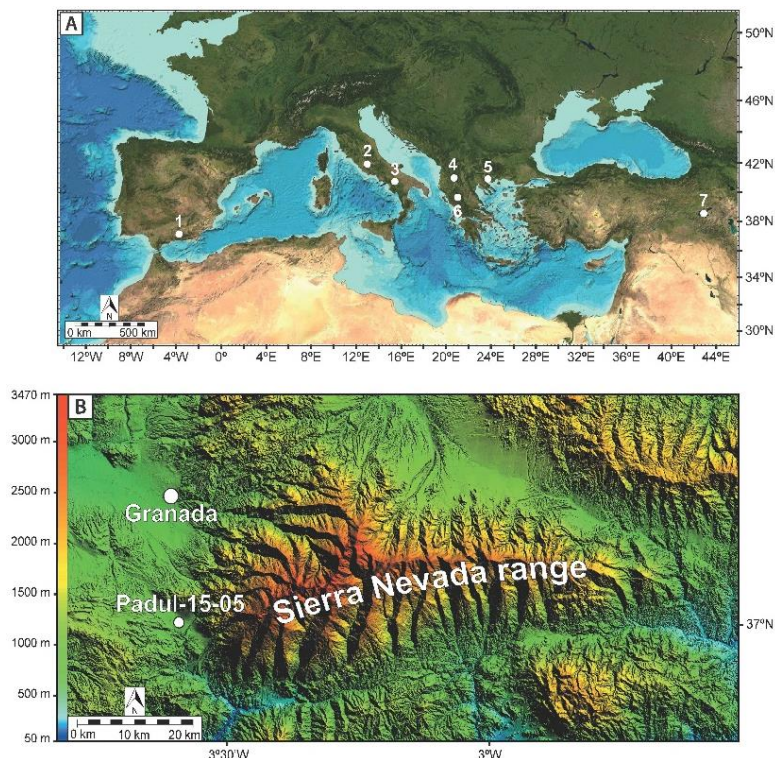


**Figure 3.1.** (A) Geographical locations of different long pollen records from the Mediterranean region numbered as: (1) Padul, (2) Valle di Castiglione, (3) Lago Grande di Monticchio, (4) Lake Ohrid, (5) Tenaghi Philippon, (6) Lake Ioannina and (7) Lake Van; (B) situation of the Padul-15-05 core in the western Sierra Nevada range and south of Granada city.

The intensive monitoring weather stations located in different sites of the Sierra Nevada, have recorded meteorological data ever hour since 2008, showing a mean annual temperature (MAT) of 11°C at 1735 m a.s.l. (Robledal de Cañar station) and a MAT of 2.5°C at 3097 m a.s.l. (Veleta station) (Pérez-Luque et al., 2012) (available in [http://wiki.obsnev.es/index.php/Estaciones\\_Monitoreo\\_Intensivo](http://wiki.obsnev.es/index.php/Estaciones_Monitoreo_Intensivo)). According to discontinuous records between 1965 and 1993, at ~2500 m a.s.l. the MAT is ~4.4°C with an annual precipitation of ~750 mm (García-Alix et al., 2018) (<http://linaria.obsnev.es/>). Precipitation at the highest altitudes areas of the Sierra Nevada (>2500 m a.s.l.) is mostly as snow and concentrated between October and April (Oliva et al., 2009). Precipitation in the Sierra Nevada is strongly controlled by humidity brought to the area by the westerlies and the North Atlantic Oscillation plays a major role controlling these.

The Sierra Nevada is one of the most important regions of plant diversity in the western Mediterranean, representing almost the 30% of the vascular plants of the Iberian Peninsula (Blanca et al., 2002). Vegetation in the Sierra Nevada range is strongly influenced by thermal and precipitation gradients (Valle, 2003), distributed in four different vegetation belts according to elevation. *Quercus coccifera* and *Pistacia lentiscus* are the main taxa in the lowest elevation thermomediterranean belt (~0 – 600 m a.s.l.). In the mesomediterranean vegetation belt (~600 – 1400 m a.s.l.), *Quercus rotundifolia* is the principal taxa, whereas the supramediterranean belt (~1400 – 1900 m a.s.l.) is characterized by *Quercus pyrenaica*, *Q. faginea*, *Q. rotundifolia*, *Acer opalus* subsp. *granatense* and *Fraxinus angustifolia* among other trees/shrubs and some herbs such as *Artemisia glutinosa*. The oromediterranean belt (~1900 – 2800 m a.s.l.) is mostly characterized by conifers, such as *Pinus sylvestris*, *P. nigra*, *Juniperus hemisphaerica*, *J. sabina* and *J. communis* subsp. *nana*, as well as some Fabaceae, Cistaceae and Brassicaceae. Finally, the crioromediterranean belt (>2800 m a.s.l.) is mainly depicted by tundra vegetation composed by different species of Poaceae, Asteraceae, Brassicaceae and Plantaginaceae between other herbs and also several endemic plants, such as *Erigeron frigidus*, *Saxifraga nevadensis* and *Viola crassiuscula*. For a more detailed information about vegetation occurring in the different Mediterranean vegetation belts, see Table 3.1.

Vegetation belt	Elevation (m)	Most characteristic taxa
Crioromediterranean	> 2800	<i>Festuca clementei</i> , <i>Hormathophylla purpurea</i> , <i>Erigeron frigidus</i> , <i>Saxifraga nevadensis</i> , <i>Viola crassiuscula</i> , <i>Linaria glacialis</i> and <i>Artemisia granatensis</i>
Oromediterranean	1900 - 2800	<i>Pinus sylvestris</i> , <i>P. nigra</i> , <i>Juniperus hemisphaerica</i> , <i>J. sabina</i> , <i>J. communis</i> subsp. <i>nana</i> , <i>Genista versicolor</i> , <i>Cytisus oromediterraneus</i> , <i>Hormathophylla spinosa</i> , <i>Prunus prostrata</i> , <i>Deschampsia iberica</i> and <i>Astragalus sempervirens</i> subsp. <i>nevadensis</i>
Supramediterranean	1400 - 1900	<i>Quercus pyrenaica</i> , <i>Q. faginea</i> , <i>Q. rotundifolia</i> , <i>Acer opalus</i> subsp. <i>granatense</i> , <i>Fraxinus angustifolia</i> , <i>Sorbus torminalis</i> , <i>Adenocarpus decorticans</i> , <i>Helleborus foetidus</i> , <i>Daphne gnidium</i> , <i>Clematis flammula</i> , <i>Cistus laurifolius</i> , <i>Berberis hispanicus</i> , <i>Festuca scariosa</i> and <i>Artemisia glutinosa</i>
Mesomediterranean	700 - 1400	<i>Quercus rotundifolia</i> , <i>Retama sphaerocarpa</i> , <i>Paeonia coriacea</i> , <i>Juniperus oxycedrus</i> , <i>Rubia peregrina</i> , <i>Asparagus acutifolius</i> , <i>Daphne gnidium</i> , <i>Ulex parviflorus</i> , <i>Genista umbellata</i> , <i>Cistus albidus</i> and <i>C. laurifolius</i>
Thermomediterranean	0 - 600	<i>Quercus coccifera</i> , <i>Pistacia lentiscus</i> , <i>Ceratonia siliqua</i> , <i>Osyris quadripartita</i> , <i>Aristolochia baetica</i> , <i>Chamaerops humilis</i> , <i>Lavandula multifida</i> , <i>Cistus</i> spp., <i>Pinus halepensis</i> and <i>P. pinea</i>

**Table 3.1.** Modern vegetation belts from the Sierra Nevada with the most characteristic taxa. Based and modified from El Aallali et al. (1998), Blanca et al. (2002) and Valle (2003).

## 2.2. Padul basin and wetland: geography, climate and vegetatio

The Padul wetland (726 m a.s.l.) is located in the western margin of the Sierra Nevada, 20 km south of Granada city (Andalusia, Spain). It covers an area of about 4 km<sup>2</sup>, within the NW-SE elongated Padul-Nigüelas extensional endorheic basin. The Padul-Nigüelas basin started to form during the Alpine orogeny, resulting in a basin of 12 km length, 4 km width and an area of 45 km<sup>2</sup>, delimited by normal faults related to extensional activity (still active today). The different displacement of the NE and the SW faults generated an asymmetric basin, allowing deeper sedimentation in the NE edge (Domingo García et al., 1983). Consequently, previous works on Padul presented different sedimentation rates depending on the drilling location, and

therefore, same lithological and vegetation changes occur at different depths. Sedimentary infilling seems to reach a thickness of at least 100 m (Domingo García et al., 1983; Nestares and Torres, 1998), mostly composed by peats and carbonate/marl intervals.

The Padul-Nigüelas basin is characterized by a Mediterranean climate with strong continental influence. Mean annual precipitation between 1971 and 2000 in Padul is around 445 mm/yr, being July and August the driest months (2 mm of rainfall) and December the most humid (68 mm). Mean annual temperature is 14.4°C, with warmest average temperature of 24.2°C during July and August and coldest average temperature of 6.4°C during January (agroclimap.aemet.es) (Fig. 3.2).

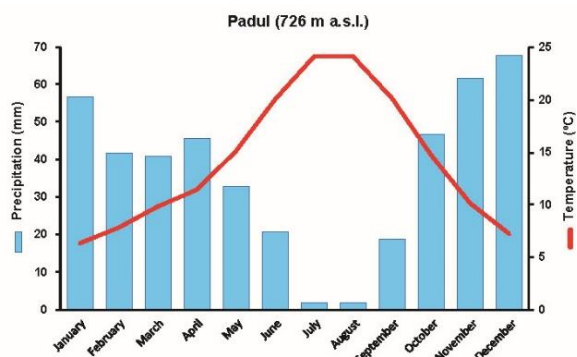


**Figure 3.2.** Climograph from Padul showing monthly distributed mean precipitation and temperature values.

Modern vegetation in the Padul wetland is principally dominated by wetland and aquatic communities, such as *Phragmites australis*, *Chara vulgaris*, *Myriophyllum spicatum*, *Potamogeton pectinatus*, *P. coloratus* and *Typha domingensis* among others. The surrounding areas of Padul are mostly characterized by the mesomediterranean vegetation with *Quercus rotundifolia*, *Q. faginea*, *Q. coccifera*, *Pistacia terebinthus*, *Populus alba*, *Ulmus minor*, *Fraxinus angustifolia*, *Celtis australis* and *Salix* spp. as principal tree taxa. With respect to shrubs, *Juniperus oxycedrus*, *Crataegus monogyna*, *Retama sphaerocarpa* and *Sambucus nigra* are the most common (Pérez Raya and López Nieto, 1991). For a more detailed vegetation of the Padul wetland see Table 3.2.

Vegetation	Most characteristic taxa
Trees	<i>Quercus rotundifolia</i> , <i>Q. faginea</i> , <i>Q. coccifera</i> , <i>Pistacia terebinthus</i> , <i>Populus alba</i> , <i>P. nigra</i> , <i>Ulmus minor</i> , <i>Tamarix gallica</i> , <i>Fraxinus angustifolia</i> , <i>Celtis australis</i> , <i>Ficus carica</i> and <i>Salix</i> spp.
Shrubs	<i>Juniperus oxycedrus</i> , <i>Crataegus monogyna</i> , <i>Daphne gnidium</i> , <i>Ruscus aculeatus</i> , <i>Retama sphaerocarpa</i> , <i>Genista cinerea</i> subs. <i>spectosa</i> and <i>Sambucus nigra</i>
Herbs	<i>Paeonia broteroi</i> and <i>Stipa tenacissima</i>
Creepers	<i>Lonicera implexa</i> , <i>Rubia peregriana</i> , <i>Hedera helix</i> and <i>Asparagus acutifolius</i>
Wetland and aquatic communities	<i>Phragmites australis</i> , <i>Chara vulgaris</i> , <i>Myriophyllum spicatum</i> , <i>Potamogeton pectinatus</i> , <i>P. coloratus</i> , <i>Typha domingensis</i> , <i>Apium nodiflorum</i> , <i>Juncus subnodulosus</i> , <i>J. bufonius</i> , <i>Carex hispida</i> and <i>Ranunculus muricatus</i>

**Table 3.2.** Most characteristic taxa around the Padul wetland. Based and modified from Pérez Raya and López Nieto (1991) and Ramos-Román (2018).

### 3. Materials and methods

#### 3.1. Padul-15-05 core: drilling and sampling

The 42.64 m long Padul-15-05 sedimentary core was taken in July 2015 at the edge of the actual Padul wetland (37°00′39″N, 3°36′14″W), using a Rolatec RL-48-L hydraulic percussion coring machine from the Scientific Instrumentation Center of the University of Granada. The core was sampled and stored in a cooler at 4°C in the Stratigraphy and Paleontology Department at the University of Granada.

#### 3.2. Chronology and age-depth model

The Holocene age-depth model of the Padul-15-05 core was previously carried out by Ramos-Román et al. (2018a, b). Later on, the Holocene part (0 – 3.67 m depth) along with the age-depth model until 23.27 m depth was developed based on a total of 42 AMS-Standard radiocarbon samples (including 3 samples from specific compounds) and 4 Amino Acid Racemization (AAR) samples from gastropods (3 of them averaged because they were within the errors of one another), using R-code package “Clam 2.2” software (Blaauw, 2010) under a locally weighted spline age-depth model at 95% confidence range. The age model from 23.27 m to 42.64 m depth (core bottom) was created using linear extrapolation with the peat and carbonate/marl sediment accumulation rates from the well dated upper part of the core ( $SAR_{peat} = 0.0365$  cm/yr and  $SAR_{carb} = 0.0136$  cm/yr) (Camuera et al., 2018). Following this method, the Padul-15-05 core contains a record of the last ~197,000 years (Fig. 3.3).



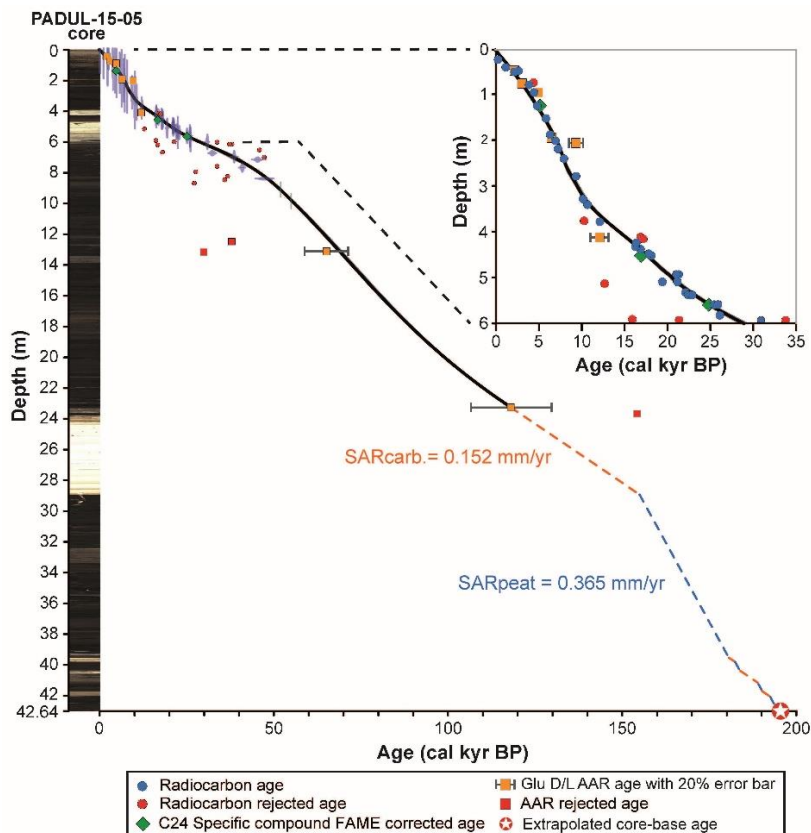


**Figure 3.3.** Age-depth model of the Padul-15-05 core along with the scanner photograph of the entire Padul-15-05 core. The right panel shows the detailed age-depth model of the upper 6 meters. Taken from Camuera et al. (2018).

### 3.3. Palynological analysis

A total of 414 samples including 176 samples from the Holocene (0 – 3.67 m depth) (Ramos-Román et al., 2018a, b) and 238 samples from the rest of the core (3.67 – 42.64 m depth) (this study) were studied for pollen analyses. Pollen extraction was done following a modified Faegri and Iversen (1989) methodology. Processing starts adding *Lycopodium* spores to 1 cm<sup>3</sup>/sample of sediment for the calculation of pollen concentration, followed by HCl, HF, NaOH and acetolysis procedures in order to remove carbonates, silicates, humic acid and organic matter, respectively. Sediment was also sieved at 250 µm and at 10 µm, with the purpose of removing the unnecessary remains. The final pollen residue was mixed with glycerin and prepared in slides for counting, using a Zeiss transmitted light microscope mainly at 400x magnification. A minimum of 300 terrestrial pollen grains per sample were identified. Pollen percentages were calculated based on the terrestrial pollen sum, not including aquatic plants (*Cyperaceae*, *Typha*, *Myriophyllum*, *Utricularia* and *Potamogeton*). Mediterranean forest pollen taxa is composed of

*Quercus* total, *Olea*, *Phillyrea* and *Pistacia*, whereas the sclerophyllous forest group (*Quercus* evergreen, *Olea*, *Phillyrea* and *Pistacia*) excludes deciduous *Quercus*. The temperate-humid forest includes *Quercus* deciduous, *Fraxinus*, *Acer*, *Alnus*, *Betula*, *Carpinus*, *Castanea*, *Celtis*, *Corylus*, *Salix*, *Ulmus*, *Abies* and *Taxus*. A xerophytes group was also made, which included *Artemisia*, *Amaranthaceae* and *Ephedra*. Differentiation between small (alpine) and large (Mediterranean) *Pinus* was not easy due to the high occurrence of undifferentiated pollen sizes, so it was plotted as *Pinus* total. However, slight size variations are perceptible between episodes of high climatic difference (e.g. Holocene and Last Glacial Maximum). Pollen zonation was made using the Tilia software cluster analysis Coniss, using *Quercus* total, *Olea*, *Pinus* total, *Pistacia*, *Artemisia*, Asteraceae Cichorioideae, Asteraceae Asteroideae, *Amaranthaceae* and *Poaceae* (Grimm, 1987). The most characteristic Non-Pollen Palynomorphs (NPPs) including algal and fungal spores are also included in the pollen analysis (Figs. 3.4 and 3.5). Algae are not included in the total pollen, therefore their relative values can exceed 100%. Lake level from Padul has also been reconstructed using pollen data from algae (*Pediastrum* + *Botryococcus* + *Mougeotia* + *Zygnema* type total), hygrophytes (*Cyperaceae* + *Typha*) and *Poaceae* as: Algae / (Algae + Hygrophytes + *Poaceae*).

#### 3.4. Pollen Climate Index (PCI)

The Pollen Climate Index (PCI) proposed by Joannin et al. (2011) and based on the mesothermic/steppic taxa ratio from Combourieu Nebout et al. (1999) was calculated in order to discriminate between cold/arid-glacial/stadial and warm/humid-interglacial/interstadial phases. Joannin et al. (2008, 2011), Bertini et al. (2015) and Toti (2018) used this pollen derived climate index for a relative paleotemperature reconstruction. However, some of the taxa used are not only responding to temperature but also to precipitation variability. As mesothermic taxa we included *Quercus* total, *Olea*, *Fraxinus*, *Phillyrea*, *Acer*, *Betula*, *Alnus*, *Ulmus*, *Taxus*, *Salix*, *Pistacia*, *Corylus* and *Carpinus* while as steppic taxa we included *Artemisia*, *Ephedra*, *Hippophaë* and *Amaranthaceae*. We follow the threshold value to separate between cold/arid and warm/humid periods defined by Bertini et al. (2015) and Toti (2018) at  $\sim 2$ , with lower values suggesting glacial/stadial phases ( $PCI < \sim 2$ ) and higher values suggesting interglacial/interstadials ( $PCI > \sim 2$ ).

#### 3.5. Principal Component Analysis (PCA)

PCA was developed with the aim of classifying different pollen species in simple groups of vegetation responding to different environmental and climate conditions. All the pollen data were normalized as:  $X = (x - \text{mean}) / \text{standard deviation}$ . This analysis was run using the PAST software (Hammer et al., 2001) on the most representative pollen taxa: *Quercus* evergreen, *Quercus* deciduous, *Olea*, *Pistacia*, *Pinus* total, *Cupressaceae*, *Artemisia*, *Amaranthaceae*, *Ephedra*, *Ericaceae*, *Poaceae*, *Cyperaceae*, *Botryococcus* and *Pediastrum*.

### 3.6. Spectral analysis

Spectral analysis was done using the entire time series data from the Mediterranean forest, *Pinus* and Pollen Climate Index (PCI) with the aim of obtaining periodicities of the regional vegetation, climate and local lake conditions in the Padul-15-05 core. Cyclicities were obtained using the PAST software (Hammer et al., 2001) under a Redfit spectral analysis type, based on a rectangular window function with the standard value of 2 for both segments and oversample parameters. We focused on statistically significant peaks with frequencies below 0.000225 (4,500 years) with the purpose of highlighting the orbital-scale amplitude cycles (Fig. 3.7). The higher frequency cycles are not statistically representative when studying the entire record, as the pollen analysis from ~50 to 197 kyr BP presents relatively lower resolution (~1,500 year resolution) with respect to age range between ~50 – 11.5 kyr BP (~250 year resolution) and the Holocene section studied by Ramos-Román et al. (2018b) (~65 year resolution). Mediterranean forest has been proven to be a good indicator of Mediterranean climate changes (Tzedakis, 2007; Sánchez Goñi et al., 2008; Fletcher et al., 2010a; Jiménez-Moreno et al., 2013; Ramos-Román et al., 2018a). Therefore, Mediterranean forest data has been filtered based on the frequency of the most statistically significant spectral peak obtained (see sections 4.3 and 5.2.1) in order to compare with insolation cycles.

## 4. Results

### 4.1 Palynological results

The most representative 57 taxa (18 trees, 5 shrubs, 24 herbs and grasses, 4 aquatic plants, 4 algae and 2 NPPs), with percentages higher than 1% are presented in Figures 3.4 and 3.5. *Pinus* seems to be overrepresented as in many palynological studies from the Iberian Peninsula (Franco Múgica et al., 1998; García-Antón et al., 2011; Morales-Molino et al., 2011), so it has been described after the rest of the taxa when explaining species percentages for the different pollen zones (explained below). Note that the resolution is much higher from ~60 kyr BP until present, and therefore, smaller millennial-scale oscillations in all taxa are more common.

The Padul-15-05 pollen record was divided in 4 pollen zones with some subdivisions using cluster analysis. Pollen zones are described below, starting from the oldest part of the core until present:

#### 4.1.1. Zone 4 (~197 kyr – 135 kyr BP / 42.64 m – 26 m depth)

Zone 4 is divided in 3 subzones (Zones 4c, 4b and 4a), generally characterized by the abundance of herbs and grasses such as *Artemisia* or *Amaranthaceae*, and low percentages of trees such as *Quercus* or *Olea*.

Zone 4c (~197 kyr – 181 kyr BP / 42.64 m – 39 m depth) is the oldest zone composed by high average percentages of xerophytes (~15%), including *Artemisia* (~9% average), *Amaranthaceae* (~4% average) and *Ephedra* (~2% average). On the contrary, the most abundant

trees (excluding *Pinus*) *Quercus* evergreen and deciduous never reach 5%. The average *Quercus* total is lower than 2%, while Cupressaceae presents some peaks that reach a 9%. Average percentages of hygrophytes are around 24% while algae only present some isolated peaks, with maximum values of 31%. *Pinus* average in this subzone is ~66%.

Zone 4b (~181 kyr – 153 kyr BP / 39 m – 28.5 m depth) presents slightly higher tree abundances and lower amounts of herbs and grasses. In this sense, *Quercus* total presents maximum values of 20% with an average of ~6% while xerophytes show an average percentage decrease (~10%). Poaceae increases until reaching maximum peaks of ~48% and average values of ~20%. According to *Fraxinus*, *Acer*, *Alnus* and *Betula*, they all present some isolated peaks (<2%). Note that *Abies* occurs for the first time in the core with a maximum peak of ~4%. Hygrophytes and algae do not present very important changes with respect to the previous zone. *Pinus* average values are ~52%.

Zone 4a (~153 kyr – 135 kyr BP / 28.5 m – 26 m depth) again shows an increase in herbs and grasses, but the most representative tree taxa (*Quercus* total) keeps similar percentages than in the previous zone (~8% average). Xerophytes increase their average values up to ~25%, with maximum *Artemisia* peaks of ~42% (~16% average), maximum Amaranthaceae of ~19% (~8% average) and maximum *Ephedra* of ~3% (~1% average), similar to Zone 4c. Poaceae decreases to ~5% average as also occur with hygrophytes, changing from ~22% average (Zones 4c and 4b) to practically nonexistent (<1% average). On the contrary, algae increase, with minimum values of 16% and average values of ~37%. Note that Cupressaceae also increases again up to ~4% average with maximum peaks of ~9%. *Pinus* average percentage is ~53%.

#### 4.1.2. Zone 3 (~135 kyr – 60 kyr BP / 26 m – 11 m depth)

Zone 3 is divided in 4 subzones (Zones 3d, 3c, 3b and 3a) with important vegetation changes.

Zone 3d (~135 kyr – 104 kyr BP / 26 m – 21 m depth) is composed of varying but overall abundant tree pollen content. Maximum Mediterranean forest percentages are around 57% with average value of ~34%. Moreover, *Quercus* deciduous reaches the highest peak of the entire record (~43%) at 121 kyr BP. The presence of *Olea*, *Fraxinus*, *Alnus*, *Betula* and *Pistacia* is common, even if percentages are low (<5%). It must be mentioned the noteworthy decrease in the Mediterranean forest taxa (mainly in *Quercus* evergreen, *Quercus* deciduous and *Pistacia*) between ~120 – 117 kyr BP. On the other hand, herbs and grasses are very low. The average percentage of xerophytes is ~3%, with maximum values never exceeding 9%. Note that the first half of this Zone 3d (~135 – 125 kyr BP) presents high algae (~50% average) (mainly *Botryococcus*), and low Poaceae and hygrophytes values (~5% and ~3% average, respectively), while during the second part (~125 – 112 kyr BP), algae decrease (~5% average) and Poaceae and hygrophytes increase (~12% and ~17% average, respectively). During the second half of this pollen zone, the abundance of Cistaceae also increases. The occurrence of *Carpinus* is also remarkable in this zone, even if its maximum abundance does not reach 1%. Average values of *Pinus* are ~44%.

Zone 3c (~104 kyr – 79 kyr BP / 21 m – 15.5 m depth) shows an important vegetation change with respect to the previous Zone 3d. Tree pollen abundance decreases, well reflected in the

decline in the Mediterranean forest average values (~4%). On the contrary, xerophytes increase to ~19% average, with a maximum peak of ~48%. The maximum peak of *Artemisia* reaches the ~27%, Amaranthaceae the ~21% and *Ephedra* the ~4%. Even if hygrophytes present relatively high average percentages (~35%), a distinctive decrease occur between ~98 – 91 kyr BP. Note that *Botryococcus* shows an increase in the second half of the zone, from ~90 kyr to 81 kyr BP. *Pinus* presents average percentage of ~61%.

Zone 3b (~79 kyr – 71 kyr BP / 15.5 m – 13.5 m depth) again shows an increase in the abundance of tree pollen and a decline in herbs and grasses. This is evident in the increase of the Mediterranean forest (~36% average), produced by high average values of *Quercus* total (~26%), *Olea* (~5%), *Pistacia* (~4%) and *Phillyrea* (~1%). *Olea* presents relatively high percentages in this zone, reaching maximum values of 8% similar to the most recent pollen Zone 1. Most characteristic herb and grass taxa disappear, such as *Artemisia*, Amaranthaceae and *Ephedra*. The occurrence of Ericaceae increases in this zone, with average values of ~4% and maximum peaks of ~9%. Average hygrophyte values decrease to ~18%, while algae almost disappear (<1% average). Average *Pinus* values decrease with respect to previous and next zones, presenting a ~29%.

Zone 3a (~71 kyr – 60 kyr BP / 13.5 m – 11 m depth) is characterized by a slight decline in arboreal pollen due to the decrease in almost all tree taxa, such as *Quercus* total (~10% average). *Alnus* presents some peaks reaching 1.5%, as also occurs with *Abies* and *Cedrus*. With respect to herbs and grasses, xerophytes are very low (~1% average), while Ericaceae shows a number of peaks reaching ~12%. Moreover, Cistaceae presents the highest values of the record (~6%), as also occurs with *Glomus* NPP (~22%). Hygrophytes slightly increase to average values ~28%, while algae do not show changes (<1% average). *Pinus* average percentage is ~57%.

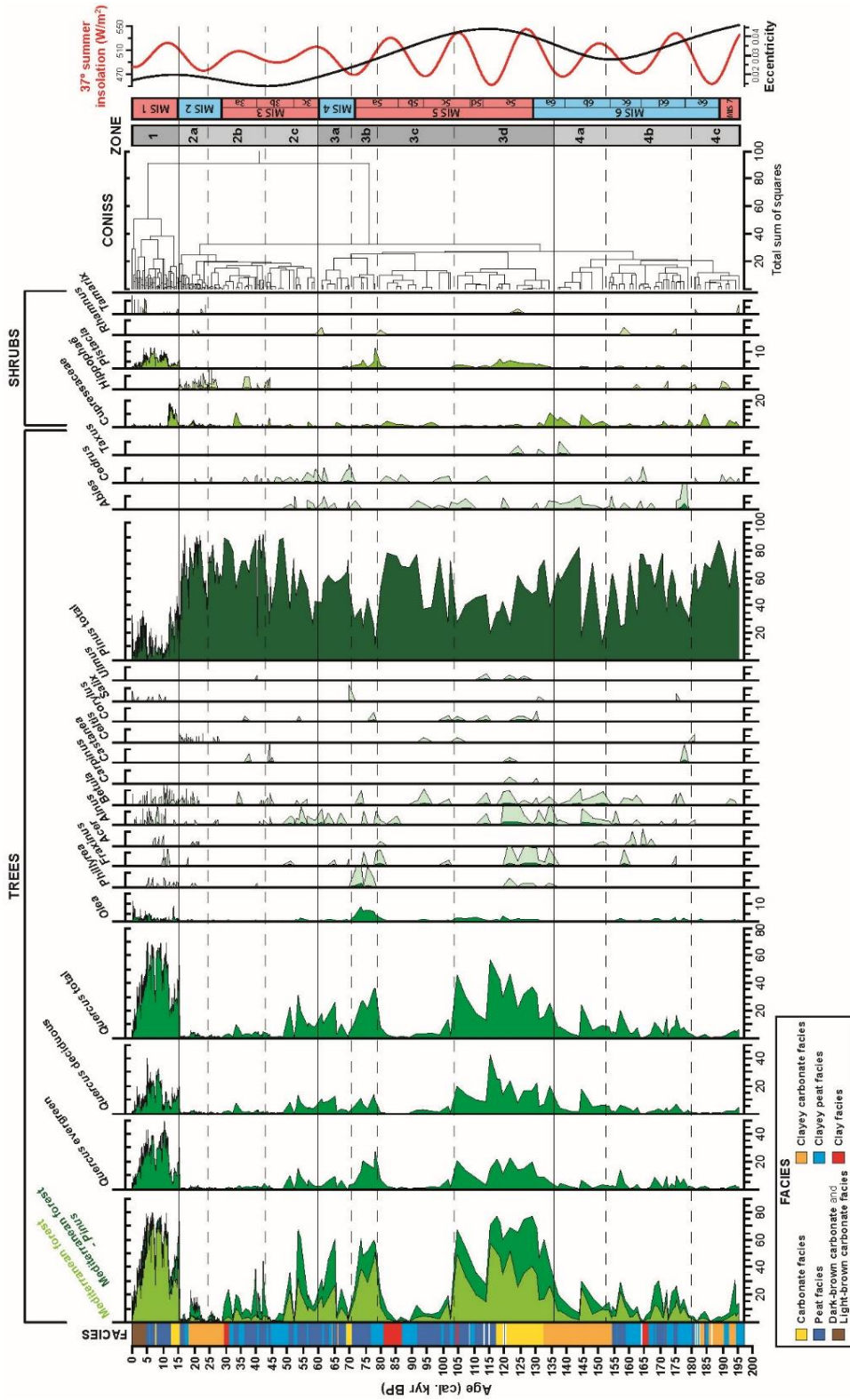


**Figure 3.4.** Percentages of the most characteristic selected tree (green) and shrub (light green), calculated with respect to the total terrestrial pollen sum. Silhouettes in lighter color show 10x exaggeration percentages. The Mediterranean forest taxa category is composed by *Quercus* total, *Olea*, *Phillyrea* and *Pistacia*. Facies are shown on the left. Pollen zones, Marine Isotope Stages (MISs), and summer insolation and eccentricity are shown on the right.



Vegetation and climate changes during the last two glacial-interglacial cycles in the western Mediterranean: a new long pollen record from Padul (southern Iberian Peninsula)

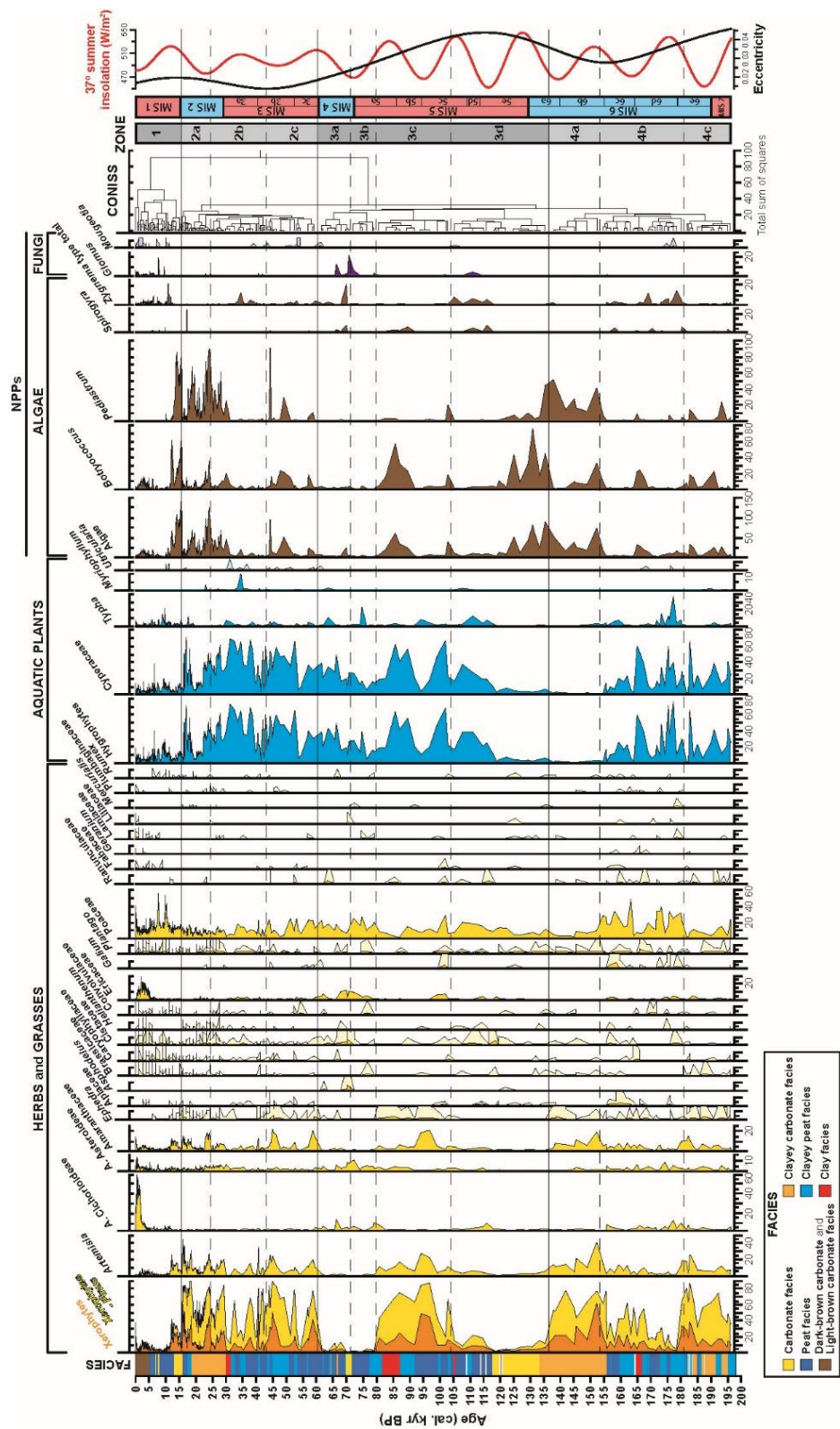


**Figure 3.5.** Percentages of the most characteristic selected herbs/grasses (yellow), aquatic plants (blue), algae (brown) and NPP (purple) taxa. Herbs/grasses were calculated with respect to the total terrestrial pollen sum. Silhouettes in lighter color show 10x exaggeration percentages. The xerophyte taxa category is composed by *Artemisia*, *Amaranthaceae* and *Ephedra*. Facies are shown on the left. Pollen zones, Marine Isotope Stages (MISs), and summer insolation and eccentricity are shown on the right.

#### 4.1.3. Zone 2 (~60 kyr – 15 kyr BP / 11 m – 4.17 m depth)

Zone 2c (~60 – 43 kyr BP / 11 m – 8 m depth) is characterized by a significant pollen change, with relatively high Mediterranean forest values during the first half until ~51 kyr (~12% average) and considerably decreasing during the second half of the zone until ~43 kyr BP (~1% average). In addition, the last occurrence of *Abies* in the core also occurs at ~51 kyr BP. *Alnus* occurs with small amounts (maximum values of 1.5%) throughout this zone. On the contrary, xerophytes experience a very high increase in average values (~21%) due to high relative percentages of *Artemisia* (~12% average), *Amaranthaceae* (~8% average) and *Ephedra* (~1% average). With respect to hygrophytes and algae, both increase with respect to the previous Zone 3a (~40% and 16% average, respectively). *Pinus* average is ~53%.

Zone 2b (~43 – 24.5 kyr BP / 8 m – 5.5 m depth) presents very low Mediterranean forest percentages (~2% average), in particular during the second half of this Zone 2b (~33 – 24.5 kyr BP). *Quercus* and *Cupressaceae* present a small peak at ~34 kyr BP. Xerophytes occur with average values of ~11%. Some herbs are more common during the second half (~36 – 24.5 kyr BP), such as *Asteroidae* (max. values of 6%) and small increases in *Cistaceae* (and *Helianthemum*) and *Convolvulaceae* (both with maximum peaks of 2%). Moreover, algae also increase notably in the final part of this zone between ~30 and 24.5 kyr, changing from ~3% to 34% average values. Hygrophytes have average percentages of 37%, with lower abundance during the beginning and the final part of the zone. *Pinus* reach the highest average values in the core (~72%).

Zone 2a (~24.5 – 15 kyr BP / 5.5 m – 4.17 m depth) shows a similar general pattern with respect to the Mediterranean forest (~1.5% average) and xerophyte taxa (~18% average) than in the previous zone, with small millennial-scale changes. *Hippophaë* is more common than in previous pollen zones even if percentages are low (max. values of ~1%). Aquatic plants (hygrophytes) and algae show several oscillations, with average values of ~21% for hygrophytes and ~30% for algae. *Pinus* has average values of 67%.

#### 4.1.4. Zone 1 (~15 kyr BP – present / 4.17 m – 0 m depth)

Zone 1 (15 – 0 kyr BP / 4.17 – 0 m depth) is composed of a remarkable increase in the arboreal forest, reflected in a drastic Mediterranean forest increase (~42% average with maximum peaks of ~77%) due to increase in both evergreen and deciduous *Quercus* (~23% and 9% average, respectively), *Pistacia* (~4% average) and *Olea* (~2% average). Other tree taxa are also very common, such as *Betula* or *Alnus*. In contrast to tree taxa, percentages of herbs/grasses, aquatic plants and algae decrease, reflected in low xerophyte (~6% average), hygrophyte (~7% average) and algae values (13% average). It must be mentioned that during the first 3,500 years of the zone (~15 to 11.5 kyr BP), the Mediterranean forest percentages are not as high as during the Holocene (the last 11.5 kyr), and xerophyte values are higher. Moreover, *Pinus*, *Cupressaceae* and algae also present totally different trends during the first 3,500 years, showing much higher percentages. The average *Pinus* percentage in the entire zone presents the lowest



values of the core (~14%). For more specific and detailed results and interpretations of the Holocene pollen data see Ramos-Román et al. (2018a, b).

#### 4.2. Principal Component Analysis (PCA)

The PCA results are represented on a scatter plot (Fig. 3.6), showing the Principal Component 1 (PC1) and Principal Component 2 (PC2). PC1 explains a 31.66% of the total variance and PC2 the 13.26%. The rest of the Principal Components represent percentages lower than 10%. Data results have been assembled in 3 main groups, classified as Group 1 (GR1), Group 2 (GR2) and Group 3 (GR3). The GR1 was separated with respect to GR2 and GR3 because of its negative loading to PC1, whereas GR2 and GR3 were separated according to their opposite loading to PC2. Consequently, groups are composed by: a) GR1: *Quercus* evergreen, *Quercus* deciduous, *Pistacia*, *Olea*, Ericaceae and Poaceae; b) GR2: *Artemisia*, Amaranthaceae, *Ephedra*, Cupressaceae, *Botryococcus* and *Pediastrum*; and c) GR3: *Pinus* total and Cyperaceae.

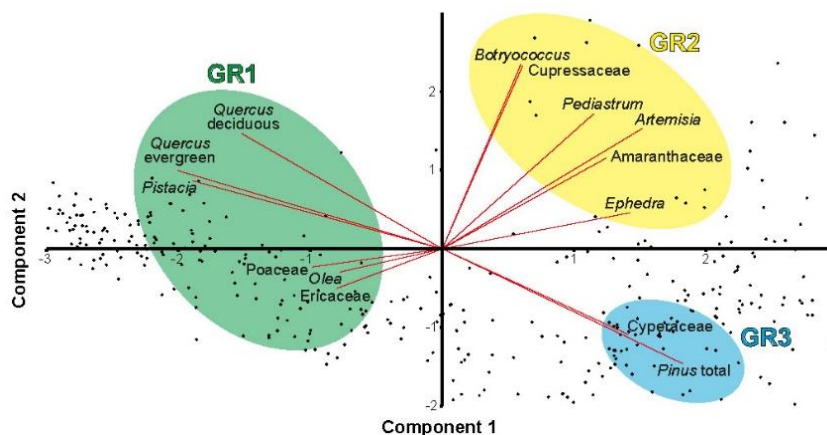


**Figure 3.6.** The Principal Component Analysis (PCA) from different pollen taxa showing the scatter plot with PC1 and PC2 axis.

#### 4.3. Spectral analysis

The spectral analysis was performed on the most characteristic climate proxy (PCI) and pollen group (Mediterranean forest), and on one of the most abundant pollen genus (*Pinus* total), focusing on the lowest frequency cycle with the purpose of comparing with orbital-scale oscillations. This analysis shows significant spectral peaks at ca. 23.7, 23 and 21.8 kyr periodicities for *Pinus* total, Mediterranean forest and PCI, respectively, all above >80% confidence interval (Fig. 3.7).

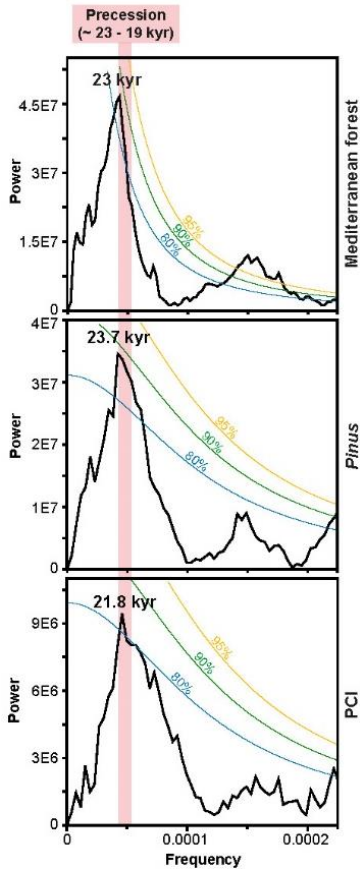


**Figure 3.7.** Spectral analysis developed on the Mediterranean forest, *Pinus* and Pollen Climate Index (PCI) data. Cycles below frequencies of 0.000225 (4,500 years) are shown. Confidence intervals of 80% (blue), 90% (green) and 95% (yellow) are shown. The age range of the precession cycle (~23 – 19 kyr) has also been marked.

## 5. Discussion

### 5.1. Vegetation and climate reconstruction: from MIS 6 to MIS 1

Pollen data from the Padul-15-05 core allow us to characterize vegetation and climate changes during the last two glacial-interglacial cycles of the last ~197 kyr. The Padul wetland is located within the Mesomediterranean vegetation belt and movement of forest species in elevation, towards higher elevation during warmings and towards lower elevation during coolings, and variations in the forest composition and density depending of climate, are expected through time. Here we describe chronologically vegetation changes associated to environmental and climate changes, starting from the penultimate glacial period until the present interglacial. Note that the chronological limits of Marine Isotope Stages/Substages (MIS) added in the Figures 3.4, 3.5, 3.8, 3.11 and 3.12 (in red and blue colors) do not perfectly fit with climate changes in Padul due to age uncertainties, leads and/or lags. Therefore, we used the ages from the Padul chronology [examples: MIS 6d (~178 – 168 kyr BP) or MIS 5a (~80 – 71 kyr BP)] when describing vegetation changes in Padul associated with Marine Isotope Stages/Substages.

### *5.1.1. Penultimate glacial period (MIS 6)*

The age data from Padul-15-05 indicates that the first glacial phase identified by the pollen record is the penultimate glacial period MIS 6. The beginning of this glacial cycle (MIS 6e between ~190 – 181 kyr BP, pollen Zone 4c) occurred after a Mediterranean forest decline from the previous interglacial MIS 7 and was characterized by the coldest and most arid climate in the region during the penultimate glacial period, indicated by high xerophyte and the lowest PCI values (Figs. 3.5 and 3.8a). This matches well with dry and cold conditions at  $185.13 \pm 13$  kyr BP deduced from a mammalian molar tooth from the Iberian Peninsula studied by (Cortés-Sánchez et al., 2016). During MIS 6d and 6c (~181 – 153 kyr BP, pollen Zone 4b), a slight increase in the Mediterranean taxa and in temperate-humid forest, along with the occurrence of the highest *Abies* peak at ~178 kyr BP, suggested relatively higher moisture climate conditions compared with the previous MIS 6e (Figs. 3.4 and 3.8d, e). In addition, the PCI and sclerophyllous trees also indicated warmer climate especially during MIS 6d (~178 – 168 kyr BP) (Fig. 3.8a, c). These data corroborate the high humid conditions at the beginning of MIS 6d (~180 kyr BP) expressed by different evidences in the Mediterranean region, such as the continental and marine pollen records from Lake Ioannina (Roucoux et al., 2011) and MD01-2444 (Margari et al., 2010, 2014), the  $\delta^{13}\text{C}$  and  $\delta^{18}\text{O}$  isotope records from speleothems in the Gitana Cave (SE Spain) (Hodge et al., 2008) and Soreq Cave (Israel) (Bar-Matthews et al., 2003), and isotopes from foraminifera (Kallel et al., 2000) and the sapropel S6 deposition (Bard et al., 2002; Kallel et al., 2004) in the Mediterranean Sea. All these data show higher pluvial conditions and/or higher runoff in the Mediterranean region at that time.

*Artemisia*, *Ephedra* and *Amaranthaceae* (i.e., crioromediterranean vegetation) dominated the vegetation during the MIS 6b and 6a (~150 – 135 kyr BP) but decreased with time, suggesting the disappearance of the cold and arid climate taxa at the end of the penultimate glacial cycle (Fig. 3.5). Furthermore, the decreasing trend between ~144 to 135 kyr BP of the cold/dry tolerant *Pinus* taxa (along with *Cupressaceae*, mainly *Juniperus* type) characteristic from the supra- and oromediterranean belt could have also been related to a treeline movement towards higher elevations due to the glacial-interglacial transitional climate warming (Fig. 3.4). At ~135 kyr BP, xerophytes presented a drastic decrease, reaching values below 5%, while warmer/wetter taxa such as Mediterranean forest and temperate-humid forest developed (especially, *Quercus* deciduous, *Fraxinus* and *Alnus*). Nevertheless, the Mediterranean forest and AP/NAP ratio did not show a definitive increase until ~131 kyr BP, when *Cupressaceae* totally disappeared (Figs. 3.4 and 3.8b, c, d). The decrease in the Mediterranean forest, and specially, in the temperate-humid forest between 133 – 131 kyr BP should be remarked (Fig. 3.8c, d), which could be related to the Heinrich Stadial 11 (in particular, HS11.2 and HS11.3), similar to that recently recorded by Tzedakis et al. (2018). The ~4,000-year-long transition (between ~135 and ~131 kyr BP) points into Termination II, with a similar time duration of about 5,000 years suggested by Tzedakis (2005).

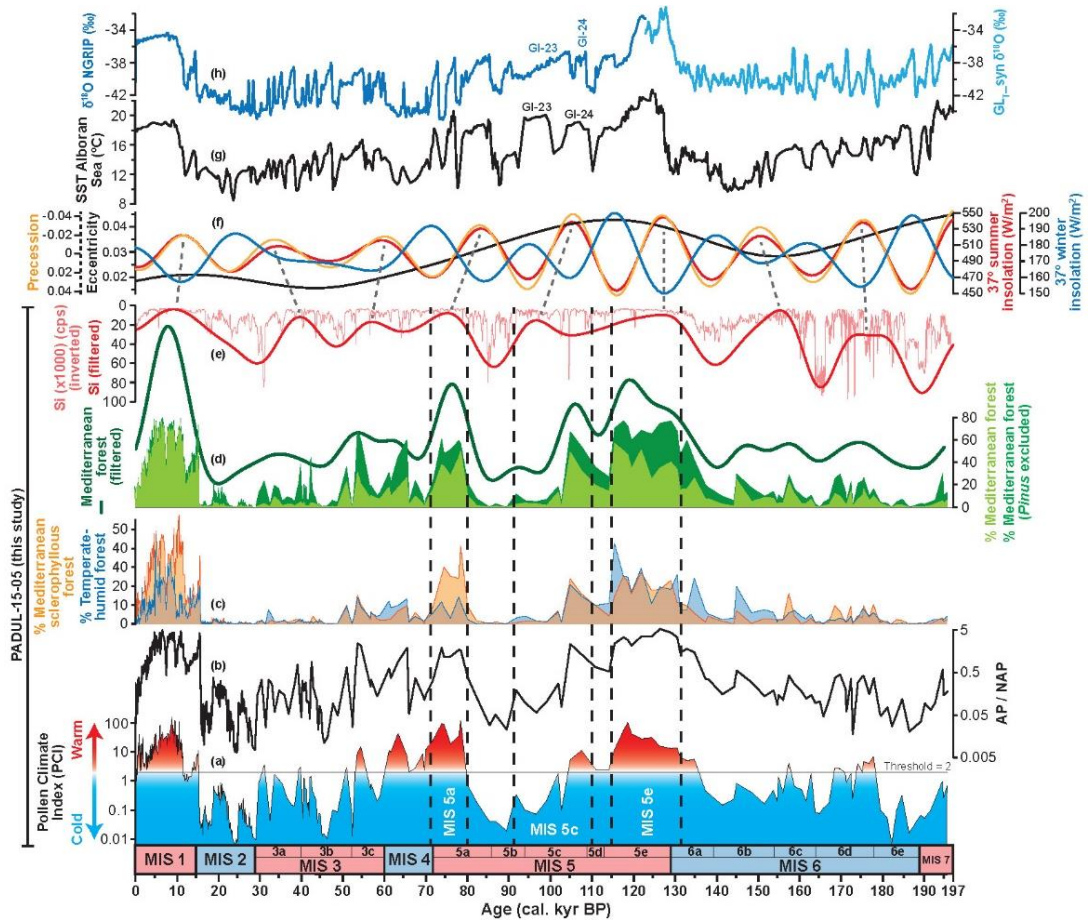


**Figure 3.8.** Representation of different plots showing from bottom to top: (a) the Pollen Climate Index (PCI) with the horizontal black line (value  $\sim 2$ ) indicating the boundary between glacial/stadial and interglacial/interstadial phases; (b) AP/NAP (Arboreal Pollen/Non Arboreal Pollen) ratio (the AP also includes *Pinus*), on a logarithmic scale; (c) Percentages of the Mediterranean sclerophyllous forest (orange) and temperate-humid forest (blue); (d) Mediterranean forest pollen percentages including *Pinus* (light green) and excluding *Pinus* (dark green) with respect to the total terrestrial pollen sum along with the filtered Mediterranean forest data (green line); (e) silica data (in counts per second) (inverted scale) and filtered silica data (red line); (f) precession (orange), eccentricity (black), and summer and winter insolation at  $37^\circ\text{N}$  ( $\text{W}/\text{m}^2$ ) (red and blue, respectively). Summer insolation has been correlated with the Padul data (based on silicon and Mediterranean forest filtering) with grey dashed lines; (g) Sea Surface Temperature (SST) ( $^\circ\text{C}$ ) record from Alboran Sea (Martrat et al., 2004) of the last two glacial-interglacial cycles; (h)  $\delta^{18}\text{O}$  values from NGRIP ( $\text{‰ VSMOW}$ ) (NGRIP-Members, 2004) and  $\text{GL}_{\text{syn}} \delta^{18}\text{O}$  record ( $\text{‰ VSMOW}$ ) (Barker et al., 2011). Marine Isotope Stage (MIS) 6 and substages have been ascribed following the Table 1 from Sun and An (2005). MIS 5 and substages are based on the SST from (Martrat et al., 2004) and vegetation data from Milner et al. (2016). Finally, MIS 4, 3, 2 and 1 have been delimited according to vegetation changes from Fletcher et al. (2010a). Vertical black dashed lines (in graphs from a to e; data from this study) are delimiting the MIS 5e, 5c and 5a (written in white letters on graph a) according to our Padul-15-05 data and chronology, not exactly fitting with the MIS chronology shown in the age axis.

### 5.1.2. Last interglacial period (MIS 5)

After ~131 kyr ago during the MIS 5e, the oromediterranean vegetation continued to decrease (principally because of *Pinus* and Cupressaceae) whereas the mesomediterranean vegetation belt established around the Padul wetland. The gradual increase in the Mediterranean sclerophyllous taxa such as *Quercus ilex-coccifera* and *Pistacia*, along with the occurrence of moisture-demanding species such as *Quercus* deciduous, *Betula*, *Alnus* and *Fraxinus*, among others, between ~131 – 124 kyr BP is indicative of the beginning of a warm and wet interglacial climate. However, maximum moisture conditions in the southern Iberian Peninsula were reached between ~124 – 115 kyr BP (maximum at ~115 kyr BP), shown by the expansion of the temperate-humid forest mainly as result of the higher increase of *Quercus* deciduous, *Alnus*, *Betula*, *Carpinus* and *Abies* (Fig. 3.4 and 3.8c). Tzedakis (2007) suggested that the mediterranean sclerophyllous and summer-drought resistant taxa expanded during the maximum summer insolation, whereas humid-demanding species developed later in relation with decreasing summer insolation and less-seasonal climate, which is well represented in the Padul pollen record (Fig. 3.8c). The MD99-2331 marine record from the NW Iberian Margin also recorded a similar pattern, with an increase in temperate-humid taxa at ~123 kyr BP and later on, higher moisture conditions with decreasing sea surface temperature represented by the highest presence of *Carpinus betulus* at ~115 kyr BP [see Fig. 3 from Sánchez Goñi et al. (2005)].

A evident decrease in the Mediterranean forest in Padul between ~115 and 110 kyr BP suggest a relatively fast cold event that could be related to the MIS 5d stadial, while the later warm period from ~110 to 104 kyr BP could be linked to the Greenland interstadial 24 (GI-24) from the first half of the MIS 5c, similar to the Sea Surface Temperature (SST) record from Alboran Sea (Martrat et al., 2004) (Fig. 3.8g). Nevertheless, the second part of the MIS 5c well described in the Greenland ice-core record as Greenland interstadial 23 (GI-23) (Fig. 3.8h) is not well represented in Padul as other interglacial and interstadial periods. The Mediterranean forest in Padul shows very low occurrences during the second part of MIS 5c (also called Saint Germain Ic interstadial), whereas xerophytes and *Pinus* were well represented. This suggests a less marked ocean advection and higher continental climate conditions with a deficit in winter precipitation (Pons et al., 1992), which might have favored the expansion of coniferous forest in this area.

The transition from the MIS 5c to MIS 5a (~97 – 71 kyr BP) in the Padul-15-05 record is characterized by a sequence of vegetation changes, starting with the high occurrence of xerophytes at ~97 – 92 kyr BP (second half of MIS 5c) representing coldest/driest conditions, changing to high *Pinus* values from ~92 – 80 kyr BP (MIS 5b) and concluding with a significant Mediterranean forest and temperate-humid forest increase indicative of warm and more humid conditions between ~80 – 71 kyr ago (MIS 5a *sensu lato*, the age difference with respect to MIS 5a could be due to dating uncertainties) (Figs. 3.4, 3.5 and 3.8c, d). This transition shows glacial/stadial-interglacial/interstadial vegetation changes similar to the idealized glacial-interglacial vegetation cycle described by Tzedakis (2007) for southern Europe. The *Pinus* occurrence (most likely *P. sylvestris* and *P. nigra*) along with Cupressaceae and high silica

values during MIS 5b suggest a lowering in elevation of the oromediterranean belt and treeline due to cooling, reducing the density of the forest and allowing a higher erosion and siliciclastic input into lower elevation areas (i.e., Padul) (Figs. 3.4 and 3.9). On the other hand, MIS 5a interstadial corresponding to pollen Zone 3b suggested warm and relatively humid climate without intense droughts deduced by increasing Mediterranean forest taxa (especially *Olea*, compared with the rest of the core), sclerophyllous and temperate-humid forest and PCI, and decreasing *Pinus*, total absence of xerophytes and low silica values, which resulted from higher forest cover and lower erosion (Figs. 3.4, 3.5 and 3.8a to 8e).

### 5.1.3. Last glacial period (MIS 4, MIS 3 and MIS 2)

The earliest part of MIS 4 is characterized by the abundance of Ericaceae that suggest decreasing summer insolation but still humid conditions (with minimum xerophytes) (Fig. 3.5). This agrees with Fletcher and Sánchez Goñi (2008), who suggested that the expansion of Ericaceae is related to minimum boreal summer insolation which reduced seasonality, and therefore, declined summer aridity and increased availability in annual moisture. Thereafter, the last glacial cycle started with a transitional forest cover during MIS 4 (pollen Zone 3a, ~71 – 60 kyr BP) mainly represented by *Pinus* and Ericaceae during the early MIS 4 pointing into cool and humid conditions, changing into also humid but warmer taxa represented by *Quercus* deciduous during the late MIS 4. This pattern from cold/humid to warm/humid climate for the MIS 4 is also represented by the increasing PCI and temperate-humid forest values during this period (Fig. 3.8a, c).

The MIS 3c is characterized by an early dry period between ~60 – 55 kyr BP with high xerophytes changing into warmer/wetter phase at ~55 kyr BP with *Quercus* evergreen and deciduous as principal taxa. This PCI, Mediterranean forest and arboreal pollen increase between ~55 – 50 kyr BP seems to be related to the warmest climate conditions in this region during both MIS 3 and MIS 2, also recorded by the highest SST in the Alboran Sea (Martrat et al., 2004) and in Greenland (Greenland interstadial 14) (NGRIP-Members, 2004) (Fig. 3.8a, b, c, d, g, h). The MIS 3b showed a very cold and arid period recorded by high xerophytes, absence of Mediterranean forest and very low PCI values (Figs. 3.5 and 3.8a, d). Moreover, moisture-demanding taxa such as *Quercus* deciduous and *Abies* disappeared during the beginning of MIS 3b ~52 kyr ago (Fig. 3.4). The MIS 3a showed a recovery of the forest cover represented by slightly higher Mediterranean forest and PCI values, with lower silica and xerophytes (Figs. 3.5 and 3.8a, d, e).

The MIS 2 is characterized by the most extreme glacial conditions at ~24 kyr BP during the Last Glacial Maximum (LGM) expressed by the lowest PCI values, which seems to be coincident in time with the SST from Alboran Sea (Martrat et al., 2004; Jiménez-Espejo et al., 2007) (Fig. 3.8a, g).

The last glacial period, from the beginning of MIS 4 to the end of MIS 2, is characterized by a decreasing trend in warm and humid taxa, such as the Mediterranean forest (mainly *Quercus* evergreen and deciduous), *Alnus* and *Abies*, as well as in PCI values, opposite to the increasing occurrence of *Pinus* and *Hippophaë* (Figs. 3.4 and 3.8a, d). Xerophytes presented high values



during the entire glacial period, but pointing into progressively colder and more arid conditions with significant smaller-scale oscillations probably due to millennial-scale variability (Fig. 3.5). Some of these millennial-scale oscillations observed in the xerophytes, Mediterranean forest and PCI values have also been recorded in the Alboran Sea and SW Iberian Margin and have been linked to Heinrich and D-O-like variability during the last glacial period (Sánchez Goñi et al. 2000, 2002). Furthermore, even if Mediterranean and alpine *Pinus* have not been differentiated due to their difficulty for classification, during the final part of the last glacial cycles (mainly during MIS 2) *Pinus* pollen grains were generally smaller than during previous periods, which could be indicating the abundance of subalpine pine species adapted to colder conditions, which are characterized by its smaller pollen size (Desprat et al., 2015). During cold/arid phases higher altitude vegetation belts from the Sierra Nevada probably moved to lower elevations, allowing the presence of supramediterranean, oromediterranean and crioromediterranean herbs and alpine tree species (e.g. *Pinus sylvestris* and *P. nigra*) into lower elevation areas such as Padul (Fig. 3.9).

Regardless of the above-mentioned findings, the continuous occurrences of *Quercus*, and the sporadic presence of other thermophytes such as *Olea* support the view that glacial refugia for temperate woods may have lied in the surrounding mountain valleys of the Betic Ranges (Carrión, 2002; Manzano et al., 2017).

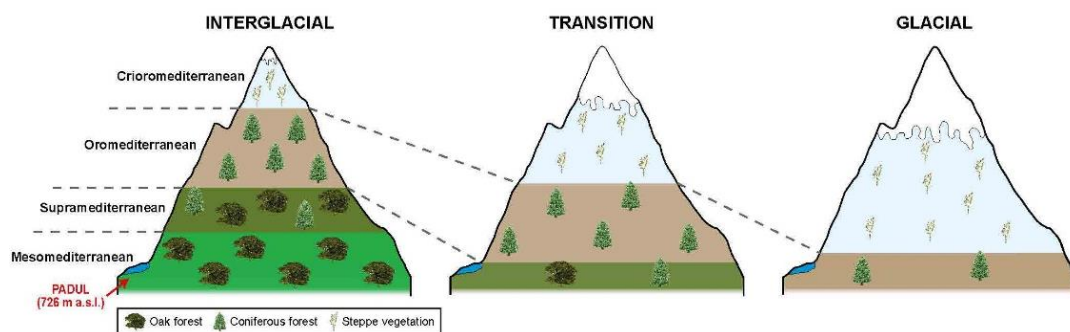


**Figure 3.9.** Schematic representation of vegetation belts oscillations in the Sierra Nevada range and related vegetation during interglacial, transitional and glacial periods.

#### 5.1.4. Recent interglacial (MIS 1) and comparison with the last interglacial period (MIS 5)

The pollen Zone 1 corresponding to MIS 1 is composed by the Bølling-Allerød (B-A) interstadial and the Younger Dryas (YD) stadial (Greenland Interstadial and Stadial 1, respectively) and the Holocene. The B-A is characterized by a drastic increase in Mediterranean forest decreasing into the YD before entering the Holocene. However, xerophytes and Cupressaceae did not totally disappear during the B-A and YD, still indicating relative dry climate conditions but under higher summer-winter temperature contrast (Figs. 3.4 and 3.5). The pollen record from the Holocene part has been described in Ramos-Román et al. (2018a, b) and

is characterized by high occurrences of Mediterranean forest representing warm and humid conditions in this area.

There are significant differences in the *Pinus* occurrences for both recorded interglacial periods (MIS 5e and Holocene), showing higher values during the early MIS 5e (Fig. 3.4). The higher dominance of *Pinus* over the Mediterranean forest during the last interglacial period compared to the early Holocene suggest more marked summer drought (Pérez-Sanz et al., 2013), probably related to the higher summer-winter insolation contrast (Laskar et al., 2004; Berger et al., 2007). Nevertheless, the occurrence of temperate-humid forest composed by *Quercus* deciduous, *Carpinus*, *Corylus* and *Abies* among other high humid taxa along with *Pinus* during the early MIS 5e (Fig. 3.4 and 3.8c), could be indicative of extreme seasonal temperature differences (strong difference between summer and winter insolation, Fig. 3.8f), probably resulting in very high autumn-winter precipitation. All this agrees with other pollen records from the Mediterranean region that denote different climate with warmer and/or wetter conditions during the MIS 5e compared to the Holocene, such as in Lake Ioannina (Tzedakis and Bennett, 1995), Lake Urmia (Djamali et al., 2008) and Lake Van (Litt et al., 2014).

In addition, the higher abundance of algae (mainly *Botryococcus*) during the MIS 5e with respect to the Holocene suggest a deeper water column at the Padul wetland probably linked to the higher autumn-winter precipitation, resulting in a more positive precipitation/evapotranspiration balance during the last interglacial period. In contrast, the lower abundance of mesophyte taxa (e.g., absence of *Abies* and *Carpinus*) during the Holocene shows that autumn-winter precipitation should have been lower than summer evapotranspiration at that time. This might have resulted in negative precipitation/evapotranspiration balance, and therefore, low lake levels and peat formation. The occurrence of Ericaceae during the middle-late Holocene and the total absence during the MIS 5e also points into differences in seasonality between the two interglacials, with a more reduced seasonality with cooler summers (reduced dryness) and warmer winters for the recent Holocene interglacial period (Carrión et al., 2007). Moreover, different proxy records from the Mediterranean region, such as the  $\delta^{18}\text{O}$  values from Soreq Cave (Bar-Matthews et al., 2003), the pollen data from Ioannina Lake (Tzedakis et al., 2003a) and the sapropel S5 deposition in the Mediterranean Sea (Ziegler et al., 2010) also suggest higher precipitation during the last interglacial than during the Holocene. This is related to the increasing land-ocean temperature contrast during the maximum difference between summer and winter insolation (Berger and Loutre, 1991), favoring transport of higher moisture air masses into the continent during autumn and winter seasons.

The Holocene and MIS 5a present similarities with respect to similar abundance in *Olea*, whereas the MIS 5e did not show such a high *Olea* expansion. This could be related to the higher autumn-winter precipitation during the last interglacial as explained above, which could not have allowed the optimum development of *Olea* taxa due to the presence of strong high-moisture woodland competitors. Similar increases in *Olea* during the MIS 5a interstadial are observed in the nearby pollen record from the Cueva de la Carihuela cave (Carrión et al., 1998; Fernández et al., 2007), which points to the same pattern of vegetation response to similar climate conditions. In addition, the relationship between the Mediterranean sclerophyllous and the temperate-humid forest during the Holocene is more similar to the MIS 5a than to the MIS 5e.



This suggests that environmental conditions during the Holocene seem to be more similar to the MIS 5a interstadial than to the last interglacial period (Fig. 3.8c).

## 5.2. *Orbital forcing: regional climate and local environmental changes*

### 5.2.1. *Regional climate changes*

The cyclostratigraphic study on the Padul-15-05 pollen record shows that vegetation in Padul is influenced by a strong orbital-scale precession cycle (Laskar et al., 2004). This is deduced by the statistically significant 23.7, 23 and 21.8 kyr cycles presented respectively in *Pinus* total, Mediterranean forest and in the PCI (Fig. 3.7). The Mediterranean forest data has been filtered using the given frequency of 4.3317E-5 (23 kyr) and the pollen data shows a good correlation with insolation, which is highly influenced by precession cycles at this relatively low latitude (Berger et al., 2007) (Fig. 3.8). Several studies such as Tzedakis (2007) and Fletcher and Sánchez Goñi (2008) also showed the strong relationship between vegetation/forest expansion and precession orbital forcing at Mediterranean latitudes. In Padul, increases in the Mediterranean forest and PCI seem to also covary and be related to increasing summer insolation, such as during MIS 5e, 5a and MIS 1 (subjected to dating uncertainties, especially for MIS 5a as a result of lack of chronological data for this period) (Fig. 3.8). In addition, the strong precessional signal was also previously described affecting sedimentation in the Padul-15-05 core, deduced by the inorganic geochemistry (i.e., Si), organic geochemistry and magnetic susceptibility data (Camuera et al., 2018).

### 5.2.2. *Local environmental changes – lake level reconstruction based on different proxies*

The palynological data from Padul-15-05 has allowed reconstructing the lake level variations of the Padul wetland during the last 197 kyr. A previous study, based on lithology, facies, magnetic susceptibility and inorganic and organic geochemistry of the Padul-15-05 core, showed that the lake level varied with the climate regime and that it was mostly controlled by the precipitation/evapotranspiration balance (Camuera et al., 2018). In this study, palynological data have also been used for the same goal and the comparison between the two, lithological vs. palynological, lake level reconstructions show very similar results. For this reconstruction, the ratio between high lake levels represented by algae (mainly *Botryococcus* and *Pediastrum*) and shallower conditions shown by hygrophytes (Cyperaceae and *Typha*) and Poaceae have been used as: Algae / (Algae + Hygrophytes + Poaceae) (Fig. 3.11). This lake level proxy ratio is explained below.

Algae are principally composed of *Botryococcus* and *Pediastrum*, which are floating planktonic organisms related to oxygenated lake habitats (Guy-Ohlson, 1992) and used as indicator of open lake waters (Rawson, 1956; Whiteside, 1965). Moreover, the capability of *Botryococcus* to resist cold/drought periods and environmental changes allow these green algae to generate massive blooms when normal lake conditions are restored (Clausing, 1999). Due to

this fact, our sediment record presents several blooms of *Botryococcus* when lithology, and therefore, lake conditions changed benefiting this alga. *Botryococcus* occurred abundantly at ~135 kyr BP (until ~123 kyr BP) when carbonate lithology took place and oxygenation increased, and at ~90 kyr BP (until ~80 kyr BP) when sedimentation changed from peat sediments, which are indicative of very shallow and no oxygenated water, to clay deposition during a slightly deeper lake phase. Conditions that determine the occurrence of *Pediastrum* in lake waters are really wide (erosion in catchment, turbidity, nutrient status, pH, etc.) because palynological records lump different *Pediastrum* species together (Van Geel, 2001). Nevertheless, the occurrence of *Pediastrum* in the Padul-15-05 record seems to be more related to *Clayey carbonate facies* linked to deep water column under colder glacial conditions (e.g. MIS 6b, 6a and MIS 2) with respect to *Botryococcus*, which is more common in *Carbonate facies* and *Clay facies* during relatively warmer periods (MIS 5e and 5b-5a) (Fig. 3.5). Therefore, the occurrence of *Botryococcus* and *Pediastrum* along with carbonate/marl lithology with low organic matter and low C/N (Camuera et al., 2018) seem to be similar to the palynological, sedimentological and organic matter analysis recorded by Kaufman et al. (2010), suggesting changes from a wetland with low water column to open lake conditions. Although *Botryococcus* occurred during several interglacial and interstadial phases, the algae as a group presented similar trends with respect to xerophyte taxa throughout the entire core and shows a positive correlation to the xeric group in the PCA (GR2 in Fig. 3.6 and Supplementary Table 3.S1). Therefore, there is a close relationship between high lake levels and cold/arid climatic periods observed during MIS 6b, 6a and MIS 2 (Fig. 3.11), which could be linked to positive precipitation/evapotranspiration balance due to very low evapotranspiration during summer insolation minima, occurring during glacial and stadial phases. This is concordant with the General Circulation Models proposed by Kutzbach and Guetter (1986) and COHMAP-Members (1988), suggesting cold/dry air stream transported from the North Atlantic into the Mediterranean region that produced cloudy summers with lack of precipitation and also cold/dry air masses carried from the North European glacial anticyclone into the Iberian Peninsula during winter times. Consequently, cold/arid xerophyte taxa fit well with lake level increases in Padul and concordant with enhanced siliciclastic input represented by silica cycles and magnetic susceptibility, suggesting stronger erosion and detrital input from the Sierra Nevada due to the lower forest cover during glacial/stadial climate conditions (Camuera et al., 2018). It cannot be ruled out that meltwater from the higher altitude permafrost of the Sierra Nevada could have also supplied with more water to the lower areas (e.g., Padul-Nigüelas basin), also favoring higher lake level.

Singh et al. (1990) explained that both Cyperaceae and *Typha* (hygrophytes) are indicative of local freshwater marsh environment and do not directly indicate regional climate but local moisture conditions (Swain et al., 1983). However, in the Padul wetland, local variations in lake level do also reflect regional environmental changes, as can be deduced by the PCA (Fig. 3.6). These hygrophytes seem to covary with conifers (mainly *Pinus*), denoting lower lake levels during transitional climate phases with respect to previously described predominant algae periods during cold and arid glacial phases.

Finally, Poaceae seem to indicate shallowest wetland and lake shore conditions, which triggered peat sedimentation and generally occurred during warm and humid interglacial and interstadials periods. This is confirmed by the positive correlation between Poaceae and the Mediterranean forest taxa in the PCA and with correlation coefficients (Fig. 3.6 and Supplementary Table 3.S1). An exception occurred during the warm/humid MIS 5e, showing high water lake level. In this case, the temperate-humid forest with high humid taxa such as *Quercus* deciduous, *Betula* or *Alnus* along with *Carpinus*, *Corylus* and *Abies* suggest higher moisture conditions. Even if summer temperatures during the last interglacial period were higher than today (Kaspar et al., 2005), maxima in summer insolation favored humid storm track activity due to strong land-ocean temperature contrast. Therefore, precipitation mostly occurring during autumn-winter in the last interglacial period should have exceeded the annual evapotranspiration (mainly during summer season), resulting in relatively higher lake level.

Lake level reconstruction based on palynological data ratio shown above shows a very strong correlation ( $r = 0.8143$ ;  $p = 2.0269E-93$ ) with the previous reconstruction from the same Padul-15-05 core using independent lithological proxies such as magnetic susceptibility and the most characteristic inorganic and organic geochemistry data (Fig. 3.11a, b). This indicates an immediate respond in both lithology/sedimentology and vegetation as a consequence of climate change and subsequent lake level oscillations.

### *5.3. Comparison with previous palynological records from Padul*

This study has allowed a comparison of the Mediterranean forest (mainly composed by *Quercus*) and xerophytes data (principally formed by *Artemisia*) pollen data from Padul-15-05 with respect to the two previous pollen studies from Padul wetland (Florschütz et al., 1971; Pons and Reille, 1988). Starting from the Holocene, all the studies present high forest development represented by high occurrence of *Quercus* and other Mediterranean forest taxa. The last glacial cycle and the LGM occurred in the different records represented by arid vegetation with *Artemisia* and xerophyte taxa, and also with lithological changes in which the LGM seem to be related to clay lithology in Florschütz et al. (1971) (~6 – 11 m depth) and with marls in Pons and Reille (1988) (~5 – 7 m depth) and in our Padul-15-05 record (~5 – 6 m depth) (Fig. 3.10). Lithological differences between records are probably related to the asymmetric shape of the basin (distance to the close Padul-Nigüelas fault) and the coring location within the wetland. Discrepancies in the age control occur in the different records from the last glacial cycle to their core bottoms. Taking into account the diverse age controls from both previous studies, already explained in the *Introduction* (see *section 1*), and our Padul-15-05 record, we decided to compare the three pollen records and their lithological changes in order to clarify their correlation with global climate events. In this way, we suggest that the interval between ~12 and 24 m depth at Padul IVa and Padul IV records, related to the early Glacial (~70 – 115 kyr BP) and Eemian interglacial period (~115 – 130 kyr BP) by Florschütz et al. (1971) could be better assigned to the late MIS 3-MIS 5a climate stages (Fig. 3.10). This is justified by: a) the absence of any other interstadial (e.g. MIS 5a) with high Mediterranean forest/*Quercus* values between their supposed early Glacial and the Holocene [~from 12 to 5 m depth, ~115 – 12 kyr BP according to the

interpretation from Florschütz et al. (1971)]; b) the assumption by Florschütz et al. (1971) would imply an extraordinary low sediment accumulation rate between the supposed early Glacial (~115 kyr BP) at ~12 m depth and the beginning of the Holocene (~12 kyr BP) at ~5 m depth for a rather continuous sedimentary record; and c) the peat lithology from the supposed Eemian interglacial interpreted by Florschütz et al. (1971) does not correspond to the marl lithology described occurring in the Padul-15-05 record (~26 – 23 m depth). Thereafter, from ~24 m depth to the bottom of the Padul IVa record (Florschütz et al., 1971) the age control seems to also be imprecise, so the correlation with our core was done based on palynological and lithological features (Fig. 3.10). Based on this, it looks like the Padul IVa core also contained a record of the last interglacial (MIS 5e), MIS 6 glacial, the previous MIS 7 interglacial and even reached into MIS 8 glacial, contrary to their assumptions of a record older than the Holsteinian interglacial (or older than MIS 11) (>400 kyr BP).

Our record shows a slightly better correlation with the study from Pons and Reille (1988), especially for the uppermost 8 meters (Padul 3). However, the base of the record at 24 m depth (Padul 2) was interpreted as the first Prewürm interstadial (MIS 5c, ~105 kyr BP), which does not fit with our pollen data. Their high *Quercus* and relatively low *Artemisia* values between ~24 – 15 m depth at Padul 2 seem to be very similar to the MIS 5a, MIS 4 and beginning of MIS 3 from the Padul-15-05 record (~16 – 9 m depth). Furthermore, the section between ~15 – 10 m depth in Padul 2 looks very similar to the Padul-15-05 record between ~9 – 6 m depth (Fig. 3.10). Therefore, according to the palynological and lithological correlations to our chronologically-improved record we suggest that the study from Pons and Reille (1988) could have recorded approximately the last 60 kyr (MIS 5a), contrary to their assumptions of recording until the St. Germain interstadial Ia corresponding to the early MIS 5c (~105 kyr BP).

Vegetation and climate changes during the last two glacial-interglacial cycles in the western Mediterranean: a new long pollen record from Padul (southern Iberian Peninsula)

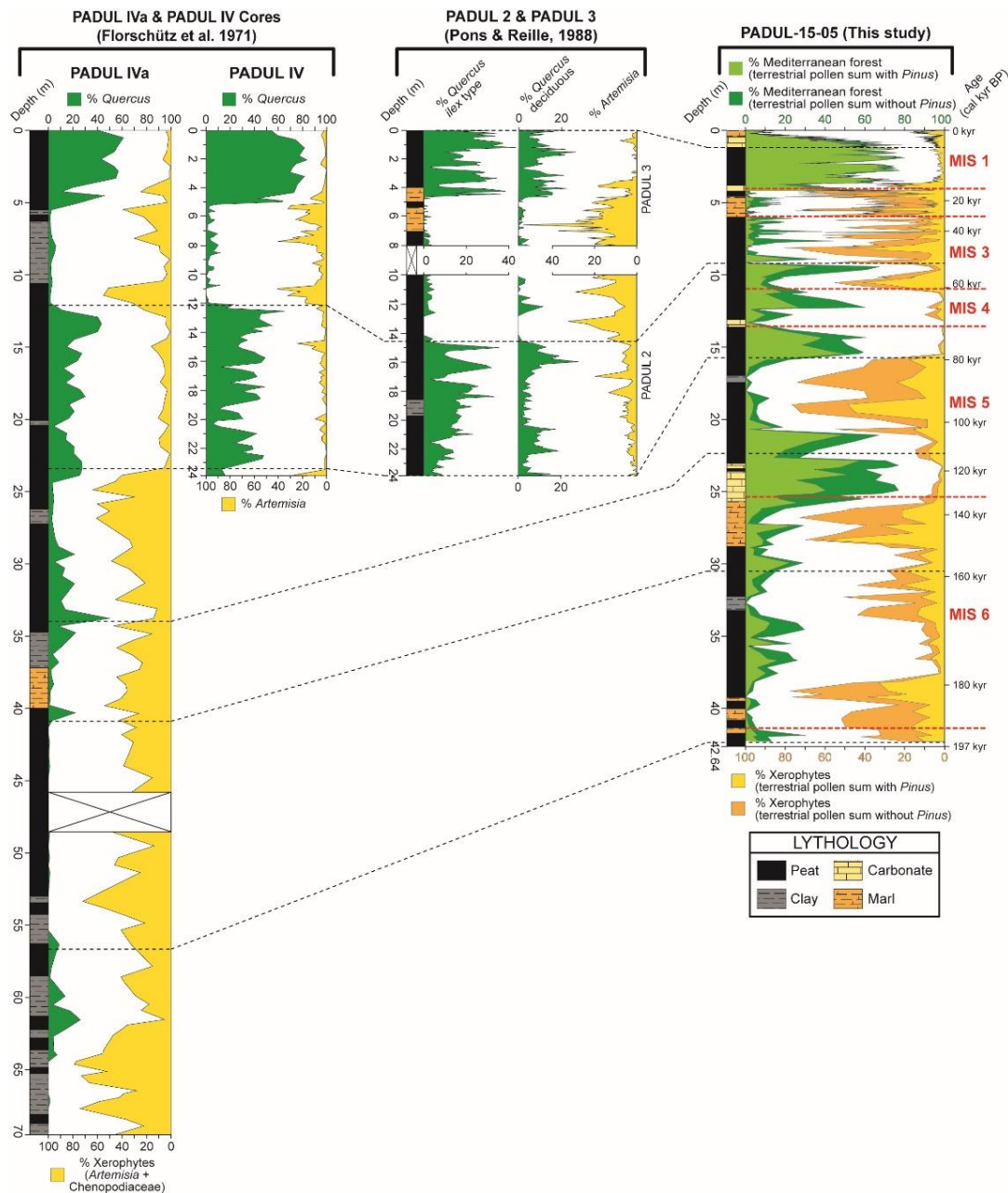


**Figure 3.10.** Correlation of the Padul-15-05 pollen data (this study) with respect to the two previous palynological works from Padul (Florschütz et al., 1971; Pons and Reille, 1988). Lithology and pollen percentages [Mediterranean forest/*Quercus* (green) and xerophytes/*Artemisia* (yellow)] are shown. Florschütz et al. (1971) presented percentages from *Quercus* total, *Artemisia* and xerophytes (*Artemisia* + *Chenopodiaceae*/*Amaranthaceae*) while Pons and Reille (1988) recorded percentages from *Quercus ilex* type, *Quercus deciduous* and *Artemisia*. Suggested correlations based on the lithology, pollen and age control from Padul-15-05 core have been represented using dashed lines between different records. The age control (with 20 kyr intervals) and Marine Isotope Stages (MISs) are shown at the right of the Padul-15-05 record.

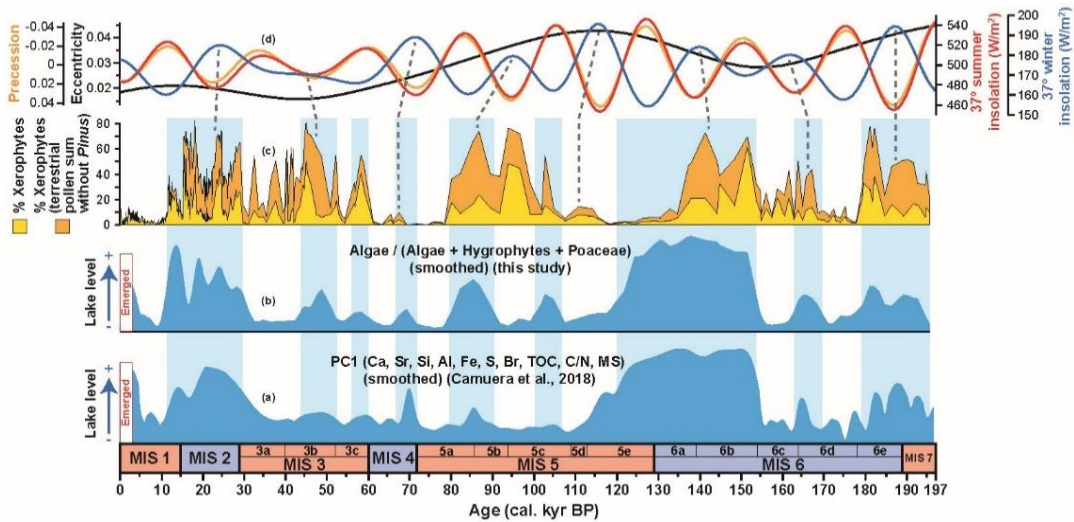


**Figure 3.11.** Representation of: (a) the previous lake level reconstruction based on the most characteristic inorganic geochemistry, organic geochemistry and magnetic susceptibility data (Ca, Sr, Si, Al, Fe, S, Br, TOC, C/N and MS) from Padul-15-05 core (Camuera et al., 2018); (b) the lake level reconstruction based on palynological data (Algae / Algae + Hygrophytes + Poaceae) from this study; (c) percentages of xerophytes with *Pinus* included (yellow) and excluded (orange) from the total terrestrial pollen sum; (d) precession (orange), eccentricity (black), and summer and winter insolation at 37°N ( $W/m^2$ ) (red and blue, respectively). Winter insolation has been correlated with the Padul paleoclimate chronological data using grey dashed lines. Bands (light blue) represent the correlation of high water depth from both lake level reconstructions and the relation with cold/arid periods represented by high xerophyte values.

#### 5.4. Padul and other Mediterranean pollen records

The Padul-15-05 pollen data show similar trends but also some differences compared with other Mediterranean pollen records (Fig. 3.12). The base of the Padul-15-05 core presenting the last millennia of MIS 7 is not well represented, as also occurred in Lake Van (Turkey). During the MIS 6, the Arboreal Pollen (AP) – *Pinus* signal shows low values almost in all records with several millennial-scale variability oscillations, such as those occurring during MIS 6d.

The AP increases during Termination II (between MIS 6 and MIS 5e) in some records (e.g. Lake Ioannina or Padul) are characterized by a more transitional change with respect to the sharp increases during Termination I, very characteristic in almost all records. The MIS 5c showed important forest cover increase after the previous MIS 5d (Greenland stadial 25 or Melisey I stadial) and later on it is interrupted by the cold Montaigu event (Greenland stadial 24), which is also recorded in Lake Ohrid, Lago Grande di Monticchio, Valle di Castiglione, Tenaghi Philippon and Padul (Figs. 3.8 and 3.12). Nevertheless, after the Montaigu event, Padul did not record the subsequent Greenland interstadial 23 (or Saint Germain Ic), corresponding to the second half of the MIS 5c, with such a high forest expansion as in other Mediterranean pollen records (e.g. Tenaghi Philippon, Lago Grande di Monticchio, Lake Ioannina) (Fig. 3.12) (explained above in section 5.1.2).

MIS 5a is well represented in Padul as well as in other Mediterranean lakes. However, the forest development in Padul at this time seems to be delayed ~5,000 years, probably due to age uncertainties. This interstadial showed a shorter duration and lower AP values with respect to the MIS 5e interglacial, as it is also noted in other mediterranean sites such as Lake Ioannina and Lake Van (Fig. 3.12).

From MIS 4 to MIS 2, the Mediterranean region was characterized by a general arboreal decreasing trend. However, some interstadials are well represented in some areas, such as that from the MIS 3c in Lake Ioannina, Lago Grande di Monticchio and Padul (Fig. 3.12). Forest species are absent (0% AP) during the coldest and most arid stadials from the last glacial in Mediterranean sites where present-day annual rainfall is low such as in Padul and Lake Van. On the contrary, Lake Ioannina and Lake Ohrid, characterized by higher present-day mean annual precipitation and probably higher precipitation during the last glacial period with respect to other Mediterranean places, never showed AP values below 7 – 8% (even without *Pinus*, *Juniperus* and *Betula*) during the coldest and most arid phases (Fig. 3.12). The wetter climate partially related to rougher topography and higher orographic precipitation in these areas (Popovska, 2002; Roucoux et al., 2008) would have allowed the survival of specific tree species during the most extreme glacial phases, buffering cold/arid glacial conditions. Therefore, topographic features from some Mediterranean regions would have been more important climate conditioner than the latitude for tree survival in certain refuge areas.

Finally, the MIS 1 shows an important climatic change at ~15 kyr BP with significant increases in AP. Our record shows a very similar trend than the Lago Grande di Monticchio, with a drastic AP increase due to the warm Bølling-Allerød interstadial and a decrease during the Younger Dryas before entering the Holocene with another arboreal forest development (Fig. 3.12).



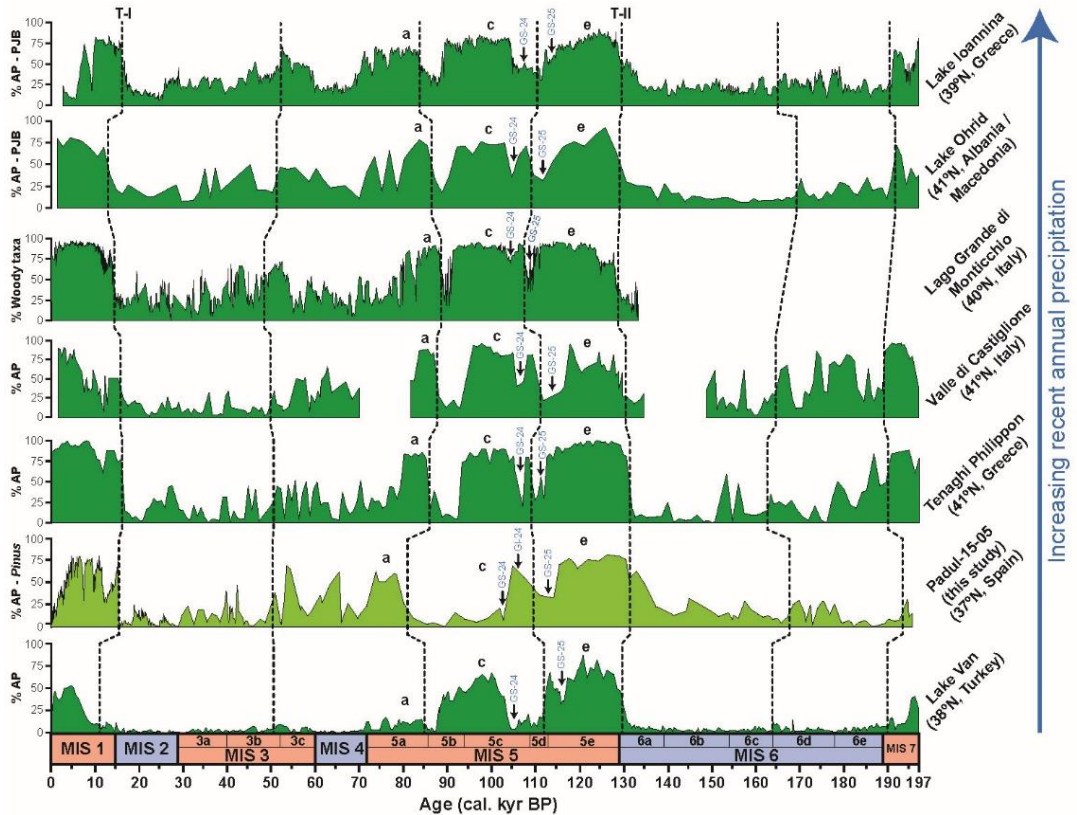


**Figure 3.12.** Comparison of different Mediterranean pollen records for the last 197,000 years, including (from bottom to top): Lake Van (Litt et al., 2014; Pickarski et al., 2015a, b; Pickarski and Litt, 2017), Padul (green light, this study), Tenaghi Philippon (Wijmstra, 1969; Mommersteeg et al., 1995; Tzedakis et al., 2006), Valle di Castiglione (Follieri et al., 1989; Magri, 1989), Lago Grande di Monticchio (Watts et al., 1996; Allen et al., 1999; Allen and Huntley, 2009), Lake Ohrid (Sadori et al., 2016) and Lake Ioannina (Roucoux et al., 2008, 2011). Depending on the record, percentages of Arboreal Pollen (% AP), Arboreal Pollen minus *Pinus* (% AP-*Pinus*), Arboreal Pollen minus *Pinus*, *Juniperus* and *Betula* (% AP-PJB) and Woody taxa are represented. Vertical dashed lines show suggested correlations between records. Termination I and II are represented as T-I and T-II, respectively. The Greenland stadials 24 and 25 are shown in blue as GS-24 and GS-25, respectively. The recent annual precipitation on these Mediterranean sites are (increasing from bottom to top): Lake Van = 379 mm/yr (Stockhecke et al., 2012), Padul = 445 mm/yr (agroclimap.aemet.es), Tenaghi Philippon = 459 mm/yr (Pross et al., 2015), Valle di Castiglione = 800 mm/yr (Follieri et al., 1998), Lago Grande di Monticchio = 815 mm/yr (Watts et al., 1996; Martín-Puertas et al., 2014), Lake Ohrid watershed = 907 mm/yr (Popovska and Bonacci, 2007) and Lake Ioannina = 1200 mm/yr (Tzedakis et al., 2002; Roucoux et al., 2008).



## **6. Conclusions**

The palynological analysis of the new Padul-15-05 sediment record allowed a detailed study of vegetation and climate changes of the last two glacial-interglacial cycles (~200,000 years) in the southern Iberian Peninsula and western Mediterranean region. This study shows that:

1. In this area vegetation is mainly forced by insolation, dominated by orbital-scale changes represented by precession and eccentricity.
2. Vegetation changes at Padul are closely related to the variations in the elevation of forest species from bioclimatic vegetation belts in the Sierra Nevada linked to climate oscillations.
3. The pollen data from Padul-15-05 present discrepancies on the age control and the correlations of the observed vegetation changes with climatic phases with respect to the two previous palynological studies from Padul (Florschütz et al., 1971; Pons and Reille, 1988). Therefore, a robust and high-resolution age-depth control based on updated dating techniques is essential in order to reconstruct and compare paleoenvironmental and climate changes more accurately.
4. Lake level oscillations in the Padul wetland were closely related to climate variations. High water level (represented by high algae) occurred during cold and arid glacial/stadial periods (high xerophytes) due to positive precipitation/evapotranspiration balance mainly as a result of low evapotranspiration. On the contrary, during warm interglacial/interstadial phases (recorded by high Mediterranean forest) evapotranspiration rates greatly exceeded rainfall (except for the MIS 5e), producing a negative precipitation/evapotranspiration balance and decreasing lake levels.
5. The comparison between the lake level reconstruction from Padul based on palynological data with previous lake level reconstruction from the same record but based on inorganic and organic geochemistry and magnetic susceptibility shows very high correlation. This suggests that both methodologies are good proxies for lake level oscillations and useful for water level reconstructions in lakes/wetlands with similar hydrological and sedimentological features.
6. Mediterranean lake sites located in abrupt topographic areas with high precipitation rates could have buffered extreme cold and arid climates, resulting in tree refugia with higher forest cover during the most extreme glacial conditions with respect to other Mediterranean sites characterized by lower precipitation levels. This indicates that the orographic precipitation in some regions is more important climate conditioner for tree refugia than the latitude.

## Acknowledgments

This research is supported by the projects CGL2013-47038-R and CGL-2017-85415-R funded by Ministerio de Economía y Competitividad of the Spanish Government, project P11-RNM-7332 from the Junta de Andalucía and the research group RNM0190 (Junta de Andalucía). Jon Camuera acknowledges the PhD funding (BES-2014-069117) provided by the Ministerio de Economía y Competitividad of the Spanish Government under the project CGL2013-47038-R. María J. Ramos-Román also acknowledges the PhD and post-PhD fellowship (P11-RNM-7332) from the Conserjería de Economía, Innovación, Ciencia y Empleo of the Junta de Andalucía. Antonio García-Alix was supported by a Ramón y Cajal fellowship (RYC-2015-18966) from the Ministerio de Economía y Competitividad of the Spanish Government. Thanks to Javier Jaimez for helping with the coring (CIC-UGR). José Carrión thanks the Ministerio de Economía y Competitividad of the Spanish Government (grant number CGL-BOS-2012-34717 and CGL-BOS 2015-68604) and Fundación Séneca (grant number 19434/PI/14). Authors want to thank Katherine Roucoux, Alessia Masi, Judy Allen, and Nadine Pickarski and Thomas Litt for providing the pollen data from Lake Ioannina, Lake Ohrid, Lago Grande di Monticchio and Lake Van, respectively. Also thanks to the editor Danielle Schreve, Vasiliki Margari and one anonymous reviewer for their very useful comments and suggestions on a previous version of the manuscript.

## Supplementary Information

### Vegetation and climate changes during the last two glacial-interglacial cycles in the western Mediterranean: a new long pollen record from Padul (southern Iberian Peninsula)

Jon Camuera<sup>1</sup>, Gonzalo Jiménez-Moreno<sup>1</sup>, María J. Ramos-Román<sup>1</sup>, Antonio García-Alix<sup>1, 2</sup>, Jaime L. Toney<sup>3</sup>, R. Scott Anderson<sup>4</sup>, Francisco Jiménez-Espejo<sup>2, 5</sup>, Jordon Bright<sup>6</sup>, Cole Webster<sup>4</sup>, Yurena Yanes<sup>7</sup>, José S. Carrión<sup>8</sup>

<sup>1</sup> Departamento de Estratigrafía y Paleontología, Universidad de Granada, Spain

<sup>2</sup> Instituto Andaluz de Ciencias de la Tierra (IACT), Consejo Superior de Investigaciones Científicas-Universidad de Granada (CSIC-UGR), Granada, Spain

<sup>3</sup> School of Geographical and Earth Sciences, University of Glasgow, UK

<sup>4</sup> School of Earth Sciences and Environmental Sustainability, Northern Arizona University, USA

<sup>5</sup> Department of Biogeochemistry, Japan Agency for Marine-Earth Science and Technology (JAMSTEC), Japan

<sup>6</sup> 7351 E. Speedway Blvd, 30C, Tucson AZ, USA

<sup>7</sup> Department of Geology, University of Cincinnati, USA

<sup>8</sup> Departamento de Biología Vegetal, Facultad de Biología, Universidad de Murcia, Spain

### Supplementary Table

	Quercus evergreen	Quercus deciduous	Olea	Pistacia	Ericaceae	Poaceae	Artemisia	Amaranthaceae	Ephedra	Cupressaceae	Botryococcus	Pediastrum	Pinus total	Cyperaceae
Quercus evergreen		6.55E-39	2.82E-01	5.60E-115	1.06E-03	8.97E-09	1.44E-14	2.35E-15	8.25E-14	5.19E-03	1.38E-01	5.18E-09	5.48E-72	1.72E-21
Quercus deciduous	0.58		1.14E-01	1.40E-37	8.26E-02	3.66E-01	1.29E-08	2.61E-11	8.49E-09	5.87E-01	1.32E-01	5.74E-03	5.76E-32	9.76E-14
Olea	0.05	0.08		2.51E-01	3.14E-03	1.21E-06	2.15E-08	5.63E-01	3.19E-06	7.46E-02	6.25E-02	4.27E-03	3.72E-13	1.62E-08
Pistacia	0.65	0.57	0.05		2.92E-02	4.39E-07	2.97E-13	1.34E-14	9.43E-11	1.01E-03	1.65E-02	1.12E-06	2.23E-49	2.90E-15
Ericaceae	0.16	0.09	0.14	0.11		3.18E-04	2.96E-06	6.59E-05	1.52E-05	1.34E-03	5.08E-01	3.07E-06	1.84E-09	2.21E-07
Poaceae	0.28	0.04	0.24	0.25	-0.18		1.23E-06	7.39E-01	7.57E-06	3.36E-02	1.85E-06	4.21E-06	6.84E-28	6.08E-03
Artemisia	-0.37	-0.27	-0.27	-0.35	-0.23	-0.24		9.67E-51	1.50E-18	1.71E-06	1.56E-06	8.58E-15	5.29E-04	1.02E-07
Amaranthaceae	-0.38	-0.32	0.03	-0.37	-0.19	-0.02	0.65		6.67E-15	2.16E-03	7.02E-03	8.52E-07	8.62E-01	1.97E-03
Ephedra	-0.36	-0.28	-0.23	-0.31	-0.21	-0.22	0.41	0.37		5.20E-03	4.30E-03	2.02E-05	3.93E-11	8.57E-15
Cupressaceae	-0.14	0.03	-0.09	-0.16	-0.16	-0.10	0.23	0.15	0.14		2.48E-16	5.33E-11	6.99E-01	1.12E-01
Botryococcus	-0.07	0.07	-0.09	-0.12	-0.03	-0.23	0.23	0.13	0.14	0.39		6.04E-13	3.54E-01	6.77E-01
Pediastrum	-0.28	-0.14	-0.14	-0.24	-0.23	-0.22	0.37	0.24	0.21	0.32	0.34		1.65E-07	3.66E-03
Pinus total	-0.74	-0.53	-0.35	-0.64	-0.29	-0.50	0.17	0.01	0.32	0.02	0.05	0.25		5.66E-28
Cyperaceae	-0.44	-0.35	-0.27	-0.37	-0.25	-0.13	0.26	0.15	0.37	-0.08	0.02	0.14	0.50	

**Supplementary Table 3.S1.** Correlation table of the most characteristic pollen taxa. Pollen species have been colored as the groups from the PCA (see Figure 3.6): Group 1 (green), Group 2 (yellow) and Group 3 (blue). Correlation coefficients above 0.2 have been colored in green, while correlation coefficients below -0.2 are in red.

# *Chapter*4

*Organic biomarkers (n-alkanes, diols, fatty acids) as a proxy for  
environmental changes in the Padul wetland and southern  
Iberian Peninsula*



## **Chapter 4: Organic biomarkers (*n*-alkanes, diols, fatty acids) as a proxy for environmental changes in the Padul wetland and southern Iberian Peninsula**

### **1. Introduction**

Organic biomarkers preserved in marine and lake sediments present different features as result of the distinct occurrence of microalgae, bacteria and other microorganisms living there (Cranwell et al., 1987; D'Anjou et al., 2013). In the last decades, various classes of organic molecules (lipids) have been proven to be useful as paleoenvironmental indicators due to their relative resistance to degradation and preservation in the sedimentary record (Volkman, 1986).

Aliphatic hydrocarbons (*n*-alkanes) are organic compounds derived from autochthonous and allochthonous sources linked to algae, bacteria and vascular plants living around the lake (Meyers and Ishiwatari, 1993; D'Anjou et al., 2013). Often, the number of carbons in the molecular chain of *n*-alkanes, and therefore, the molecular length, are related with a specific producing organisms. In this way, the organic leaf waxes characterized by short-chain *n*-alkanes (C<sub>15</sub>-C<sub>21</sub>) are commonly linked to algae and photosynthetic bacteria (Meyers, 2003 and references therein), mid-chain *n*-alkanes (C<sub>21</sub>-C<sub>25</sub>) with submerged plants (Ficken et al., 2000) and long-chain *n*-alkanes (C<sub>25</sub>-C<sub>33</sub>) are characteristic of higher order terrestrial plants (Cranwell et al., 1987). Previous studies show that temperature conditions affect the algal structure and diols from marine and continental environments (Brassell et al., 1986; Rampen et al., 2012). With respect to fatty acids, the molecular lengths have been associated with the occurrence of different producers. In particular, the long-chain fatty acids (C<sub>24</sub>, C<sub>26</sub>, C<sub>28</sub>) are major components of wax coating of land-plant leaves, flowers and pollen, whereas short-chain molecules (C<sub>12</sub>, C<sub>14</sub>, C<sub>16</sub>) are dominant lipid components of algae (Bourbonniere and Meyers, 1996). These organic biomarkers can thus provide with useful information about paleoenvironmental and paleoclimatic changes in the study area through time, such as oscillations in the vegetation, in paleotemperatures and/or in the terrestrial vs aquatic producer lipid ratios, among others (Bourbonniere and Meyers, 1996; Meyers and Teranes, 2001; Martrat et al., 2014).

Lacustrine environments, such as the Padul wetland, are excellent sites for paleoclimate reconstructions due to the high-sensitivity of its paleoenvironmental record to climate changes (Zhang et al., 2011; Camuera et al., 2018, 2019). However, less is known about biomarkers in lacustrine ecosystems in comparison with marine environments (Zhang et al., 2011). Therefore, studies focusing on paleoenvironmental and paleoclimate interpretations of biomarkers in terrestrial areas can provide new information about how to interpret these proxies, and how they responded to different environmental and climate conditions in wetland sedimentary records.

This chapter aims to provide additional information, mainly about local environmental changes in the Padul wetland, given by *n*-alkane (including analysis of  $\delta D$ ), diol and fatty acid data from the Padul-15-05 record during the last ~36 kyr BP. This was done through comparing

the organic biomarker data with the regional vegetation (pollen analysis) and the local sedimentation (analysis of inorganic geochemistry) data.

## **2. Methodology**

In this study, a ratio representing short-chain *n*-alkanes ( $A = C_{17} + C_{19}$ ) divided by the sum of short-chain, mid-chain ( $B = C_{21} + C_{23}$ ) and long-chain ( $C = C_{29} + C_{31}$ ) *n*-alkanes has been included as  $A/(A+B+C)$  to observe the presence of algae and aquatic organisms in the wetland (Fig. 4.1c). The long-chain *n*-alkanes divided by the sum of short-, mid- and long-chain *n*-alkanes have also been included as  $C/(A+B+C)$ , which could provide with information about the occurrence of lipids from trees and land-plants in the Padul sedimentary record (Fig. 4.1d). The hydrogen isotopes ( $\delta D$ ) from the *n*-alkanes have commonly been used in paleoclimatic studies to infer changes in precipitation, evapotranspiration and/or the origin of the water source (Araguas-Araguas and Diaz Teijeiro, 2005; Hou et al., 2006; Seki et al., 2011). In particular, in Padul we used the  $\delta D$  (ice volume corrected; see methods in *Chapter 1*) data from the  $C_{31}$  alkane (Fig. 4.1e).

The Long-chain Diol Index [ $LDI = C_{30} \text{ 1,15-diol} / (C_{28} \text{ 1,13-diol} + C_{30} \text{ 1,13-diol} + C_{30} \text{ 1,15-diol})$ ] has been calculated according to the analysis and the obtained data from the third neutral lipid fraction corresponding to diols. In the literature this index has been related with paleotemperatures in marine and terrestrial sediments (Rampen et al., 2012; García-Alix et al., submitted) (Fig. 4.1f).

The fatty acids obtained from the Total Acid Fraction (TAF) in the Padul-15-05 record also allow calculating the Terrestrial to Aquatic Ratio [ $TAR_{fa} = (C_{24} + C_{26} + C_{28}) / (C_{16} + C_{18})$ ] that can also provide with information about the source of the organic matter, revealing the contribution of the land-derived and aquatic-derived organic matter (Bourbonniere and Meyers, 1996) (Fig. 4.1g).

The correlation coefficients between  $A/(A+B+C)$  and  $C/(A+B+C)$  ratios, and between  $\delta D$  from  $C_{31}$  alkanes and the pollen P index were calculated using the PAST 3.15 software (Hammer et al., 2001). In order to obtain the most aseptic correlation results, only the P index data corresponding to the lower resolution samples from the  $\delta D$  analysis has been used (Fig. 4.2).

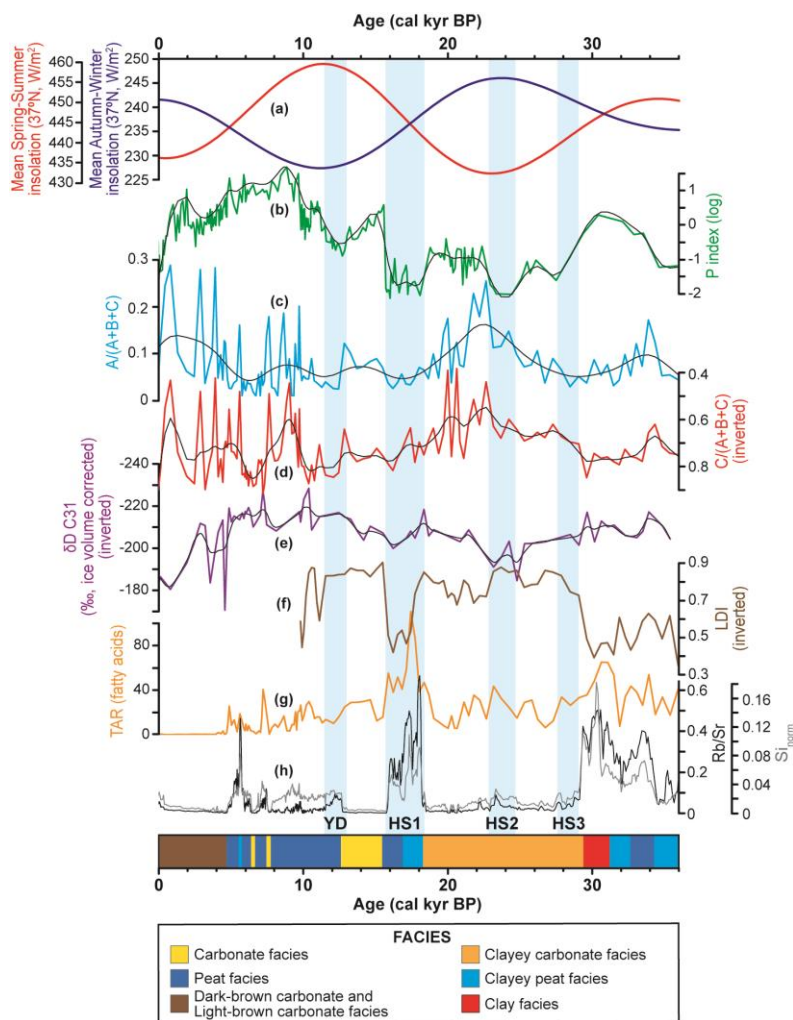


**Figure 4.1.** The record of organic biomarkers, palynological analysis and XRF for the last ~36 kyr BP. (a) Mean spring-summer insolation (red) and mean autumn-winter insolation (blue) at 37°N latitude (Laskar et al., 2004). (b) P index with the optimized smoothing data (black line, smooth value 2.125). (c)  $A/(A+B+C)$  ratio with the optimized smoothing (black line, smooth value 8.1). (d)  $C/(A+B+C)$  ratio with the optimized smoothing (black line, smooth value 6.925) (vertical axis inverted). (e)  $\delta D$  C<sub>31</sub> *n*-alkane values (ice volume corrected) with a smooth value of 4.9 (black line) (vertical axis inverted). (f) LDI data from diols (vertical axis inverted). (g) TAR from fatty acids. (h) Rb/Sr (black) and normalized silicon data (grey) from XRF. HSs (including YD) are shown in blue shading.

### 3. Results and discussion

The *n*-alkanes from organic biomarkers in the Padul-15-05 record have been synthesized using the two ratios described above, i.e.,  $A/(A+B+C)$  and  $C/(A+B+C)$ , depicting the distribution through the time of the short-chain and long-chain *n*-alkanes, respectively. The correlation between the raw data of these two ratios is -0.715 ( $p = 5.38E-21$ ), indicating opposite



environmental signals. The distribution of the short-chain *n*-alkanes are usually associated to algae and bacteria, associated with relatively high lake level with oxygenated water in the Padul wetland. This can be deduced in the Padul record from the documentation of the lowest values between ~36 kyr BP and the end of the YD (at 11.6 kyr BP), during sedimentation of *Peat facies*, in which the water column and oxygen availability was lower, whereas the highest values mainly occurred during the deposition of the higher lake level *Carbonate* and *Clayey Carbonate facies* (Camuera et al., 2018, 2019) (Fig. 4.1c). The long-chain *n*-alkanes represented by the ratio  $C/(A+B+C)$  show the highest values during the sedimentation of *Peat facies*, contrary to that recorded by the short-chain *n*-alkanes. This could indicate the relative higher presence of lipids from higher order plants in the wetland consequence of the low occurrence of short- and mid-chain *n*-alkanes that have been linked to algae and/or photosynthetic bacteria and submerged plants, respectively (Ficken et al., 2000; Meyers, 2003). In contrast, during the *Peat facies* deposition of the early Holocene between ~10 – 7 kyr BP, the Padul wetland recorded a relatively low long-chain *n*-alkanes (Fig. 4.1d). This could be related with the dense *Typha* type and Poaceae (probably *Phragmites*) cover in the lake shore at that time (see Figure 5 from Ramos-Román et al., 2018b), which could have provided the lake water with mid-chain *n*-alkanes (see the positive correlation between mid-chain *n*-alkanes and *Typha* type and Poaceae in Figures 5 and 6 from Ramos-Román et al., 2018b) and could have also acted as a natural vegetal barrier, preventing the lipid input of the surrounding higher order plants and the longest *n*-alkane chains. This is supported by the low Rb/Sr and Si values recorded during this period, suggesting a low siliclastic/detrital input in the lake transported from the Sierra Nevada range, probably also due to the dense submerged vegetal cover (e.g., Poaceae) acting as a sedimentary barrier (Fig. 4.1h).

The hydrogen isotopic composition of the  $C_{31}$  alkane has previously been used a proxy of the environmental source water used by terrestrial plants, and therefore, can be used to reconstruct environmental changes related to precipitation dynamics and/or the rainfall water source during different periods (Niedermeyer et al., 2010; Collins et al., 2013b). In this study, the linkage between the hydrogen isotopic composition of the precipitation and that of the  $\delta D_{C_{31}}$  sedimentary alkane is verified by the similar values of Padul  $\delta D$  annual rainfall, calculated using the OIPC models (-42‰ V-SMOW; Bowen and Revenaugh, 2003), and the  $\delta D_{water}$  (-43.1‰) obtained from the  $\delta D_{C_{31}}$  of currents plants in the Padul catchment basin after applying the fractionation factor of -141‰, according to Sachse et al. (2004).

In this study, the raw  $\delta D$  data and P index values for the last ~36 kyr BP from the Padul-15-05 record have been compared, obtaining a correlation coefficient of -0.576 ( $p = 3.40E-8$ ). In order to obtain a correlation coefficient without background signal, an optimized smoothing was run on both  $\delta D$  (smooth value 6.225) and P index (smooth value 2.125) data with the PAST software. This smoothed value is based on a multiple data set converging to a single point by weighted averaging and following the algorithm from de Boer (2001). The obtained correlation coefficient of -0.777 ( $p = 6.07E-17$ ) show the strong opposite correlation between  $\delta D_{C_{31}}$  and P index at long-terms (Fig. 4.2) and also highlight the relationship between precipitation and the hydrogen isotopic composition of the  $C_{31}$  alkane, which is ultimately related to the isotopic composition of the water source. In particular, the depleted  $\delta D$  values and the increased in P index occurred during enhanced precipitation conditions, whereas the  $\delta D$  enrichment is closely

related with arid climate periods in the western Mediterranean. The smoothed  $\delta D_{C_{31}}$  alkane and P index data revealed that both paleoclimatic records are closely related to insolation values at Padul's 37°N latitude, pointing into enhanced precipitation (low  $\delta D$  and high P index) during spring-summer insolation maxima and arid periods (high  $\delta D$  and low P index) during spring-summer insolation minima (Fig. 4.2). In short-term variability, changes in the  $\delta D$  values could be related with different rainfall water sources and/or linked to distinct precipitation/evapotranspiration conditions in the wetland (García-Alix et al., submitted).

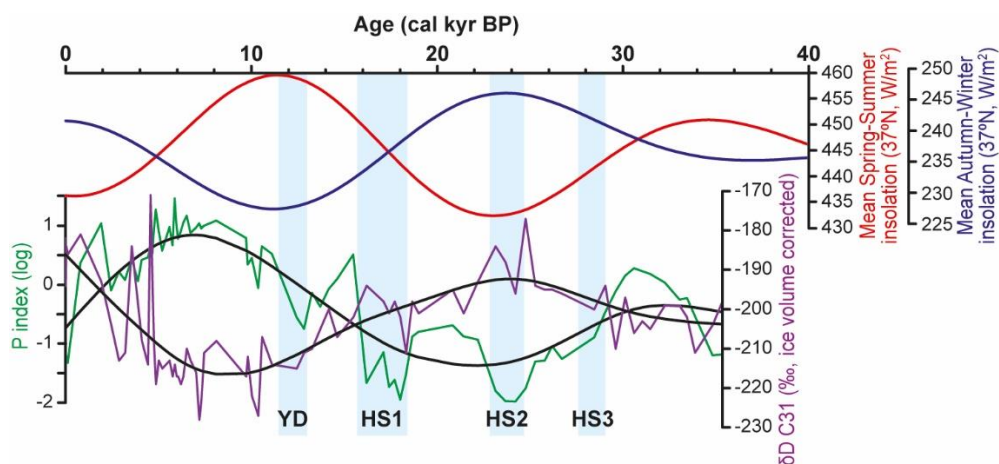


**Figure 4.2.** Comparison between the  $\delta D_{C_{31}}$  *n*-alkane (the black line shows the optimized smoothing with a value of 6.225) and P index (log) data (the black line shows the data under a smooth value of 4.7) and the mean spring-summer and autumn-winter insolation at 37°N latitude. Note the good visual correlation between spring-summer insolation and P index and the anti-correlation with  $\delta D_{C_{31}}$ . HSs (including YD) are shown in blue shading.

The LDI calculated from the diol fraction shows values ranging between 0.35 and 0.9. Generally, the highest LDI values are recorded during carbonate lithologies (*Carbonate* and *Clayey carbonate* facies) and lowest values occur during peat sedimentation (*Peat* and *Clayey peat* facies). Several studies have related the LDI with lake paleotemperatures (García-Alix et al., submitted). Nevertheless, our LDI data from the Padul-15-05 record seems to be rather related with the lithology, and therefore, the lithology would be strongly conditioning the LDI data and buffering the paleotemperature signal. A detailed calibration of diols in the recent Padul wetland would be then necessary for obtaining an accurate paleotemperature record.

The Padul-15-05  $TAR_{fa}$  is based on the data from the acid fraction and shows the highest values during *Clay* and *Clayey peat* facies deposited during low lake level conditions. In general, the  $TAR_{fa}$  data show similar trends with respect to the Rb/Sr and Si data from the XRF analysis. This suggests a higher input of lipids from terrestrial plants into the Padul wetland as result of the higher soil erosion during lower vegetal cover (low P index), similar to that occurred during HS1. The signal in carbonate lithologies is buffered due to the higher presence of aquatic lipids. However, similar trends with increasing  $TAR_{fa}$  and Rb/Sr and Si values can also be observed during HS2.

#### **4. Conclusions**

The organic biomarkers from the Padul-15-05 record, including *n*-alkanes, diols and fatty acids, have provided with information about local and regional environmental changes in the Padul wetland during the last ~36 kyr BP.

On a long-term scale, the  $\delta D$  values from C<sub>31</sub> alkane display an opposite correlation with respect to the P index from the palynological analysis, pointing into the same precipitation signal. The good correlation between these results and insolation values suggest that rainfall in southern Iberian Peninsula was mainly affected by the insolation factor, with higher rainfall during insolation maxima and lower rainfall during insolation minima. At short-term scale, the  $\delta D$  data could also suggest the rainfall water source and/or the different precipitation/evapotranspiration conditions in this region during specific periods.

With respect to the local signal from the wetland, short- and long-chain *n*-alkanes indicate the presence of algae and/or photosynthetic bacteria, and higher order plants, respectively. The concentrations of the different *n*-alkanes are related with lake level conditions but also with the occurrence of low or high forest cover and submerged plants around the wetland.

The terrestrial against aquatic ratio from fatty acids represented by TAR<sub>fa</sub> seems to be closely related with the detrital/siliciclastic input from the Sierra Nevada, and therefore, pointing into a good indicator of external runoff input favored by the higher soil erosion during lower forest cover.

Finally, diols seem to provide with information about the local environment, as they are conditioned by the lithological features. Recent and detailed calibrations of the organic biomarkers would be necessary for a further and more accurate interpretation of paleotemperature signal in the Padul wetland.

# *Chapter* 5

*Millennial- and centennial-scale climate variability during the  
last 65 kyr BP in the southern Iberian Peninsula*



## **Chapter 5: Millennial- and centennial-scale climate variability during the last 65 kyr BP in the southern Iberian Peninsula**

### **1. Introduction**

In the last decades, several paleoclimatic studies have focused on the study of millennial- and centennial-scale climate oscillations in the past, and in particular during the last glaciation. This was done with the main goal of understanding rapid climate changes that also occurred during the Holocene and that will affect future climate change and our society. Some of these fast climate oscillations occurring during the last glacial period resulted from Dansgaard-Oeschger (D-O) variability (including stadials and interstadials) and from the extreme cold events known as Heinrich events (HEs) (Moreno et al., 2002; Penaud et al., 2010). HEs are characterized by massive discharge of IRD into the North Atlantic from high-latitude ice-sheets. The D-O variability, characterized by the most often ~1500-yr cyclicality, was described in detail in the high-resolution ice core paleoclimatic records from Greenland (Alley et al., 2001; Ganopolski and Rahmstorf, 2001). The interval between two consecutive HEs is called “Bond cycle” and is characterized by D-O variability featuring abrupt and progressively cooler interstadials (D-O interstadials), culminating in a Heinrich Stadial (HS) during which HEs occurred (Barker et al., 2009).

Few pollen records from western Europe and the Mediterranean region show high-resolution vegetation data interpreting environmental changes related with HSs and D-O variability (Combourieu Nebout et al., 2002; Masson-Delmotte et al., 2005; Sánchez Goñi et al., 2008; Fletcher et al., 2010a). Complex patterns of vegetation responses were identified related with HSs during the last glacial period in the western Mediterranean (Skinner and Elderfield, 2007; Fletcher and Sánchez Goñi, 2008) and high-frequency climate changes corresponding to D-O oscillations were also observed in this region under high-resolution multiproxy studies (including vegetation data) (Moreno et al., 2005; Margari et al., 2009).

Most of the studies focusing on these short-scale vegetation changes have been done on marine sediment cores, taking advantage of the continuous and high sediment accumulation rates and thus providing with higher resolution data with respect to continental sites. However, some terrestrial sites can also provide with high-resolution paleoenvironmental data with reliable results for the identification and interpretation of HEs and D-O cycles (Allen et al., 1999; Tzedakis et al., 2002; Jiménez-Moreno et al., 2007; Margari et al., 2009; Fletcher et al., 2013). A further study on these rapid changes (including HSs as well as D-O events) in terrestrial environments from the western Mediterranean is necessary in order to obtain a more complete vision of the regional climate variability in this area.

This chapter aims to interpret climate conditions of the last 65 kyr BP focusing on millennial- and centennial-scale variability, in particular on Heinrich Stadials [from Heinrich Stadial 6 (HS6) to the Younger Dryas (YD), also called Heinrich Stadial 0 (HS0)] and D-O

oscillations. Possible causes and mechanisms forcing these environmental oscillations in the Iberian Peninsula and in the Padul wetland during this period are also discussed.

## **2. Methodology**

The local and regional environmental and climate reconstructions of the last 65 kyr BP, with special attention to the D-O variability and Heinrich Stadials, have been done using detailed pollen data from the Padul-15-05 record.

The palynological analysis of the last 65 kyr BP is based on 353 samples [including 176 samples from the Holocene analyzed by Ramos-Román et al. (2018a, b)], presenting an average pollen data resolution of ~184 years. The age-range between 65 kyr to 30 kyr BP (including HS6, HS5 and HS4) show relatively low-resolution data (average resolution of ~813 yr). However, the pollen data resolution of the last 30 kyr BP is much higher, presenting a resolution of ~136 yr for the age-range between 30 kyr and 11.7 kyr BP (including HS3, HS2, HS1 and YD) and ~66 yr for the last 11.7 kyr BP (Holocene).

Millennial- and centennial-scale environmental and climate variability from the Padul-15-05 record was studied using the pollen data, specifically the Pollen Climate Index (PCI) and xerophyte pollen group, which are sensitive paleoclimate proxies. The specific methodology about the palynological analysis, including the PCI and the vegetation taxa composing the xerophyte pollen group is explained in *Chapter 1*. The PCI data have been smoothed (smooth value of 4.7) using the smoothing spline from the PAST 3.15 software (Hammer et al., 2001) with the purpose of comparing with insolation values.

## **3. Results and discussion**

### *3.1. Environmental and climatic response to HSs and D-O variability in the western Mediterranean*

The high-resolution pollen data (in particular, xerophytes and PCI) from the Padul-15-05 record have been used for the identification and environmental reconstruction of HSs and smaller scale D-O events during the last 65 kyr BP. The Padul-15-05 data have been compared with pollen and SST data of the MD95-2043 record from the nearby Alboran Sea, the Ioannina-284 terrestrial record from Greece and  $\delta^{18}\text{O}$  data from Greenland ice-cores, in order to observe environmental/climatic similarities and differences between distinct records from the Mediterranean area and high-latitude environments (Fig. 5.1).

Xerophyte data show maxima during HSs (between ~30 and 60%), whereas during D-O stadials xerophyte peaks are commonly between 10% and 30%, clearly showing that driest climate conditions in the last glaciation were reached during HSs. Here below, the identification and interpretation of every single HS and D-O event has been explained.

The Padul-15-05 record shows a peak in PCI at ~63 kyr BP, which could be interpreted as an environmental response to the D-O interstadial 18, even if the resolution for the age period is relatively low. Later on, a significant drop in PCI and an increase in xerophyte values to ~41%

were recorded between ~60 and 57 kyr BP, suggesting an environmental response due to colder and more arid climate conditions in the area during HS6. The end of HS6 in the Padul wetland presents then a delayed record (~2,000 – 3,000 years) with respect to the end of the correspondent Greenland Stadial 18 (GS-18) recorded by the NGRIP (~59.4 kyr BP, Rasmussen et al., 2014). This could be related to a slight age uncertainty from the age-depth model of Padul due to the absence of dates between ~65 and 55 cal kyr BP (Camuera et al., 2018) or to a delayed response of the Padul environment to this climatic event.

In this study, D-O cycles 17 to 13 that occurred after HS6 have not been recorded with enough resolution, resulting in 3 cycles (D-O 17-16?, D-O 15-14? and D-O 13) in comparison with the 5 cycles observed in Greenland (NGRIP-Members, 2004). In addition, it is interesting to highlight the low intensity record of the D-O interstadial 13 in both Padul and Ioannina terrestrial records, whose interpretation will be detailed below (Fig. 5.1b, f). The record of HS5 in Padul is evidenced by a peak in xerophytes of ~50% between ~47 and 44 kyr BP, which also seems to be delayed (~2,000 years) with respect to high-latitude areas (Fig. 5.1b-e and g). In this case, the evidences shown by the higher resolution and better constrained age-depth model of the Padul-15-05 during this period (Camuera et al., 2018) along with the paleoclimatic information given by the record from the Alboran Sea, suggest that HS5 could have been recorded with a certain delay in the mid-latitude western Mediterranean region compared to the high-latitude Greenland record. Nevertheless, uncertainties in the age-depth control of the Padul-15-05 and MD95-2043 records cannot be completely discarded. This delay is also shown in the Ionnina pollen record, but with a less degree (Fig. 5.1f).

Another difference of the Padul-15-05 record with respect to the paleoclimate record from Greenland is that the D-O cycles 12 to 9 are only evidenced by 3 main cycles, being D-O events 10 and 9 only recorded as a single cycle (Fig. 5.1b, c). Similarly, these D-O events were not well represented in Alboran Sea and the D-O interstadial 9 occurred with a very low amplitude in the Ionnina-284 record (Fig. 5.1d-f), suggesting that this millennial-scale climatic variability might have been different in the Mediterranean area during these events compared to high-latitude regions. Another important cooling/drying, deduced by a maximum in xerophyte values of ~50% and probably related with HS4, occurred in Padul between ~41 and 39 kyr BP. This HS is only represented by 2 samples but presents a good correlation with respect to the Alboran Sea, Ioannina and Greenland records, showing synchronicity at global scale and a rapid environmental response in the Padul area.

Our record from the Padul wetland shows millennial-scale climate variability probably related with D-O cycles 8 to 5. These warm interstadials show higher PCI values with respect to the previous D-O events 13 to 9, and can be correlated with other regional and global paleoclimate records (Alboran Sea, Ioannina and NGRIP). However, D-O cycles 7 and 6 would need a higher resolution analysis in order to be identified more accurately and interpret their paleoenvironmental impact in southern Iberian Peninsula. The high-resolution data from the last ~30 kyr BP from the Padul-15-05 record allow for a better identification of HSs and D-O variability in the study area. Another maximum in xerophytes with an abundance of ~28% was recorded between ~29 and 27.5 kyr BP (Fig. 5.1c). This cold/dry event could have been related with HS3 and is different from the previous HSs in that it seems to be milder, representing the



least cold/dry HS of the last glaciation period. This is also supported by the lowest semi-desert taxa percentages from the MD95-2043 record and one of the smallest drops in Arboreal Pollen values from the Ioannina-284 record of all the HSs from the last 65 kyr BP (Fig. 5.1d, f).

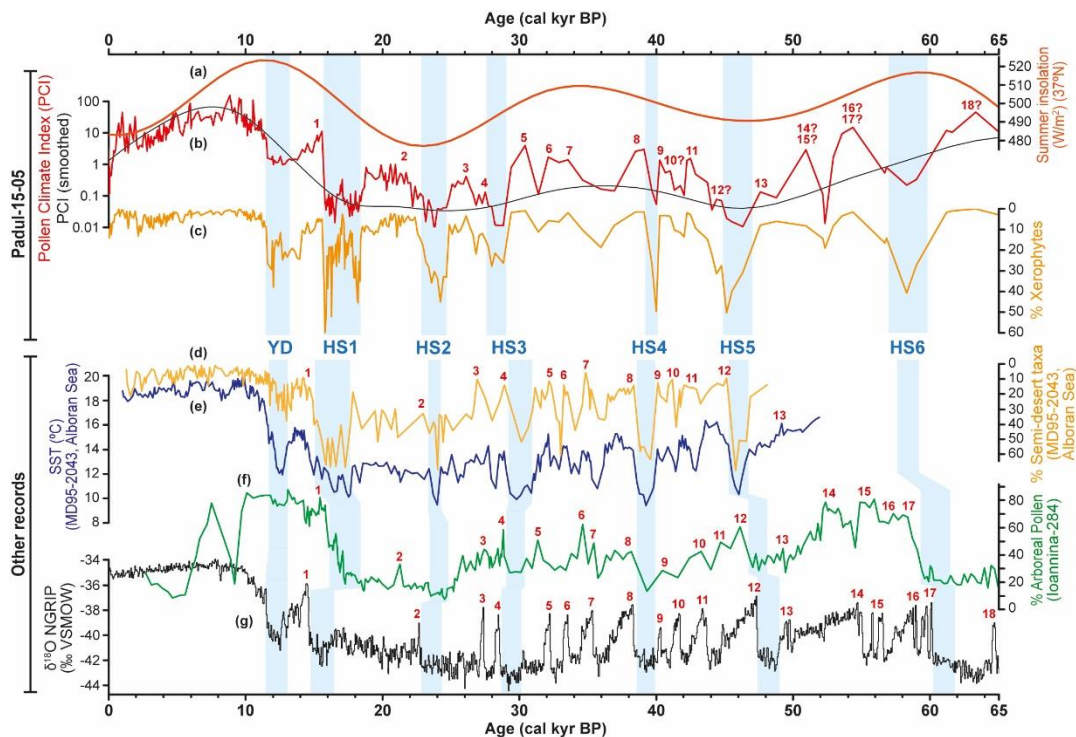


**Figure 5.1.** Paleoclimatic data from the Padul-15-05 record based on palynological analysis in comparison with other paleoclimatic records for the last 65 kyr BP. (a) Summer insolation values at 37° latitude (Laskar et al., 2004). (b) Pollen Climate Index (PCI) and smoothed PCI data and (c) xerophyte percentages from the Padul-15-05 record. (d) Semi-desert taxa (Fletcher and Sánchez Goñi, 2008) and (e) SST from the MD95-2043 record from the Alboran Sea (Cacho et al., 1999; 2001; 2006). (f) Arboreal Pollen percentages from the Ioannina-284 record (Tzedakis et al., 2002; Lawson et al., 2004; Roucoux et al., 2008, 2011) (g)  $\delta^{18}\text{O}$  values (‰, VSMOW) from NGRIP (NGRIP-Members, 2004).

The Padul wetland has also recorded the environmental response of the D-O cycles 4 and 3 but with low amplitude signals, similar to the low amplitude D-O cycle 3 recorded in the Ioannina lake, also suggesting a low magnitude for this interstadial climate signal. Later on, an increase in xerophytes with maximum values of ~45% occurred between ~24.5 and 22.5 kyr BP, suggesting enhanced cold and arid conditions in southern Iberian Peninsula in relation with HS2.

Climate ameliorated again between ~22.5 and 18.4 kyr BP in relation with warm D-O interstadial 2. However, this D-O interstadial 2 in Padul, along with the previous D-O interstadials 4-3 and 13-12, present one of the lowest PCI values of all the D-O interstadials of the last 65 kyr BP (Fig. 5.1b). In the paleoclimatic record from the Ioannina lake, some of these D-O interstadials, in particular the D-O interstadials 13, 3 and 2, were also recorded with a very low amplitude (Fig. 5.1f). In contrast, the previously described D-O interstadials 17 to 14 and 8

to 5 were characterized in Padul by higher PCI, suggesting warmer and more humid climate conditions. This is also supported by the strong warm/humid environmental signal recorded by the Arboreal Pollen in Ioannina mainly during D-O cycles 17 to 14. This seems to be related with the precessional forcing, which has strongly conditioned insolation in the past at mid-latitudes and the western Mediterranean, and therefore, affected the amplitude of the small-scale D-O events in the Padul area. This modulation by insolation on the impact of D-O variability was previously observed by Sánchez Goñi et al. (2008), who noticed latitudinal differences related with middle and high latitudes being mostly controlled by precession and obliquity, respectively. The smoothed PCI data also corroborates the good correlation between the paleoenvironmental vegetation signal at Padul and insolation values at 37° latitude (Fig. 5.1a, b). The coldest and driest period of the last 65 kyr BP was recorded between 18.4 and 15.6 kyr BP during HS1, in which xerophytes reached the highest values ~60%. Extreme cold and arid conditions during HS1 are supported by the MD95-2043 record from Alboran Sea, which also recorded the highest semi-desert taxa with similar values of ~65-70%. Coldest and most arid conditions were also recorded during the previously described HS5, suggesting that these two HSs (HS1 and HS5) were the most arid climate phases of the last glacial period in the southern Iberian Peninsula (Fig. 5.1c, d). The expansion of these arid vegetation species during HSs in both records are strongly related with decreasing SST in the Alboran Sea (Fig. 5.1e). The entrance of polar North Atlantic water into the Mediterranean during HEs contributed to the extreme decrease in SST in western Mediterranean (Cacho et al., 1999), producing low evaporation rates and low moisture content of the low-pressure systems moving across the Mediterranean, and therefore, an intensification of arid conditions in this region (Tzedakis et al., 2004).

Finally, this study shows a very rapid increase in warm and moisture conditions in the Padul area at 15.6 kyr BP and continuing warm/humid conditions until 12.9 kyr BP. This is shown by the abrupt increase in PCI data, which seems to be related with warming during D-O interstadial 1 or Bølling-Allerød (BA). The Padul-15-05 data show a very similar pattern of climate change compared with the  $\delta^{18}\text{O}$  data from Greenland (Fig. 5.1b, c, g). However, the pattern of climate change from HS1 to BA seems to be sharper in the Padul-15-05 record than in the paleoclimatic record from Alboran Sea. The increase in xerophytes in Padul with maximum values of ~38% between 12.9 and 11.6 kyr BP and corresponding to the YD, is not characterized by such extreme arid conditions as the previously recorded HSs. A less extreme cold/arid HS during the YD is also recorded in the paleoclimatic data from Alboran Sea, Ioannina lake and Greenland (Fig. 5.1b-g).

#### 4. Conclusions

The detailed pollen analysis from the Padul wetland, providing new moderate- to high-resolution vegetation data of the last 65 kyr BP from the southern Iberian Peninsula, shows millennial- and centennial-scale vegetation changes related with abrupt HSs and high-frequency D-O variability during the last glacial period. This study also shows the good correlation between vegetation data from the terrestrial Padul-15-05 (southern Iberian Peninsula) with other

terrestrial paleoclimate records such as the Ioannina-284 (Greece) record, and vegetation and SST data from the marine MD95-2043 record (Alboran Sea) in the western Mediterranean region. This shows that both marine and terrestrial environments from the western Mediterranean region were very sensitive and overall synchronic to the same short-scale climate variability, pointing to a same climate control.

Cold and arid conditions are recorded in the Padul-15-05 record during every HSs [HS6 through HS0 (or YD)]. However, xerophyte and semi-desert taxa from Padul and Alboran Sea recorded the most extreme arid conditions of the last glacial period in the southern Iberian Peninsula during HS5 and, in particular, during HS1. Enhanced aridity during cold HSs could have been conditioned by the decrease in SST, producing low evaporation rates and low moisture content moving across the Mediterranean. Environments in the Padul area also sensitively responded to D-O millennial-scale variability. The amplitude of the warmest and most humid D-O interstadials (i.e., D-O interstadials 17 to 15 and 8 to 5) seems to be conditioned by insolation maxima at this latitude, whereas other D-O interstadials (mainly D-O interstadials 13 to 12 and 4 to 2) show lower amplitude and were cooler, most-likely buffered by insolation minima. However, a further palynological study of the Padul-15-05 record increasing data resolution would be necessary for a better environmental and climate interpretation of HSs and D-O variability, principally between ~65 and 30 kyr BP as result of the low-resolution data for this age period. This would allow obtaining one of the highest resolution pollen and paleoenvironmental record of the last 65 kyr BP in the Mediterranean region.

# *Chapter* 6

*Early record of Heinrich Stadial 1 in southern Europe and the  
Mediterranean region*



## **Chapter 6: Early record of Heinrich Stadial 1 in southern Europe and the Mediterranean region**

Jon Camuera<sup>1</sup>, Gonzalo Jiménez-Moreno<sup>1</sup>, María J. Ramos-Román<sup>1</sup>, Antonio García-Alix<sup>1,2</sup>, Francisco Jiménez-Espejo<sup>2</sup>, Jaime L. Toney<sup>3</sup>, R. Scott Anderson<sup>4</sup>, Cole Webster<sup>4</sup>

<sup>1</sup> *Departamento de Estratigrafía y Paleontología, Universidad de Granada, Spain*

<sup>2</sup> *Instituto Andaluz de Ciencias de la Tierra (IACT), Consejo Superior de Investigaciones Científicas-Universidad de Granada (CSIC-UGR), Granada, Spain*

<sup>3</sup> *School of Geographical and Earth Sciences, University of Glasgow, UK*

<sup>4</sup> *School of Earth and Sustainability, Northern Arizona University, USA*

### **Under review:**

Geophysical Research Letters

Impact factor: 4.339

### **Key Points:**

- The compilation of paleoclimatic data from Southern Europe and the Mediterranean area show an early record of Heinrich Stadial 1 (HS1).
- Median age boundaries for HS1 based on marine and continental records from this region ranged between 17,780 and 15,080 cal yr BP.
- Marine records showed a delayed response to this stadial with respect to continental environments.
- Several hypotheses have been proposed for the early mid-latitude environmental record of HS1 with respect to high-latitude records.

## **Abstract**

Previous studies recording Heinrich Stadial 1 (HS1) show disagreement in the timing and the duration of this event. This is probably due to multiple reasons, including the lack of an accurate age control or errors in dating. Records are often tuned to the Greenland ice-core chronology, assuming a synchronicity of this climate event worldwide. However, this prevents the study of possible regional leads/lags in the paleoclimatic records to this event. Here we present a synthetic HS1 age-range for southern Europe and the Mediterranean region based on 18 independently-dated high-resolution records. A Kernel Density Estimation within a Bayesian approach for continental, marine, and the sum of both continental and marine records shows median age boundaries for HS1 at 18,340 – 15,410, 17,700 – 15,040, and 17,780 – 15,080 cal yr BP, respectively. This suggests an earlier and asynchronous record of the terrestrial environments to HS1, with respect to marine and Greenland ice-core records.

## **Plain language summary**

Establishing an accurate age control of past climatic events observed worldwide is essential to understanding future paleoenvironmental studies about these time periods and the underlying processes affecting climate variability in separate geographical areas. Previous studies from southern Europe and the Mediterranean region recording the most extreme glacial conditions occurring during Heinrich Stadial 1 (HS1) present disagreement in the timing and the duration of this period. The median ages obtained from the compiled marine and continental paleoclimatic records from this area show an early record in both the onset and end of HS1 (between 17,780 and 15,080 years ago) with respect to high-latitude ice-core records from Greenland (17,480 – 16,692 years ago). The most probable hypothesis for the early onset of HS1 might have been related to an early deglaciation of the European alpine glaciers during the onset of HS1, enhancing meltwater supply into the Mediterranean, which could have influenced the Mediterranean thermohaline circulation favoring earlier cold/arid climate conditions in this region. The record of an early end of HS1 in this area could have been related to several processes, including the earlier enhanced of the Mediterranean Outflow Water towards the Atlantic, and/or the increased in (a) summer insolation, (b) Mediterranean sea surface temperature and/or (c) atmospheric CO<sub>2</sub>.

## **1. Introduction**

The difference between Heinrich Events (HEs), Heinrich Layers (HLs) and Heinrich Stadials (HSs) has caused much confusion in the scientific literature. HEs are characterized by massive discharge of ice-rafted debris (IRD) from Laurentide, Fennoscandian and Greenland ice sheets into the North Atlantic, resulting in the deposition of detrital and carbonate-rich sediment layers called HLs (Heinrich, 1988; Hemming, 2004; Hodell et al., 2017). HSs were described as cold temperature intervals revealed in the North Atlantic records during which HEs occurred

(Barker et al., 2009). These periods and events represent the most extreme glacial conditions culminating in the decreasing temperature trends of Bond cycles (Bond et al., 1993).

Many HSs registered in the North Atlantic sedimentary records do not present the exact duration and synchronicity with respect to the chronologically corresponding GSs, as defined by isotopic records from Greenland ice-cores (Sánchez Goñi and Harrison, 2010). Researchers are often faced with a choice of using a chronology based on dates obtained from their own record or, alternatively, generating an age model using age correlations (tuning) to Greenland ice-cores. For example, the MD95-2040 [Schönfeld et al. (2003) and de Abreu et al. (2003)], MD95-2042 (Bard et al., 2004), MD03-2697 (Naughton et al., 2016) and ODP 975 (Jiménez-Espejo et al., 2008) records typify the latter. When tuning one paleoclimate record to another, it is assumed that climate events must have been produced by major global-scale changes occurring simultaneously over wide and distant areas. This does not allow possible interpretations of asynchronicities and regional temporal variabilities that could be provided by independent chronological controls (Blaauw, 2012).

During the last two decades, several studies from marine and continental records have focused on the paleoenvironmental reconstructions of HSs (Fletcher and Sánchez Goñi, 2008; Moreno et al., 2010; Stanford et al., 2011). However, the age control of HS1, ostensibly corresponding to Greenland Stadial 2.1a [GS-2.1a; 17,480 – 14,692 yr BP according to Rasmussen et al. (2014)], has not been thoroughly examined in marine and continental paleoclimatic records. Current records show chronological discrepancies in the onset and the end of this period (Fletcher et al., 2010b; Moreno et al., 2010; Sánchez Goñi and Harrison, 2010). Causes in age differences in the environmental responses obtained from different records in the same region to HS1 can be a consequence of: a) errors/uncertainties from radiocarbon dating techniques, b) poor age control produced by low sample resolution, c) very low sedimentary rates, precluding an accurate chronological control, d) the large and variable reservoir effect mainly in marine sediments deposited during HS1 in the North Atlantic [~500 – 1300 <sup>14</sup>C years according to Stern and Lisiecki (2013)] and Mediterranean Sea [~800 years according to Siani et al. (2001)] and/or e) the reworked materials in both marine and continental areas.

This study aims to review and define the age-range for HS1 in southern Europe and the Mediterranean region through comparing HS1 ages boundaries (onset and end) from the new high-resolution paleoclimate record from Padul-15-05 (southern Iberian Peninsula) with other independently and objectively dated high-resolution continental and marine paleoclimatic records, using a Kernel Density Estimation (*KDE*) under a Bayesian approach. The obtained age results differ considerably between terrestrial and marine sites in the study area and with ice-core records from Greenland, demonstrating event asynchronicity. Ultimately, we propose several hypotheses to explain such age differences.

## 2. Material and methods

### 2.1. Padul-15-05 paleoclimatic record of HS1



The 42.64 m-long continuous Padul-15-05 sedimentary record was retrieved from the Padul wetland lakeshore in 2015 (37°00′39″N, 3°36′14″W; Fig. 6.1). Padul-15-05 is characterized by alternation of peat and carbonate/marl lithologies deposited during the last ~200,000 years (Camuera et al., 2018). In this study, the age-depth model of the sediment core has been improved for the 20,000 – 11,000 cal yr BP interval (including HS1) with addition of six new AMS radiocarbon samples from 4.88 to 3.52 m depth, resulting in a total of 15 dates for the interval, from which two of them have been rejected in this study and other three in the previous work from Camuera et al. (2018). The new age-depth model for the Padul-15-05 sedimentary record is shown in Figure 6.2 (see supplementary methods for explanation, Fig. 6.S1 and Table 6.S1).

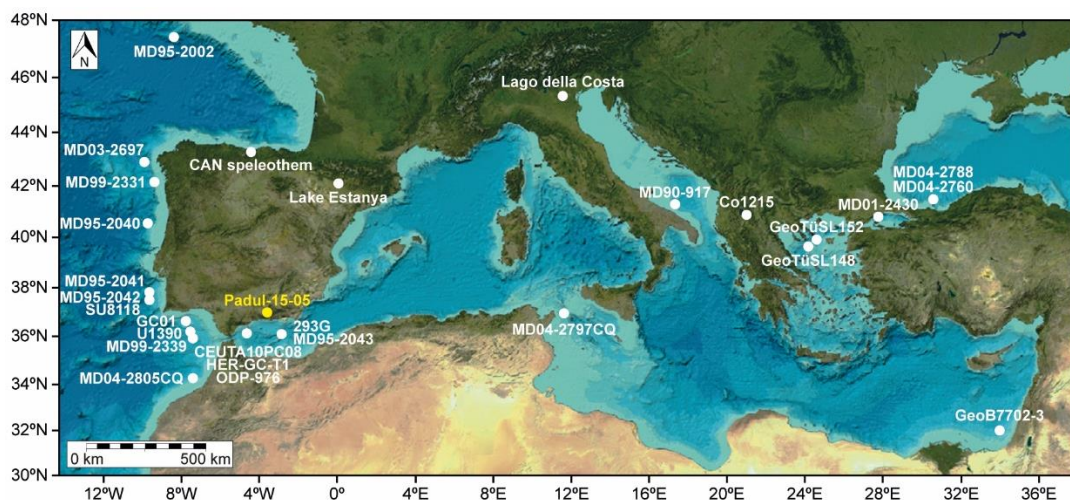


**Figure 6.1.** Location map showing the Padul-15-05 continental record (yellow) and other records, both marine and continental, compared in this study. Individual records were chosen due to their high-resolution paleoenvironmental data during HS1 and location (southern Europe and the Mediterranean region). All these records document well-dated numerical ages for HS1 boundaries in their respective studies. See text, Figure 6.S2, and Tables 6.S2a and b for more information about the archives compiled for this study.

This study focuses on the palynological analysis of 92 pollen samples of the Padul-15-05 record distributed between 4.88 – 3.52 m depth (20,000 – 11,000 cal yr BP). In particular, the delimitation of HS1 is based on 44 pollen samples (between 4.16 and 4.61 m depth), improving the temporal data resolution with respect to the previously published study from Camuera et al. (2019) up to a maximum resolution of ~61 years. Here we show pollen abundances of Mediterranean forest (*Quercus* total, *Olea*, *Phillyrea* and *Pistacia*) and xerophytes (sum of *Artemisia*, *Ephedra* and *Amaranthaceae*; Fig. 6.2). Xerophytes are a good proxy for aridity, especially during the most arid climate conditions (Pini et al., 2009), and a reliable paleoclimatic proxy for the identification of HS1 in the southern Iberian Peninsula (Camuera et al., 2019). Therefore, xerophytes have been taken as the more appropriate pollen taxa for HS1 age delimitation in Padul.

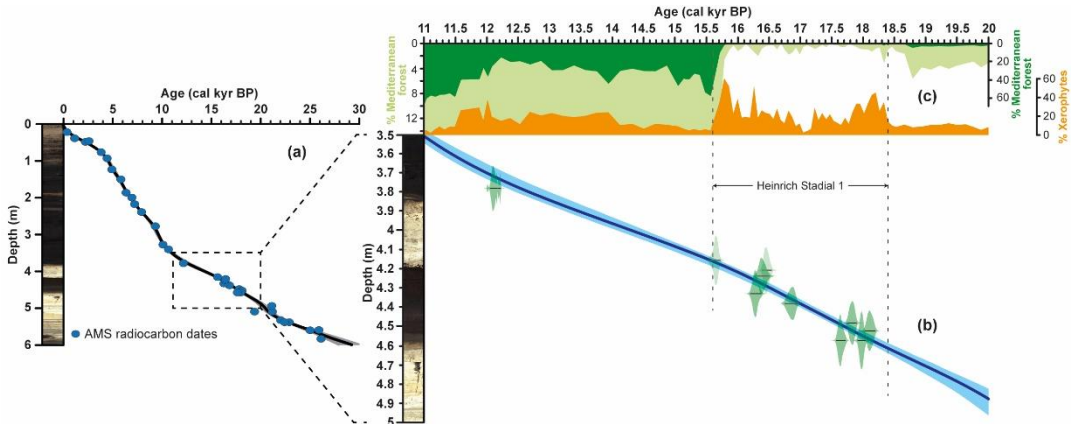


**Figure 6.2.** The chronological control and percentages of xerophyte and Mediterranean forest pollen data from Padul-15-05. (a) The age-depth model with the AMS radiocarbon dates used for the last 30,000 cal years. (b) The age-depth model between 20,000 and 11,000 cal yr BP. (c) Percentages of xerophyte and Mediterranean forest (light green = exaggerated vertical scale) obtained for the time period between 20,000 and 11,000 cal yr BP. During cold/arid periods (e.g., HS1) xerophytes increase and Mediterranean forest values decrease. The upper and lower boundaries of HS1 have been delimited based on xerophyte data.

## 2.2. Synthetic HS1 age-range boundaries for southern Europe and the Mediterranean region

The age-range (onset and end) for HS1 in southern Europe and the Mediterranean region was statistically calculated using a compilation of detailed ages from Padul-15-05 and other available marine and continental (lakes, speleothems) sites recording HS1 in this area, according to the following criteria:

- Marine and terrestrial records are located in southern Europe and the Mediterranean region, specifically, between latitude 31°N and 48°N, and between longitude 10°W and 34°E (Fig. 6.1).
- Records are of high-resolution data only, where HS1 is represented with at least 10 samples (ca. >250-yr mean resolution) (Fig. 6.S2).
- Records should not be tuned to ice-core chronologies or to other nearby records, and ages for HS1 should be based on independent absolute dates providing an objective age-depth model.
- Records should have an exact numerical age-range for HS1 suggested or mentioned in the correspondent original studies.

Data from twenty non-tuned and independently dated high-resolution marine and continental paleoclimatic records (including Padul-15-05) have been compiled following the above criteria (Fig. 6.S2). HS1 age boundaries previously published were revised (Fig. 6.S2) and the median ages from a *KDE* were calculated (Fig. 6.3; see Supplementary methods for more information and Table 6.S2a). The median ages for HS1 boundaries including all marine and continental records (*KDE Total*) were obtained running a *KDE\_plot* function within a Bayesian model using the Oxcal software (Ramsey, 2017). In addition, we also calculated boundaries for

HS1 based on the original age delimitations that authors provided in their studies for comparison (Fig. 6.S2 and 6.S3, Table 6.S2a and Supplementary Information).

This methodology was also applied to individual groupings of 4 continental records and 12 marine cores with 15 paleoclimatic records (Fig. 6.3) with the purpose of observing possible leads and lags between the different environments (*KDE Continental* and *KDE Marine*, respectively; Fig. 6.3 and 6.S3) (see Supplementary Information for more accurate methodology). Even if the compiled paleoclimatic proxies represent different environmental signals (aridity, freshwater pulses, presence of cold water, etc.), the lack of enough records displaying the same signal as in Padul (aridity) under the criteria mentioned above does not allow us to suggest an age-range for HS1 based on a unique climate signal.

### 3. Results and discussion

The accurately-constrained age model of the Padul-15-05 record shows an age range for HS1 between 18,400 and 15,600 cal yr BP (Fig. 6.2). The obtained *KDE* median ages for HS1 boundaries, including the revised independently dated high-resolution marine and continental records from southern Europe and the Mediterranean region (*KDE Total*), exhibited ages of 17,780 cal yr BP for the onset and 15,080 cal yr BP for the end of HS1. According to this, the onset and end of HS1 in southern Europe are respectively recorded at least ~300 and ~390 years earlier than in the Greenland ice-cores [GS-2.1a onset at 17,480 yr BP and end at 14,692 yr BP; Rasmussen et al. (2014)]. Sánchez Goñi and Harrison (2010) also suggested early environmental response of HS1 in the North Atlantic (between 18,000 and 15,600 yr BP) with respect to the Greenland chronology, based on the age compilation recorded from several North Atlantic cores (Elliot et al., 2001; 2002).

Regional age differences between different world areas as response to global climatic oscillations have also been recorded in several marine and continental sites. For example, opposite temperature conditions and asynchronous signals displayed in Northern and Southern Hemispheres during the last deglaciation affected the Atlantic's conveyor circulation and heat transmission between the North Atlantic and the South Atlantic (Barker et al., 2009). Other asynchronous paleoclimatic responses to climate changes were also recorded between low- and high-latitudes during the Last Termination in Lake Suigetsu (Japan) (Nakagawa et al., 2003) and during the Younger Dryas in the eastern Mediterranean (Castañeda et al., 2010).

Below we present some possible causes for the early response of the onset and the end of HS1 in southern Europe and the Mediterranean region with respect to the correspondent GS-2.1a from Greenland ice-core records.

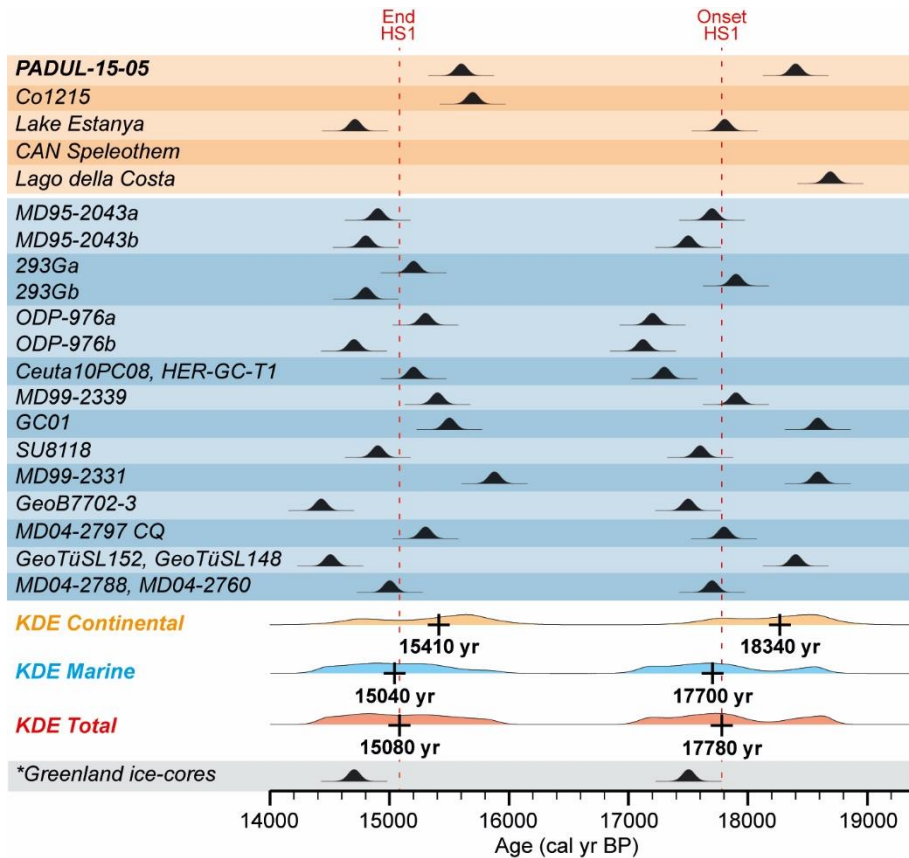


**Figure 6.3.** Median ages of HS1 boundaries, obtained by means of a *KDE* under a Bayesian modelling. Ages for each non-tuned high-resolution records have been obtained according to our revision of the age boundaries from the paleoclimatic data of different proxy records to HS1 (see Supplementary Information, Figure 6.S2 and Table 6.S2a). We assumed an error of  $\pm 50$  years for all the ages for the onset/end of HS1 from the different paleoclimatic record data. Note that the age boundaries of CAN speleothem and for the end of Lago della Costa have not been included, as they do not present data for this time periods due to hiatuses (CAN speleothem) and absence of data (Lago della Costa). Continental records are marked in orange/light orange, whereas marine records are in blue/light blue. The median ages for the boundaries of HS1 include: all the continental records (*KDE Continental*, orange), all the marine records (*KDE Marine*, blue), and the sum of all continental and marine records (*KDE Total*, red). Red vertical dashed lines indicate the median age distributions of the HS1 boundaries provided by the *KDE Total* (onset HS1 = 17,780 cal yr BP; end HS1 = 15,080 cal yr BP). The age-range of GS-2.1a from Greenland ice-cores (Rasmussen et al., 2014) is shown at the bottom of the figure.

### 3.1. Early beginning of HS1 in southern Europe and the Mediterranean area

An early onset of HS1 has been recorded in the study region with median ages of 18,340 cal yr BP for continental areas, 17,700 cal yr BP for marine sites, and 17,780 cal yr BP for both continental and marine records (*KDE continental*, *KDE marine* and *KDE total*, respectively; Fig. 6.3). Understanding what may have caused the HS1 climatic event worldwide could help us hypothesize reasons why it occurred earlier in the study area. Shakun et al. (2012) suggested

increasing temperatures associated with increased boreal summer insolation generated warming in the northern hemisphere between ~22,000 and 19,000 yr BP. This in turn generated the retreat of the Arctic ice cap and enhanced cold freshwater fluxes into the North Atlantic, lowering the temperature between 30°N and 90°N after 19,000 years ago, and an Atlantic Meridional Ocean Circulation (AMOC) slowdown occurred. Global climate models suggest that an AMOC slowdown and the reduction of the ocean heat transport could have produced a large reduction in surface heat flux inland and atmospheric thermal decrease in continental western Europe (Ganopolski and Roche, 2009; Jackson et al., 2015; Martín-García, 2019). A weak AMOC could have triggered a reduction to the amount of humidity held in the atmosphere as well as a weakening of the westerlies, and consequently, a decrease in precipitation in mid-latitude western Europe. The reduced moisture transport from the ocean to the land would have also resulted in a decrease in forest cover over this region (Jackson et al., 2015), as shown by the decrease of the Mediterranean forest (contrary to the behavior of xerophytes) during HS1 (Fig. 6.2c). Our data show that HS1 in the study area began early, in agreement with an early AMOC reduction, which could have generated a fast environmental response in mid-latitude southern Europe with especially cold and arid climate conditions. However, more studies are required in order to understand how the AMOC could have affected earlier the mid-latitude southern Europe and the Mediterranean region compared to high-latitude areas.

A more solid hypothesis for the early onset of HS1 in southern Europe and the Mediterranean region could be related to the increasing summer insolation after the minima at 23,000 yr BP that produced enhanced freshwater discharges from the European ice sheet [at ~18,200 yr BP according to Toucanne et al. (2015)] and alpine glacier melting from the Alps and Apennines, which could have led to the slowdown of the Mediterranean Sea overturning circulation (Fink et al., 2015; Jiménez-Espejo et al., 2015; Rohling et al., 2015). In the case of the Alps, the glacial retreat began ~20,000 years ago, suggesting an early meltwater influx at ~19,000 yr BP into the western Mediterranean through the large rivers from the northern Mediterranean borderlands, such as the Var River in SE France (Bonneau et al., 2014 and references therein). This early reduction of the Mediterranean thermohaline circulation could have been the cause of the early beginning of extremely cold and arid conditions in this region, as it is the main factor controlling regional climate (Rohling et al., 2015).

### *3.2. Early end of HS1 in southern Europe and the Mediterranean area*

This study also shows an early end of HS1 with a synthetic median age of 15,410 cal yr BP in continental areas, 15,040 cal yr BP in marine environment, and 15,080 cal yr BP including all continental and marine sites in the study area (*KDE continental*, *KDE marine* and *KDE total*, respectively; Fig. 6.3).

The onset of the Bølling-Allerød (B-A) seems to have been triggered by the abrupt resumption of the AMOC (McManus et al., 2004) and different processes have been proposed for this restart [Liu et al. (2009) and references therein; Thiagarajan et al. (2014) and references therein]. The Mediterranean Outflow Water (MOW) has also been suggested as an important factor influencing the switch from stadial to interstadial AMOC modes (Pénaud et al., 2011). A

coupled atmosphere-ocean General Circulation Model showed that changes in the MOW and in the Mediterranean-Atlantic water exchange play an important role on the strength of the AMOC (Rogerson et al., 2010), affecting the regional climate of the high-latitude North Atlantic, Labrador and Greenland Seas (Ivanovic et al., 2014). The enhanced MOW towards the Atlantic occurred ~15,500 years ago (Rogerson et al., 2010), several hundred years before the usually assumed onset of the B-A ~14,700 yr ago. According to that, it could be hypothesized that the early enhanced MOW and own Mediterranean Sea thermohaline reactivation could have previously affected climate at the lower latitude Mediterranean area, suggesting an earlier environmental response of the warm and humid B-A interstadial in this region.

A deglacial warming between 16,500 and 16,000 yr BP, ~1,500 years before the onset of the B-A in Greenland ice-cores, was also recorded by increasing chironomid-inferred summer temperatures and early forest expansion in Lago di Origlio (southern Alps) and in nearby areas (Vescovi et al., 2007; Samartin et al., 2012). Other records also presented an early warming/humid transition after the Heinrich Event 1 (HE1) at ~16,000 yr BP, such as the SSTs from the Gulf of Cadiz, Alboran Sea and Tyrrhenian Sea [see Figure 4 from Cacho et al. (2001) and references therein] or the  $\delta^{13}\text{C}$  ‰ values shown from Soreq and Sofular caves [see Figure 7 from Samartin et al. (2012) and references therein]. The slight SST warming in the Mediterranean Sea and Iberian margin at this time seems to be accompanied by increasing atmospheric temperature and an early vegetation response in western Mediterranean and southern Iberian Peninsula (Naughton et al., 2009). This early beginning of the B-A could have been related to higher summer insolation triggering higher temperatures, but also with the early increase in atmospheric  $\text{CO}_2$  concentration that started to rise ~17,000 years ago (Lourantou et al., 2010) favoring the expansion of the forest cover in continental realms. In addition, the low heat transport along the North Atlantic due to the slowdown of the AMOC during HS1, as explained above, was probably sufficient to restrict the entrance of cold Atlantic water into the Mediterranean, and therefore, causing an early ocean and atmospheric B-A warming in the Mediterranean area as result of the increasing insolation and/or  $\text{CO}_2$  concentration (Samartin et al., 2012).

Another hypothesis for the earlier environmental record in this area could have been related with increasing summer insolation that could have resulted in a faster mid-latitude land and SST increase favored by the higher insolation values at Mediterranean latitude compared to higher latitudes (Laskar et al., 2004). This is strongly related to the precessional forcing on insolation that dominates climate at low- and mid-latitudes (e.g., Mediterranean region), highly influencing temperature in this area and being a more important climate factor here than at high-latitudes (Tzedakis, 2007). This hypothesis is supported by a study also showing an early environmental response during the beginning of the B-A in Lake Suigetsu (Japan) with respect to the Cariaco basin and ice-core data (Nakagawa et al., 2003). This study suggested that the northwestern Pacific and the Sea of Japan could have responded faster to increasing insolation than the North Atlantic and high-latitude areas, which could have been similar to what occurred in mid-latitude southern Europe and the Mediterranean region.

### 3.3. HS1 age discrepancies between continental and marine environments

The Padul-15-05 record as well as the median ages for continental records obtained from the *KDE* based on Bayesian modelling suggest an earlier terrestrial environmental response with respect to marine environments from southern Europe and the Mediterranean and Greenland during both onset and end of HS1 (Fig. 6.3). The age differences between *KDE continental* and *KDE marine* are ~640 years for the onset and ~370 years for the end of HS1. However, it should be taken carefully as the continental median age boundaries of HS1 (*KDE continental*) are only based on the compilation of three terrestrial records.

Several hypotheses have been suggested favoring asynchronous responses to climate changes between continental and marine environments in the study area, such as a lagged response of the marine biological signals (resulting in a paleoclimatic proxy) to physical climate forcing due to different productivity, dynamical and biogeographical features (Sicre et al., 2016). Temporal delays were also observed in marine environments between alkenone-derived and GDGT (glycerol dialkyl glycerol tetraether)-derived SST reconstructions. Alkenones, commonly in association with fine sediments, presented a lagged response of a few hundred years with respect to the GDGTs, which are linked to larger sedimentary particles. The different ages provided by both SST reconstructions are conditioned by grain size fraction, and therefore, subjected to the water flow velocities and densities (Magill et al., 2018). Moreover, the same marine record can provide different HS1 age boundaries depending on the paleoclimatic proxy used, such as the alkenone SST and pollen data from MD95-2043 record, the alkenone SST and foraminifera data from the OPD-976 record, or the Zr/Al and SST reconstruction from the 293G record (Fig. 6.S2 and Table 6.S2a).

Radiocarbon dating on terrestrial environments (e.g., lakes or peatlands) could have produced older radiocarbon ages, especially in relation with reworked materials or reservoir effect on the measured samples (Björck and Wohlfarth, 2002). However, the analyzed samples from Padul were pretreated to remove any carbonate remains that could contaminate the plant remains with older carbon, avoiding age errors related with bulk material and with carbonate and clay sediments transported from the Sierra Nevada range (see Supplementary Information and Table 6.S1).

The previously exposed hypotheses could explain, at least partially, the lagged response of some marine proxy data with respect to the terrestrial paleoclimatic indicators, and consequently, the more modern median ages of marine environments compared to continental areas. Nevertheless, more specific studies focusing on factors affecting the lagged marine and/or early continental records of HS1 in southern Europe and the Mediterranean region are necessary.

## 4. Conclusions

Our recent high-resolution paleoclimatic study of the Padul-15-05 sedimentary record from S Spain, together with other 17 well-dated paleoclimatic continental and marine records documenting HS1 from southern Europe and the Mediterranean area shows that:

- 1) The synthetic median ages for the onset and the end of HS1 in this area are 17,780 and 15,080 cal yr BP, respectively. This shows an early record of Heinrich Stadial 1 in southern Europe and the Mediterranean region, compared to the high-latitude Greenland ice core records [GS-2.1a; 17,480 – 14,692 yr BP according to Rasmussen et al. (2014)]. The mid-latitude location as well as the geographical features of southern Europe and the Mediterranean area could have somehow conditioned the early environmental record of HS1 in this area. However, further studies focusing on more detailed interpretations of possible causes leading to this early environmental record in this region are necessary.
- 2) Continental records show an earlier evidence of HS1 (onset = 18,340 cal yr BP; end = 15,410 cal yr BP) compared to marine records (onset = 17,700 cal yr BP; end = 15,040 cal yr BP) from the study area. This age difference that could have lagged the paleoclimatic signal in marine environments could be explained by different processes, such as the lagged biological response to climate forcing and/or the ocean water flow velocities and densities.
- 3) This study highlights the importance of well-dated continental sedimentary records with continuous and high sedimentation rates (e.g., Padul wetland), providing excellent sites for paleoclimate reconstructions, especially for rapid climate changes such as the HS1, and showing good environmental signal under accurate chronological control.

Tuning to Greenland ice-core records should be avoided outside northernmost Atlantic climatic realm, since climate events might be asynchronous in different worldwide areas as result of the different geographical location and environmental features affecting them.

### **Acknowledgments**

This study and research have been supported by the projects CGL2013-47038-R and CGL-2017-85415-R, the PhD funding BES-2014-069117 (Jon Camuera) and the Ramón y Cajal fellowship RYC-2015-18966 (Antonio García-Alix), provided by the Ministerio de Economía y Competitividad of the Spanish Government. Additional funding was also provided by the research group RNM0190 and the project P11-RNM-7332 with a postdoctoral fellowship (María J. Ramos-Román) from the Junta de Andalucía. We acknowledge all the authors that have provided us with the paleoclimatic data from Figure 6.S2. Our pollen data from Padul will be provided on request.



## Supplementary Information

### Early record of Heinrich Stadial 1 in southern Europe and the Mediterranean region

Jon Camuera<sup>1</sup>, Gonzalo Jiménez-Moreno<sup>1</sup>, María J. Ramos-Román<sup>1</sup>, Antonio García-Alix<sup>1,2</sup>, Francisco Jiménez-Espejo<sup>2</sup>, Jaime L. Toney<sup>3</sup>, R. Scott Anderson<sup>4</sup>, Cole Webster<sup>4</sup>

<sup>1</sup> *Departamento de Estratigrafía y Paleontología, Universidad de Granada, Spain*

<sup>2</sup> *Instituto Andaluz de Ciencias de la Tierra (IACT), Consejo Superior de Investigaciones Científicas-Universidad de Granada (CSIC-UGR), Granada, Spain*

<sup>3</sup> *School of Geographical and Earth Sciences, University of Glasgow, UK*

<sup>4</sup> *School of Earth and Sustainability, Northern Arizona University, USA*

### Supplementary text

#### *Chronology of the Padul-15-05 record*

The age-depth model of the Padul-15-05 core was based on 42 accelerator mass spectrometry (AMS) radiocarbon dates (including dating on specific compounds), 4 amino acid racemization (AAR) dates and sediment accumulation rates for the bottom part of the core (Camuera et al., 2018; 2019). Two new age-depth models were developed with the R-code package “Clam 2.2” software (Blaauw, 2010) using the smooth spline model type and IntCal13.14C calibration curve at 95% confidence range for the time period between 20,000 and 11,000 cal yr BP in order to obtain a more precise chronological control for HS1. The “Padul age model 2” was rejected due to our assessment of two radiocarbon samples being too old (460.35 cm depth; 19,410 and 19,481 cal yr BP; Fig. 6.S1 and Table 6.S1), probably resulting from a reservoir effect. Even if carbonate samples have been pretreated and dating was done on the organic residue, a small carbon reservoir effect could be associated to these samples, as carbonate sediments from lakes are commonly linked to carbon-reservoir age errors varying between 500 and 2000 years (Grimm et al., 2009). Therefore, the “Padul age model 1”, in which we excluded these two samples from carbonate layers showing too old ages, has been assumed as the best age-depth model, providing a good chronological control for HS1 (Fig. 6.1 and 6.S1).

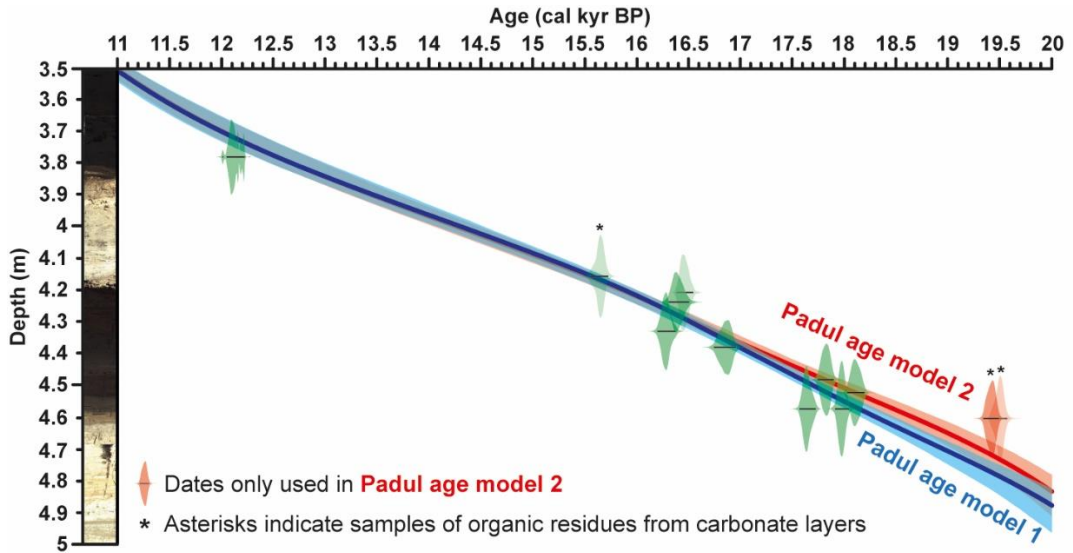


**Figure 6.S1.** Age-depth models (Padul age model 1 and 2) of the Padul-15-05 record between 20,000 and 11,000 cal yr BP. The selected “Padul age model 1” was developed excluding two samples of organic residues from carbonate layers, as discussed above. Dates marked in green (10 samples) were used in both age models, whereas dates marked in red (2 samples) were only used for the “Padul age model 2”.

Lab. reference	Material	Depth (cm)	$\delta^{13}\text{C}$ (‰)	Age ( $^{14}\text{C}$ yr BP $\pm 1\sigma$ )	Calibrated age (cal yr BP) 95% confidence interval	Median age (cal yr BP)
Reference age		0		2015 CE	-65	-65
D-AMS 008531	Plant remains	21,67	-11,3	103 $\pm$ 24	23 - 264	127
Poz-77568	Org. bulk sed.	38,46	-31	1205 $\pm$ 30	1014 - 1239	1130
BETA-437233	Plant remains	46,04	-24,3	2480 $\pm$ 30	2385 - 2722	2577
Poz-77569	Org. bulk sed.	48,21	-29,2	2255 $\pm$ 30	2158 - 2344	2251
BETA-415830	Gastropods	71,36	-10,1	3910 $\pm$ 30	4248 - 4421	4343
BETA-437234	Plant remains	76,34	-28	3550 $\pm$ 30	3722 - 3956	3838
BETA-415831	Org. bulk sed.	92,94	-26,7	3960 $\pm$ 30	4297 - 4519	4431
Poz-74344	Plant remains	122,96	-26,4	4295 $\pm$ 35	4827 - 4959	4871
BETA-415832	Plant remains	150,04	-26,8	5050 $\pm$ 30	5728 - 5900	5814
Poz-77571	Plant remains	186,08	-29,2	5530 $\pm$ 40	6281 - 6402	6341
Poz-74345	Plant remains	199,33	-29,7	6080 $\pm$ 40	6797 - 7154	6935
BETA-415833	Org. bulk sed.	217,36	-26,8	6270 $\pm$ 30	7162 - 7262	7212
Poz-77572	Org. bulk sed.	238,68	-29,6	7080 $\pm$ 50	7797 - 7999	7910
Poz-74347	Plant remains	277,24	-29,6	8290 $\pm$ 40	9138 - 9426	9293
BETA-415834	Plant remains	327,29	-26,4	8960 $\pm$ 30	9932 - 10221	10107
Poz-77573	Plant remains	340,04	-29,8	9420 $\pm$ 50	10514 - 10766	10640
Poz-74348	Plant remains	375,62	-26,7	9120 $\pm$ 50	10199 - 10412	10305
Poz-79815	Org. bulk sed.	377,83	-28,6	10310 $\pm$ 50	11847 - 12388	12144
Poz-79817	Gastropods	411,02	-7,2	13910 $\pm$ 60	16588 - 17088	16838
Poz-79818	Gastropods	414,89	-6,8	14130 $\pm$ 50	17001 - 17419	17210
BETA-506210 *	Organic residue	415,46	-27,1	13060 $\pm$ 40	15400 - 15852	15658
BETA-506209 *	Organic residue	420,59	-31,2	13630 $\pm$ 40	16238 - 16639	16365
Poz-77574	Org. bulk sed.	423,65	-27,2	13580 $\pm$ 80	16113 - 16654	16384
Poz-79819	Org. bulk sed.	432,82	-31,3	13500 $\pm$ 60	16047 - 16494	16270
Poz-19821	Org. bulk sed.	437,92	-29,7	13910 $\pm$ 70	16570 - 17113	16841
Poz-79822	Org. bulk sed.	448,12	-29,7	14640 $\pm$ 70	17618 - 18011	17814
Poz-77575	Org. bulk sed.	452,2	-28,6	14890 $\pm$ 80	17898 - 18325	18111
BETA-506207 *	Organic residue	457,29	-29,7	14480 $\pm$ 50	17473 - 17863	17650
BETA-506208 *	Organic residue	457,29	-29,9	14780 $\pm$ 50	17815 - 18157	17980
BETA-506205 *	Organic residue	460,35	-30,4	16140 $\pm$ 60	19256 - 19661	19481
BETA-506206 *	Organic residue	460,35	-29,7	16080 $\pm$ 60	19210 - 19592	19410
Poz-79837	Org. bulk sed.	493,43	-28,7	17580 $\pm$ 80	20966 - 21527	21246
Poz-79838	Pollen residue	493,43	-32	17450 $\pm$ 80	20813 - 21352	21082
Poz-79839	Org. bulk sed.	509,26	-28,2	17510 $\pm$ 80	20885 - 21429	21157
Poz-79843	Pollen residue	509,26	-29,8	16060 $\pm$ 70	19173 - 19587	19380
Poz-74349	Plant remains (vertical roots)	513,22	-26,9	10740 $\pm$ 60	12582 - 12737	12659
Poz-79841	Pollen residue	532,24	-31,9	18210 $\pm$ 90	21836 - 22329	22082
Poz-77576	Org. bulk sed.	537,84	-27,5	19010 $\pm$ 120	22538 - 23255	22896
Poz-79842	Pollen residue	537,84	-26,5	18570 $\pm$ 80	22280 - 22628	22454
Poz-77820	Org. bulk sed.	559,25	-30,5	21650 $\pm$ 130	25691 - 26132	25911
Poz-79844	Pollen residue	559,76	-27,6	20790 $\pm$ 90	24660 - 25378	25019
BETA-437235	Plant remains	582,92	-15,7	21900 $\pm$ 80	25916 - 26331	26123

**Table 6.S1.** AMS-standard radiocarbon dates of the last 30,000 cal years from the Padul-15-05 record [modified from Camuera et al. (2018)]. Six new radiocarbon samples pretreated (HCl + HF) were analyzed for this study and have been marked with an asterisk (\*) in the *Lab. reference* column. Ages excluded from the age-depth model are marked in red.

### Palynological analysis

In this study, the temporal sample resolution of the palynological analysis has been improved with respect to the previously published work about the paleoenvironmental reconstruction of the last ~197,000 years from the entire Padul-15-05 record (Camuera et al., 2019). The pollen extraction followed a modified methodology of Faegri and Iversen (1989),

whereas the analysis was developed identifying a minimum of 300 terrestrial pollen grains per sample using a Zeiss transmitted light microscope. Xerophyte taxa percentages were calculated based on terrestrial pollen sum excluding aquatic plants (*Cyperaceae*, *Typha*, *Myriophyllum*, *Utricularia* and *Potamogeton*).

### *Synthetic HS1 age-range estimation*

The revision of HS1 age boundaries of the proxy data from every record was obtained by taking the middle points of climate transitions (i.e., Last Glacial Maximum-HS1 transition for the onset of HS1 and HS1-Bølling Allerød transition for the end of HS1), trying to not highly differ from the ages provided by authors in their original studies. Our revision of HS1 boundaries for continental records exhibit a median age-range between 15,410 and 18,340 cal yr BP, and a mean age of  $15,330 \pm 462$  cal yr BP for the onset and  $18,290 \pm 397$  cal yr BP for the end of HS1. Marine records show a median age boundaries between 15,040 and 17,700 cal yr BP, and a mean age of  $15,060 \pm 398$  cal yr BP for the onset and  $17,770 \pm 460$  cal yr BP for the end of HS1. Finally, the sum of all marine and continental paleoclimatic data presented a median age boundaries between 15,080 cal yr BP and 17,780 cal yr BP, and a mean age of  $15,100 \pm 419$  cal yr BP for the onset and  $17,860 \pm 489$  cal yr BP for the end of HS1. The median age boundaries from continental, marine and sum of continental and marine records are shown in Figure 6.3.

For comparison with the median ages obtained for the age-range of HS1, which are based on our revision of the boundaries from every paleoclimatic record data, we have also calculated the median ages of HS1 based on the original age boundaries provided by authors in their studies (Fig. 6.S2). This calculation including all marine and continental records (*KDE Total*) has resulted on the onset of HS1 occurring at 17,920 cal yr BP and the end at 15,050 cal yr BP (Fig. 6.S3). Note that some studies working on the same record and under the same chronological control displayed different delimitations for HS1 as result of the different proxy data used (Fig. 6.3 and 6.S3, and Table 6.S2a). Nine records tuned with ice-cores or with other nearby records from this region (sometimes also tuned to Greenland) were excluded from the Kernel Density Estimation (*KDE*) modellings in order to avoid circular reasoning (Blaauw, 2012).

The median ages of HS1 boundaries provided by a *KDE* under a Bayesian modelling were calculated using the OxCal distribution V4.3 (<http://c14.arch.ox.ac.uk/index.html>). The median ages for HS1 boundaries in continental (*KDE Continental*), marine (*KDE Marine*), and sum of continental and marine environments (*KDE Total*) were obtained using the *KDE\_plot* function (Ramsey, 2017). In addition, for the *KDE Total* we also carried out the *KDE\_model* function for a double-check of the median ages previously obtained with the *KDE\_plot* method (Ramsey, 2017). We decided to only display median ages from the *KDE\_plot* in Figures 6.3 and 6.S3, as both *KDE\_plot* and *KDE\_model* methods show the same ages for HS1 boundaries. Note that an age error of  $\pm 50$  years has been assumed for all the proxy data boundaries from every paleoclimatic record data before running the *KDE*.

Early record of Heinrich Stadial 1 in southern Europe and the Mediterranean region

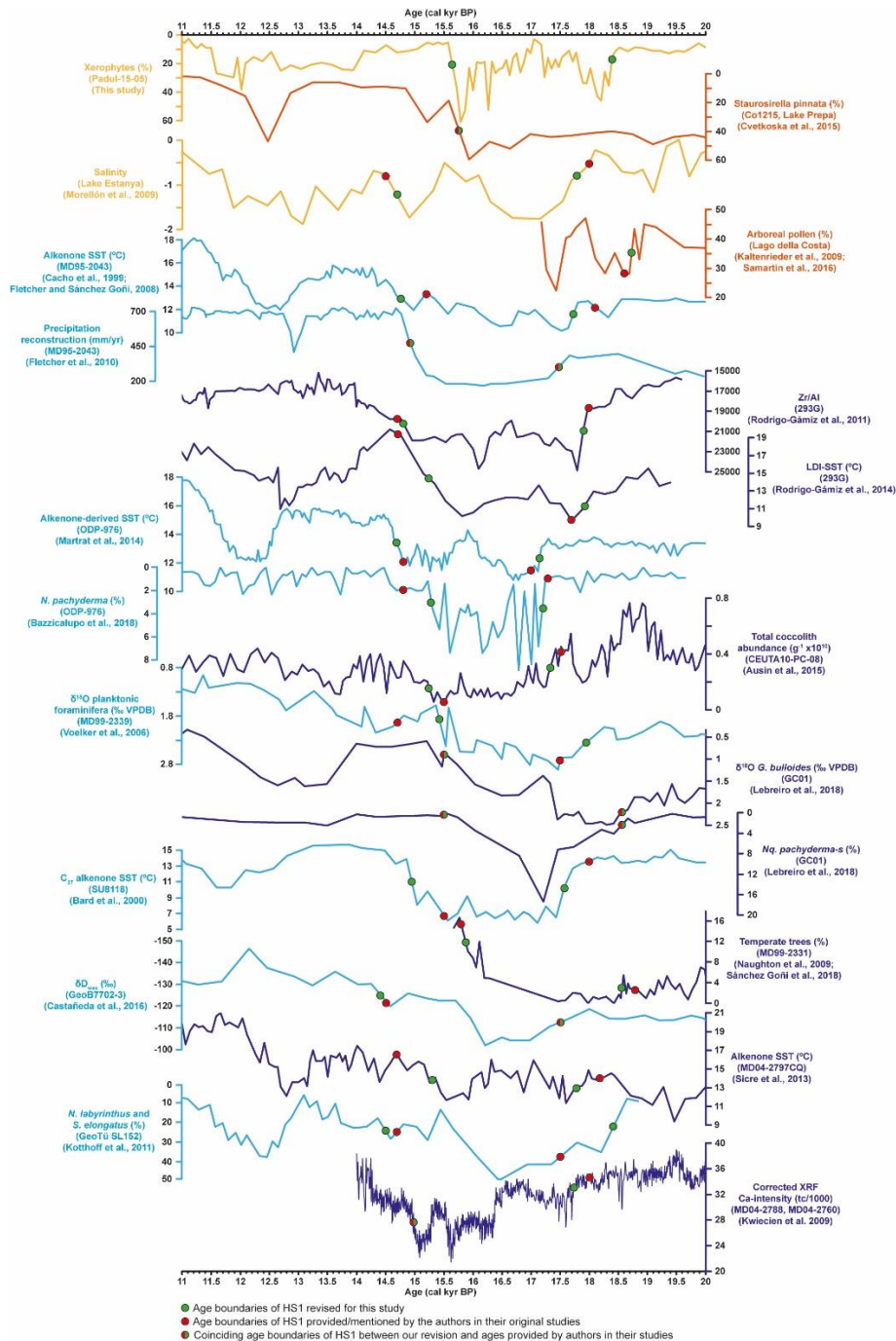


**Figure 6.S2.** All the proxy data from the non-tuned and independently dated high-resolution records from southern Europe and the Mediterranean region between 20,000 and 11,000 cal yr BP. Green dots represent the ages boundaries (onset and end) of HS1 according to our detailed revision of the multiproxy data from the different paleoclimatic records, whereas red dots show the original age boundaries of HS1 exposed by the authors in their previously published studies. Continental records are represented in orange/light orange and marine records are displayed in blue/light blue.

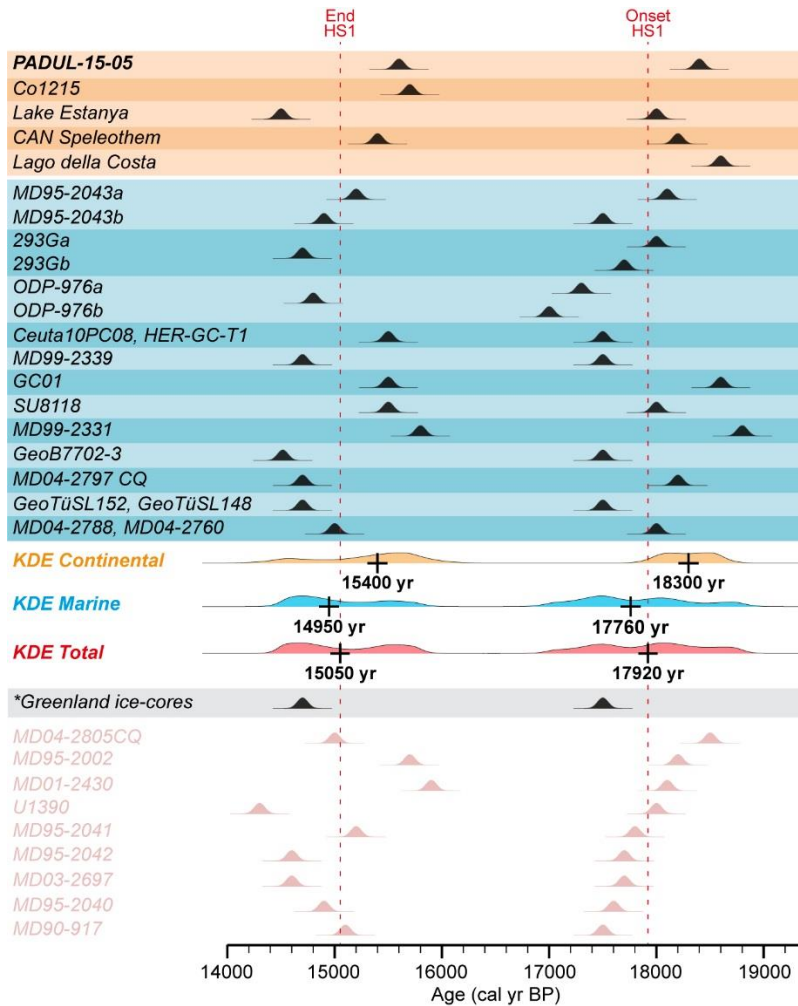


**Figure 6.S3.** The median ages of HS1 obtained from the original age boundaries provided by authors in their studies. On the top of the figure are high-resolution non-tuned sites (orange/light orange = continental records including Padul-15-05; blue/light blue = marine records) showing ages based on data previously published (Figure 6.S2 and Table 6.S2a). It has been assumed an error of  $\pm 50$  years for all the age boundaries from all paleoclimatic data. The median ages for the HS1 boundaries are represented as: *KDE Continental* (including all continental records, orange), *KDE Marine* (including all marine records, blue) and *KDE Total* (including all continental and marine records, red). Red vertical dashed lines indicate the median age distribution of HS1 boundaries provided by the *KDE Total* (onset HS1 = 17,920 cal yr BP; end HS1 = 15,050 cal yr BP). The age range of GS-2.1a, an equivalent for HS1 from Greenland ice-cores, is also represented (Rasmussen et al., 2014). At the bottom part (light pink), records with tuned age-depth models for HS1 have been included. These tuned records and ages provided by authors have not been used for the modelling of the *KDEs*, and therefore, for the median ages (see Supplementary Information above and Table 6.S2b).



Record	Archive	Location	Latitude (°)	Longitude (°)	Dating	Proxy	Heinrich Stadial 1				Reference	Comments
							Revised ages (this study)	End (cal kyr BP)	Onset (cal kyr BP)	End (cal kyr BP)		
Padul-5-05	Continental	S Iberian Peninsula	37° 00' N	3° 35' W	<sup>14</sup> C AMS plant remains, bulk organic matter	Pollen	8.4	5.6	8.4	5.6	This study	-
Co 216	Continental	Macedonia/Greece	40° 58' N	20° 58' E	<sup>14</sup> C AMS plant, fish and shell remains, bulk organic matter, Tepeiras	Diatoms	-	5.7	-	5.7	Cvetkoska et al. (2015)	4 tie-points from NGRIP record (North Greenland Ice Core Project members, 2004) based on Greenland Ice Core Chronology 2005 (GICC05) between -60,000 and 90,000 cal yr BP [according to Damascchke et al. (2013)].
Lake Estanya	Continental	NE Iberian Peninsula	42° 02' N	0° 32' E	<sup>14</sup> C AMS plant remains, bulk organic matter	XRF elements (PCA)	7.8	4.7	8	4.5	Morelin et al. (2009)	4 tie-points between 4800 and 6200 cal yr BP.
CAN Spoletohem	Continental	N Iberian Peninsula	43° 23' N	4° 30' W	230Th dating	Mg/Ca, Ba/Ca	No record (hiatus)	-	8.2	5.4	Moreno et al. (2010)	-
Lago della Costa	Continental	N Italy	45° 16' N	11° 44' E	<sup>14</sup> C AMS plant remains	Pollen	8.7	-	8.6	-	Samartin et al. (2016)	-
MD95-2043	Marine	Alboran Sea	36° 09' N	2° 37' W	<sup>14</sup> C AMS foraminifera	Alkenone-SST	7.7	4.8	8.1	5.2	Fletcher and Sánchez-Goni (2008)	The two age models developed in MD95-2043 (Cacho et al., 1999) used 39 tie-points from GISP2 between -2,000 and 52,000 cal yr BP, including isotopic events and peak to peak correlations. The age limit of HS1 from Fletcher and Sánchez-Goni (2008) was defined based on the sea surface temperature data from Cacho et al. (1999), whereas Fletcher et al. (2010) defined the age range on the basis of the pollen data.
293G	Marine	Alboran Sea	36° 10' N	2° 45' W	<sup>14</sup> C AMS foraminifera	Zr/Al LDI-SST	7.9	4.8	8	4.7	Rodrigo-Gámiz et al. (2011)	The age ranges from Rodrigo-Gámiz et al. (2011) was based on Zr/Al values (among other data) whereas HS limits from Rodrigo-Gámiz et al. (2014) was based on the LDI-SST.
ODP-976	Marine	Alboran Sea	36° 12' N	4° 16' W	<sup>14</sup> C AMS foraminifera	Alkenone-SST	7.1	4.7	7	4.8	Martrat et al. (2014)	1 tie-point at 56,960 cal yr BP (Combourieu-Nebout et al., 2002) from RC 11-20 record after Marinson et al. (1987).
CEUTA OPC08, HER-GC-11	Marine	Alboran Sea	~36° 20' N	~4° 50' W	<sup>14</sup> C AMS foraminifera	Foraminifera, coccoliths	7.2	5.3	7.3	4.8	Bazzicalupo et al. (2018)	-
MD99-2339	Marine	Iberian margin	35° 58' N	7° 53' W	<sup>14</sup> C AMS foraminifera, pteropod fragment	Foraminifera, isotopes	7.3	5.2	7.5	5.5	Austin et al. (2016)	3 tie-points from GISP2 chronology (Grootes and Stuiver, 1997) at 23,800, 45,400 and 46,940 cal yr BP.
GC01	Marine	Iberian margin	36° 43' N	7° 45' W	<sup>14</sup> C AMS foraminifera	Foraminifera, isotopes	8.6	5.5	8.6	5.5	Voelker et al. (2006)	-
SLJ118	Marine	Iberian margin	37° 46' N	10° 11' W	<sup>14</sup> C AMS foraminifera	Alkenone-SST	7.6	4.9	8	5.5	Bard et al. (2000)	25 tie-points from the nearby MD95-2039 record of Thouveny et al. (2000) beyond 20,000 cal yr BP.
MD95-2331	Marine	Iberian margin	42° 09' N	9° 41' W	<sup>14</sup> C AMS foraminifera	Pollen	8.6	5.9	8.6	5.8	Naughton et al. (2007, 2009), Sánchez-Goni et al. (2018)	5 tie-points from the MD95-2042 record of Bard et al. (2004) for ages older than 21,786 ± 170 14C yr BP.
GeoB 7702-3	Marine	E Mediterranean	31° 39' N	34° 04' E	<sup>14</sup> C AMS foraminifera	δD leaf wax	7.5	4.4	7.5	4.5	Castañeda et al. (2016)	-
MD04-2797 CQ	Marine	Siculo-Tunisian strait	36° 57' N	11° 40' E	<sup>14</sup> C AMS foraminifera	Alkenone-SST	7.8	5.3	8.2	4.7	Sicre et al. (2015), Desprat et al. (2016)	Age range of HS1 in M 11s based on Desprat et al. (2015). However, data resolution from Desprat et al. (2015) is too low so the C37 alkenone SST from Sicre et al. (2015) has been represented in Figure S2.
GeoTu SL152, GeoTu SL148	Marine	Aegean Sea	~40° N	~24° 20' E	<sup>14</sup> C AMS foraminifera	Foraminifera	8.4	4.5	7.5	4.7	Kothhoff et al. (2011)	-
MD04-2788, MD04-2760	Lacustrine/ Marine	Black Sea	41° 32' N	30° 53' E	<sup>14</sup> C AMS ostracods, gastropods	XRF elements	7.7	5	8	5	Kwiecien et al. (2008, 2009)	Age model developed using 8 Holocene dates from the nearby GeoB-7022-2 record (Lamy et al., 2006) and a tephral layer (Friedrich et al., 2006) between -800 and 8000 cal yr BP [according to Kwiecien et al. (2008)].

(a)

Tuned records									
Record	Archive	Location	Latitude (°)	Longitude (°)	Heinrich Stadial 1		Reference	Comments	
					Onset (cal kyr BP)	End (cal kyr BP)			
MD04-2805 CQ	Marine	Moroccan margin	34° 31' N	7° 01' W	18.5	16	Penaud et al. (2011)	Correlation using 27 tie-points from the MD99-2339 record of Voelker et al. (2006) between 5890 and 27 730 cal yr BP. Voelker et al. (2006) used 3 tie-points from GISP2 between 23,800 and 46,940 cal yr BP.	
U1390	Marine	Iberian margin	36° 8' N	7° 43' W	18	14.3	Van Dijk et al. (2018)	9 tie-points from the North Atlantic U1308 (Hodell et al., 2017) and NGRIP (Steffensen et al., 2008) records between 10,850 and 18,050 cal yr BP.	
MD95-2041	Marine	Iberian margin	37° 83' N	9° 52' W	17.8	15.2	Voelker et al. (2009)	3 tie-points from GISP2 at 41,500, 29,000 and 30,220 cal yr BP.	
MD95-2042	Marine	Iberian margin	37° 45' N	10° 10' W	17.7	14.6	Bard et al. (2004) Daniau et al. (2007) Sánchez-Goni et al. (2008)	About 45 tie-points from GRIP and GISP2 ice-core records between for the last 10,000 cal yr BP (according to Bard et al. (2004) and Daniau et al. (2007)).	
MD95-2040	Marine	Iberian margin	40° 35' N	9° 52' W	17.6	14.9	Schönfeld et al. (2003) De Abreu et al. (2003)	37 tie-points from GISP2 record [based on Meese et al. (1997), Martinson et al. (1987) and Stuiver and Grootes (2000)] between 11547 and 73,650 cal yr BP.	
MD03-2897	Marine	Iberian margin	42° 10' N	9° 42' W	17.7	14.6	Naughton et al. (2016)	3 tie-points from Greenland ice-core records (average ages of NEEEM, GISP2 and NGRIP) at the beginning of the Bølling-Allerød, Younger Dryas and Holocene.	
MD95-2002	Marine	Bay of Biscay	47° 27' N	8° 32' W	18.2	15.7	Toucanne et al. (2016)	9 tie-points from NGRIP ice-core between 11500 and 39,600 cal yr BP. The end of HS1 (15.7 kyr BP) is based on the MD04-2790 record from Soulet et al. (2013), which also refined the age model based on Soulet et al. (2013a, b). The MD04-2790 chronology from Soulet et al. (2013a, b) was also tied with the Hulu cave chronology (Wang et al., 2001).	
MD01-2430	Marine	Marmara Sea	40° 48' N	27° 44' E	18.1	15.9	Londeix et al. (2009)	Age model developed using 6 dates from the nearby MAR98-2 and MAR97-1 records (Aksu et al., 2002; Mudie et al., 2007), and a tephra layer (Pichler and Friedrich, 1976; Vuur et al., 2002) between 4200 ± 100 and 15,590 ± 90 14C yr BP (4279 and 21877 cal yr BP).	
MD90-917	Marine	Adriatic Sea	41° 17' N	17° 37' E	17.5	15.1	Combouret-Nebout et al. (1998)	Age model developed using 10 dates from the Adriatic KET 82-16 records of Fontugne et al. (1989) between 1640 ± 100 and 18,540 ± 250 14C yr BP.	

(b)

**Table 6.S2.** Summary of all high-resolution continental and marine records from southern Europe and the Mediterranean region that provided exact age limits for the onset and the end of HS1. (a) Non-tuned and independently dated records used for obtaining the median ages based on *KDE* under a Bayesian modelling. (b) Records tuned with Greenland ice-cores or other nearby records and excluded from the *KDEs*, and therefore, not used for obtaining the median ages for HS1 boundaries.





# *Chapter* 7

*Climatic subdivision of Heinrich Stadial 1 based on centennial-scale paleoenvironmental changes observed in western Mediterranean area*



## **Chapter 7: Climatic subdivision of Heinrich Stadial 1 based on centennial-scale paleoenvironmental changes observed in western Mediterranean area**

Jon Camuera<sup>1</sup>, Gonzalo Jiménez-Moreno<sup>1</sup>, María J. Ramos-Román<sup>1</sup>, Antonio García-Alix<sup>1,2</sup>, Jaime L. Toney<sup>3</sup>, R. Scott Anderson<sup>4</sup>, Francisco Jiménez-Espejo<sup>2</sup>, Cole Webster<sup>4</sup>

<sup>1</sup> *Departamento de Estratigrafía y Paleontología, Universidad de Granada, Spain*

<sup>2</sup> *Instituto Andaluz de Ciencias de la Tierra (IACT), Consejo Superior de Investigaciones Científicas-Universidad de Granada (CSIC-UGR), Granada, Spain*

<sup>3</sup> *School of Geographical and Earth Sciences, University of Glasgow, UK*

<sup>4</sup> *School of Earth and Sustainability, Northern Arizona University, USA*

**Under review:**

Geology

Impact factor: 5.073

## **Abstract**

Heinrich Stadial 1 (HS1) is one of the most extreme climate periods of the last glacial cycle, generating extremely low sea surface temperatures (SST) and significant changes in terrestrial landscape (e.g., vegetation). Previous studies show that overall cold/dry conditions occurred during HS1, but the lack of high-resolution records precludes whether climate was stable or instead characterized by instability. A high-resolution paleoclimatic record from Padul (southern Iberian Peninsula), supported by a robust chronology, shows that climate during HS1 was non-stationary and centennial-scale variability in moisture is superimposed on this overall cold climatic period. In this study we improve the resolution and suggest a novel subdivision of HS1 in 7 sub-phases, including: i) 3 sub-phases (a.1–a.3) during an arid early phase (HS1a; ~18.4–17.2 kyr BP), ii) a humid middle phase (HS1b; ~17.2–16.7 kyr BP), and iii) 3 sub-phases (c.1–c.3) during an arid late phase (HS1c; ~16.7–15.6 kyr BP). This climatic subdivision is regionally supported by oscillations in SST records from the Mediterranean Sea, suggesting a strong land-ocean relationship. A cyclostratigraphic analysis of our pollen data indicates that HS1 climate variability, and thus this subdivision, is characterized by ~2000 and ~800-yr periodicities, suggesting solar forcing controlling climate in this area.

## **1. Introduction**

Understanding the background of natural climatic variability underlying abrupt anthropogenic climate change is a main goal in paleoclimate research. In this respect, deciphering rapid (e.g., millennial-scale) climate change and environmental impacts due to Dansgaard/Oeschger (D/O) and Heinrich-like climatic oscillations during the last glacial period and deglaciation have been the aim of ice, marine and terrestrial paleoclimate investigations (Cacho et al., 2006; Höbig et al., 2012; Panagiotopoulos et al., 2014).

Several paleoclimatic records evidenced the effect of especially cold conditions recorded during Heinrich Stadials (HSs) in marine and terrestrial environments (Martrat et al., 2014). However, few studies focus on shorter-scale internal climate variability of HSs, and in particular within HS1 (Fletcher and Sánchez Goñi, 2008). In this regard, a division of HS1 into two and three phases has previously been observed in very few marine records (Supplementary Information and Table 7.S1). Nevertheless, the studies showing a three-phase division of HS1 disagree in the paleoenvironmental characterization of each phase (Table 7.S1) and a complete knowledge of the variability within HS1 has yet to be achieved (Hodell et al., 2017).

Here, we present pollen and sedimentation data between 20 and 11 kyr BP from the new Padul-15-05 terrestrial sedimentary record (southern Iberian Peninsula; Fig. 7.1), registering regional and local paleoenvironmental responses to climate changes during HS1 and deglaciation, i.e., Bølling-Allerød (BA) and Younger Dryas (YD). The high-resolution data (~61-yr) from 18.4 to 15.6 kyr BP revealed centennial-scale variability during HS1, which is replicated in other Mediterranean paleoclimatic records and enables us to suggest, for the first time, an accurate internal climatic subdivision of HS1.

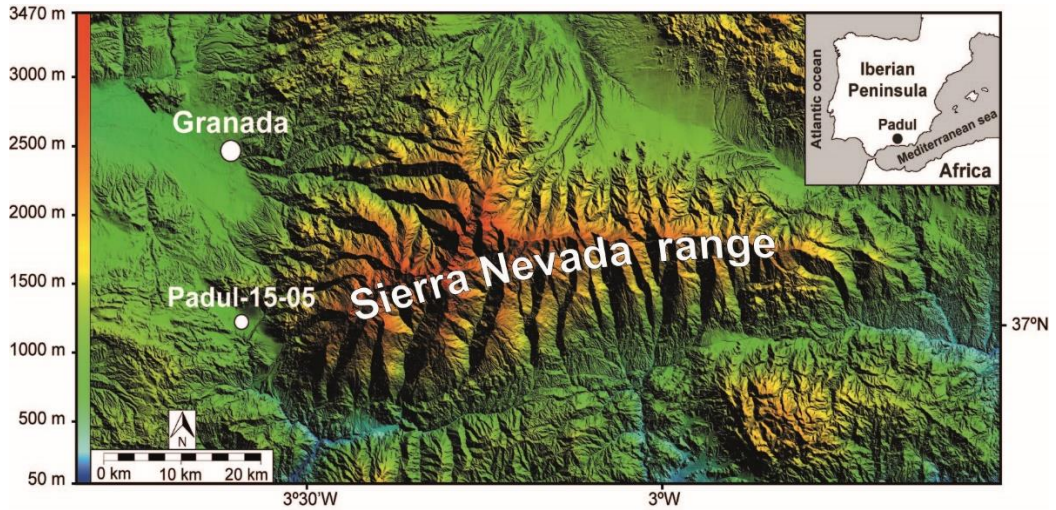


**Figure 7.1.** Geographical location of the Padul-15-05 record in the western margin of Sierra Nevada range and south of Granada city (southern Iberian Peninsula) [modified from Camuera et al. (2018)].

## 2. Materials and methods

In this study we used 10 AMS radiocarbon dates to obtain an accurate chronological control between 20 and 11 kyr BP from the Padul-15-05 record (Fig. 7.2A and Table 7.S2; Supplementary Information for more precise methodology).

The Mediterranean forest, xerophytes, Pollen Climate Index (PCI) and Precipitation Index ( $I_p$ ) were used as pollen paleoclimatic proxies. The PCI is useful for temperature and precipitation related climate changes, whereas  $I_p$  is a proxy for precipitation reconstruction in this region. In addition, normalized silicon data from XRF analysis was used as indicator of the siliciclastic input from the Sierra Nevada into the wetland (Camuera et al., 2018) (Methods, Supplementary Information).

For the purpose of identifying cyclicities related to regional climate oscillations, a cyclostratigraphic spectral analysis was performed on xerophyte data due to their high abundance and sensitivity to climate changes, especially during cold/arid glacial conditions (Pini et al., 2009). A spectral analysis was also run on GRIP  $^{10}\text{Be}$  flux data between 18.6 and 11 kyr BP (Adolphi et al., 2014) in order to observe cyclicities related to solar activity (Fig. 7.3; Methods, Supplementary Information).

## 3. Results and discussion

### 3.1. Heinrich Stadial 1 (HS1)

The terrestrial paleoclimate record from Padul shows overall cold and arid conditions during HS1, deduced by the decrease in mesic forest and abundance of xerophytes between 18.4 and 15.6 kyr BP (Fig. 7.2C, D). Centennial-scale variability is also observed during HS1 that can be

divided into 3 main climatic phases (i.e., HS1a from 18.4 to 17.2 kyr BP, HS1b from 17.2 to 16.7 kyr BP, and HS1c from 16.7 to 15.6 kyr BP) and a further subdivision in 7 smaller-scale phases within them (i.e., HS1a.1, HS1a.2, HS1a.3, HS1b, HS1c.1, HS1c.2 and HS1c.3) (Fig. 7.2E, F).

The first of the three main climatic phases in Padul, HS1a (early HS1; 18.4–17.2 kyr BP), is characterized by low temperatures with significant variability in precipitation but under generally arid conditions, deduced by high xerophytes and low PCI and  $I_p$  values (Fig. 7.2C, E, F). Especially cold/arid conditions during this early phase are confirmed by high  $Si_{norm}$  values, which show that high siliciclastic input from the Sierra Nevada range into the wetland are caused by enhanced erosion during decreased forest cover (Camuera et al., 2019). The general cold/arid conditions shown in Padul during the early HS1a were also documented in nearby marine records presenting the 3 main phases for HS1, such as the pollen records from NW Iberia (Naughton et al., 2016), or the pollen data, SST reconstructions and foraminifera/coccolithophore assemblages from Alboran Sea (Fletcher and Sánchez Goñi, 2008; Martrat et al., 2014; Bazzicalupo et al., 2018).

HS1b (middle HS1; 17.2–16.7 kyr BP) is characterized in Padul by a moderate increase in temperature and precipitation, deduced by low xerophytes, and higher PCI and  $I_p$  values. This is further supported by low  $Si_{norm}$ , indicative of low erosion precluding siliciclastic input in the wetland. A similar slightly warmer climate during this phase was recorded in SST records from the Mediterranean (Cacho et al., 1999; 2006; Sicre et al., 2013), and in particular, from Alboran Sea (Martrat et al., 2014) (Fig. 7.2G-I, subjected to age uncertainties for onset/ending of HS1). This warmer/wetter conditions agree with increases in temperate forest recorded in the Iberian margin (Danianu et al., 2007), and in runoff in Lake Estanya (NE Spain) (Morellón et al., 2009).

HS1c (late HS1; 16.7–15.6 kyr BP) was climatically similar to HS1a, characterized by cold/dry conditions. This is deduced by the observed increase in xerophytes and  $Si_{norm}$  and lowering in  $I_p$  between ~16.9 and 15.8 kyr BP, related with the decreasing moisture (Fig. 7.2B, C, E). The general cold/arid climate in Padul during this phase is concordant with low SST from Alboran Sea (Martrat et al., 2014) (Fig. 7.2I), and with increasing salinity and low lake level in Lake Estanya (Morellón et al., 2009).

Our high-resolution record also revealed shorter centennial-scale climatic variability during HS1a and HS1c with a further climatic subdivision of HS1 into 7 sub-phases (i.e., HS1a.1, HS1a.2, HS1a.3, HS1b, HS1c.1, HS1c.2 and HS1c.3):

HS1a.1 was characterized by a cold/arid phase between 18.4 and 17.8 kyr BP recorded by high xerophytes, and low PCI and  $I_p$  values. Climate changed towards more humidity in HS1a.2 sub-phase at 17.8–17.5 kyr BP, and returned to enhanced aridity during HS1a.3 between 17.5–17.2 kyr BP. This arid-humid-arid climatic pattern is further confirmed by oscillations in  $Si_{norm}$ .

HS1c also presents a three-phase subdivision, namely HS1c.1, HS1c.2 and HS1c.3. HS1c.1 was characterized by a decrease in precipitation and temperature (low  $I_p$  and lowest PCI values), registering the coldest conditions of HS1 at 16.7–16.4 kyr BP. Temperature and moisture conditions increased during HS1c.2 at 16.4–16 kyr BP, whereas similar temperatures but under more arid climate conditions are recorded during HS1c.3 at 16–15.6 kyr BP. This arid-humid-arid climatic pattern is similar to the earlier HS1a.

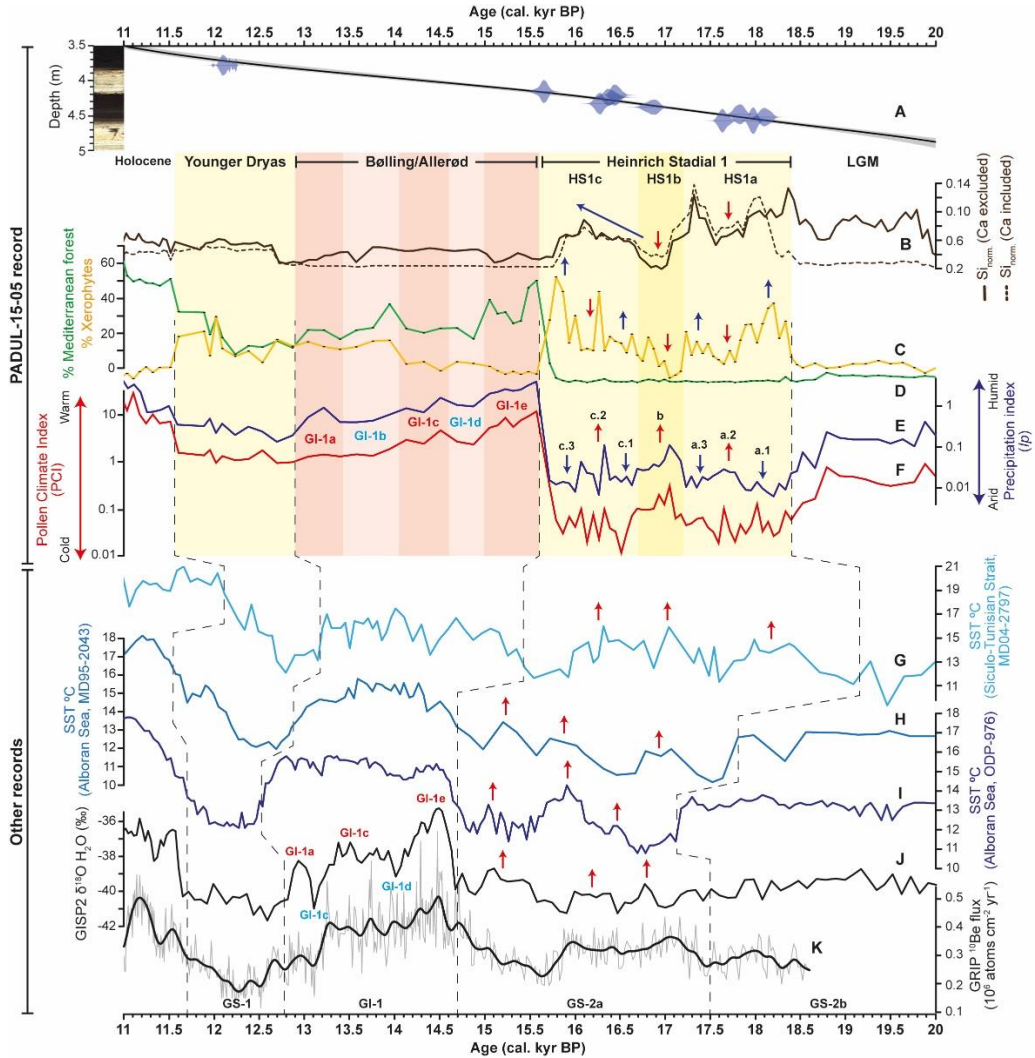


**Figure 7.2.** Paleoclimatic proxies from the Padul-15-05 sediment core, Mediterranean Sea and Greenland ice-cores for the time period between 20 and 11 kyr BP. Data from Padul-15-05: (A) Photograph and age-depth model. (B) Normalized silicon values, with calcium excluded (continuous line) and included (dashed line) from total counts (Methods, Supplementary Information). (C) Percentage of xerophytes. (D) Percentage of Mediterranean forest. (E) Precipitation Index ( $I_p$ ). (F) Pollen Climate Index (PCI). Data from other records: (G) SST from the Siculo-Tunisian Strait (Sicre et al., 2013). (H) SST (degrees Celsius) from MD95-2043 record of Alboran Sea (Cacho et al., 1999; 2006). (I) SST (degrees Celsius) from ODP-976 record of Alboran Sea (Martrat et al., 2014). (J) Raw  $\delta^{18}\text{O}$   $\text{H}_2\text{O}$  values (‰) from GISP2 (Grotes et al., 1993). (K) Raw  $^{10}\text{Be}$  flux values ( $10^6$  atoms  $\text{cm}^{-2} \text{yr}^{-1}$ ) (grey line) and smoothed data (black line) from GRIP (Adolphi et al., 2014). Yellow shadings show the Younger Dryas (YD) and Heinrich Stadial 1 (HS1). Dark yellow shading within HS1 indicates the slightly warmer/wetter middle phase (HS1b). Red-pink shading shows the Bølling-Allerød (BA). In particular, red shadings correspond to the warmer/wetter Greenland Interstadials 1a, 1c and 1e, and pink shadings to the colder/more arid Greenland Interstadial 1b and 1d. Vertical dashed lines show transitions between LGM-HS1 (GS-2b – GS-2a), HS1-BA (GS-2a – GI-1), BA-YD (GI-1 – GS-1) and YD-Holocene for each study. Red arrows indicate moderately warmer/wetter sub-phases within HS1, whereas blue arrows show cold/arid sub-phases or trends (graphs b, c, e and f). In the three SST and Greenland records (graphs g-j) relatively warmer temperatures are also marked with red arrows.



Environmental changes recorded in Padul represent centennial-scale climate oscillations during HS1, which can be correlated with other regional records. The centennial-scale arid-humid-arid trends recorded during HS1a and HS1c, and the increase in temperature/precipitation during HS1b, are also observed in the SST records from the Alboran Sea and Siluco-Tunisian Strait in western/central Mediterranean (Cacho et al., 1999; 2006; Sicre et al., 2013; Martrat et al., 2014) and in the GISP2 ice core (Grootes et al., 1993) (Fig. 7.2G-J), suggesting a similar response in continental, marine and ice sheet environments to climatic forcing (see section below). The presented age offsets between records could be related with major variations in reservoir ages of the Atlantic and Mediterranean promoted by thermohaline circulation collapse in both areas during HS1 (Sierro et al., 2005). In addition, the significant decrease in the atmospheric  $^{14}\text{C}$  between 17.5 and 14.5 kyr also difficult age models during this period (Broecker and Barker, 2007), whereas dating on different foraminifera species can also produce large differences on radiocarbon ages, especially during HS1 (up to 1000 years) (Ausín et al., 2019). Despite the offsets of SST reconstructions from Mediterranean Sea, environmental oscillations in both areas should have been synchronous. Therefore, warming peaks recorded in Padul and in SST records during HS1 were coetaneous, result of the strong land-ocean interaction (Sánchez Goñi et al., 2018).

### *3.2. Bølling-Allerød (BA) and Younger Dryas (YD)*

The BA recorded in Padul between 15.6 and 12.9 kyr BP is characterized by significant increase in the Mediterranean forest, and thus  $I_p$  and PCI values, indicating warmer/wetter climate than during HS1. In addition, Padul is one of the few continental records to detect the 5 centennial-scale sub-phases during the BA, similar to the GI-1e to GI-1a from Greenland ice cores (Johnsen et al., 1992; Grootes et al., 1993) (Fig. 7.2E, F, J).

Cold/arid climate during the YD stadial also affected the paleoenvironments in this area between 12.9-11.6 kyr BP. The beginning of the YD is marked by a Mediterranean forest decrease with the most arid conditions recorded 12.7–12.5 kyr ago, deduced by high xerophytes and low  $I_p$  values (Fig. 7.2C-E).

### *3.3. Climate variability and solar forcing in the Iberian Peninsula*

Centennial- and millennial-scale climate variability have been recorded during HS1, BA and YD period in Padul. The spectral analysis on xerophytes presented ~2000, 800, 500 and 200-yr cycles (Fig. 7.3A, B) that could be related to solar forcing, as similar cyclicities have been obtained analyzing solar activity with  $^{14}\text{C}$  production rates (Damon and Jirikowic, 1992; Turney et al., 2005). Several studies have determined a relation between paleoenvironmental data oscillations linked to climate changes through variations in solar activity (Bond et al., 2001; Lüning and Vahrenholt, 2016). In particular, climate variability during the Last Glacial and Holocene periods was strongly controlled by solar activity, specifically during cold glacial phases, in which solar variability caused larger climate changes (Van Geel et al., 1999). In

addition, more recent temperature estimations showed that they also seem to be forced by solar variability (Soon et al., 2015).

The obtained ~2000-yr climatic cyclicality forced millennial-scale paleoenvironmental variability in Padul and permitted the three-phase division of HS1 (Fig. 7.3D, E). This cyclicality could be linked to D/O-like variability, which presents a 1–2 kyr periodicity during the last glaciation (Bond et al., 1999), such as the ~1.8-kyr cycle identified on the hematite-stained grain record from North Atlantic cores (Bond et al., 1999). Paleoclimatic records from the Equator and Southern Hemisphere also determined periodic surface temperature variations of around 2000 yrs in relation with solar irradiance (Bütikofer, 2007).

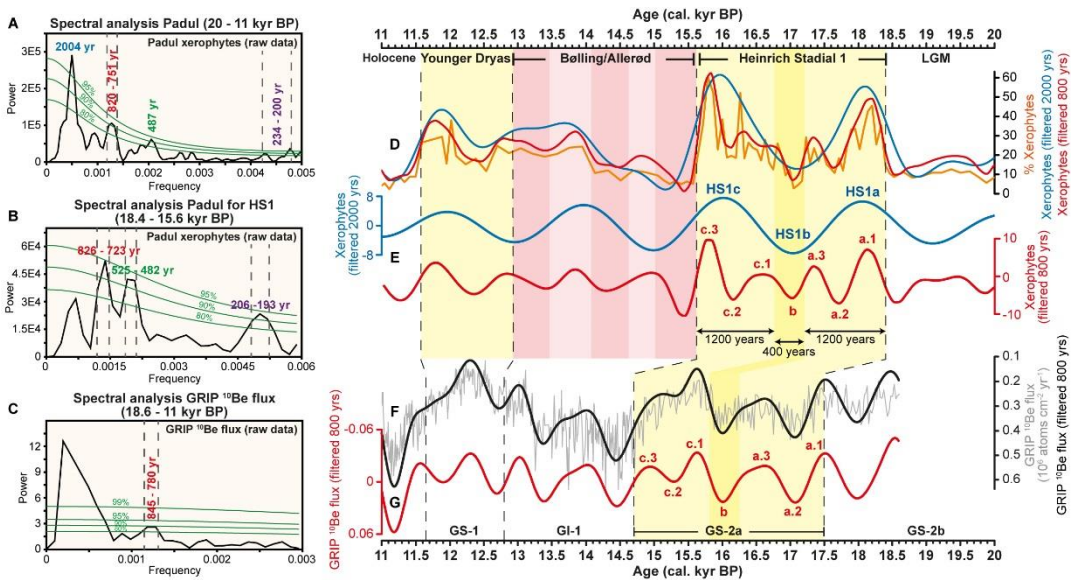


**Figure 7.3.** Left panels show the spectral analysis run on: (A) Xerophyte percentages from the Padul-15-05 record for the age range between 20 and 11 kyr BP. (B) Xerophyte percentages for HS1 (18.4 – 15.6 kyr BP). (C) GRIP  $^{10}\text{Be}$  flux data between 18.6 – 11 kyr BP. Note that the spectral peak of the GRIP  $^{10}\text{Be}$  between 0.0001973 and 0.0005919 frequencies (a cycle with a periodicity between 5068 and 1689 years) seems to be an artefact, as the longer periodicity cycles (closer to 5 kyr) cannot be significant in a time series of data spanning 7600 years. Right graphs show: (D) Raw percentages of xerophyte taxa (orange) along with the filtered xerophyte taxa based on the obtained ~2000-yr cycle (blue) and the ~800-yr cycle (red) (Fig. 7.3A, B). (E) Xerophyte data filtered using a bandwidth parameter of 0.0001 for the ~2000-yr cycle (blue) and 0.0006 for the ~800-yr cycle (red). Note that the 3 main phases (HS1a, HS1b and HS1c) are marked within HS1 in relation with the ~2000-yr cycle, and the internal sub-phases (a.1-a.3, b, and c.1-c.3) in relation with the ~800-yr cycle. The length of the HS1a, HS1b and HS1c have also been marked. (F) GRIP  $^{10}\text{Be}$  flux data ( $10^6$  atoms  $\text{cm}^{-2} \text{yr}^{-1}$ ; values inverted) (grey line) filtered to the obtained cyclicality of ~800 yr (black line) (Fig. 7.3C). (G) GRIP  $^{10}\text{Be}$  flux data filtered using a bandwidth parameter of 0.0006 for the ~800-yr cycle. Vertical dashed lines on graphs F and G have been marked according to the Greenland Stadials (GS-2b, GS-2a, GS-1) and Interstadial (GI-1) delimitations (Rasmussen et al., 2014).

The ~800-yr cycle identified in Padul forced the centennial-scale climatic subdivision of HS1 in 7 sub-phases (Fig. 7.3D, E). A similar ~800 yr cyclicality characterizes the  $^{10}\text{Be}$  flux data indicative of changes in solar activity (Adolphi et al., 2014) (Fig. 7.3C, F, G). Other global paleoclimatic studies also show similar frequencies caused by solar variability. For example, an

~800-yr cycle was observed in Irish oak tree chronologies (Turney et al., 2005) and in Mg/Ca SST from the Pacific Ocean (Marchitto et al., 2010), both records closely related to solar irradiance. A 890-yr cycle was also found in the  $\delta^{18}\text{O}$  Holocene time series from Greenland and interpreted as linked to solar radiation (Schulz and Paul, 2002). Consequently, the ~800-yr cycle detected in Padul and in other worldwide records suggests a linkage between centennial-scale paleoenvironmental changes and solar activity.

The data from Padul display a good correlation between environmental changes in the southern Iberian Peninsula and Mediterranean SSTs during HS1 (Fig. 7.2B-I), suggesting a close land-ocean relationship in response to solar variability. The Mediterranean SST could have been affected by solar activity, similar to the North Atlantic cooling episodes linked to reduced solar irradiance (Bond et al., 2001). In addition, observed variations in the Padul data suggest a southward shift of the North Atlantic polar front during HS1 (Repschläger et al., 2015), which could have produced a penetration of colder Atlantic surface waters into the Mediterranean (Cacho et al., 1999; Sierro et al., 2005). These conditions, along with the southward displacement of the North Atlantic atmospheric polar front, could have produced a low land-ocean temperature contrast and weak moisture advection between both environments, and therefore, increasing aridity in the western Mediterranean during cold sub-phases HS1a.1, HS1a.3, HS1c.1 and HS1c.3. Similar conditions linked to weak moisture advection were interpreted in the eastern Mediterranean during HS1 and HS2 (Kwiecien et al., 2009) and in the Corchia Cave during HS11 (Drysdale et al., 2009). In contrast, during warmer sub-phases in Padul (i.e., HS1a.2, HS1b and HS1c.2) and in Mediterranean SSTs, enhanced marine evaporation and moisture advection toward the continent could have provoked wetter climate conditions in southern Iberian Peninsula.

#### **4. Conclusion**

The high-resolution analysis of the Padul-15-05 continental record for the 20–11 kyr BP interval shows that:

- 1) Centennial-scale climate oscillations affected southern Iberian Peninsula during HS1, with three main phases HS1a (18.4–17.2 kyr BP), HS1b (17.2–16.7 kyr BP) and HS1c (16.7–15.6 kyr BP) characterized by general arid(cold), humid(cool) and arid(cold) climate, respectively.
- 2) We suggest for the first time a further subdivision within these 3 main climatic phases of HS1 in 7 sub-phases: 3 sub-phases (a.1–a.3) during HS1a, HS1b, and 3 sub-phases (c.1–c.3) during HS1c. The climatic variability is also identified in Mediterranean SST records, confirming this climatic pattern at regional-scale.
- 3) The main periodicities obtained for climatic oscillations of ~2000 and ~800 yrs within HS1, BA and YD seem to be related to solar forcing. Variations in solar activity could have influenced latitudinal shifts of the North Atlantic and atmospheric polar fronts, affecting the land-ocean temperature contrast, marine evaporation and moisture advection toward the continent.

## **Acknowledgments**

This research is supported by the projects CGL2013-47038-R and CGL-2017-85415-R, PhD funding BES-2014-069117 (Jon Camuera) and Ramón y Cajal fellowship RYC-2015-18966 (Antonio García-Alix) provided by the Ministerio de Economía y Competitividad of the Spanish Government. Additional funding was provided by the research group RNM0190 and the project P11-RNM-7332 with a postdoctoral fellowship (María J. Ramos-Román) from the Junta de Andalucía.

## **Supplementary Information**

### **Climatic subdivision of Heinrich Stadial 1 based on centennial-scale paleoenvironmental changes observed in western Mediterranean area**

Jon Camuera<sup>1</sup>, Gonzalo Jiménez-Moreno<sup>1</sup>, María J. Ramos-Román<sup>1</sup>, Antonio García-Alix<sup>1,2</sup>, Jaime L. Toney<sup>3</sup>, R. Scott Anderson<sup>4</sup>, Francisco Jiménez-Espejo<sup>2</sup>, Cole Webster<sup>4</sup>

<sup>1</sup> *Departamento de Estratigrafía y Paleontología, Universidad de Granada, Spain*

<sup>2</sup> *Instituto Andaluz de Ciencias de la Tierra (IACT), Consejo Superior de Investigaciones Científicas-Universidad de Granada (CSIC-UGR), Granada, Spain*

<sup>3</sup> *School of Geographical and Earth Sciences, University of Glasgow, UK*

<sup>4</sup> *School of Earth and Sustainability, Northern Arizona University, USA*

### **Supplementary introduction**

Heinrich Stadial 1 (HS1) is one of the most recent and coldest Heinrich Stadials of the last glaciation, described in several marine sedimentary records close to the study area (Salgueiro et al., 2014; Naughton et al., 2016). In this region, some marine records with high sedimentation rates presented two and three-phase division of HS1. For example, two phases were described in Iberian margin marine sedimentary records (Naughton et al., 2009; Salgueiro et al., 2014; Sánchez Goñi et al., 2018) and Neil River Basin (Castañeda et al., 2016), with similar wet conditions during the first phase and arid climate during a second phase. Other paleoclimate studies based on different proxies recorded a three-phase division for HS1, such as those from the Alboran Sea (Fletcher and Sánchez Goñi, 2008; Bazzicalupo et al., 2018), northwestern Mediterranean (Sierro et al., 2005), Iberian margin (Naughton et al., 2016) and off NW Africa (Bouimtarhan et al., 2012). However, these studies showed different paleoenvironmental reconstructions for these three phases (early, middle and late HS1), which are shown in Table 7.S1.

Study	Location	Record	Environmental reconstruction	Proxy	Early HS1 (HS1a)	Middle HS1 (HS1b)	Late HS1 (HS1c)
Fletcher and Sánchez Goñi (2008)	Alboran Sea	MD95-2043	Marine	<i>N. pachyderma-s</i> (cold water indicator)	Cool	Cold	Cool
			Continental	Vegetation	Cold/humid	Arid	Cool/less arid
Bazzicalupo et al. (2018)	Alboran Sea	ODP-976	Marine	Calcareous plankton	Cold	Fresher water	Cooler
			Continental	Vegetation	Increase aridity	Maximum aridity	Cold/arid
Sierro et al. (2005)	Northwestern Mediterranean	MD99-2343	Marine	$\delta^{18}\text{O}$ <i>G. bulloides</i> (SST, iceberg meltwater)	Cold	Cool	Cold
Naughton et al. (2016)	Iberian margin	MD03-2697	Marine	Alkenone-based SST and % <i>N. pachyderma-s</i>	Extreme cooling	Warmer (still cool)	Cooling (warmer than HS1a)
			Continental	Vegetation	Extreme cold/wet	Warmer (still cool)/increase aridity	Warming/wet
Bouimetarhan et al. (2012)	Off NW Africa	GeoB9508-5	Continental	Vegetation	Dryness	Wetter	Extreme dry

**Table 7.S1.** Marine records presenting a division of HS1 in three phases (Sierro et al., 2005; Fletcher and Sánchez Goñi, 2008; Bouimetarhan et al., 2012; Naughton et al., 2016; Bazzicalupo et al., 2018). Marine and continental reconstructions of the early, middle and late HS1 have been schematized below. Note the diversity in the interpretations for the three phases identified within HS1.

### *Regional and local settings*

Padul is located at the foothill of the Sierra Nevada, which is an approximately 85 km long E-W aligned mountain range located in southern Spain. The precipitation in the Sierra Nevada is highly controlled by the humidity carried from the westerlies and the North Atlantic Oscillation (Jiménez-Moreno and Anderson, 2012; Lionello, 2012).

The Padul wetland (724 m a.s.l.) is located in the western margin of the Sierra Nevada range, 20 km south of Granada city (Andalusia, Spain) (Fig. 7.1) and covers an area of 4 km<sup>2</sup> in the Padul-Nigüelas basin. The NW-SE elongated Padul-Nigüelas endorheic basin developed as a consequence of extensional activity of the main normal fault that delimits the NE edge of the basin (Santanach et al., 1980). It bears an estimated sedimentary sequence of about 100 m in the depocenter of the basin (Ortiz et al., 2004a). The Padul area is at present characterized by a semiarid Mediterranean climate with high temperature and low precipitation during summertime (summer drought), presenting a mean annual temperature of 14.4°C and mean annual precipitation of 445 mm (AEMET, 2016).

### *Chronology*

The 42.64 m-long Padul-15-05 sediment core was drilled in the Padul wetland lakeshore (37°00'39"N, 3°36'14"W) in July 2015. The chronological control of the Padul-15-05 core is based on 43 Accelerator Mass Spectrometry (AMS) radiocarbon dates, 4 Amino Acid Racemization (AAR) dates from gastropods (hydrobiid *Milesiana schuelei*) and two different sediment accumulation rates (SAR) for both peat and carbonate/marl lithologies for the bottom part of the core (Camuera et al., 2018). The age-depth control for the new Padul-15-05 record between 20 and 11 kyr BP (4.88 – 3.52 m depth) was built using 10 AMS radiocarbon dates, from a total of 15 radiocarbon samples analyzed (Table 7.S2). Five dates were rejected because they provided ages that are too young due to root penetration from above (1 sample), and ages too old due to reservoir effect (2 samples from gastropods and 2 samples from bulk carbonates).

This record presented high sediment accumulation rates (SAR, 0.151 mm/yr) during this time period and therefore permitted us to perform high-resolution multiproxy analyses for regional paleoclimate reconstructions.

The age-depth model was developed using the R-code package Clam 2.2 software (Blaauw, 2010), under the IntCal13.14C calibration curve (Reimer et al., 2013) at 95% confidence level. Note that 6 new radiocarbon dates between 415.46 and 460.35 m depth (15658 – 19481 cal. yrs BP) were analyzed in this study and added to the age model for an accurate delimitation of HS1.

	Material	Depth (cm)	Age ( <sup>14</sup> C yr BP ± 1σ)	Calibrated age (cal yr BP) 95% confidence interval	Median age (cal yr BP)
Poz-74348	Plant remains	375.62	9120 ± 50	10199 - 10412	10305
Poz-79815	Org. bulk sed.	377.83	10310 ± 50	11847 - 12388	12144
Poz-79817	Gastropods	411.02	13910 ± 60	16588 - 17088	16838
Poz-79818	Gastropods	414.89	14130 ± 50	17001 - 17419	17210
BETA-506210	Bulk carbonate	415.46	13060 ± 40	15400 - 15852	15658
BETA-506209	Org. bulk sed.	420.59	13630 ± 40	16238 - 16639	16365
Poz-77574	Org. bulk sed.	423.65	13580 ± 80	16113 - 16654	16384
Poz-79819	Org. bulk sed.	432.82	13500 ± 60	16047 - 16494	16270
Poz-19821	Org. bulk sed.	437.92	13910 ± 70	16570 - 17113	16841
Poz-79822	Org. bulk sed.	448.12	14640 ± 70	17618 - 18011	17814
Poz-77575	Org. bulk sed.	452.2	14890 ± 80	17898 - 18325	18111
BETA-506207	Org. bulk sed.	457.29	14480 ± 50	17473 - 17863	17650
BETA-506208	Org. bulk sed.	457.29	14780 ± 50	17815 - 18157	17980
BETA-506205	Bulk carbonate	460.35	16140 ± 60	19256 - 19661	19481
BETA-506206	Bulk carbonate	460.35	16080 ± 60	19210 - 19592	19410

**Table 7.S2.** AMS-standard radiocarbon ages of the Padul-15-05 record between 4.88 - 3.52 m depth (according to the age-depth model, between 20000 and 11000 calibrated years BP). In red are the dates that were rejected for the age model.

### *Palynological analysis*

For this study a total of 92 pollen samples were analyzed between 4.88 and 3.52 m depth (20 - 11 kyr BP) with a resolution of ~77 years for the last part of the Last Glacial Maximum (LGM) and HS1 (20 – 15.6 kyr BP) and ~131 years for the BA, YD and the beginning of the Holocene (15.6 – 11 kyr BP), augmenting the resolution with respect to the previous study on the entire Padul-15-05 core about vegetation and climate changes during the last ~197 kyr (Camuera et al., 2018; 2019). Pollen extraction was done following a modified methodology of Faegri and Iversen (1989). After the final extraction of the pollen residue, a minimum of 300 terrestrial pollen grains per sample were identified using a Zeiss transmitted light microscope under a magnification of 400x.

The Mediterranean forest includes *Quercus* total, *Olea*, *Phillyrea* and *Pistacia*. The xerophyte pollen group includes *Artemisia*, *Ephedra* and *Amaranthaceae*. Pollen Climate Index (PCI) includes *Quercus* total, *Olea*, *Fraxinus*, *Phillyrea*, *Acer*, *Betula*, *Alnus*, *Ulmus*, *Taxus*, *Salix*, *Pistacia*, *Corylus* and *Carpinus*. Finally, the Precipitation Index ( $I_p$ ) is expressed as:  $I_p = [Quercus\ deciduous / (Artemisia + Ephedra + Amaranthaceae + Quercus\ deciduous)]$ . Pollen

percentages were calculated based on the terrestrial pollen sum excluding aquatic plants (Cyperaceae, *Typha*, *Myriophyllum*, *Utricularia* and *Potamogeton*).

The Mediterranean forest group taxa have previously been shown to be a good indicator of climate changes in the Mediterranean region (Fletcher and Sánchez Goñi, 2008). The PCI is based on the mesothermic/steppic taxa ratio (Combourieu Nebout et al., 1999; Joannin et al., 2011), and has been useful in identifying climate changes mainly related to temperature in this region. However, some taxa included in the PCI respond not only to temperature, but also to different precipitation conditions, hence a more precise reconstruction of the precipitation in this area has been obtained using the *Ip* (Fletcher et al., 2010a).

### *Inorganic geochemistry*

Inorganic geochemical composition of the Padul-15-05 core was analyzed every 1 cm (~70 years resolution between 20 – 11 kyr BP) in a continuous XRF Avaatech core scanner from the CORELAB at the University of Barcelona (Spain). From a total of 34 elements analyzed, Si was taken as the most representative data for climate reconstruction in this study (Camuera et al., 2018). This element has been used as Si normalized, represented by the silicon data divided by the sum of the total counts (in cps) from the most important elements as:  $Si_{norm} = Si / (Si, K, Ca, Fe, Zr, Br, Sr, Al, Rb, Cl, Zn, Mn, S, Pb, U, Ni, Ti)$ . However, calcium data present very high values in carbonate lithologies. Therefore, a normalized Si values excluding Ca from the total counts have also been represented in order to observe more accurate changes in carbonate sediments. Elements with low representation, negative values and/or elements providing background values have been excluded.

### *Spectral analysis and filtering*

The spectral analysis was developed on xerophyte taxa from Padul with the PAST 3.19 software (Hammer et al., 2001) using the REDFIT procedure of Schulz and Mudelsee (2002) under the rectangular window function and the standard value of 2 for the segments parameter and value of 3 for the oversample parameter. Two spectral analyses were run on xerophytes, including the age range between 20 – 11 kyr BP and for HS1 (18.4 – 15.6 kyr ago). A periodicity of ~2000 years ( $f = 0.0004990$ ; > 95 Confidence Interval) was obtained in the spectral analysis for the age range between 20 – 11 kyr BP. Cyclicities of ~800 years ( $f = 0.001384 - 0.001211$ ), ~500 years ( $f = 0.002075 - 0.001905$ ) and ~200 years ( $f = 0.005181 - 0.004273$ ) (all above > 90% CI) were identified in both spectral analysis (Fig. 7.3A, B).

A spectral analysis was also run on  $^{10}Be$  flux values ( $10^6$  atoms  $cm^{-2} yr^{-1}$ ) from GRIP (Adolphi et al., 2014) using the same REDFIT procedure as on xerophyte data from Padul under the rectangular window function and the standard value of 2 for segments and oversample parameters, with the purpose of observe cyclicities related to solar activity. A periodicity of ~800 years was obtained from the  $^{10}Be$  flux data with a confidence interval of ~90% (Fig. 7.3C).

The obtained periodicities of ~2000 and ~800 years were filtered using the Analyseries 2.0 software (Paillard et al., 1996) for the visual comparison of cyclicities between different records.





# *Chapter* 8

*Holocene geochemical footprint from semi-arid alpine wetlands  
in southern Spain*



## Chapter 8: Holocene geochemical footprint from semi-arid alpine wetlands in southern Spain

Antonio García-Alix<sup>1,2,3</sup>, Francisco J. Jiménez-Espejo<sup>3,4</sup>, Gonzalo Jiménez-Moreno<sup>1</sup>, Jaime L. Toney<sup>2</sup>, María J. Ramos-Román<sup>1</sup>, Jon Camuera<sup>1</sup>, R. Scott Anderson<sup>5</sup>, Antonio Delgado-Huertas<sup>3</sup>, Francisca Martínez-Ruiz<sup>3</sup>, Ignasi Queralt<sup>6</sup>

<sup>1</sup> *Departamento de Estratigrafía y Paleontología, Universidad de Granada, Granada, Spain*

<sup>2</sup> *School of Geographical and Earth Sciences, University of Glasgow, UK.*

<sup>3</sup> *Instituto Andaluz de Ciencias de la Tierra (IACT), CISC-UGR, Armilla, Spain*

<sup>4</sup> *Department of Biogeochemistry (JAMSTEC), Yokosuka, Japan*

<sup>5</sup> *School of Earth Sciences and Environmental Sustainability, Northern Arizona University, Flagstaff, AZ, USA*

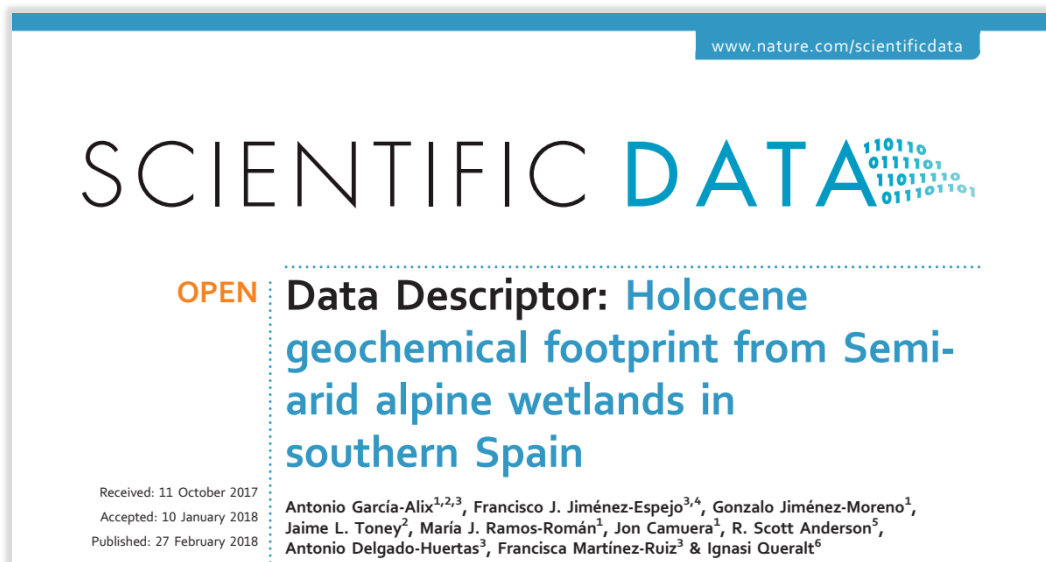
<sup>6</sup> *Institute of Environmental Assessment and Water Research (IDAEA), CSIC, Barcelona, Spain*

### Published in:

Scientific Data, v. 5, n. 180024 (2018)

Doi: 10.1038/sdata.2018.24

Impact factor: 5.311



## **Abstract**

Here we provide the geochemical dataset that our research group has collected after 10 years of investigation in the Sierra Nevada National Park in southern Spain. These data come from Holocene sedimentary records from four alpine sites (ranging from ~2500 to ~3000 m a.s.l.): two peatlands and two shallow lakes. Different kinds of organic and inorganic analyses have been conducted. The organic matter in the bulk sediment was characterised using elemental measurements and isotope-ratio mass spectrometry (EA-IRMS). Leaf waxes in the sediment were investigated by means of chromatography with flame-ionization detection and mass spectrometry (GC-FID, GC-MS). Major, minor and trace elements of the sediments were analysed with atomic absorption (AAS), inductively coupled plasma mass spectrometry (ICP-MS), as well as X-ray scanning fluorescence. These data can be reused by environmental researchers and soil and land managers of the Sierra Nevada National Park and similar regions to identify the effect of natural climate change, overprinted by human impact, as well as to project new management policies in similar protected areas.

## **1. Background and summary**

Arid Mediterranean ecosystems, especially alpine wetlands, are particularly vulnerable to climate oscillations, and their management and protection requires a complete knowledge of their response to past natural climate fluctuations and human-induced biochemical changes (Escudero et al., 2004; Schröter et al., 2005; Regato and Salman, 2008; García-Alix et al., 2017). Recent works in the protected Sierra Nevada National Park in southern Spain have shown that the environmental evolution of neighbouring alpine wetlands can develop different sensitivities and long-term environmental responses during the Holocene, regardless of similar natural forcings (García-Alix et al., 2012; Jiménez-Moreno et al., 2013; Jiménez-Espejo et al., 2014; García-Alix et al., 2017). This feature, which is common in areas under extreme climate conditions, supports the importance of datasets like those described here to understand past, present and potential future behaviours of vulnerable areas under similar climate and human pressure.

Additional climatic stresses exist for high altitude alpine wetlands in the Sierra Nevada, which are covered by snow from ~November to ~April. Due to limited access, only few and irregular meteorological records have been collected since 1960 ([http://www.aemet.es/es/datos\\_abiertos/AEMET\\_OpenData](http://www.aemet.es/es/datos_abiertos/AEMET_OpenData), <http://linaria.obsnev.es/>). As an example, an observatory at 2500 m a.s.l. registered mean annual temperatures (MAT) of ~4.4°C and annual precipitation of ~750mm from discontinuous records between 1965 and 1993 ([http://www.aemet.es/es/datos\\_abiertos/AEMET\\_OpenData](http://www.aemet.es/es/datos_abiertos/AEMET_OpenData), <http://linaria.obsnev.es/>). Meteorological data are even more scarce at higher elevations. Data collected from ~3020 m a.s.l. recorded a MAT of ~2.8°C in the 2000s (<http://linaria.obsnev.es/>) while additional collections at ~3100 m a.s.l. registered a MAT of 2.1°C in 2016 (<http://www.mapama.gob.es/es/red-parques-nacionales/red-seguimiento/>). Although precipitation and isotopic records are rare at these elevations, monitoring programs from 2001

to 2003 succeeded in measuring isotopes from precipitation (snow) between 1030 and 3020 m a.s.l. ( $\delta D = -111.9 \pm 12.7\text{‰}$  and  $\delta^{18}O = -16.1 \pm 1.9\text{‰}$ ) (Raya Garrido, 2003). These values are much lower than the ones at lower elevations in the south of the Iberian Peninsula (García-Alix, 2015). Similarly, scarce data from the alpine lakes show mean  $\delta^{18}O$  values of  $-7.7 \pm 1.8\text{‰}$ , although they can reach  $-4.5\text{‰}$  due to evaporative process in the shallowest lakes (Mladenov et al., 2011).

Previous paleoecological studies conducted in Sierra Nevada alpine areas have mostly focused on regional environmental and climate evolution within the context of the western Mediterranean climate domain (Anderson et al., 2011; Jiménez-Moreno and Anderson, 2012; Oliva and Gómez-Ortiz, 2012; Jiménez-Moreno et al., 2013; Oliva et al., 2014). In this respect, some inorganic geochemical records preserved at these elevations are extraordinary archives for tracking past regional and north-hemispheric scale teleconnections (e.g., Zr content, and La/Lu ratio) (Jiménez-Espejo et al., 2014; García-Alix et al., 2017; Jiménez et al., 2018). On the other hand, despite the Pb and Hg deposition occurs widely throughout the Northern Hemisphere, these metals also record local mining, metallurgy and industrial atmospheric pollution sources (Rosman et al., 1997; García-Alix et al., 2017). Local alpine environmental conditions in these sites can be specifically reconstructed by means of these and other inorganic elements related to catchment evolution, as well as organic bulk sediment and biomarker proxies that evidence past local biogeochemical cycles (García-Alix et al., 2012; Jiménez-Moreno et al., 2013; Jiménez-Espejo et al., 2014; Jiménez et al., 2015; García-Alix et al., 2017) (Fig. 8.1).

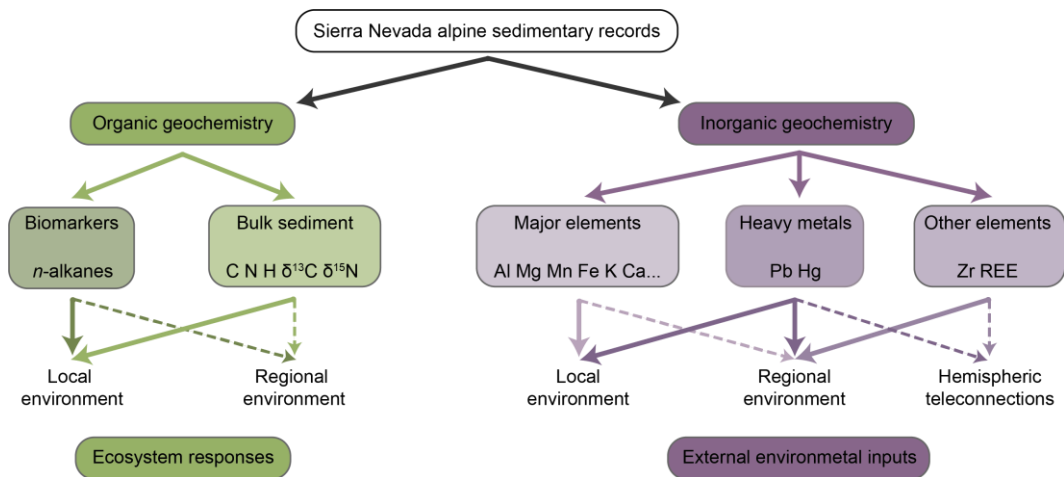


**Figure 8.1.** Schematic overview of the environmental proxies analysed in Sierra Nevada alpine wetlands. Solid lines represent environmental signals with high influence in the proxies (high sensitivity to these signals); dashed lines represent environmental signals with medium influence in the proxies (moderate sensitivity to these signals). Figure created by A. García-Alix using Adobe Illustrator [5.5] (<https://www.adobe.com/>).

The most important factors controlling local biogeochemical behaviour in Sierra Nevada alpine wetlands are: 1) the length of the ice free season, which typically extends from May to October (Pulido-Villena et al., 2005; Morales-Baquero et al., 2006; Jiménez et al., 2015; García-Alix et al., 2017), 2) the water availability, since Sierra Nevada is located in a semi-arid region

(García-Alix et al., 2012, 2017), and 3) the allochthonous nutrient inputs, as these wetlands are oligotrophic and their main nutrient input is via atmospheric deposition (Pulido-Villena et al., 2005, 2006; Morales-Baquero et al., 2006). In addition, human activities have had isolated impacts on the sites, especially during the last hundred years (García-Alix et al., 2013, 2017).

This data descriptor includes all the organic and inorganic geochemical data from previously studied Holocene sedimentary records that characterise past alpine wetland environments in Sierra Nevada. These data have been only partially published (~45% of the data) and come from four sites at different elevations, ranging from 2497 to 3020 m a.s.l. They are, from west to east: Laguna de la Mula (LdlM), Borreguiles de la Virgen (BdlV), Laguna de Río Seco (LdRS), and Borreguil de la Caldera (BdlC) (Table 8.1; Fig. 8.2). Each of the sites, located in former glacial valleys or cirques, are within a 1.25 km<sup>2</sup> area, with a maximum distance of ~8km between the westernmost (LdlM) and the easternmost (BdlC) site (Fig. 8.2). Their catchment basins consist of bare mica-schist rocks without soil development and scarce vegetation (<20% in catchment surface) (Mladenov et al., 2011; Jiménez et al., 2018) mainly concentrated around the water bodies. The main water bodies in the wetlands are shallow lakes without thermal stratification and an almost neutral pH (from 6 to 8) (Sánchez-Castillo et al., 1989; Jiménez et al., 2015). There are no available pH data from peaty areas. Vegetation mainly consists of graminoid-dominated (Cyperaceae and Poaceae) alpine meadows, although bryophytes predominate in the wetland-pond transitions. Vegetation distribution in Sierra Nevada is primarily controlled by precipitation and temperature, determining elevational belts. Only LdlM occurs near the local tree line (~2500 m a.s.l.). The other records are in the tundra-like zone above ~2900 m a.s.l. (Valle, 2003; Anderson et al., 2011).

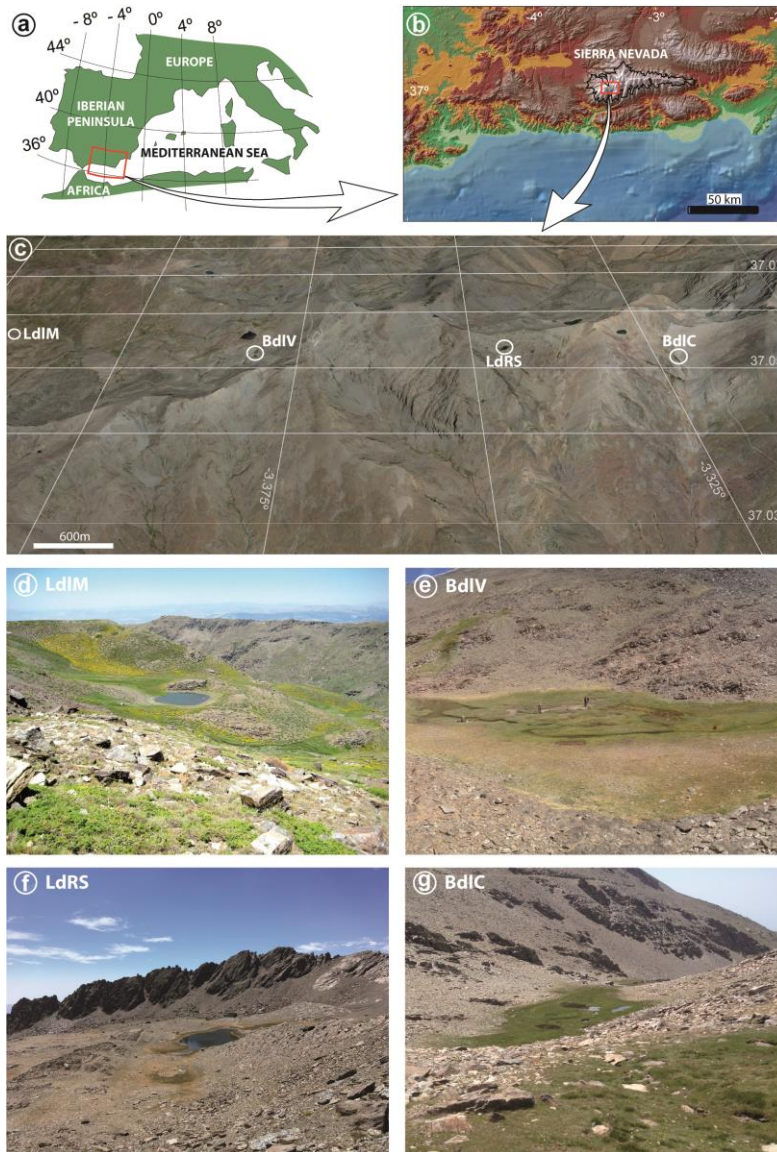


**Figure 8.2.** Geographical setting. (a) Studied area in the western Mediterranean region, and (b) location of the Sierra Nevada National Park (black line). (c) Situation of studied sites: Laguna de la Mula (LdIM), Borreguil de la Virgen (BdIV), Laguna de Río Seco (LdRS), and Borreguil de la Caldera site (BdIC). Detailed pictures of (d) Laguna de la Mula, (e) Borreguil de la Virgen, (f) Laguna de Río Seco, and (g) Borreguil de la Caldera. Data source and software: (a-c) modified from García-Alix et al. (2017), (a) map created by P. Ruano using Adobe Illustrator [5.5] (<https://www.adobe.com/>), (b) data from Shuttle Radar Tomography Mission (SRTM-90: <http://www2.jpl.nasa.gov/srtm/>)47 plotted by means of ArcMap [10.1] (<http://www.esri.com/software/arcgis/arcgis-for-desktop>), (c) map from Google Earth Pro [7.1.5.1557] (<https://www.google.es/earth/download/gep/agree.html>) using the data provided by Google 2016 and DigitalGlobe 2016. (d) Picture from R.S. Anderson, (e and g) pictures from G. Jiménez-Moreno, (f) picture from A. García-Alix.



Site	Type	Record length (cm -- ky)	Location	Elevation (m a.s.l.)	Surface (ha)		Orientation
					Site	Catchment	
LdlM	Lake	32.5 cm 4.1 ky	37°3'35''N 3°25'01''W	2497	0.10	25	NW
BdlV	Bog (present) Lake (early –middle Holocene)	169 cm 8.5 ky	37°03'10''N 3°22'43''W	2945	0.18	30	NW
LdRS	Lake	150 cm 12.0 -12.5 ky	37°03'08''N 3°20'44''W	3020	0.42	9.9	S
BdlC	Bog	56 cm 4.5 ky	37°03'02''N 3°19'24''W	2992	0.17	62	S

**Table 8.1.** Main features of the studied sites. Acronyms: Laguna de la Mula (LdlM), Borreguil de la Virgen (BdlV), Laguna de Río Seco (LdRS), Borreguil de la Caldera (BdlC).

## 2. Methods

A multi-proxy approach based on geochemical analyses has been developed in four sedimentary cores collected in two peat bogs and two shallow lakes facing different hillslopes (Table 8.1). To track the source of the organic matter in the sediments several indexes in bulk sediment samples have been selected: total organic carbon (TOC), total nitrogen (TN), total hydrogen (TH), atomic hydrogen – carbon ratio (H/C), atomic carbon – nitrogen ratio (C/N), and carbon and nitrogen isotopes (Meyers, 2003). The organic matter has been also characterised more specifically by means of leaf wax (*n*-alkanes) indices (Meyers, 2003). In this regard, the length of the carbon chain in *n*-alkanes can be related to different kinds of vegetation in the catchment basins, as well as potential water stress: short *n*-alkanes are related to aquatic environments, and long *n*-alkanes usually to terrestrial plants in the extreme environments of Sierra Nevada (García-Alix et al., 2017). So, three *n*-alkane indices from leaf wax biomarkers, assessing the length of the carbon chain length, are used to constrain the source of organic matter and the water availability in the environments: the average chain length (ACL), the portion aquatic (P<sub>aq</sub>) (Ficken et al., 2000), and the carbon preference index CPI (Bush and McInerney, 2013). The potential detrital and aeolian input in these areas are depicted by means of La/Lu (Martínez-Ruiz et al., 2000; Gallego-Torres et al., 2007; Jiménez-Espejo et al., 2014) (sources of N African aeolian dust), Zr/Th, and Zr/Al ratios (amount of N African aeolian inputs) (Jiménez-Espejo et al., 2014; Rodrigo-Gámiz et al., 2015; García-Alix et al., 2017) as well as Mg/Al (catchment basin runoff), among others Jiménez-Espejo et al., 2007, 2014). Mn/Al ratios are usually related to the redox conditions in aquatic environments (Naeher et al., 2013); nevertheless, the complex Mn behaviour makes the reconstruction of oxygen conditions difficult based solely on this proxy. The anthropogenic heavy metal atmospheric pollution at these high elevation wetlands can be tracked by means of the Pb, Pb/Al and Hg records (Jiménez-Espejo et al., 2014; Guédron et al., 2016; García-Alix et al., 2017). All these raw data along with other unpublished geochemical data are specified in the datasets (Data Citation 1).

## 2.1. Sampling methods and sediment core and age models

Four sedimentary records were extracted in the studied areas from 2006 to 2013 using a Livingstone piston corer and an Aquatic Research corer. They are named according to the year when they were retrieved and the number of cores extracted: Laguna de la Mula, LdlM 10-02; Borreguiles de la Virgen, BdlV 06-01; Laguna de Río Seco, LdRS 06-01 and LdRS 06-02; and Borreguil de la Caldera, BdlC 13-01. Their lengths were: 32.5cm (LdlM 10-02), 169 cm (BdlV 06-01), 150cm (LdRS 06-01 + LdRS 06-02: LdRS 06-02-uppermost 10cm; LdRS 06-01-140cm), and 56cm (BdlC 13-01). Only one drive was retrieved from cores LdlM 10-02, BdlC 13-01, and LdRS 06-02 and four and seven drives were retrieved in cores LdRS 06-01 and BdlV 06-01, respectively. Drives 01 and 02 from BdlV 06-01 and drive 01 from LdRS 06-01 were compacted during drilling and the real coring depth in these cases has been reconstructed. This is specified in each file (Data Citation 1). Sediment samples for the different analyses were taken from the cores at different resolution, depending on the proxy studied (Table 8.2). Age models from the cores were computed using  $^{14}\text{C}$  ages in LdlM 10-02 (Jiménez-Moreno et al., 2013), BdlV 06-01 (Jiménez-Moreno and Anderson, 2012), LdRS 06-01 (Anderson et al., 2011), and BdlC 13-01 (Ramos-Román et al., 2016) as well as Cs-Pb (LdRS 06-02) (Anderson et al., 2011) by means of Clam package (<http://www.chrono.qub.ac.uk/blaauw/clam.html>) (Blaauw, 2010) for R open-source software (<https://www.r-project.org/>) and the calibration curves IntCal09 (Reimer et al., 2009) and IntCal13 (Reimer et al., 2013) (Table 8.3).

Site	Organic analyses							Inorganic analyses					
	Elemental Analyser				EA-IRMS		GC-FID	Data files in Data Citation	AAS	ICP-MS	Mercury Analyser	XRF scanner	Data files in Data Citation
	TOC, TN	TH	C/N	H/C	$\delta^{13}\text{C}$	$\delta^{15}\text{N}$	<i>n</i> -alkanes						
LdlM	31		31		31	31		LdlM_organic (Data Citation 2)					
BdlV	73		79		79	74	93	BdlV_organic (Data Citation 3)					
LdRS	68	68	68		68	68		LdRS_organic (Data Citation 4)	68	68			LdRS_inorganic (Data Citation 6)
BdlC	81	81	82	82	56	51	50	BdlC_organic (Data Citation 5)			18	78	BdlC_inorganic (Data Citation 7) BdlC_Hg: (Data Citation 8)

**Table 8.2.** Organic and inorganic analyses conducted in the sedimentary cores as well as number of samples measured with the different techniques and the file name where these data are stored (Data Citation 1). AAS data: Al, Mn, Ca, Fe, Mg, and K; ICP data: Li, Rb, Cs, Be, Sr, Ba, Sc, V, Cr, Co, Ni, Cu, Zn, Ga, Y, Nb, Ta, Hf, Mo, Sn, Tl, U, Ce, Pr, Nd, Sm, Eu, Gd, Tb, Dy, Ho, Er, Tm, Yb, Lu, Zr, Pb, Th, and La; XRF-scanner data: Al, Si, S, K, Ca, Ti, Fe, Zr, Br, Rb, and Sr. Acronyms: EA, Elemental Analyser; IRMS, Isotope-ratio mass spectrometry; GC-FID, Gas Chromatography with Flame-Ionization Detection; AAS, Atomic Absorption; ICP-MS, Inductively coupled plasma mass spectrometry; XRF-scanner, X-ray fluorescence scanner.

Laboratory Code	Core	Depth (cm)	Material Dated	Dating Method	<sup>14</sup> C age (yr BP)	SD (±)	Calibrated Age (cal yr BP/AD)
Reference age	LdlM 10-02	0.0		Present			-60
DirectAMS-1203-006	LdlM 10-02	2.5	OBS	<sup>14</sup> C	834	19	739
DirectAMS-1203-007	LdlM 10-02	9.5	OBS	<sup>14</sup> C	2038	24	1990
DirectAMS-1203-008	LdlM 10-02	14.5	OBS	<sup>14</sup> C	2535	28	2624
DirectAMS-1203-009	LdlM 10-02	18.0	OBS	<sup>14</sup> C	2887	20	3018
DirectAMS-1203-010	LdlM 10-02	22.0	OBS	<sup>14</sup> C	3397	20	3650
<i>DirectAMS-1203-011</i>	<i>LdlM 10-02</i>	<i>27.5</i>	<i>OBS</i>	<i><sup>14</sup>C</i>	<i>3913</i>	<i>22</i>	<i>4356</i>
UCIAMS81595	LdlM 10-02	30.5	OBS	<sup>14</sup> C	3720	20	4042
Reference age	BdlV 06-01	0.0		Present			-56
UCIAMS-51248	BdlV 06-01	34.5	VR	<sup>14</sup> C	730	15	675
UCIAMS-69120	BdlV 06-01	44.2	VR	<sup>14</sup> C	3220	20	3428
<i>UCIAMS-67124</i>	<i>BdlV 06-01</i>	<i>47.5</i>	<i>VR</i>	<i><sup>14</sup>C</i>	<i>5435</i>	<i>25</i>	<i>6240</i>
<i>UCIAMS-67125</i>	<i>BdlV 06-01</i>	<i>53.96</i>	<i>VR</i>	<i><sup>14</sup>C</i>	<i>5000</i>	<i>20</i>	<i>5722</i>
UCIAMS-67126	BdlV 06-01	61.8	VR	<sup>14</sup> C	3960	20	4430
UCIAMS-51249	BdlV 06-01	72.4	VR	<sup>14</sup> C	4395	15	4941
UCIAMS-51250	BdlV 06-01	100.0	VR	<sup>14</sup> C	5410	15	6241
Beta-22171	BdlV 06-01	144.0	VR	<sup>14</sup> C	6470	40	7375
UCIAMS-51251	BdlV 06-01	159.0	VR	<sup>14</sup> C	7245	20	8052
Reference age	LdRS 06-02	0.0		Present			-56
USC-LdRS 06-02-1	LdRS 06-02	5.0	BS	<sup>137</sup> Cs			1963 AD
USC-LdRS 06-02-2	LdRS 06-02	15.0	BS	<sup>210</sup> Pb			1891 AD
UCIAMS-51255	LdRS 06-01	20.0	VR	<sup>14</sup> C	1520	15	1398
UCIAMS-63003	LdRS 06-01	26.75	VR	<sup>14</sup> C	2255	20	2234
UCIAMS-51256	LdRS 06-01	40.0	VR	<sup>14</sup> C	3060	15	3295
UCIAMS-63004	LdRS 06-01	46.0	VR	<sup>14</sup> C	3525	20	3786
UCIAMS-51257	LdRS 06-01	60.0	VR	<sup>14</sup> C	4010	15	4480
UCIAMS-51258	LdRS 06-01	80.0	VR	<sup>14</sup> C	5450	30	6246
UCIAMS-63005	LdRS 06-01	83.25	VR	<sup>14</sup> C	5505	20	6298
UCIAMS-63006	LdRS 06-01	109.5	VR	<sup>14</sup> C	6550	20	7453
UCIAMS-32495	LdRS 06-01	123.5	VR	<sup>14</sup> C	8570	60	9540
Reference age	BdlC 01	0.0		Present			-63
DirectAMS-004385	BdlC 01	13.7	VR	<sup>14</sup> C	388	24	469
DirectAMS-004386	BdlC 01	23.2	VR	<sup>14</sup> C	474	26	517
DirectAMS-004387	BdlC 01	36.8	VR	<sup>14</sup> C	1036	31	950
DirectAMS-004388	BdlC 01	46.4	VR	<sup>14</sup> C	2563	30	2725
DirectAMS-004389	BdlC 01	56.0	VR	<sup>14</sup> C	4066	29	4551

**Table 8.3.** Age data from the studied cores. <sup>14</sup>C ages were calibrated using IntCal09 curve35 in LdlM7, LdRS11, and BdlV12, and IntCal13 curve36 in BdlC33. Dates in italics: old carbon ages not used in the age model. Acronyms: OBS, organic bulk sediment; BS, bulk sediment; VR, vegetal remains; DirectAMS#, Accium BioSciences, Seattle, USA; Beta#, Beta Analytic, Inc. Miami, USA; UCIAMS#, University of California at Irvine W.M. Keck Carbon Cycle Accelerator Mass Spectrometry Laboratory, Irvine, USA. USC, University of Southern California, Los Angeles, USA.

## 2.2. Organic geochemistry

### 2.2.1. Elemental analysis in bulk sediment

Pre-weighted and freeze-dried samples were decarbonated overnight by means of acid digestion (HCl 1M). The acid concentration was 1M because carbonate content in the samples was low. When all the carbonate was digested, the solution was centrifuged to remove the acid, and samples were rinsed with Milli-Q water and centrifuged five times. After reaching a neutral pH, the obtained carbonate-free product was freeze-dried again. When samples were totally dry, they were split in two aliquots: one for elemental analyses and another one for C and N isotope analyses. The elemental composition of the samples was measured using a Thermo Scientific Flash 2000 elemental analyser with He as carrier gas at the Centre for Scientific Instrumentation of the University of Granada, Spain (hereafter CIC-UGR). A flash combustion was produced at 1000°C, and the obtained gas, after passing through a reduction column with Cu, was separated by means of a chromatographic column and quantified with a Thermal Conductivity Detector CTD (Data Citations 2–5).

### 2.2.2. Carbon and Nitrogen analyses in bulk sediment

C and N isotopes were measured in the other aliquot of the decarbonated bulk samples by means of isotope-ratio mass spectrometry (IRMS) with a coupled elemental analyser (EA). In this case, the obtained gases from the EA (N<sub>2</sub> and CO<sub>2</sub>) were analysed in the IRMS in order to obtain their isotopic composition. We used two different configurations: Carlo Erba Ba 1500 series 2 Elemental Analyser attached to a Thermo Finnigan Delta plus XL IRMS (Instituto Andaluz de Ciencias de la Tierra CSIC-UGR, Spain) in samples from LdlM, BdIV, and LdRS, and an Euro EA 300 Elemental Analyser attached to an Isoprime 50V IRMS (CIC-UGR) in samples from BdIC. The isotopic measurements were calibrated using internal and international standards (see Technical Validation section), and expressed using the  $\delta$  notation, which relates the isotopic abundance of an element in the sample and that of the same element in a reference material:  $\delta \text{‰} = [(R_{\text{sample}}/R_{\text{Ref}}) - 1] \times 1000$ . This reference is VPDB in the case of  $\delta^{13}\text{C}$  and AIR, in the case of  $\delta^{15}\text{N}$  (Data Citations 2–5).

### 2.2.3. Specific compound analyses

Pre-weighted, homogenized and freeze-dried samples were dissolved by means of sonication (20 min) and temperature (38°C for 1 hour) using DCM:MeOH (3:1) solution. The supernatant solvent was collected after centrifuging at 3300 rpm and dried in a nitrogen stream. These steps were repeated at least two more times to make sure that all the lipids had been extracted from the samples. The neutral fraction of this total lipid extract was obtained by means of aminopropyl-silica gel chromatography and a solution of 1:1 DCM:isopropanol. Afterwards, the aliphatic hydrocarbon fraction, with the *n*-alkanes, was extracted using the elution of the neutral fraction with hexane through a 230–400 mesh/35–70micron silica-gel chromatographic

column. Finally, the *n*-alkanes were analysed by means of a GC-FID (Shimadzu 2010) in order to quantify them, and a GC-MS (Shimadzu OP2010-Plus Mass Spectrometer interfaced with a Shimadzu 2010 GC) at the BECS laboratory (University of Glasgow, UK) in order to identify the compounds of the most complicated samples (Data Citations 3 and 5).

### *2.3. Inorganic geochemistry*

#### *2.3.1. Inductively Coupled Plasma Mass Spectrometry and Atomic Absorption Analyses*

About 0.1-0.2g of sediment samples were dissolved using HNO<sub>3</sub> (65% Panreac PA-AR) + HF (40% Suprapur) in Teflon-lined vessels at high temperature and pressure during 150 min. Afterwards, they were completely evaporated and re-dissolved in 100ml of 4 vol.% HNO<sub>3</sub>. This solution was split in two aliquots. One was analysed by means of inductively coupled plasma mass spectrometry (ICP-MS) using a Perkin Elmer Sciex Elan 5000 (for Li, Rb, Cs, Be, Sr, Ba, Sc, V, Cr, Co, Ni, Cu, Zn, Ga, Y, Nb, Ta, Hf, Mo, Sn, Tl, U, Ce, Pr, Nd, Sm, Eu, Gd, Tb, Dy, Ho, Er, Tm, Yb, Lu, Zr, Pb, Th, and La). The other aliquot was analysed by means of flame Atomic Absorption (AAS) using a Perkin-Elmer 5100 ZL spectrometer with an analytic error of 2% (for Al, Mn, Ca, Fe, Mg, and K). Two different flames were used: one of acetylene / nitrous oxide for the determination of Al and another of acetylene / air for the other elements. These inorganic analyses were conducted at the CIC-UGR. Although raw data are expressed in ppm, the concentration of some selected paleoenvironmental proxies (Zr, Mg, Mn, Pb, among others) are normalised by refractory elements (i.e., Al, or Th, in this case) (Taylor and McClennan, 1985; Cochran et al., 1986) in order to correct the dilution caused by sedimentary barren phases of a particular element (Calvert and Pedersen, 1993; Morford and Emerson, 1999) (Data Citation 6).

#### *2.3.2. X-Ray fluorescence Scanner analyses*

High-resolution elemental profiles (Al, Si, S, K, Ca, Ti, Fe, Zr, Br, Rb, and Sr) at the BdIC core were obtained by means of an Avaatech X-Ray fluorescence (XRF) core Scanner at the XRF-Core Scanner Laboratory (University of Barcelona, Spain). The core was scanned two times with a point sensor: one at 10s count time (10kV X-ray voltage and 650mA X-ray current for light elements, such as Al, Si, S, K, Ca, Ti, and Fe), and another one at 35s count time (30kV X-ray voltage and 1700mA X-ray current for heavy elements, such as Zr, Br, Rb, Sr). Triplicate measurements were analysed every 25 analyses. Results were expressed in intensities (counts per second, cps) as well as normalized for the total sum of cps in every measure in order to avoid the influence of the water content and the sediment surface conditions (Data Citation 7).

#### *2.3.3. Mercury analyses*

Total mercury concentrations were determined using an Advanced Mercury Analyser

(LECO AMA-254) with an absolute mass detection limit of 0.01 ng of Hg, following analogous procedures than reported by Díez et al. (2007) at the Institute of Environmental Assessment and Water Research (IDAEA-CSIC, Spain). This instrumentation, originally developed by Altec, Ltd., Czech Republic, is a single-purpose atomic absorption spectrometer for determination of mercury traces in solid and liquid specimens without sample pre-treatment or pre-concentration. Sediment samples and quality control materials with masses of 20mg to 100mg were automated, introduced into a quartz combustion tube in a nickel boat and dried at 120°C for 50s. Subsequently the instrument self-seals the tubes. Afterwards, samples were combusted in an oxygen-rich atmosphere (99.5%) and the released gasses were transported using oxygen as carrier gas through specific catalytic converter (a Mn<sub>3</sub>O<sub>4</sub>/CaO-based catalyst at 750°C), in order to obtain a complete oxidation as well as the retention of halogens, nitrogen, and sulphur oxides. As a consequence, the different mercury species are converted into elemental Hg vapour, which is collected in a gold-plated ceramic amalgamator. Subsequently, the mercury is released by means of an oxygen flush for 150s and the amalgamator heating up to approx. 700°C. The gas is driven to a cuvette at ~120°C in order to prevent condensation and to minimize potential carry-over effects. The source was a low-pressure mercury vapour lamp at of 253.65nm wave-length, and a detector, with a working range between 0.05ng and 500ng, acquired the signal. Data are expressed in ppb (Data Citation 8).

#### 2.4. Code availability

The database includes seven datasets stored in seven files (Data Citation 1). The files with the different datasets are named with the acronym of the site and the data source; i.e. BdlV\_organic. The files and the information they contain are listed in Table 8.2. Each data file includes the following fields for each sample:

*Core ID*  
*Drive*  
*Top sampling depth*  
*Bottom sampling depth*  
*Top real depth*  
*Bottom real depth*  
*Mean real depth*  
*Top age Cal yr BP*  
*Bottom age Cal yr BP*  
*Mean age Cal yr BP*  
*Proxy#1*  
*Proxy#2*  
*Proxy#n-n+1*

Data from XRF scanner in the file *BdlC\_inorganic* do not contain the fields: *bottom sampling depth*, *bottom real depth*, *mean real depth*, *bottom age Cal yr BP* and *mean age Cal yr BP* since measurement were taken with a point sensor in specific locations (*top sampling depth*).

Proxy units are showed between brackets when are needed. Each single data can be named as follows: core-ID#top\_real\_depth/top\_age#proxy, i.e., *BdlV 06-01#10cm/155cal yr BP# $\delta^{13}C$* . New paleochemical data can be easily added to this database when they are available so that this database will always be updated with the latest geochemical findings in these sites.

### 3. Data records

The dataset presented in this paper shows information of the organic and inorganic content from four alpine sites at the Sierra Nevada National Park: LdlM, BdlV, LdRS, and BdlC (Table 8.1). These geochemical records have different lengths, registering the environmental evolution of these shallow lakes and peatlands from the last 4.1 ky (LdlM, the shortest sedimentary record in the area) to the last 12-12.5 ky (LdRS, the longest sedimentary record in the area) (Table 8.1).

Regarding the organic data, we present the total organic carbon (TOC), total nitrogen (TN), total hydrogen (TH), atomic hydrogen – carbon ratio (H/C), atomic carbon – nitrogen ratio (C/N), carbon isotopic composition ( $\delta^{13}C$ ), nitrogen isotopic composition ( $\delta^{15}N$ ), and several *n*-alkane indices (average change length, ACL; portion aquatic,  $P_{aq}$ ; carbon preference index, CPI), as well as the *n*-alkane concentration in each sample. ACL, CPI and  $P_{aq}$  have been worked out from the *n*-alkane concentrations ( $C_{xx}$ ) following these equations:

$ACL = (25 \times C_{25} + 27 \times C_{27} + 29 \times C_{29} + 31 \times C_{31} + 33 \times C_{33}) / (C_{25} + C_{27} + C_{29} + C_{31} + C_{33})$  after Poynter and Eglinton (1990).

$CPI = 0.5 \times [(C_{25} + C_{27} + C_{29} + C_{31} + C_{33}) / (C_{24} + C_{26} + C_{28} + C_{30} + C_{32}) + (C_{25} + C_{27} + C_{29} + C_{31} + C_{33}) / (C_{26} + C_{28} + C_{30} + C_{32} + C_{34})]$  after Bray and Evans (1961).

$P_{aq} = (C_{23} + C_{25}) / (C_{23} + C_{25} + C_{29} + C_{31})$  according to Ficken et al. (2000).

The inorganic geochemical data available are the concentrations of Al, Si, Mn, Ca, Fe, Mg, K, S, Li, Rb, Br, Cs, Ti, Be, Sr, Ba, Sc, V, Cr, Co, Ni, Cu, Zn, Ga, Y, Nb, Ta, Hf, Mo, Sn, Tl, U, Ce, Pr, Nd, Sm, Eu, Gd, Tb, Dy, Ho, Er, Tm, Yb, Lu, Zr, Pb, Th, and Hg, as well as the ratios Mg/Al, Mn/Al, Zr/Th, Zr/Al, La/Lu, and Pb/Al (Table 8.2).

All of these data are related to 1) the external mechanisms that generated the sedimentary record: i.e. runoff, aeolian input/atmospheric deposition, or the redox conditions in water environments, which are mainly related to the inorganic geochemical data, that eventually were boosted either by climate/environmental or indirect human influence; and 2) the environmental responses of these extreme environments to the climate/environmental and human pressures (mostly organic geochemical data) (Fig. 8.1). We present all these raw data in the datasets (Data Citation 1); however, the interpretation of these data in the context of our research can be found in the original publications (García-Alix et al., 2012, 2013; Jiménez-Moreno et al., 2013; Jiménez-Espejo et al., 2014; García-Alix et al., 2017).

## 4. Technical validation

### 4.1. Organic geochemistry

#### 4.1.1. Elemental analysis in bulk sediment

The equipment was calibrated every day using a certified Sulfanilamide standard, whose elemental composition is: N 16.27%, C 41.84%, H 4.68%, and S 18.62%. The calculated precision of the measurements was better than  $\pm 0.1\%$ . The CIC-UGR works under a Quality Management System following the requirements of the UNE-EN-ISO-9001, which certifies the technical quality of the obtained data.

#### 4.1.2. Carbon and Nitrogen analyses in bulk sediment

The analyses that were conducted in the EA-Thermo Finnigan DELTA plus XL IRMS used four internal standards EEZ14 -phthalic acid- ( $\delta^{13}\text{C}$ :  $-30.63\%$  VPDB) and EEZ 21 -sucrose- ( $\delta^{13}\text{C}$ :  $-11.65\%$  VPDB), EEZ17 -urea Merk- ( $\delta^{15}\text{N}$ :  $-1.02\%$  air), and EEZ23 -shark cartilage- ( $\delta^{15}\text{N}$ :  $16.01\%$  air), contrasted with the IAEA international references NBS-22-oil- ( $\delta^{13}\text{C}$ :  $-30.03\%$  VPDB), IAEA-CH-6 -sucrose- ( $\delta^{13}\text{C}$ :  $-10.45\%$  VPDB), and IAEA-N1 -ammonium sulphate- ( $\delta^{15}\text{N}$ :  $+0.4\%$  air). The calculated precision of the measurements was better than  $\pm 0.1\%$  for  $\delta^{13}\text{C}$  and  $\delta^{15}\text{N}$ .

The analyses that were conducted in the EA-Isoprime 50V IRMS used Certified Elemental Microanalysis standards: Sorgo Flour Standard ( $\delta^{13}\text{C}$ :  $-13.68\%$  VPDB and  $\delta^{15}\text{N}$ :  $+1.58\%$  air), Wheat Flour Standard ( $\delta^{13}\text{C}$ :  $-27.1\%$  VPDB and  $\delta^{15}\text{N}$ :  $+2.85\%$  air), and Casein Standard ( $\delta^{13}\text{C}$ :  $-26.98\%$  VPDB and  $\delta^{15}\text{N}$ :  $+5.94\%$  air). These standards were calibrated to the international standards IAEA-CH-6 sucrose- ( $\delta^{13}\text{C}$ :  $-10.45\%$  VPDB) and IAEA-N1 -ammonium sulphate- ( $\delta^{15}\text{N}$ :  $+0.4\%$  air). The calculated precision of the measurements was better than  $\pm 0.1\%$  for  $\delta^{13}\text{C}$  and  $\delta^{15}\text{N}$ . The analyses were conducted under a Quality Management System following the requirements of the UNE-EN-ISO-9001 at the CIC-UGR.

#### 4.1.3. Specific compound analyses

The reproducibility of the measurements was checked by means of an external standard with a mixture of *n*-alkanes ( $\text{C}_{16}$ ,  $\text{C}_{18}$ ,  $\text{C}_{19}$ ,  $\text{C}_{20}$ ,  $\text{C}_{23}$ ,  $\text{C}_{25}$ ,  $\text{C}_{26}$ ,  $\text{C}_{28}$ ,  $\text{C}_{30}$ ,  $\text{C}_{32}$ ,  $\text{C}_{37}$ ) measured every five samples. The standard reproducibility was better than 97%. The concentration of the *n*-alkanes was worked out with the  $\text{C}_{25}$  *n*-alkane of the same external alkane mixture mentioned above. The concentration of this  $\text{C}_{25}$  *n*-alkane was  $10 \mu\text{g/ml}$ .



## *4.2. Inorganic geochemistry*

### *4.2.1. ICP analyses*

Each sample was measured in triplicate. Re and Rh (25 ppb) internal standards (25 ppb) were used to test the performance of the equipment. In addition, data were contrasted with several reference geo-standards: UBN, PMS, WSE, BEN, BR, AGV, DRN, GSN GA and GH (Govindaraju, 1994). The instrumental errors during the measurement of the sample batches were  $\pm 2\%$  for elemental concentrations  $>50$  ppm and  $\pm 5\%$  for concentrations between 50 to 5 ppm (Bea, 1996). The technical validation of the analyses is certified by the Quality Management System of the CIC-UGR that follows the requirements of the UNE-EN-ISO-9001.

### *4.2.2. Atomic Absorption analyses*

The Perkin-Elmer 5100 spectrometer has an analytic error lower than 2%. Certified Perkin Elmer standards for AA (ISO Guide 34 and ISO 17025 – certified by A2LA) at a concentration of  $1000\mu\text{g}/\text{m}$  in a solution of 2% of  $\text{HNO}_3$  were used for each element. Blank samples were measured for each element to establish their detection limit, which was:  $<190\text{ppm}$  (Mn),  $<5\text{ppm}$  (Al),  $<200\text{(Ca)}$ ,  $<5\text{ppm}$  (Fe),  $<340\text{ppm}$  (Mg), and  $<190\text{ppm}$  (K). The analyses were conducted following the UNE-EN-ISO-9001 requirements of the Quality Management System at the CIC-UGR.

### *4.2.3. X-Ray fluorescence Scanner analyses*

Measurements of the SARM4 standard of the National Institute of Standards and Technology (NIST) were performed in order to test the stability of the X-ray tube at the beginning and at the end of the measurement session every day. In addition, samples were measured in triplicate every 25 analyses. The % mean error of the measurements  $[(\text{stdes}/\text{mean}) * 100]$  was 3.5% (Al), 0.9% (Si), 1.4% (S), 1.1% (K), 2.6% (Ca), 1.4% (Ti), 0.6% (Fe), 2.5% (Zr), 4.3% (Br), 4.4% (Rb), 2.8% (Sr).

### *4.2.4. Mercury analyses*

The absolute mass detection limit of the LECO AMA-254 was 0.01 ng of Hg. The entire analytical procedure was validated by analysing certified reference material DORM-3 (Fish tissue, NRCC, Canada) at the beginning and end of each set of samples, ensuring that the instrument remained calibrated during the course of the analytical routine.

**Data citations**

1. García-Alix, A., Jiménez-Espejo, F.J., Jiménez-Moreno, G., Toney, J.L., Ramos-Román, M.J., Camuera, J., Anderson, R.S., Delgado Huertas, A., Martínez Ruiz, F., and Queralt, I. *PANGAEA* <https://doi.org/10.1594/PANGAEA.883651> (2017)
2. García-Alix, A., Jiménez-Espejo, F.J., Jiménez-Moreno, G., Toney, J.L., Ramos-Román, M.J., Camuera, J., Anderson, R.S., Delgado Huertas, A., Martínez Ruiz, F., and Queralt, I. *PANGAEA* <https://doi.org/10.1594/PANGAEA.883647> (2017)
3. García-Alix, A., Jiménez-Espejo, F.J., Jiménez-Moreno, G., Toney, J.L., Ramos-Román, M.J., Camuera, J., Anderson, R.S., Delgado Huertas, A., Martínez Ruiz, F., and Queralt, I. *PANGAEA* <https://doi.org/10.1594/PANGAEA.883646> (2017)
4. García-Alix, A., Jiménez-Espejo, F.J., Jiménez-Moreno, G., Toney, J.L., Ramos-Román, M.J., Camuera, J., Anderson, R.S., Delgado Huertas, A., Martínez Ruiz, F., and Queralt, I. *PANGAEA* <https://doi.org/10.1594/PANGAEA.883649> (2017)
5. García-Alix, A., Jiménez-Espejo, F.J., Jiménez-Moreno, G., Toney, J.L., Ramos-Román, M.J., Camuera, J., Anderson, R.S., Delgado Huertas, A., Martínez Ruiz, F., and Queralt, I. *PANGAEA* <https://doi.org/10.1594/PANGAEA.883645> (2017)
6. García-Alix, A., Jiménez-Espejo, F.J., Jiménez-Moreno, G., Toney, J.L., Ramos-Román, M.J., Camuera, J., Anderson, R.S., Delgado Huertas, A., Martínez Ruiz, F., and Queralt, I. *PANGAEA* <https://doi.org/10.1594/PANGAEA.883648> (2017)
7. García-Alix, A., Jiménez-Espejo, F.J., Jiménez-Moreno, G., Toney, J.L., Ramos-Román, M.J., Camuera, J., Anderson, R.S., Delgado Huertas, A., Martínez Ruiz, F., and Queralt, I. *PANGAEA* <https://doi.org/10.1594/PANGAEA.883642> (2017)
8. García-Alix, A., Jiménez-Espejo, F.J., Jiménez-Moreno, G., Toney, J.L., Ramos-Román, M.J., Camuera, J., Anderson, R.S., Delgado Huertas, A., Martínez Ruiz, F., and Queralt, I. *PANGAEA* <https://doi.org/10.1594/PANGAEA.883644> (2017)

## **Acknowledgments**

This study was supported by the project P11-RNM-7332 of the Junta de Andalucía, the projects CGL2013-47038-R of the Ministerio de Economía y Competitividad of Spain and Fondo Europeo de Desarrollo Regional FEDER and the research group RNM0190 and RNM309 (Junta de Andalucía). Antonio García-Alix was also supported by a Marie Curie Intra-European Fellowship of the 7th Framework Programme for Research, Technological Development and Demonstration of the European Commission (NAOSIPUK. Grant Number: PIEF-GA-2012-623027) and by a Ramón y Cajal Fellowship RYC-2015-18966 of the Spanish Government (Ministerio de Economía y Competitividad). Jaime L. Toney was also supported by a Small Research Grant by the Carnegie Trust for the Universities of Scotland and hosted the NAOSIPUK project (PIEF-GA-2012-623027). María J. Ramos-Román acknowledges the PhD funding provided by Consejería de Economía, Innovación, Ciencia y Empleo de la Junta de Andalucía (P11-RNM 7332). Jon Camuera acknowledges the PhD funding provided by Ministerio de Economía y Competitividad of Spain and Fondo Europeo de Desarrollo Regional FEDER.

## **Author contributions**

Antonio García-Alix conceived the idea, retrieved some of the studied cores, conducted both bulk organic (including isotopes) and specific compound analyses, and wrote this work with contributions from all authors. Francisco J. Jiménez-Espejo conducted bulk inorganic analyses in discrete samples and processed these data. Gonzalo Jiménez-Moreno retrieved all the studied cores, studied the stratigraphy, and conducted the XRF scanner analyses. Jaime L. Toney retrieved some of the studied cores, conducted the specific compound analyses, and processed these data. María J. Ramos-Román conducted the XRF scanner analyses and processed these data. Jon Camuera conducted the XRF scanner analyses and processed these data. R. Scott Anderson retrieved all of the studied cores and studied the stratigraphy. Antonio Delgado Huertas conducted the isotopic analyses in bulk sediment samples and processed these data. Francisca Martínez-Ruiz conducted bulk inorganic analyses in discrete samples and processed these data. Ignasi Queralt conducted the mercury analyses in the sediments and processed these data. All the co-authors discussed the data together.

# *Chapter 9*

*Conclusions and future perspectives*



## ***Chapter 9: Conclusions and future perspectives***

### **Conclusions**

The multiproxy study of the new ~200 kyr Padul-15-05 sedimentary record show that the Padul wetland is an extraordinary site for paleoenvironmental and paleoclimatic reconstructions in the western Mediterranean region. This study has provided insight about past climate variability in this area in relation with Earth's orbital and sub-orbital oscillations through the understanding of local (e.g., sedimentation, lake level) and regional (e.g., vegetation) responses to high-amplitude glacial-interglacial cycles (from MIS 7 to MIS 1) as well as to abrupt and rapid millennial- and centennial-scale variability (such as Heinrich Stadials or Dansgaard-Oeschger variability).

The main conclusions of this PhD thesis have been synthesized below:

1. The Padul wetland is confirmed as an ideal continental site for high-resolution paleoenvironmental and paleoclimatic reconstructions for the Quaternary. This is deduced by the excellent preservation of biological, physical and geochemical paleoclimatic signals in a long (42.64 m) and continuous sedimentary record of the last ~200 kyr, which allowed obtaining paleoclimate inferences at orbital- and sub-orbital-scales.
2. The new Padul-15-05 sedimentary record has improved the chronological control of the Padul wetland sedimentary sequence with respect to the previous studies. This results from up-to-date dating techniques such as high-resolution AMS radiocarbon dating and amino acid racemization dating. The improvement of the age-depth control has permitted correlating paleoenvironmental changes in this site to orbital- and suborbital-scale paleoclimatic changes more precisely.
3. Insolation, principally controlled by orbital-scale precession and to a lesser extent by eccentricity oscillations, was the principal factor controlling climate variability in the Padul area and forced local and regional environmental changes. Significant changes in the abundance of the Mediterranean forest were mainly forced by insolation values, increasing and decreasing during interglacials (and interstadials) and glacials (and stadials), respectively. The local sedimentary signal (lithology and sedimentary facies) was also conditioned by insolation. For example, insolation minima triggered arid climate conditions and lower forest cover, which allowed a higher soil erosion and higher siliciclastic input transported from Sierra Nevada into the Padul wetland.

4. Lake level reconstructions using: (1) statistical analysis on inorganic geochemistry (XRF), organic geochemistry (elemental analysis) and magnetic susceptibility data and, (2) palynological data (in particular, algae, hygrophytes and Poaceae) show high correlation, suggesting that both biological and physical/geochemical signals are good proxies for lake level oscillations. Generally, higher lake water levels occurred during cold and arid glacial and stadial conditions (recorded by high xerophyte values from palynological analysis) as result of the low evapotranspiration and positive precipitation/evapotranspiration balance. On the contrary, warmer and higher moisture conditions of interglacial and interstadial phases (recorded by high Mediterranean forest and arboreal pollen values) are characterized by lower lake levels due to negative precipitation/evapotranspiration balance consequence of the high evapotranspiration rates that highly exceeded rainfall. An exception occurred during the Last Interglacial period, during which the high rainfall (recorded by the highest AP/NAP values and the occurrence of hygrophilous pollen taxa, such as *Abies* and *Carpinus*) could have resulted on positive precipitation/evapotranspiration balance (rainfall exceeding evapotranspiration) and high lake level.
5. Sedimentation in Padul during the Last Interglacial differs with respect to the recent Holocene Interglacial, resulting from the distinct seasonality and temperature/precipitation conditions owing to the different orbital parameters and insolation values. Sediments that accumulated during the Last Interglacial period were characterized by a carbonate lithology, probably conditioned by the previously mentioned positive precipitation/evapotranspiration balance in which precipitation highly exceeded evapotranspiration. In contrast, the Holocene period was mainly characterized by the accumulation of peat sediments that accumulated during very low lake levels, resulting from the high evapotranspiration rates exceeding rainfall.
6. The comparison of the pollen data from the Padul-15-05 record with other long Mediterranean pollen records for the last two glacial-interglacial cycles such as Lake Ioannina, Tenaghi Philippon, Lago Grande di Monticchio or Lake Ohrid allowed to identify similarities and differences between the past vegetation and climate records and generates a long-term pollen data repository from the Mediterranean region for future studies. Mediterranean sites located in environments characterized by high rainfall (partially due to the high elevation and high orographic precipitation) buffered cold and arid climate conditions and generated tree refugia during the most extreme glacial periods.
7. The high-resolution pollen analysis from the Padul wetland show millennial- and centennial-scale environmental variability, providing a perfect record for observing fast and abrupt vegetation changes in the southern Iberian Peninsula during the last ~65 kyr BP. In particular, these data evidence cold and arid climate conditions during HSs (from HS6 to

Younger Dryas) as well as millennial-scale climatic variability due to D-O cycles (from D-O cycle 18 to 1). In addition, the amplitude of the D-O interstadials recorded in Padul seem to be conditioned by insolation values at this mid-latitude.

8. High-resolution inorganic geochemistry and pollen data from Padul-15-05 show centennial-scale oscillations during Heinrich Stadial 1 (HS1), presenting 3 main phases (HS1a, HS1b and HS1c) characterized by arid(cold), more humid(warmer) and arid(cold) climate conditions, respectively. This suggests, for the first time, a subdivision of HS1 in 7 sub-phases: 3 sub-phases during HS1a (i.e., HS1a.1, HS1a.2 and HS1a.3; ~18.4 – 17.2 kyr BP), HS1b (~17.2 – 16.7 kyr BP) and other 3 sub-phases during HS1c (i.e., HS1c.1, HS1c.2 and HS1c.3; ~16.7 – 15.6 kyr BP). This variability has also been recorded in other Mediterranean SST records, confirming this climatic pattern at regional-scale.
9. The pollen data from Padul-15-05, together with other 17 well- and independently-dated (not tuned) high-resolution continental and marine records from southern Europe and the Mediterranean region show an early record of Heinrich Stadial 1 in this area (17,780 – 15,080 cal kyr BP) with respect to the climatically equivalent Greenland Stadial 2.1a (GS-2.1a, 17,480 – 14,692 cal kyr BP; Rasmussen et al., 2014) from high-latitude Greenland ice-core records. Several causes and mechanisms have been suggested for the early record of cold and arid HS1 in the Mediterranean region, probably related with the AMOC, the Mediterranean thermohaline circulation and/or the different insolation dynamics that affected land and sea surface temperatures differently in our study area compared to higher latitudes. Continental sites also present earlier evidence of HS1 compared to the marine sedimentary records, which could be related to the lagged response of marine biological signal to physical climate forcing. Nevertheless, further studies focusing on factors affecting the early record of HS1 in southern Europe and the Mediterranean region and the early continental record with respect to marine environments are still necessary.
10. The analysis of organic biomarkers (including *n*-alkanes, diols and fatty acids) from the Padul-15-05 record during the last ~36 kyr BP show that these data are mainly related with lithological/sedimentological features and local variability in the Padul wetland, but also with the regional changes mostly conditions by climate recorded by the palynological analysis. At long-term time-scales, the  $\delta D$  from *n*-alkanes show a good correlation with pollen data, pointing into insolation as the main conditioner for precipitation changes in the southern Iberian Peninsula. At short-term time-scales, *n*-alkanes and fatty acids could be related with precipitation/evapotranspiration conditions, lake levels and/or with the input of terrestrial lipids from the surrounding Padul area that depends on the vegetal cover, and therefore, on the regional environmental conditions.



## **Future perspectives**

This PhD thesis is just a further step toward more knowledge of past environmental and climate changes during the last ~200 kyr in southern Iberian Peninsula and western Mediterranean region. However, many questions arise regarding to specific abrupt and rapid climate changes observed in the Padul-15-05 record that could not be dealt with in this study due to lack of time for a higher resolution pollen or organic biomarkers analyses. In particular, it would be interesting to understand similarities/differences of the Heinrich Stadials from the penultimate glacial cycle or a more detailed analysis of fast vegetation changes that occurred during the Last Interglacial period (Eemian), similar to the millennial- and centennial-scale variability observed in the Holocene (Combourieu Nebout et al., 2009; Peyron et al., 2011; Ramos-Román et al., 2018b). The accurate identification and environmental interpretation of the D-O cycles in the Mediterranean region is also important to learn about causes and mechanism affecting environments in mid-latitude regions such as the western Mediterranean during rapid centennial-scale oscillations.

In addition, it would be interesting to reconstruct quantitative temperature and precipitation values during the last two glacial-interglacial cycles in the southern Iberian Peninsula using the pollen data from this study, similar to the recently published quantitative temperature/precipitation reconstructions based on pollen data from the Villarquemado paleolake (Wei et al., 2019). This could permit a comparison of quantitative estimations of temperature and precipitation conditions between different records from this region. Moreover, the compilation of all the available pollen-based quantitative temperature/precipitation data obtained from the different continental sites of the Iberian Peninsula could also allow a highly accurate past temperature/precipitation reconstruction for this region.

With respect to the organic biomarkers, a higher resolution data and a calibration of algal lipids (long-chain diols) to instrumental data from the Padul wetland would be really useful for reconstructing the quantitative freshwater temperature of the Padul-15-05 record for the last two glacial-interglacial cycles. The temperature-dependent biomarkers, such as those produced by algae (alkenones) or bacteria/archaea (glycerol dialkyl glycerol tetraethers: GDGTs) have been used in several marine records as quantitative paleothermometers and their application in lake environments has increased in the last decade (Castañeda and Schouten, 2011; Foster et al., 2016; Longo et al., 2018). Nevertheless, very few quantitative paleotemperature reconstructions have been done in long terrestrial records, being an interesting and promising area of study.

## References

- Adolphi, F., Muscheler, R., Svensson, A., Aldahan, A., Possnert, G., Beer, J., Sjolte, J., Björck, S., Matthes, K., Thiéblemont, R., 2014. Persistent link between solar activity and Greenland climate during the Last Glacial Maximum. *Nature Geoscience* 7, 662-666. Doi: 10.1038/NGEO2225.
- AEMET, 2016. Agencia Estatal de Meteorología, Visor del Atlas climático de la Península y Baleares, 1971-2000, <http://agroclimap.aemet.es>.
- Ahn, J., Brook, E.J., 2008. Atmospheric CO<sub>2</sub> and Climate on Millennial Time Scales During the Last Glacial Period. *Science* 322, 83-85. Doi: 10.1126/science.1160832.
- Allen, J.R., Brandt, U., Brauer, A., Hubberten, H.-W., Huntley, B., Keller, J., Kraml, M., Mackensen, A., Mingram, J., Negendank, J.F., 1999. Rapid environmental changes in southern Europe during the last glacial period. *Nature* 400, 740-743. Doi: 10.1038/23432.
- Allen, J.R., Watts, W.A., Huntley, B., 2000. Weichselian palynostratigraphy, palaeovegetation and palaeoenvironment; the record from Lago Grande di Monticchio, southern Italy. *Quaternary International* 73, 91-110. Doi: 10.1016/S1040-6182(00)00067-7.
- Allen, J.R.M., Huntley, B., 2009. Last Interglacial palaeovegetation, palaeoenvironments and chronology: a new record from Lago Grande di Monticchio, southern Italy. *Quaternary Science Reviews* 28, 1521-1538. Doi: 10.1016/j.quascirev.2009.02.013.
- Alley, R.B., Anandakrishnan, S., Jung, P., 2001. Stochastic resonance in the North Atlantic. *Paleoceanography* 16, 190-198. Doi: 10.1029/2000pa000518.
- Alonso Zarza, A.M., Calvo, J.P., García del Cura, M.A., 1992. Palustrine sedimentation and associated features—grainification and pseudo-microkarst—in the Middle Miocene (intermediate unit) of the Madrid Basin, Spain. *Sedimentary Geology* 76, 43-61. Doi: 10.1016/0037-0738(92)90138-H.
- Álvarez-Lao, D.J., Kahlke, R.-D., García, N., Mol, D., 2009. The Padul mammoth finds — On the southernmost record of *Mammuthus primigenius* in Europe and its southern spread during the Late Pleistocene. *Palaeogeography, Palaeoclimatology, Palaeoecology* 278, 57-70. Doi: 10.1016/j.palaeo.2009.04.011.
- Anderson, R.S., Jiménez-Moreno, G., Carrión, J.S., Pérez-Martínez, C., 2011. Postglacial history of alpine vegetation, fire, and climate from Laguna de Río Seco, Sierra Nevada, southern Spain. *Quaternary Science Reviews* 30, 1615-1629. Doi: 10.1016/j.quascirev.2011.03.005.
- Araguas-Araguas, L., Diaz Teijeiro, M., 2005. Isotope composition of precipitation and water vapour in the Iberian Peninsula: first results of the Spanish network of isotopes in precipitation. International Atomic Energy Agency Technical Report 1453, 173-190.
- Aranbarri, J., González-Sampéris, P., Valero-Garcés, B., Moreno, A., Gil-Romera, G., Sevilla-Callejo, M., García-Prieto, E., Di Rita, F., Mata, M.P., Morellón, M., Magri, D., Rodríguez-Lázaro, J., Carrión, J.S., 2014. Rapid climatic changes and resilient vegetation during the Lateglacial and

## References

Holocene in a continental region of south-western Europe. *Global and Planetary Change* 114, 50-65. Doi: 10.1016/j.gloplacha.2014.01.003.

Ausín, B., Haghypour, N., Wacker, L., Voelker, A.H., Hodell, D., Magill, C., Looser, N., Bernasconi, S.M., Eglinton, T.I., 2019. Radiocarbon age offsets between two surface dwelling planktonic foraminifera species during abrupt climate events in the SW Iberian margin. *Paleoceanography and Paleoclimatology* Doi: 10.1029/2018PA003490.

Bahr, A., Jiménez-Espejo, F.J., Kolasinac, N., Grunert, P., Hernández-Molina, F.J., Röhl, U., Voelker, A.H.L., Escutia, C., Stow, D.A.V., Hodell, D., Alvarez-Zarikian, C.A., 2014. Deciphering bottom current velocity and paleoclimate signals from contourite deposits in the Gulf of Cádiz during the last 140 kyr: An inorganic geochemical approach. *Geochemistry, Geophysics, Geosystems* 15, 3145-3160. Doi: 10.1002/2014gc005356.

Baldini, L.M., McDermott, F., Baldini, J.U.L., Arias, P., Cueto, M., Fairchild, I.J., Hoffmann, D.L., Matthey, D.P., Müller, W., Nita, D.C., Ontañón, R., Garcá-Moncó, C., Richards, D.A., 2015. Regional temperature, atmospheric circulation, and sea-ice variability within the Younger Dryas Event constrained using a speleothem from northern Iberia. *Earth and Planetary Science Letters* 419, 101-110. Doi: 10.1016/j.epsl.2015.03.015.

Bar-Matthews, M., Ayalon, A., Gilmour, M., Matthews, A., Hawkesworth, C.J., 2003. Sea-land oxygen isotopic relationships from planktonic foraminifera and speleothems in the Eastern Mediterranean region and their implication for paleorainfall during interglacial intervals. *Geochimica et Cosmochimica Acta* 67, 3181-3199. Doi: 10.1016/s0016-7037(02)01031-1.

Bard, E., Delaygue, G., Rostek, F., Antonioli, F., Silenzi, S., Schrag, D.P., 2002. Hydrological conditions over the western Mediterranean basin during the deposition of the cold Sapropel 6 (ca. 175 kyr BP). *Earth and Planetary Science Letters* 202, 481-494. Doi: 10.1016/S0012-821X(02)00788-4.

Bard, E., Rostek, F., Ménot-Combes, G., 2004. Radiocarbon calibration beyond 20,000 14 C yr BP by means of planktonic foraminifera of the Iberian Margin. *Quaternary research* 61, 204-214. Doi: 10.1016/j.yqres.2003.11.006.

Barker, S., Diz, P., Vautravers, M.J., Pike, J., Knorr, G., Hall, I.R., Broecker, W.S., 2009. Interhemispheric Atlantic seesaw response during the last deglaciation. *Nature* 457, 1097-1102. Doi: 10.1038/nature07770.

Barker, S., Knorr, G., Edwards, R.L., Parrenin, F., Putnam, A.E., Skinner, L.C., Wolff, E., Ziegler, M., 2011. 800,000 years of abrupt climate variability. *Science* 334, 347-351. Doi: 10.1126/science.1203580.

Barreiro-Lostres, F., Brown, E., Moreno, A., Morellón, M., Abbott, M., Hillman, A., Giralt, S., Valero-Garcés, B., 2015. Sediment delivery and lake dynamics in a Mediterranean mountain watershed: Human-climate interactions during the last millennium (El Tobar Lake record, Iberian Range, Spain). *Sci Total Environ* 533, 506-519. Doi: 10.1016/j.scitotenv.2015.06.123.

Barry, R.G., Chorley, R.J., 2009. *Atmosphere, weather and climate*. Routledge, 536. Doi: 10.4324/9780203871027.

- Bartov, Y., Stein, M., Enzel, Y., Agnon, A., Reches, Z.e., 2002. Lake Levels and Sequence Stratigraphy of Lake Lisan, the Late Pleistocene Precursor of the Dead Sea. *Quaternary Research* 57, 9-21. Doi: 10.1006/qres.2001.2284.
- Bazzicalupo, P., Maiorano, P., Girone, A., Marino, M., Combourieu-Nebout, N., Incarbona, A., 2018. High-frequency climate fluctuations over the last deglaciation in the Alboran Sea, Western Mediterranean: Evidence from calcareous plankton assemblages. *Palaeogeography, Palaeoclimatology, Palaeoecology* 506, 226-241. Doi: 10.1016/j.palaeo.2018.06.042.
- Bea, F., 1996. Residence of REE, Y, Th and U in Granites and Crustal Protoliths; Implications for the Chemistry of Crustal Melts *Journal of Petrology* 37, 521–552.
- Beas, J., 1990. Acuífero del borde oeste de Sierra Nevada: Sierra del Padul-La Peza. Atlas hidrogeológico de la provincia de Granada. Instituto Tecnológico Geominero de España y Diputación Provincial de Granada.
- Berger, A., 1980. The Milankovitch astronomical theory of paleoclimates: A modern review. *Vistas in Astronomy* 24, 103-122. Doi: 10.1016/0083-6656(80)90026-4.
- Berger, A., 1988. Milankovitch Theory and climate. *Reviews of Geophysics* 26, 624-657. Doi: 10.1029/RG026i004p00624.
- Berger, A., Loutre, M., Mélice, J., 1998. Instability of the astronomical periods from 1.5 Myr BP to 0.5 Myr AP. *Paleoclimates* 2, 239-280.
- Berger, A., Loutre, M.F., 1991. Insolation values for the climate of the last 10 million years. *Quaternary Science Reviews* 10, 297-317. Doi: 10.1016/0277-3791(91)90033-Q.
- Berger, A., Loutre, M.F., Kaspar, F., Lorenz, S.J., 2007. Chapter 2: Insolation during interglacial, in: Sirocko, F., Claussen, M., Sánchez Goñi, M.F., Litt, T. (Eds.), *Developments in Quaternary Sciences*. Elsevier, 13-27. Doi: 10.1016/S1571-0866(07)80027-3.
- Berger, W.H., Jansen, E., 1994. Mid-Pleistocene Climate Shift - The Nansen Connection, The Polar Oceans and Their Role in Shaping the Global Environment, 295-311. Doi: 10.1029/GM085p0295.
- Bertini, A., 2001. Pliocene climatic cycles and altitudinal forest development from 2.7 Ma in the Northern Apennines (Italy): Evidence from the pollen record of the Stirone section (~ 5.1 to ~ 2.2 Ma). *Geobios* 34, 253-265. Doi: 10.1016/S0016-6995(01)80074-7.
- Bertini, A., Toti, F., Marino, M., Ciaranfi, N., 2015. Vegetation and climate across the Early–Middle Pleistocene transition at Montalbano Jonico, southern Italy. *Quaternary International* 383, 74-88. Doi: 10.1016/j.quaint.2015.01.003.
- Beug, H.-J., 2004. Leitfaden der Pollenbestimmung für Mitteleuropa und angrenzende Gebiete. Verlag Dr. Friedrich Pfeil, München, 542.
- Bindoff, N.L., Stott, P.A., AchutaRao, K.M., Allen, M.R., Gillett, N., Gutzler, D., Hansingo, K., Hegerl, G., Hu, Y., Jain, S., 2013. Section 10: Detection and Attribution of Climate Change: from Global to Regional, in: Stocker, T.F., Qin, D., Plattner, G.-K., Tignor, M., Allen, S.K., Boschung, J., Nauels, A., Xia, Y., Bex, V., Midgley, P.M. (Ed.), *Climate change 2013: The Physical Science Basis*.

Working Group I to the Fifth Assessment Report of the Intergovernmental Panel on Climate Change. Cambridge University Press, 1535.

Björck, S., Wohlfarth, B., 2002. 14C chronostratigraphic techniques in paleolimnology, in: Last, W.M., Smol, J.P. (Eds.), Tracking environmental change using lake sediments. Kluwer Academic Publisher, Dordrecht, The Netherlands, 205-245.

Blaauw, M., 2010. Methods and code for 'classical' age-modelling of radiocarbon sequences. *Quaternary Geochronology* 5, 512-518. Doi: 10.1016/j.quageo.2010.01.002.

Blaauw, M., 2012. Out of tune: the dangers of aligning proxy archives. *Quaternary Science Reviews* 36, 38-49. Doi: 10.1016/j.quascirev.2010.11.012.

Blanca, G., López, M., Lorite, J., Martínez, M., Molero, J., Quintas, S., Ruíz, M., Varo, M., Vidal, S., 2002. Flora amenazada y endémica de Sierra Nevada. Universidad de Granada, Consejería de Medio Ambiente de la Junta de Andalucía, Granada.

Bond, G., Broecker, W., Johnsen, S., McManus, J., Labeyrie, L., Jouzel, J., Bonani, G., 1993. Correlations between climate records from North Atlantic sediments and Greenland ice. *Nature* 365, 143. Doi: 10.1038/365143a0.

Bond, G., Heinrich, H., Broecker, W., Labeyrie, L., McManus, J., Andrews, J., Huon, S., Jantschik, R., Clasen, S., Simet, C., 1992. Evidence for massive discharges of icebergs into the North Atlantic ocean during the last glacial period. *Nature* 360, 245. Doi: 10.1038/360245a0.

Bond, G., Kromer, B., Beer, J., Muscheler, R., Evans, M.N., Showers, W., Hoffmann, S., Lotti-Bond, R., Hajdas, I., Bonani, G., 2001. Persistent solar influence on North Atlantic climate during the Holocene. *Science* 294, 2130-2136. Doi: 10.1126/science.1065680.

Bond, G.C., Showers, W., Elliot, M., Evans, M., Lotti, R., Hajdas, I., Bonani, G., Johnson, S., 1999. The North Atlantic's 1-2 kyr climate rhythm: relation to Heinrich events, Dansgaard/Oeschger cycles and the Little Ice Age. *Mechanisms of global climate change at millennial time scales* 112, 35-58. Doi: 10.1029/GM112p0035.

Bonneau, L., Jorry, S.J., Toucanne, S., Silva Jacinto, R., Emmanuel, L., 2014. Millennial-scale response of a western Mediterranean river to late Quaternary climate changes: a view from the deep sea. *The Journal of Geology* 122, 687-703. Doi: 10.1086/677844.

Bouimetarhan, I., Prange, M., Schefuß, E., Dupont, L., Lippold, J., Mulitza, S., Zonneveld, K., 2012. Sahel megadrought during Heinrich Stadial 1: evidence for a three-phase evolution of the low- and mid-level West African wind system. *Quaternary Science Reviews* 58, 66-76. Doi: 10.1016/j.quascirev.2012.10.015.

Bourbonniere, R.A., Meyers, P.A., 1996. Sedimentary geolipid records of historical changes in the watersheds and productivities of Lakes Ontario and Erie. *Limnology and Oceanography* 41, 352-359. Doi: 10.4319/lo.1996.41.2.0352.

Bowen, G.J., Revenaugh, J., 2003. Interpolating the isotopic composition of modern meteoric precipitation. *Water Resources Research* 39, 1-13. Doi: 10.1029/2003wr002086.

- Brassell, S.C., Eglinton, G., Marlowe, I.T., Pflaumann, U., Sarnthein, M., 1986. Molecular stratigraphy: a new tool for climatic assessment. *Nature* 320, 129-133. Doi: 10.1038/320129a0.
- Brauer, A., Allen, J.R., Mingram, J., Dulski, P., Wulf, S., Huntley, B., 2007. Evidence for last interglacial chronology and environmental change from Southern Europe. *Proceedings of the National Academy of Sciences of the United States of America* 104, 450-455. Doi: 10.1073/pnas.0603321104.
- Bray, E.E., Evans, E.D., 1961. Distribution of n-paraffins as a clue to recognition of source beds. *Geochimica et Cosmochimica Acta* 22, 2-15. Doi: 10.1016/0016-7037(61)90069-2.
- Broecker, W., Barker, S., 2007. A 190‰ drop in atmosphere's  $\Delta^{14}\text{C}$  during the “Mystery Interval”(17.5 to 14.5 kyr). *Earth and Planetary Science Letters* 256, 90-99. Doi: 10.1016/j.epsl.2007.01.015.
- Broecker, W., Bond, G., Klas, M., Clark, E., McManus, J., 1992. Origin of the northern Atlantic's Heinrich events. *Climate Dynamics* 6, 265-273. Doi: 10.1007/BF00193540.
- Broecker, W.S., Denton, G.H., 1989. The role of ocean-atmosphere reorganizations in glacial cycles. *Geochimica et Cosmochimica Acta* 53, 2465-2501. Doi: 10.1016/0016-7037(89)90123-3.
- Bush, R.T., McInerney, F.A., 2013. Leaf wax n-alkane distributions in and across modern plants: Implications for paleoecology and chemotaxonomy. *Geochimica et Cosmochimica Acta* 117, 161-179. Doi: 10.1016/j.gca.2013.04.016.
- Bütikofer, J., 2007. Millennial scale climate variability during the last 6000 years—tracking down the Bond cycles. University of Bern, p. 124.
- Buurman, P., 1980. Palaeosols in the Reading Beds (Paleocene) of Alum Bay, Isle of Wight, U.K. *Sedimentology* 27, 593-606. Doi: 10.1111/j.1365-3091.1980.tb01649.x.
- Cacho, I., Grimalt, J.O., Canals, M., Sbaffi, L., Shackleton, N.J., Schönfeld, J., Zahn, R., 2001. Variability of the western Mediterranean Sea surface temperature during the last 25,000 years and its connection with the Northern Hemisphere climatic changes. *Paleoceanography* 16, 40-52. Doi: 10.1029/2000PA000502.
- Cacho, I., Grimalt, J.O., Pelejero, C., Canals, M., Sierro, F.J., Flores, J.A., Shackleton, N., 1999. Dansgaard-Oeschger and Heinrich event imprints in Alboran Sea paleotemperatures. *Paleoceanography* 14, 698-705. Doi: 10.1029/1999PA900044.
- Cacho, I., Shackleton, N., Elderfield, H., Sierro, F.J., Grimalt, J.O., 2006. Glacial rapid variability in deep-water temperature and  $\delta^{18}\text{O}$  from the Western Mediterranean Sea. *Quaternary Science Reviews* 25, 3294-3311. Doi: 10.1016/j.quascirev.2006.10.004.
- Calvert, S.E., Pedersen, T.F., 1993. Geochemistry of Recent oxic and anoxic marine sediments: Implications for the geological record. *Marine Geology* 113, 67-88. Doi: 10.1016/0025-3227(93)90150-T.
- Camuera, J., Jiménez-Moreno, G., Ramos-Román, M.J., García-Alix, A., Toney, J.L., Anderson, R.S., Jiménez-Espejo, F., Bright, J., Webster, C., Yanes, Y., Carrión, J.S., 2019. Vegetation and

## References

climate changes during the last two glacial-interglacial cycles in the western Mediterranean: A new long pollen record from Padul (southern Iberian Peninsula). *Quaternary Science Reviews* 205, 86-105. Doi: 10.1016/j.quascirev.2018.12.013.

Camuera, J., Jiménez-Moreno, G., Ramos-Román, M.J., García-Alix, A., Toney, J.L., Anderson, R.S., Jiménez-Espejo, F., Kaufman, D., Bright, J., Webster, C., Yanes, Y., Carrión, J.S., Ohkouchi, N., Suga, H., Yamame, M., Yokoyama, Y., Martínez-Ruiz, R., 2018. Orbital-scale environmental and climatic changes recorded in a new ~200,000-year-long multiproxy sedimentary record from Padul, southern Iberian Peninsula. *Quaternary Science Reviews* 198, 91-114. Doi: 10.1016/j.quascirev.2018.08.014.

Carrasco Duarte, M., 1998. El Padul, 389.

Carrión, J., Munuera, M., Navarro, C., 1998. The palaeoenvironment of Carhuela Cave (Granada, Spain): a reconstruction on the basis of palynological investigations of cave sediments. *Review of Palaeobotany and Palynology* 99, 317-340. Doi: 10.1016/S0034-6667(97)00040-7.

Carrión, J.S., 2002. Patterns and processes of Late Quaternary environmental change in a montane region of southwestern Europe. *Quaternary Science Reviews* 21, 2047-2066. Doi: 10.1016/S0277-3791(02)00010-0.

Carrión, J.S., Fuentes, N., González-Sampériz, P., Sánchez Quirante, L., Finlayson, J.C., Fernández, S., Andrade, A., 2007. Holocene environmental change in a montane region of southern Europe with a long history of human settlement. *Quaternary Science Reviews* 26, 1455-1475. Doi: 10.1016/j.quascirev.2007.03.013.

Carrión, J.S., Munuera, M., Dupré, M., Andrade, A., 2001. Abrupt vegetation changes in the Segura Mountains of southern Spain throughout the Holocene. *Journal of Ecology* 89, 783-797. Doi: 10.1046/j.0022-0477.2001.00601.x.

Castañeda, I.S., Schefuß, E., Pätzold, J., Damsté, J.S.S., Weldeab, S., Schouten, S., 2010. Millennial-scale sea surface temperature changes in the eastern Mediterranean (Nile River Delta region) over the last 27,000 years. *Paleoceanography* 25 Doi: 10.1029/2009PA001740.

Castañeda, I.S., Schouten, S., 2011. A review of molecular organic proxies for examining modern and ancient lacustrine environments. *Quaternary Science Reviews* 30, 2851-2891. Doi: 10.1016/j.quascirev.2011.07.009.

Castañeda, I.S., Schouten, S., Pätzold, J., Lucassen, F., Kasemann, S., Kuhlmann, H., Schefuß, E., 2016. Hydroclimate variability in the Nile River Basin during the past 28,000 years. *Earth and Planetary Science Letters* 438, 47-56. Doi: 10.1016/j.epsl.2015.12.014.

Castillo Martín, A., 2009. *Lagunas de Sierra Nevada*. Editorial Universidad de Granada, Granada, 320.

Castillo Martín, A., Fernández-Rubio, R., 1984. Hidrogeología de la cuenca vertiente a la depresión de Padul (Granada), I Congreso Español de Geología, Tomo IV, pp. 109-121.

Clark, P.U., Pisias, N.G., Stocker, T.F., Weaver, A.J., 2002. The role of the thermohaline circulation in abrupt climate change. *Nature* 415, 863-869. Doi: 10.1038/415863a.

- Clausing, A., 1999. Palaeoenvironmental significance of the green alga *Botryococcus* in the lacustrine rotliegend (upper carboniferous - lower permian). *Historical Biology* 13, 221-234. Doi: 10.1080/08912969909386582.
- Cochran, J.K., Carey, A.E., Sholkovitz, E.R., Surprenant, L.D., 1986. The geochemistry of uranium and thorium in coastal marine sediments and sediment pore waters. *Geochimica et Cosmochimica Acta* 50, 663-680. Doi: 10.1016/0016-7037(86)90344-3.
- Cohen, A.S., 2003. *Paleolimnology: the history and evolution of lake systems*. Oxford University Press.
- COHMAP-Members, 1988. Climatic Changes of the Last 18,000 Years: Observations and Model Simulations. *Science* 241, 1043-1052.
- Collins, J.A., Govin, A., Mulitza, S., Heslop, D., Zabel, M., Hartmann, J., Röhl, U., Wefer, G., 2013a. Abrupt shifts of the Sahara–Sahel boundary during Heinrich stadials. *Climate of the Past* 9, 1181-1191. Doi: 10.5194/cp-9-1181-2013.
- Collins, J.A., Schefuß, E., Mulitza, S., Prange, M., Werner, M., Tharammal, T., Paul, A., Wefer, G., 2013b. Estimating the hydrogen isotopic composition of past precipitation using leaf-waxes from western Africa. *Quaternary Science Reviews* 65, 88-101. Doi: 10.1016/j.quascirev.2013.01.007.
- Combourieu-Nebout, N., 1993. Vegetation Response to Upper Pliocene Glacial/Interglacial Cyclicity in the Central Mediterranean. *Quaternary Research* 40, 228-236. Doi: 10.1006/qres.1993.1074.
- Combourieu Nebout, N., Londeix, L., Baudin, F., Turon, J.-L., Von Grafenstein, R., Zahn, R., 1999. Quaternary marine and continental paleoenvironments in the western Mediterranean (Site 976, Alboran Sea): palynological evidence, *Proceedings of the Ocean Drilling Program. Scientific Results. Ocean Drilling Program* 161, pp. 457-468.
- Combourieu Nebout, N., Peyron, O., Dormoy, I., Desprat, S., Beaudouin, C., Kotthoff, U., Marret, F., 2009. Rapid climatic variability in the west Mediterranean during the last 25 000 years from high resolution pollen data. *Climate of the Past* 5, 503-521. Doi: 10.5194/cp-5-503-2009.
- Combourieu Nebout, N., Turon, J.L., Zahn, R., Capotondi, L., Londeix, L., Pahnke, K., 2002. Enhanced aridity and atmospheric high-pressure stability over the western Mediterranean during the North Atlantic cold events of the past 50 k.y. *Geology* 30, 863. Doi: 10.1130/0091-7613.
- Corella, J.P., Brauer, A., Mangili, C., Rull, V., Vegas-Vilarrúbia, T., Morellón, M., Valero-Garcés, B.L., 2012. The 1.5-ka varved record of Lake Montcortès (southern Pyrenees, NE Spain). *Quaternary Research* 78, 323-332. Doi: 10.1016/j.yqres.2012.06.002.
- Cortés-Sánchez, M., Morales-Muñiz, A., Jiménez-Espejo, F., Évora, M., Simón-Vallejo, M.D., García-Alix, A., Aguirre, A.M., Riquelme-Cantal, J.A., P. Odriozola, C., Giráldez, R.P., Álvarez-Lao, D.J., 2016. Multi-purpose fossils? The reappraisal of an *Elephas antiquus* molar from El Pirulejo (Magdalenian; Córdoba, Spain). *Archaeological and Anthropological Sciences* 9, 1287-1303. Doi: 10.1007/s12520-016-0324-1.



## References

- Corzo, A., Luzon, A., Mayayo, M.J., van Bergeijk, S.A., Mata, P., García de Lomas, J., 2005. Carbonate Mineralogy Along a Biogeochemical Gradient in Recent Lacustrine Sediments of Gallocanta Lake (Spain). *Geomicrobiology Journal* 22, 283-298. Doi: 10.1080/01490450500183654.
- Cranwell, P.A., Eglinton, G., Robinson, N., 1987. Lipids of aquatic organisms as potential contributors to lacustrine sediments—II. *Organic Geochemistry* 11, 513-527. Doi: 10.1016/0146-6380(87)90007-6.
- D'Anjou, R.M., Wei, J.H., Castañeda, I.S., Brigham-Grette, J., Petsch, S.T., Finkelstein, D.B., 2013. High-latitude environmental change during MIS 9 and 11: biogeochemical evidence from Lake El'gygytgyn, Far East Russia. *Climate of the Past* 9, 567-581. Doi: 10.5194/cp-9-567-2013.
- Damon, P.E., Jirikowic, J.L., 1992. The sun as a low-frequency harmonic oscillator. *Radiocarbon* 34, 199-205. Doi: 10.1017/S003382220001362X.
- Daniau, A.-L., Sánchez-Goñi, M., Beaufort, L., Laggoun-Défarge, F., Loutre, M.-F., Duprat, J., 2007. Dansgaard-Oeschger climatic variability revealed by fire emissions in southwestern Iberia. *Quaternary Science Reviews* 26, 1369-1383. Doi: 10.1016/j.quascirev.2007.02.005.
- Dansgaard, W., Johnsen, S., Clausen, H., Dahl-Jensen, D., Gundestrup, N., Hammer, C., Oeschger, H., 1984. North Atlantic climatic oscillations revealed by deep Greenland ice cores. *Climate processes and climate sensitivity* 29, 288-298. Doi: 10.1029/GM029p0288.
- de Abreu, L., Shackleton, N.J., Schönfeld, J., Hall, M., Chapman, M., 2003. Millennial-scale oceanic climate variability off the Western Iberian margin during the last two glacial periods. *Marine Geology* 196, 1-20. Doi: 10.1016/S0025-3227(03)00046-X.
- de Boor, C., 2001. *A practical guide to splines*. Springer.
- Deines, P., 1980. The isotopic composition of reduced organic carbon. *Handbook of environmental isotope geochemistry* 1, 329-406.
- Delgado, J., Alfaro, P., Galindo-Zaldivar, J., Jabaloy, A., López Garrido, A.C., Sanz de Galdeano, C., 2002. Structure of the Padul-Nigüelas Basin (S Spain) from H/V Ratios of Ambient Noise: Application of the Method to Study Peat and Coarse Sediments. *pure and applied geophysics* 159, 2733-2749. Doi: 10.1007/s00024-002-8756-1.
- Desprat, S., Díaz Fernández, P.M., Coulon, T., Ezzat, L., Pessarossi-Langlois, J., Gil, L., Morales-Molino, C., Sánchez Goñi, M.F., 2015. *Pinus nigra* (European black pine) as the dominant species of the last glacial pinewoods in south-western to central Iberia: a morphological study of modern and fossil pollen. *Journal of Biogeography* 42, 1998-2009. Doi: 10.1111/jbi.12566.
- Develle, A.L., Gasse, F., Vidal, L., Williamson, D., Demory, F., Van Campo, E., Ghaleb, B., Thouveny, N., 2011. A 250ka sedimentary record from a small karstic lake in the Northern Levant (Yammoûneh, Lebanon). *Palaeogeography, Palaeoclimatology, Palaeoecology* 305, 10-27. Doi: 10.1016/j.palaeo.2011.02.008.
- Díez, S., Montuori, P., Querol, X., Bayona, J.M., 2007. Total mercury in the hair of children by combustion atomic absorption spectrometry (Comb-AAS). *Journal of Analytical Toxicology* 313, 144-149.

- Digerfeldt, G., Olsson, S., Sandgren, P., 2000. Reconstruction of lake-level changes in lake Xinias, central Greece, during the last 40 000 years. *Palaeogeography, Palaeoclimatology, Palaeoecology* 158, 65-82. Doi: 10.1016/S0031-0182(00)00029-8.
- Djamali, M., de Beaulieu, J.-L., Shah-hosseini, M., Andrieu-Ponel, V., Ponel, P., Amini, A., Akhiani, H., Leroy, S.A.G., Stevens, L., Lahijani, H., Brewer, S., 2008. A late Pleistocene long pollen record from Lake Urmia, Nw Iran. *Quaternary Research* 69, 413-420. Doi: 10.1016/j.yqres.2008.03.004.
- Domingo García, M., Fernández-Rubio, R., López González, J.D., González Gómez, C., 1983. Portación al conocimiento de la Neotectónica de la depresión de Padul (Granada). *Tecniterrae* 53, 6-16.
- Drysdale, R., Hellstrom, J., Zanchetta, G., Fallick, A., Sánchez Goñi, M., Couchoud, I., McDonald, J., Maas, R., Lohmann, G., Isola, I., 2009. Evidence for obliquity forcing of glacial termination II. *Science* 325, 1527-1531. Doi: 10.1126/science.1170371.
- El Aallali, A., López Nieto, J.M., Pérez Raya, F., Molero Mesa, J., 1998. Estudio de la vegetación forestal en la vertiente sur de Sierra Nevada (Alpujarra Alta granadina). *Itinera Geobotanica* 11, 387-402.
- Elliot, M., Labeyrie, L., Dokken, T., Manthé, S., 2001. Coherent patterns of ice-rafted debris deposits in the Nordic regions during the last glacial (10–60 ka). *Earth and Planetary Science Letters* 194, 151-163. Doi: 10.1016/S0012-821X(01)00561-1.
- Elliot, M., Labeyrie, L., Duplessy, J.-C., 2002. Changes in North Atlantic deep-water formation associated with the Dansgaard–Oeschger temperature oscillations (60–10 ka). *Quaternary Science Reviews* 21, 1153-1165. Doi: 10.1016/S0277-3791(01)00137-8.
- Emiliani, C., 1955. Pleistocene temperature variations in the Mediterranean.
- Ertel, J.R., Hedges, J.I., 1985. Sources of sedimentary humic substances: vascular plant debris. *Geochimica et Cosmochimica Acta* 49, 2097-2107. Doi: 10.1016/0016-7037(85)90067-5.
- Escudero, A., Giménez-Benavides, L., Iriondo, J.M., Rubio, A., 2004. Patch Dynamics and Islands of Fertility in a High Mountain Mediterranean Community. *Arctic, Antarctic, and Alpine Research* 36, 518-527.
- Fægri, K., Iversen, J., 1989. *Textbook of pollen analysis* (4th edition). Wiley, New York.
- Fang, J., Wu, F., Xiong, Y., Li, F., Du, X., An, D., Wang, L., 2014. Source characterization of sedimentary organic matter using molecular and stable carbon isotopic composition of n-alkanes and fatty acids in sediment core from Lake Dianchi, China. *Sci Total Environ* 473-474, 410-421. Doi: 10.1016/j.scitotenv.2013.10.066.
- Fernández, S., Fuentes, N., Carrión, J.S., González-Sampériz, P., Montoya, E., Gil, G., Vega-Toscano, G., Riquelme, J.A., 2007. The Holocene and Upper Pleistocene pollen sequence of Carhuela Cave, southern Spain. *Geobios* 40, 75-90. Doi: 10.1016/j.geobios.2006.01.004.

## References

- Ficken, K.J., Li, B., Swain, D.L., Eglinton, G., 2000. An n-alkane proxy for the sedimentary input of submerged/floating freshwater aquatic macrophytes. *Organic Geochemistry* 31, 745-749. Doi: 10.1016/S0146-6380(00)00081-4.
- Fink, H.G., Wienberg, C., De Pol-Holz, R., Hebbeln, D., 2015. Spatio-temporal distribution patterns of Mediterranean cold-water corals (*Lophelia pertusa* and *Madrepora oculata*) during the past 14,000 years. *Deep Sea Research Part I: Oceanographic Research Papers* 103, 37-48. Doi: 10.1016/j.dsr.2015.05.006.
- Fletcher, W.J., Boski, T., Moura, D., 2007. Palynological evidence for environmental and climatic change in the lower Guadiana valley, Portugal, during the last 13 000 years. *The Holocene* 17, 481-494. Doi: 10.1177/0959683607077027.
- Fletcher, W.J., Müller, U.C., Koutsodendris, A., Christanis, K., Pross, J., 2013. A centennial-scale record of vegetation and climate variability from 312 to 240 ka (Marine Isotope Stages 9c-a, 8 and 7e) from Tenaghi Philippon, NE Greece. *Quaternary Science Reviews* 78, 108-125. Doi: 10.1016/j.quascirev.2013.08.005.
- Fletcher, W.J., Sánchez Goñi, M.F., 2008. Orbital- and sub-orbital-scale climate impacts on vegetation of the western Mediterranean basin over the last 48,000 yr. *Quaternary Research* 70, 451-464. Doi: 10.1016/j.yqres.2008.07.002.
- Fletcher, W.J., Sánchez Goñi, M.F., Allen, J.R.M., Cheddadi, R., Combourieu-Nebout, N., Huntley, B., Lawson, I., Londeix, L., Magri, D., Margari, V., Müller, U.C., Naughton, F., Novenko, E., Roucoux, K., Tzedakis, P.C., 2010a. Millennial-scale variability during the last glacial in vegetation records from Europe. *Quaternary Science Reviews* 29, 2839-2864. Doi: 10.1016/j.quascirev.2009.11.015.
- Fletcher, W.J., Sánchez Goñi, M.F., Peyron, O., Dormoy, I., 2010b. Abrupt climate changes of the last deglaciation detected in a Western Mediterranean forest record. *Climate of the Past* 6, 245-264. Doi: 10.5194/cp-6-245-2010.
- Florschütz, F., Menéndez-Amor, J., Wijmstra, T.A., 1971. Palynology of a thick Quaternary succession in Southern Spain. *Palaeogeography, Palaeoclimatology, Palaeoecology* 10, 233-264. Doi: 10.1016/0031-0182(71)90049-6.
- Follieri, M., Giardini, M., Magri, D., Sadori, L., 1998. Palynostratigraphy of the Last Glacial period in the volcanic region of Central Italy. *Quaternary International* 47-48, 3-20. Doi: 10.1016/S1040-6182(97)00065-7.
- Follieri, M., Magri, D., Sadori, L., 1989. Pollen stratigraphical synthesis from Valle di Castiglione (Roma). *Quaternary International* 3-4, 81-84. Doi: 10.1016/1040-6182(89)90076-1.
- Foster, L.C., Pearson, E.J., Juggins, S., Hodgson, D.A., Saunders, K.M., Verleyen, E., Roberts, S.J., 2016. Development of a regional glycerol dialkyl glycerol tetraether (GDGT)-temperature calibration for Antarctic and sub-Antarctic lakes. *Earth and Planetary Science Letters* 433, 370-379. Doi: 10.1016/j.epsl.2015.11.018.
- Francke, A., Wagner, B., Just, J., Leicher, N., Gromig, R., Baumgarten, H., Vogel, H., Lacey, J.H., Sadori, L., Wonik, T., Leng, M.J., Zanchetta, G., Sulpizio, R., Giaccio, B., 2016. Sedimentological

processes and environmental variability at Lake Ohrid (Macedonia, Albania) between 637 ka and the present. *Biogeosciences* 13, 1179-1196. Doi: 10.5194/bg-13-1179-2016.

Franco Múgica, F., García Antón, M., Sainz Ollero, H., 1998. Vegetation dynamics and human impact in the Sierra de Guadarrama, Central System, Spain. *The Holocene* 8, 69-82. Doi: 10.1191/095968398675691171.

Gallego-Torres, D., Martínez-Ruiz, F., Paytan, A., Jiménez-Espejo, F.J., Ortega-Huertas, M., 2007. Pliocene–Holocene evolution of depositional conditions in the eastern Mediterranean: Role of anoxia vs. productivity at time of sapropel deposition. *Palaeogeography, Palaeoclimatology, Palaeoecology* 246, 424-439. Doi: 10.1016/j.palaeo.2006.10.008.

Ganopolski, A., Rahmstorf, S., 2001. Rapid changes of glacial climate simulated in a coupled climate model. *Nature* 409, 153. Doi: 10.1038/35051500.

Ganopolski, A., Roche, D.M., 2009. On the nature of lead–lag relationships during glacial–interglacial climate transitions. *Quaternary Science Reviews* 28, 3361-3378. Doi: 10.1016/j.quascirev.2009.09.019.

García-Alix, A., 2015. A multiproxy approach for the reconstruction of ancient continental environments. The case of the Mio–Pliocene deposits of the Granada Basin (southern Iberian Peninsula). *Global and Planetary Change* 131, 1-10. Doi: 10.1016/j.gloplacha.2015.04.005.

García-Alix, A., Jiménez-Espejo, F.J., Jiménez-Moreno, G., Toney, J.L., Ramos-Román, M.J., Camuera, J., Anderson, R.S., Delgado-Huertas, A., Martínez-Ruiz, F., Queralt, I., 2018. Holocene geochemical footprint from Semi-arid alpine wetlands in southern Spain. *Scientific data* 5, 180024. Doi: 10.1038/sdata.2018.24.

García-Alix, A., Jiménez-Espejo, F.J., Lozano, J.A., Jiménez-Moreno, G., Martínez-Ruiz, F., García Sanjuan, L., Aranda Jiménez, G., García Alfonso, E., Ruiz-Puertas, G., Anderson, R.S., 2013. Anthropogenic impact and lead pollution throughout the Holocene in Southern Iberia. *Sci Total Environ* 449, 451-460. Doi: 10.1016/j.scitotenv.2013.01.081.

García-Alix, A., Jiménez-Espejo, F.J., Toney, J.L., Jiménez-Moreno, G., Ramos-Román, M.J., Anderson, R.S., Ruano, P., Queralt, I., Delgado Huertas, A., Kuroda, J., 2017. Alpine bogs of southern Spain show human-induced environmental change superimposed on long-term natural variations. *Scientific Reports* 7, 7439. Doi: 10.1038/s41598-017-07854-w.

García-Alix, A., Jiménez-Moreno, G., Anderson, R.S., Jiménez Espejo, F.J., Delgado Huertas, A., 2012. Holocene environmental change in southern Spain deduced from the isotopic record of a high-elevation wetland in Sierra Nevada. *Journal of Paleolimnology* 48, 471-484. Doi: 10.1007/s10933-012-9625-2.

García-Alix, A., Toney, J.L., Jiménez-Moreno, G., Pérez-Martínez, C., Rodrigo-Gámiz, M., Anderson, R.S., Camuera, J., Jiménez-Espejo, F., Peña-Angulo, D., Ramos-Román, M.J., submitted. Extreme warming rates affecting alpine areas in SW Europe. *Quaternary Science Reviews*.

García-Antón, M., Franco-Múgica, F., Morla-Juaristi, C., Maldonado-Ruiz, J., 2011. The biogeographical role of Pinus forest on the Northern Spanish Meseta: a new Holocene sequence. *Quaternary Science Reviews* 30, 757-768. Doi: 10.1016/j.quascirev.2010.12.023.

## References

- García-Prieto, E., 2015. Dinámica paleoambiental durante los últimos 135.000 años en el Alto Jiloca: el registro lacustre de El Cañizar. Universidad de Zaragoza.
- Gómez Ortiz, A., Schulte, L., Salvador Franch, F., Palacios Estremera, D., Sanz de Galdeano, C., Sanjosé Blasco, J.J., Tanarro García, L.M., Atkinson, A., 2005. The geomorphological unity of the Veleta: a particular area of the Sierra Nevada Guidebook. Sixth International Conference of Geomorphology, Zaragoza.
- González-Sampériz, P., Aranbarri, J., Pérez-Sanz, A., Gil-Romera, G., Moreno, A., Leunda, M., Sevilla-Callejo, M., Corella, J.P., Morellón, M., Oliva, B., Valero-Garcés, B., 2017. Environmental and climate change in the southern Central Pyrenees since the Last Glacial Maximum: A view from the lake records. *Catena* 149, 668-688. Doi: 10.1016/j.catena.2016.07.041.
- González-Sampériz, P., García-Prieto, E., Aranbarri, J., Valero-Garcés, B.L., Moreno, A., Gil-Romera, G., Sevilla-Callejo, M., Santos, L., Morellón, M., Mata, P., Andrade, A., Carrión, J.S., 2013. Reconstrucción paleoambiental del último ciclo glacial-interglacial en la Iberia continental: la secuencia del Cañizar de Villarquemado (Teruel). *Cuadernos de investigación geográfica/Geographical Research Letters*, 49-76.
- González-Sampériz, P., Valero-Garcés, B.L., Moreno, A., Morellón, M., Navas, A., Machín, J., Delgado-Huertas, A., 2008. Vegetation changes and hydrological fluctuations in the Central Ebro Basin (NE Spain) since the Late Glacial period: Saline lake records. *Palaeogeography, Palaeoclimatology, Palaeoecology* 259, 157-181. Doi: 10.1016/j.palaeo.2007.10.005.
- González Donoso, J.M., Gallego, J.A., Sáenz de Galdeano, C., 1978. Hoja Geológica MAGNA Núm. 1026 (Padul), escala 1:50.000. Instituto Geológico y Minero de España.
- Govindaraju, K., 1994. Compilation of working values and sample description for 383 geostandards. *Geostandards Newsletter* 18, 1-158. Doi: 10.1046/j.1365-2494.1998.53202081.x-i1.
- Grimm, E.C., 1987. CONISS: a FORTRAN 77 program for stratigraphically constrained cluster analysis by the method of incremental sum of squares. *Computers & Geosciences* 13, 13-35. Doi: 10.1016/0098-3004(87)90022-7.
- Grimm, E.C., Maher, L.J., Nelson, D.M., 2009. The magnitude of error in conventional bulk-sediment radiocarbon dates from central North America. *Quaternary Research* 72, 301-308. Doi: 10.1016/j.yqres.2009.05.006.
- Grootes, P.M., Stuiver, M., White, J., Johnsen, S., Jouzel, J., 1993. Comparison of oxygen isotope records from the GISP2 and GRIP Greenland ice cores. *Nature* 366, 552.
- Guédron, S., Amouroux, D., Sabatier, P., Desplanque, C., Develle, A.-L., Barre, J., Feng, C., Guiter, F., Arnaud, F., Reyss, J.L., Charlet, L., 2016. A hundred year record of industrial and urban development in French Alps combining Hg accumulation rates and isotope composition in sediment archives from Lake Luitel. *Chemical Geology* 431, 10-19. Doi: 10.1016/j.chemgeo.2016.03.016.
- Guy-Ohlson, D., 1992. Botryococcus as an aid in the interpretation of palaeoenvironment and depositional processes. *Review of Palaeobotany and Palynology* 71, 1-15. Doi: 10.1016/0034-6667(92)90155-A.

- Hammer, Ø., Harper, D., Ryan, P., 2001. PAST-Palaeontological statistics. 25, 2009.
- Harrison, S.P., Digerfeldt, G., 1993. European lakes as palaeohydrological and palaeoclimatic indicators. *Quaternary Science Reviews* 12, 233-248. Doi: 10.1016/0277-3791(93)90079-2.
- Harrison, S.P., Yu, G., Tarasov, P.E., 1996. Late Quaternary Lake-Level Record from Northern Eurasia. *Quaternary Research* 45, 138-159. Doi: 10.1006/qres.1996.0016.
- Harvey, A.M., Wigand, P.E., Wells, S.G., 1999. Response of alluvial fan systems to the late Pleistocene to Holocene climatic transition: contrasts between the margins of pluvial Lakes Lahontan and Mojave, Nevada and California, USA. *Catena* 36, 255-281. Doi: 10.1016/S0341-8162(99)00049-1.
- Hazan, N., Stein, M., Agnon, A., Marco, S., Nadel, D., Negendank, J.F.W., Schwab, M.J., Neev, D., 2005. The late Quaternary limnological history of Lake Kinneret (Sea of Galilee), Israel. *Quaternary Research* 63, 60-77. Doi: 10.1016/j.yqres.2004.09.004.
- Hedges, J.I., Clark, W.A., Quay, P.D., Richey, J.E., Devol, A.H., Santos, M., 1986. Compositions and fluxes of particulate organic material in the Amazon River1. *Limnology and Oceanography* 31, 717-738.
- Heinrich, H., 1988. Origin and consequences of cyclic ice rafting in the northeast Atlantic Ocean during the past 130,000 years. *Quaternary research* 29, 142-152. Doi: 10.1016/0033-5894(88)90057-9.
- Hemming, S.R., 2004. Heinrich events: Massive late Pleistocene detritus layers of the North Atlantic and their global climate imprint. *Reviews of Geophysics* 42 Doi: 10.1029/2003RG000128.
- Höbig, N., Mediavilla, R., Gibert, L., Santisteban, J.I., Cendón, D.I., Ibáñez, J., Reicherter, K., 2016. Palaeohydrological evolution and implications for palaeoclimate since the Late Glacial at Laguna de Fuente de Piedra, southern Spain. *Quaternary International* 407, 29-46. Doi: 10.1016/j.quaint.2016.02.051.
- Höbig, N., Weber, M.E., Kehl, M., Weniger, G.-C., Julià, R., Melles, M., Fülöp, R.-H., Vogel, H., Reicherter, K., 2012. Lake Banyoles (northeastern Spain): A Last Glacial to Holocene multi-proxy study with regard to environmental variability and human occupation. *Quaternary International* 274, 205-218. Doi: 10.1016/j.quaint.2012.05.036.
- Hodell, D.A., Nicholl, J.A., Bontognali, T.R., Danino, S., Dorador, J., Dowdeswell, J.A., Einsle, J., Kuhlmann, H., Martrat, B., Mleneck-Vautravers, M.J., 2017. Anatomy of Heinrich layer 1 and its role in the last deglaciation. *Paleoceanography* 32, 284-303. Doi: 10.1002/2016PA003028.
- Hodge, E.J., Richards, D.A., Smart, P.L., Andreo, B., Hoffmann, D.L., Matthey, D.P., González-Ramón, A., 2008. Effective precipitation in southern Spain (~266 to 46 ka) based on a speleothem stable carbon isotope record. *Quaternary Research* 69, 447-457. Doi: 10.1016/j.yqres.2008.02.013.
- Hou, J., Huang, Y., Wang, Y., Shuman, B., Oswald, W.W., Faison, E., Foster, D.R., 2006. Postglacial climate reconstruction based on compound-specific D/H ratios of fatty acids from Blood Pond, New England. *Geochemistry, Geophysics, Geosystems* 7, 1-11. Doi: 10.1029/2005GC001076.

## References

- Hughen, K.A., Southon, J.R., Lehman, S.J., Overpeck, J.T., 2000. Synchronous Radiocarbon and Climate Shifts During the Last Deglaciation. *Science* 290, 1951-1954. Doi: 10.1126/science.290.5498.1951.
- Hurrell, J.W., 1995. Decadal Trends in the North Atlantic Oscillation: Regional Temperatures and Precipitation. *Science* 269, 676-679. Doi: 10.1126/science.269.5224.676.
- Imbrie, J., Boyle, E., Clemens, S., Duffy, A., Howard, W., Kukla, G., Kutzbach, J., Martinson, D., McIntyre, A., Mix, A., 1992. On the structure and origin of major glaciation cycles 1. Linear responses to Milankovitch forcing. *Paleoceanography* 7, 701-738. Doi: 10.1029/92PA02253.
- Imbrie, J., Hays, J.D., Martinson, D.G., McIntyre, A., Mix, A.C., Morley, J.J., Pisias, N.G., Prell, W.L., Shackleton, N.J., 1984. The orbital theory of Pleistocene climate: support from a revised chronology of the marine  $\delta^{18}O$  record.
- Imbrie, J., Imbrie, J.Z., 1980. Modeling the Climatic Response to Orbital Variations. *Science* 207, 943-953. Doi: 10.1126/science.207.4434.943.
- IPCC, 2013. Climate change 2013: The Physical Science Basis. Working Group I to the Fifth Assessment Report of the Intergovernmental Panel on Climate Change. Cambridge University Press, 1535.
- Ivanovic, R.F., Valdes, P.J., Gregoire, L., Flecker, R., Gutjahr, M., 2014. Sensitivity of modern climate to the presence, strength and salinity of Mediterranean-Atlantic exchange in a global general circulation model. *Climate dynamics* 42, 859-877. Doi: 10.1007/s00382-013-1680-5.
- Jackson, L., Kahana, R., Graham, T., Ringer, M., Woollings, T., Mecking, J., Wood, R., 2015. Global and European climate impacts of a slowdown of the AMOC in a high resolution GCM. *Climate dynamics* 45, 3299-3316. Doi: 10.1007/s00382-015-2540-2.
- Jiménez-Espejo, F., Pardos-Gené, M., Martínez-Ruiz, F., García-Alix, A., Van de Flierdt, T., Toyofuku, T., Bahr, A., Kreissig, K., 2015. Geochemical evidence for intermediate water circulation in the westernmost Mediterranean over the last 20 kyr BP and its impact on the Mediterranean Outflow. *Global and Planetary Change* 135, 38-46. Doi: 10.1016/j.gloplacha.2015.10.001.
- Jiménez-Espejo, F.J., García-Alix, A., Jiménez-Moreno, G., Rodrigo-Gámiz, M., Anderson, R.S., Rodríguez-Tovar, F.J., Martínez-Ruiz, F., Giral, S., Delgado Huertas, A., Pardo-Igúzquiza, E., 2014. Saharan aeolian input and effective humidity variations over western Europe during the Holocene from a high altitude record. *Chemical Geology* 374-375, 1-12. Doi: 10.1016/j.chemgeo.2014.03.001.
- Jiménez-Espejo, F.J., Martínez-Ruiz, F., Finlayson, C., Paytan, A., Sakamoto, T., Ortega-Huertas, M., Finlayson, G., Iijima, K., Gallego-Torres, D., Fa, D., 2007. Climate forcing and Neanderthal extinction in Southern Iberia: insights from a multiproxy marine record. *Quaternary Science Reviews* 26, 836-852. Doi: 10.1016/j.quascirev.2006.12.013.
- Jiménez-Moreno, G., Anderson, R.S., 2012. Holocene vegetation and climate change recorded in alpine bog sediments from the Borreguiles de la Virgen, Sierra Nevada, southern Spain. *Quaternary Research* 77, 44-53. Doi: 10.1016/j.yqres.2011.09.006.

- Jiménez-Moreno, G., Anderson, R.S., Fawcett, P., 2007. Orbital- and millennial-scale vegetation and climate changes of the past 225ka from Bear Lake, Utah–Idaho (USA). *Quaternary Science Reviews* 26, 1713-1724. Doi: 10.1016/j.quascirev.2007.05.001.
- Jiménez-Moreno, G., García-Alix, A., Hernández-Corbalán, M.D., Anderson, R.S., Delgado-Huertas, A., 2013. Vegetation, fire, climate and human disturbance history in the southwestern Mediterranean area during the late Holocene. *Quaternary Research* 79, 110-122. Doi: 10.1016/j.yqres.2012.11.008.
- Jiménez-Amat, P., Zahn, R., 2015. Offset timing of climate oscillations during the last two glacial-interglacial transitions connected with large-scale freshwater perturbation. *Paleoceanography and Paleoclimatology* 30, 768-788. Doi: 10.1002/2014PA002710.
- Jiménez-Espejo, F., Martínez-Ruiz, F., Rogerson, M., González-Donoso, J., Romero, O., Linares, D., Sakamoto, T., Gallego-Torres, D., Rueda Ruiz, J., Ortega-Huertas, M., 2008. Detrital input, productivity fluctuations, and water mass circulation in the westernmost Mediterranean Sea since the Last Glacial Maximum. *Geochemistry, Geophysics, Geosystems* 9 Doi: 10.1029/2008GC002096.
- Jiménez, L., Romero-Viana, L., Conde-Porcuna, J.M., Pérez-Martínez, C., 2015. Sedimentary photosynthetic pigments as indicators of climate and watershed perturbations in an alpine lake in southern Spain. *Limnology* 34, 439-454.
- Jiménez, L., Rühland, K.M., Jeziorski, A., Smol, J.P., Pérez-Martínez, C., 2018. Climate change and Saharan dust drive recent cladoceran and primary production changes in remote alpine lakes of Sierra Nevada, Spain. *Global Change Biology* 24, e139-e158. Doi: 10.1111/gcb.13878.
- Joannin, S., Bassinot, F., Nebout, N.C., Peyron, O., Beaudouin, C., 2011. Vegetation response to obliquity and precession forcing during the Mid-Pleistocene Transition in Western Mediterranean region (ODP site 976). *Quaternary Science Reviews* 30, 280-297. Doi: 10.1016/j.quascirev.2010.11.009.
- Joannin, S., Ciaranfi, N., Stefanelli, S., 2008. Vegetation changes during the late Early Pleistocene at Montalbano Jonico (Province of Matera, southern Italy) based on pollen analysis. *Palaeogeography, Palaeoclimatology, Palaeoecology* 270, 92-101. Doi: 10.1016/j.palaeo.2008.08.017.
- Johnsen, S., Clausen, H.B., Dansgaard, W., Fuhrer, K., Gundestrup, N., Hammer, C.U., Iversen, P., Jouzel, J., Stauffer, B., 1992. Irregular glacial interstadials recorded in a new Greenland ice core. *Nature* 359, 311. Doi: 10.1038/359311a0.
- Jones, B., Renaut, R.W., 2010. Chapter 4 Calcareous Spring Deposits in Continental Settings, in: Alonso-Zarza, A.M., Tanner, L.H. (Eds.), *Developments in Sedimentology*. Elsevier, 177-224. Doi: 10.1016/S0070-4571(09)06104-4.
- Kageyama, M., Paul, A., Roche, D.M., Van Meerbeeck, C.J., 2010. Modelling glacial climatic millennial-scale variability related to changes in the Atlantic meridional overturning circulation: a review. *Quaternary Science Reviews* 29, 2931-2956. Doi: 10.1016/j.quascirev.2010.05.029.
- Kallel, N., Duplessy, J.-C., Labeyrie, L., Fontugne, M., Paterne, M., 2004. Mediterranean Sea palaeohydrology and pluvial periods during the Late Quaternary, in: Battarbee, R.W., Gasse, F.,



## References

Stickley, C.E. (Eds.), Past Climate Variability through Europe and Africa. Springer Netherlands, Dordrecht, 307-324. Doi: 10.1007/978-1-4020-2121-3\_15.

Kallel, N., Duplessy, J.C., Labeyrie, L., Fontugne, M., Paterne, M., Montacer, M., 2000. Mediterranean pluvial periods and sapropel formation over the last 200 000 years. *Palaeogeography, Palaeoclimatology, Palaeoecology* 157, 45-58. Doi: 10.1016/S0031-0182(99)00149-2.

Kaspar, F., Kühl, N., Cubasch, U., Litt, T., 2005. A model-data comparison of European temperatures in the Eemian interglacial. *Geophysical Research Letters* 32 Doi: 10.1029/2005gl022456.

Kaufman, D.S., Manley, W.F., 1998. A new procedure for determining dl amino acid ratios in fossils using reverse phase liquid chromatography. *Quaternary Science Reviews* 17, 987-1000. Doi: 10.1016/S0277-3791(97)00086-3.

Kaufman, D.S., Scott Anderson, R., Hu, F.S., Berg, E., Werner, A., 2010. Evidence for a variable and wet Younger Dryas in southern Alaska. *Quaternary Science Reviews* 29, 1445-1452. Doi: 10.1016/j.quascirev.2010.02.025.

Kirtman, B., Power, S., Adedoyin, A., Boer, G., Bojariu, R., Camilloni, I., Doblas-Reyes, F., Fiore, A., Kimoto, M., Meehl, G., 2013. Section 11: Near-term Climate Change: Projections and Predictability, in: Stocker, T.F., Qin, D., Plattner, G.-K., Tignor, M., Allen, S.K., Boschung, J., Nauels, A., Xia, Y., Bex, V., Midgley, P.M. (Ed.), *Climate change 2013: The Physical Science Basis. Working Group I to the Fifth Assessment Report of the Intergovernmental Panel on Climate Change*. Cambridge University Press, 1535.

Kottek, M., Grieser, J., Beck, C., Rudolf, B., Rubel, F., 2006. World map of the Köppen-Geiger climate classification updated. *Meteorologische Zeitschrift* 15, 259-263. Doi: 10.1127/0941-2948/2006/0130.

Kroon, D., Alexander, I., Little, M., Lourens, L., Matthewson, A., Robertson, A.H., Sakamoto, T., 1998. Chapter 14: Oxygen isotope and sapropel stratigraphy in the eastern Mediterranean during the last 3.2 million years, *Proceedings of the Ocean Drilling Program, Scientific Results*, 181-189.

Kutzbach, J.E., Guetter, P.J., 1986. The Influence of Changing Orbital Parameters and Surface Boundary Conditions on Climate Simulations for the Past 18 000 Years. *Journal of the Atmospheric Sciences* 43, 1726-1759. Doi: 10.1175/1520-0469.

Kwiecien, O., Arz, H.W., Lamy, F., Plessen, B., Bahr, A., Haug, G.H., 2009. North Atlantic control on precipitation pattern in the eastern Mediterranean/Black Sea region during the last glacial. *Quaternary Research* 71, 375-384. Doi: 10.1016/j.yqres.2008.12.004.

Laabs, B.J., Kaufman, D.S., 2003. Quaternary highstands in Bear Lake Valley, Utah and Idaho. *Geological Society of America Bulletin* 115, 463-478. Doi: 10.1130/0016-7606.

Larrasoaña, J.C., Roberts, A.P., Rohling, E.J., Winklhofer, M., Wehausen, R., 2003. Three million years of monsoon variability over the northern Sahara. *Climate Dynamics* 21, 689-698. Doi: 10.1007/s00382-003-0355-z.

- Laskar, J., Robutel, P., Joutel, F., Gastineau, M., Correia, A.C.M., Levrard, B., 2004. A long-term numerical solution for the insolation quantities of the Earth. *Astronomy & Astrophysics* 428, 261-285. Doi: 10.1051/0004-6361:20041335.
- Lawson, I., Frogley, M., Bryant, C., Preece, R., Tzedakis, P., 2004. The Lateglacial and Holocene environmental history of the Ioannina basin, north-west Greece. *Quaternary Science Reviews* 23, 1599-1625. Doi: 10.1016/j.quascirev.2004.02.003.
- Lézine, A.M., von Grafenstein, U., Andersen, N., Belmecheri, S., Bordon, A., Caron, B., Cazet, J.P., Erlenkeuser, H., Fouache, E., Grenier, C., Huntsman-Mapila, P., Hureau-Mazaudier, D., Manelli, D., Mazaud, A., Robert, C., Sulpizio, R., Tiercelin, J.J., Zanchetta, G., Zeqollari, Z., 2010. Lake Ohrid, Albania, provides an exceptional multi-proxy record of environmental changes during the last glacial-interglacial cycle. *Palaeogeography, Palaeoclimatology, Palaeoecology* 287, 116-127. Doi: 10.1016/j.palaeo.2010.01.016.
- Lionello, P., 2012. *The climate of the Mediterranean region: From the past to the future*. Elsevier.
- Lionello, P., Malanotte-Rizzoli, P., Boscolo, R., Alpert, P., Artale, V., Li, L., Luterbacher, J., May, W., Trigo, R., Tsimplis, M., Ulbrich, U., Xoplaki, E., 2006. The Mediterranean climate: An overview of the main characteristics and issues. *Developments in Earth and Environmental Sciences* 4, 1-26. Doi: 10.1016/S1571-9197(06)80003-0.
- Lionello, P., Sanna, A., 2005. Mediterranean wave climate variability and its links with NAO and Indian Monsoon. *Climate Dynamics* 25, 611-623. Doi: 10.1007/s00382-005-0025-4.
- Lisiecki, L.E., Raymo, M.E., 2005. A Pliocene-Pleistocene stack of 57 globally distributed benthic  $\delta^{18}\text{O}$  records. *Paleoceanography* 20, 1-17. Doi: 10.1029/2004pa001071.
- Litt, T., Pickarski, N., Heumann, G., Stockhecke, M., Tzedakis, P.C., 2014. A 600,000 year long continental pollen record from Lake Van, eastern Anatolia (Turkey). *Quaternary Science Reviews* 104, 30-41. Doi: 10.1016/j.quascirev.2014.03.017.
- Liu, Z., Otto-Bliesner, B., He, F., Brady, E., Tomas, R., Clark, P., Carlson, A., Lynch-Stieglitz, J., Curry, W., Brook, E., 2009. Transient simulation of last deglaciation with a new mechanism for Bølling-Allerød warming. *Science* 325, 310-314. Doi: 10.1126/science.1171041.
- Longo, W.M., Huang, Y., Yao, Y., Zhao, J., Giblin, A.E., Wang, X., Zech, R., Haberzettl, T., Jardillier, L., Toney, J., Liu, Z., Krivonogov, S., Kolpakova, M., Chu, G., D'Andrea, W.J., Harada, N., Nagashima, K., Sato, M., Yonenobu, H., Yamada, K., Gotanda, K., Shinozuka, Y., 2018. Widespread occurrence of distinct alkenones from Group I haptophytes in freshwater lakes: Implications for paleotemperature and paleoenvironmental reconstructions. *Earth and Planetary Science Letters* 492, 239-250. Doi: 10.1016/j.epsl.2018.04.002.
- Lourantou, A., Lavrič, J.V., Köhler, P., Barnola, J.M., Paillard, D., Michel, E., Raynaud, D., Chappellaz, J., 2010. Constraint of the CO<sub>2</sub> rise by new atmospheric carbon isotopic measurements during the last deglaciation. *Global Biogeochemical Cycles* 24, 1-15. Doi: 10.1029/2009GB003545.
- Lourens, L.J., Antonarakou, A., Hilgen, F., Van Hoof, A., Vergnaud-Grazzini, C., Zachariasse, W., 1996. Evaluation of the Plio-Pleistocene astronomical timescale. *Paleoceanography and Paleoclimatology* 11, 391-413. Doi: 10.1029/96PA01125.

## References

- Lüning, S., Vahrenholt, F., 2016. Chapter 16 - The Sun's Role in Climate, in: Easterbrook, D.J. (Ed.), Evidence-Based Climate Science (Second Edition). Elsevier, 283-305. Doi: 10.1016/B978-0-12-804588-6.00016-1.
- Magill, C.R., Ausín, B., Wenk, P., McIntyre, C., Skinner, L., Martínez-García, A., Hodell, D.A., Haug, G.H., Kenney, W., Eglinton, T.I., 2018. Transient hydrodynamic effects influence organic carbon signatures in marine sediments. *Nature communications* 9, 4690. Doi: 10.1038/s41467-018-06973-w.
- Magny, M., de Beaulieu, J.-L., Drescher-Schneider, R., Vanni re, B., Walter-Simonnet, A.-V., Miras, Y., Millet, L., Bossuet, G., Peyron, O., Brugiapaglia, E., Leroux, A., 2007. Holocene climate changes in the central Mediterranean as recorded by lake-level fluctuations at Lake Accesa (Tuscany, Italy). *Quaternary Science Reviews* 26, 1736-1758. Doi: 10.1016/j.quascirev.2007.04.014.
- Magri, D., 1989. Interpreting long-term exponential growth of plant populations in a 250000-year pollen record from Valle di Castiglione (Roma). *New Phytologist* 112, 123-128. Doi: 10.1111/j.1469-8137.1989.tb00317.x.
- Magri, D., Sadori, L., 1999. Late Pleistocene and Holocene pollen stratigraphy at Lago di Vico, central Italy. *Vegetation History and Archaeobotany* 8, 247-260. Doi: 10.1007/BF01291777.
- Manzano, S., Carri n, J.S., L pez-Merino, L., Gonz lez-Samp riz, P., Munuera, M., Fern ndez, S., Mart n-Lerma, I., G mez Ferreras, M.d.C., 2017. Mountain strongholds for woody angiosperms during the Late Pleistocene in SE Iberia. *Catena* 149, 701-712. Doi: 10.1016/j.catena.2016.03.008.
- Marchitto, T.M., Muscheler, R., Ortiz, J.D., Carriquiry, J.D., van Geen, A., 2010. Dynamical response of the tropical Pacific Ocean to solar forcing during the early Holocene. *Science* 330, 1378-1381. Doi: 10.1126/science.1194887.
- Margari, V., Gibbard, P.L., Bryant, C.L., Tzedakis, P.C., 2009. Character of vegetational and environmental changes in southern Europe during the last glacial period; evidence from Lesvos Island, Greece. *Quaternary Science Reviews* 28, 1317-1339. Doi: 10.1016/j.quascirev.2009.01.008.
- Margari, V., Skinner, L.C., Hodell, D.A., Martrat, B., Toucanne, S., Grimalt, J.O., Gibbard, P.L., Lunkka, J.P., Tzedakis, P.C., 2014. Land-ocean changes on orbital and millennial time scales and the penultimate glaciation. *Geology* 42, 183-186. Doi: 10.1130/g35070.1.
- Margari, V., Skinner, L.C., Tzedakis, P.C., Ganopolski, A., Vautravers, M., Shackleton, N.J., 2010. The nature of millennial-scale climate variability during the past two glacial periods. *Nature Geoscience* 3, 127-131. Doi: 10.1038/ngeo740.
- Mart n-Garc a, G.M., 2019. Oceanic Impact on European Climate Changes during the Quaternary. *Geosciences* 9, 119. Doi: 10.3390/geosciences9030119.
- Mart n-Puertas, C., Brauer, A., Wulf, S., Ott, F., Lauterbach, S., Dulski, P., 2014. Annual proxy data from Lago Grande di Monticchio (southern Italy) between 76 and 112 ka: new chronological constraints and insights on abrupt climatic oscillations. *Climate of the Past* 10, 2099-2114. Doi: 10.5194/cp-10-2099-2014.

- Martín-Puertas, C., Valero-Garcés, B.L., Brauer, A., Mata, M.P., Delgado-Huertas, A., Dulski, P., 2009. The Iberian–Roman Humid Period (2600–1600 cal yr BP) in the Zoñar Lake varve record (Andalucía, southern Spain). *Quaternary Research* 71, 108-120. Doi: 10.1016/j.yqres.2008.10.004.
- Martin, J.D., 2004. Using X Powder: a Software Package for Powder X-Ray Diffraction Analysis. Legal Deposit GR, 1001/04. Available at: [www.xpowder.com](http://www.xpowder.com).
- Martínez-Ruiz, F., Kastner, M., Paytan, A., Ortega-Huertas, M., Bernasconi, S.M., 2000. Geochemical evidence for enhanced productivity during S1 sapropel deposition in the eastern Mediterranean. *Paleoceanography* 15, 200-209. Doi: 10.1029/1999pa000419.
- Martrat, B., Grimalt, J.O., López-Martínez, C., Cacho, I., Sierro, F.J., Flores, J.A., Zahn, R., Canals, M., Curtis, J.H., Hodell, D.A., 2004. Abrupt temperature changes in the Western Mediterranean over the past 250,000 years. *Science* 306, 1762-1765. Doi: 10.1126/science.1101706.
- Martrat, B., Jiménez-Amat, P., Zahn, R., Grimalt, J.O., 2014. Similarities and dissimilarities between the last two deglaciations and interglaciations in the North Atlantic region. *Quaternary Science Reviews* 99, 122-134. Doi: 10.1016/j.quascirev.2014.06.016.
- Masson-Delmotte, V., Landais, A., Combourieu-Nebout, N., von Grafenstein, U., Jouzel, J., Caillon, N., Chappellaz, J., Dahl-Jensen, D., Johnsen, S.J., Stenni, B., 2005. Rapid climate variability during warm and cold periods in polar regions and Europe. *Comptes Rendus Geoscience* 337, 935-946. Doi: 10.1016/j.crte.2005.04.001.
- McManus, J.F., Francois, R., Gherardl, J.M., Kelgwin, L., Drown-Leger, S., 2004. Collapse and rapid resumption of Atlantic meridional circulation linked to deglacial climate changes. *Nature* 428, 834-837. Doi: 10.1038/nature02494.
- Menéndez-Amor, J., Florschütz, F., 1962. Un aspect de la végétation en Espagne méridionale durant la dernière glaciation et l'Holocène. *Geologie en Mijnbouw*, 131-134.
- Menéndez-Amor, J., Florschütz, F., 1964. Results of the preliminary palynological investigation of samples from a 50m broing in southern Spain. *Bol. R. Soc. Española Hist. Nat.* 62, 251-255.
- Messerli, B., 1965. *Beiträge zur Geomorphologie der Sierra Nevada (Andalusien)*. Juris Verlag.
- Meyers, P., Teranes, J., 2001. Tracking environmental change using lake sediments. *Tracking Environmental Change Using Lake Sediments* 2, 239-270.
- Meyers, P.A., 1994. Preservation of elemental and isotopic source identification of sedimentary organic matter. *Chemical Geology* 114, 289-302. Doi: 10.1016/0009-2541(94)90059-0.
- Meyers, P.A., 2003. Applications of organic geochemistry to paleolimnological reconstructions: a summary of examples from the Laurentian Great Lakes. *Organic Geochemistry* 34, 261-289. Doi: 10.1016/S0146-6380(02)00168-7.
- Meyers, P.A., Ishiwatari, R., 1993. Lacustrine organic geochemistry—an overview of indicators of organic matter sources and diagenesis in lake sediments. *Organic Geochemistry* 20, 867-900. Doi: 10.1016/0146-6380(93)90100-P.

## References

Milankovitch, M., 1920. Théorie mathématique des phénomènes thermiques produits par la radiation solaire. 340. Doi: 10.1090/S0002-9904-1923-03773-7.

Milner, A.M., Collier, R.E.L., Roucoux, K.H., Müller, U.C., Pross, J., Kalaitzidis, S., Christanis, K., Tzedakis, P.C., 2012. Enhanced seasonality of precipitation in the Mediterranean during the early part of the Last Interglacial. *Geology* 40, 919-922. Doi: 10.1130/g33204.1.

Milner, A.M., Roucoux, K.H., Collier, R.E.L., Müller, U.C., Pross, J., Tzedakis, P.C., 2016. Vegetation responses to abrupt climatic changes during the Last Interglacial Complex (Marine Isotope Stage 5) at Tenaghi Philippon, NE Greece. *Quaternary Science Reviews* 154, 169-181. Doi: 10.1016/j.quascirev.2016.10.016.

Mitchell, D.S., 1969. The ecology of vascular hydrophytes on Lake Kariba. *Hydrobiologia* 34, 448-464. Doi: 10.1007/bf00045403.

Mitterer, R.M., Kriausakul, N., 1989. Calculation of amino acid racemization ages based on apparent parabolic kinetics. *Quaternary Science Reviews* 8, 353-357. Doi: 10.1016/0277-3791(89)90035-8.

Mix, A.C., Bard, E., Schneider, R., 2001. Environmental processes of the ice age: land, oceans, glaciers (EPILOG). *Quaternary Science Reviews* 20, 627-657. Doi: 10.1016/S0277-3791(00)00145-1.

Mladenov, N., Sommaruga, R., Morales-Baquero, R., Laurion, I., Camarero, L., Diéguez, M.C., Camacho, A., Delgado, A., Torres, O., Chen, Z., Felip, M., Reche, I., 2011. Dust inputs and bacteria influence dissolved organic matter in clear alpine lakes. *Nature Communications* 2, 405. Doi: 10.1038/ncomms1411.

Mommersteeg, H.J.P.M., Loutre, M.F., Young, R., Wilmstra, T.A., Hooghiemstra, H., 1995. Orbital forced frequencies in the 975 000 year pollen record from Tenaghi Philippon (Greece). *Climate Dynamics* 11, 4-24. Doi: 10.1007/BF00220674.

Morales-Baquero, R., Pulido-Villena, E., Reche, I., 2006. Atmospheric inputs of phosphorus and nitrogen to the southwest Mediterranean region: Biogeochemical responses of high mountain lakes. *Limnology and Oceanography* 51, 830-837.

Morales-Molino, C., Postigo-Mijarra, J.M., Morla, C., García-Antón, M., 2011. Long-term persistence of Mediterranean pine forests in the Duero Basin (central Spain) during the Holocene: The case of *Pinus pinaster* Aiton. *The Holocene* 22, 561-570. Doi: 10.1177/0959683611427339.

Morellón, M., Aranbarri, J., Moreno, A., González-Sampériz, P., Valero-Garcés, B.L., 2018. Early Holocene humidity patterns in the Iberian Peninsula reconstructed from lake, pollen and speleothem records. *Quaternary Science Reviews* 181, 1-18. Doi: 10.1016/j.quascirev.2017.11.016.

Morellón, M., Valero-Garcés, B., Vegas-Vilarrúbia, T., González-Sampériz, P., Romero, Ó., Delgado-Huertas, A., Mata, P., Moreno, A., Rico, M., Corella, J.P., 2009. Lateglacial and Holocene palaeohydrology in the western Mediterranean region: The Lake Estanya record (NE Spain). *Quaternary Science Reviews* 28, 2582-2599. Doi: 10.1016/j.quascirev.2009.05.014.

Moreno, A., Cacho, I., Canals, M., Grimalt, J.O., Sánchez-Goñi, M.F., Shackleton, N., Sierro, F.J., 2005. Links between marine and atmospheric processes oscillating on a millennial time-scale. A

- multi-proxy study of the last 50,000yr from the Alboran Sea (Western Mediterranean Sea). *Quaternary Science Reviews* 24, 1623-1636. Doi: 10.1016/j.quascirev.2004.06.018.
- Moreno, A., Cacho, I., Canals, M., Prins, M.A., Sánchez-Goñi, M.-F., Grimalt, J.O., Weltje, G.J., 2002. Saharan Dust Transport and High-Latitude Glacial Climatic Variability: The Alboran Sea Record. *Quaternary Research* 58, 318-328. Doi: 10.1006/qres.2002.2383.
- Moreno, A., González-Sampériz, P., Morellón, M., Valero-Garcés, B.L., Fletcher, W.J., 2012a. Northern Iberian abrupt climate change dynamics during the last glacial cycle: A view from lacustrine sediments. *Quaternary Science Reviews* 36, 139-153. Doi: 10.1016/j.quascirev.2010.06.031.
- Moreno, A., Pérez, A., Frigola, J., Nieto-Moreno, V., Rodrigo-Gámiz, M., Martrat, B., González-Sampériz, P., Morellón, M., Martín-Puertas, C., Corella, J.P., Belmonte, Á., Sancho, C., Cacho, I., Herrera, G., Canals, M., Grimalt, J.O., Jiménez-Espejo, F., Martínez-Ruiz, F., Vegas-Vilarrúbia, T., Valero-Garcés, B.L., 2012b. The Medieval Climate Anomaly in the Iberian Peninsula reconstructed from marine and lake records. *Quaternary Science Reviews* 43, 16-32. Doi: 10.1016/j.quascirev.2012.04.007.
- Moreno, A., Stoll, H., Jiménez-Sánchez, M., Cacho, I., Valero-Garcés, B., Ito, E., Edwards, R.L., 2010. A speleothem record of glacial (25–11.6kyr BP) rapid climatic changes from northern Iberian Peninsula. *Global and Planetary Change* 71, 218-231. Doi: 10.1016/j.gloplacha.2009.10.002.
- Morford, J.L., Emerson, S., 1999. The geochemistry of redox sensitive trace metals in sediments. *Geochimica et Cosmochimica Acta* 63, 1735-1750. Doi: 10.1016/S0016-7037(99)00126-X.
- Naeher, S., Gilli, A., North, R.P., Hamann, Y., Schubert, C.J., 2013. Tracing bottom water oxygenation with sedimentary Mn/Fe ratios in Lake Zurich, Switzerland. *Chemical Geology* 352, 125-133. Doi: 10.1016/j.chemgeo.2013.06.006.
- Nakagawa, T., Kitagawa, H., Yasuda, Y., Tarasov, P.E., Nishida, K., Gotanda, K., Sawai, Y., 2003. Asynchronous climate changes in the North Atlantic and Japan during the last termination. *Science* 299, 688-691. Doi: 10.1126/science.1078235.
- Naughton, F., Sánchez Goñi, M.F., Kageyama, M., Bard, E., Duprat, J., Cortijo, E., Desprat, S., Malaizé, B., Joly, C., Rostek, F., 2009. Wet to dry climatic trend in north-western Iberia within Heinrich events. *Earth and Planetary Science Letters* 284, 329-342. Doi: 10.1016/j.epsl.2009.05.001.
- Naughton, F., Sánchez Goñi, M.F., Rodrigues, T., Salgueiro, E., Costas, S., Desprat, S., Duprat, J., Michel, E., Rossignol, L., Zaragosi, S., Voelker, A.H.L., Abrantes, F., 2016. Climate variability across the last deglaciation in NW Iberia and its margin. *Quaternary International* 414, 9-22. Doi: 10.1016/j.quaint.2015.08.073.
- Nelson, D.W., Sommers, L.E., 1982. Total carbon, organic carbon, and organic matter, *Methods of Soil Analysis, Part 2*. America Society of Agronomy, Madison, Wisconsin, USA, 539-579.
- Nestares, T., Torres, T., 1998. Un nuevo sondeo de investigación paleoambiental del Pleistoceno y Holoceno en la turbera del Padul (Granada, Andalucía). *Geogaceta* 23, 99-102.
- NGRIP-Members, 2004. High-resolution record of Northern Hemisphere climate extending into the last interglacial period. *Nature* 431, 147-151. Doi: 10.1038/nature02805.

## References

Niedermeyer, E.M., Schefuß, E., Sessions, A.L., Mulitza, S., Mollenhauer, G., Schulz, M., Wefer, G., 2010. Orbital- and millennial-scale changes in the hydrologic cycle and vegetation in the western African Sahel: insights from individual plant wax  $\delta D$  and  $\delta^{13}C$ . *Quaternary Science Reviews* 29, 2996-3005. Doi: 10.1016/j.quascirev.2010.06.039.

Ohkouchi, N., Eglinton, T.I., Hayes, J.M., 2003. Radiocarbon Dating of Individual Fatty Acids as a Tool for Refining Antarctic Margin Sediment Chronologies. *Radiocarbon* 45, 17-24. Doi: 10.1017/S0033822200032355.

Oliva, M., Gómez-Ortiz, A., 2012. Late-Holocene environmental dynamics and climate variability in a Mediterranean high mountain environment (Sierra Nevada, Spain) inferred from lake sediments and historical sources. *The Holocene* 22, 915-927. Doi: 10.1177/0959683611434235.

Oliva, M., Gómez Ortiz, A., Palacios, D., Salvador-Franch, F., Salvà-Catarineu, M., 2014. Environmental evolution in Sierra Nevada (South Spain) since the Last Glaciation, based on multi-proxy records. *Quaternary International* 353, 195-209. Doi: 10.1016/j.quaint.2014.02.009.

Oliva, M., Schulte, L., Ortiz, A.G., 2009. Morphometry and late holocene activity of solifluction landforms in the sierra Nevada, southern Spain. *Permafrost and Periglacial Processes* 20, 369-382. Doi: 10.1002/ppp.645.

Ortiz, J.E., Moreno, L., Torres, T., Vegas, J., Ruiz-Zapata, B., García-Cortés, Á., Galán, L., Pérez-González, A., 2013. A 220 ka palaeoenvironmental reconstruction of the Fuentillejo maar lake record (Central Spain) using biomarker analysis. *Organic Geochemistry* 55, 85-97. Doi: 10.1016/j.orggeochem.2012.11.012.

Ortiz, J.E., Torres, T., Delgado, A., Julià, R., Lucini, M., Llamas, F.J., Reyes, E., Soler, V., Valle, M., 2004a. The palaeoenvironmental and palaeohydrological evolution of Padul Peat Bog (Granada, Spain) over one million years, from elemental, isotopic and molecular organic geochemical proxies. *Organic Geochemistry* 35, 1243-1260. Doi: 10.1016/j.orggeochem.2004.05.013.

Ortiz, J.E., Torres, T., Delgado, A., Llamas, J.F., Soler, V., Valle, M., Julià, R., Moreno, L., Díaz-Bautista, A., 2010. Palaeoenvironmental changes in the Padul Basin (Granada, Spain) over the last 1Ma based on the biomarker content. *Palaeogeography, Palaeoclimatology, Palaeoecology* 298, 286-299. Doi: 10.1016/j.palaeo.2010.10.003.

Ortiz, J.E., Torres, T., Julià, R., Delgado, A., Llamas, F.J., Soler, V., Delgado, J., 2004b. Numerical dating algorithms of amino acid racemization ratios from continental ostracodes. Application to the Guadix-Baza Basin (southern Spain). *Quaternary Science Reviews* 23, 717-730. Doi: 10.1016/j.quascirev.2003.06.001.

Overpeck, J.T., 1995. Paleoclimatology and climate system dynamics. *Reviews of Geophysics* 33, 863-871. Doi: 10.1029/95rg01035.

Paillard, D., Labeyrie, L., Yiou, P., 1996. Macintosh program performs time-series analysis. *Eos, Transactions American Geophysical Union* 77, 379-379. Doi: 10.1029/96EO00259.

Pailler, D., Bard, E., 2002. High frequency palaeoceanographic changes during the past 140 000 yr recorded by the organic matter in sediments of the Iberian Margin. *Palaeogeography, Palaeoclimatology, Palaeoecology* 181, 431-452. Doi: 10.1016/S0031-0182(01)00444-8.

- Palacios, D., Gómez-Ortiz, A., Andrés, N., Salvador, F., Oliva, M., 2016. Timing and new geomorphologic evidence of the last deglaciation stages in Sierra Nevada (southern Spain). *Quaternary Science Reviews* 150, 110-129. Doi: 10.1016/j.quascirev.2016.08.012.
- Panagiotopoulos, K., Böhm, A., Leng, M.J., Wagner, B., Schäbitz, F., 2014. Climate variability over the last 92 ka in SW Balkans from analysis of sediments from Lake Prespa. *Climate of the Past* 10, 643-660. Doi: 10.5194/cp-10-643-2014.
- Parmesan, C., 2006. Ecological and Evolutionary Responses to Recent Climate Change. *Annual Review of Ecology, Evolution, and Systematics* 37, 637-669. Doi: 10.1146/annurev.ecolsys.37.091305.110100.
- Peck, V.L., Hall, I.R., Zahn, R., Elderfield, H., Grousset, F., Hemming, S.R., Scourse, J.D., 2006. High resolution evidence for linkages between NW European ice sheet instability and Atlantic Meridional Overturning Circulation. *Earth and Planetary Science Letters* 243, 476-488. Doi: 10.1016/j.epsl.2005.12.023.
- Pelechaty, M., Pukacz, A., Apolinarska, K., Pelechata, A., Siepak, M., Porta, G.D., 2013. The significance of Charavegetation in the precipitation of lacustrine calcium carbonate. *Sedimentology* 60, 1017-1035. Doi: 10.1111/sed.12020.
- Pénaud, A., Eynaud, F., Sánchez-Goñi, M., Malaizé, B., Turon, J.-L., Rossignol, L., 2011. Contrasting sea-surface responses between the western Mediterranean Sea and eastern subtropical latitudes of the North Atlantic during abrupt climatic events of MIS 3. *Marine Micropaleontology* 80, 1-17. Doi: 10.1016/j.marmicro.2011.03.002.
- Penaud, A., Eynaud, F., Turon, J.L., Blamart, D., Rossignol, L., Marret, F., López-Martínez, C., Grimalt, J.O., Malaizé, B., Charlier, K., 2010. Contrasting paleoceanographic conditions off Morocco during Heinrich events (1 and 2) and the Last Glacial Maximum. *Quaternary Science Reviews* 29, 1923-1939. Doi: 10.1016/j.quascirev.2010.04.011.
- Pentecost, A., 2005. *Travertine*. Springer Science & Business Media.
- Pérez-Luque, A.J., Pérez-Pérez, R., Bonet, F.J., Zamora, R., 2012. Estaciones de Monitoreo Intensivo. Proyecto: Seguimiento de los efectos de cambio global en Sierra Nevada: diseño y desarrollo de un sistema de monitorización ecológica basado en la red de estaciones multiparamétricas.
- Pérez-Sanz, A., González-Sampériz, P., Moreno, A., Valero-Garcés, B., Gil-Romera, G., Rieradevall, M., Tarrats, P., Lasheras-Álvarez, L., Morellón, M., Belmonte, A., Sancho, C., Sevilla-Callejo, M., Navas, A., 2013. Holocene climate variability, vegetation dynamics and fire regime in the central Pyrenees: the Basa de la Mora sequence (NE Spain). *Quaternary Science Reviews* 73, 149-169. Doi: 10.1016/j.quascirev.2013.05.010.
- Pérez Raya, F., López Nieto, J.M., 1991. Vegetación acuática y helofítica de la depresión de Padul (Granada). *Acta Bot. Malacitana* 16, 373-389.
- Peyron, O., Goring, S., Dormoy, I., Kotthoff, U., Pross, J., de Beaulieu, J.-L., Drescher-Schneider, R., Vannière, B., Magny, M., 2011. Holocene seasonality changes in the central Mediterranean region



## References

reconstructed from the pollen sequences of Lake Accessa (Italy) and Tenaghi Philippon (Greece). *The Holocene* 21, 131-146. Doi: 10.1177/0959683610384162.

Pickarski, N., Kwiecien, O., Djamali, M., Litt, T., 2015a. Vegetation and environmental changes during the last interglacial in eastern Anatolia (Turkey): a new high-resolution pollen record from Lake Van. *Palaeogeography, Palaeoclimatology, Palaeoecology* 435, 145-158. Doi: 10.1016/j.palaeo.2015.06.015.

Pickarski, N., Kwiecien, O., Langgut, D., Litt, T., 2015b. Abrupt climate and vegetation variability of eastern Anatolia during the last glacial. *Climate of the Past* 11, 1491-1505. Doi: 10.5194/cp-11-1491-2015.

Pickarski, N., Litt, T., 2017. A new high-resolution pollen sequence at Lake Van, Turkey: insights into penultimate interglacial–glacial climate change on vegetation history. *Climate of the Past* 13, 689-710. Doi: 10.5194/cp-13-689-2017.

Pini, R., Ravazzi, C., Donegana, M., 2009. Pollen stratigraphy, vegetation and climate history of the last 215ka in the Azzano Decimo core (plain of Friuli, north-eastern Italy). *Quaternary Science Reviews* 28, 1268-1290. Doi: 10.1016/j.quascirev.2008.12.017.

Pons, A., Guiot, J., de Beaulieu, J.L., Reille, M., 1992. Recent contributions to the climatology of the last glacial-interglacial cycle based on French pollen sequences. *Quaternary Science Reviews* 11, 439-448. Doi: 10.1016/0277-3791(92)90026-5.

Pons, A., Reille, M., 1988. The Holocene and Upper Pleistocene Pollen Record from Padul (Granada, Spain): A new study. *Palaeogeography, Palaeoclimatology, Palaeoecology* 66, 243-263. Doi: 10.1016/0031-0182(88)90202-7.

Ponton, C., West, A.J., Feakins, S.J., Galy, V., 2014. Leaf wax biomarkers in transit record river catchment composition. *Geophysical Research Letters* 41, 6420-6427. Doi: 10.1002/2014gl061328.

Popovska, C., 2002. Climate change and vulnerability assessment of the water resources. *Journal VODOPRIVREDA*, 209-210.

Popovska, C., Bonacci, O., 2007. Basic data on the hydrology of Lakes Ohrid and Prespa. *Hydrological Processes* 21, 658-664. Doi: 10.1002/hyp.6252.

Poynter, J., Eglinton, G., 1990. Molecular composition of three sediments from hole 717c: The Bengal fan, *Proceedings of the Ocean Drilling Program: Scientific results* 116, pp. 155-161. Doi: 10.2973/odp.proc.sr.116.151.1990.

Prentice, I.C., Guiot, J., Harrison, S.P., 1992. Mediterranean vegetation, lake levels and palaeoclimate at the Last Glacial Maximum. *Nature* 360, 658-660. Doi: 10.1038/360658a0.

Pross, J., Koutsodendris, A., Christanis, K., Fischer, T., Fletcher, W.J., Hardiman, M., Kalaitzidis, S., Knipping, M., Kotthoff, U., Milner, A.M., Müller, U.C., Schmiedl, G., Siavalas, G., Tzedakis, P.C., Wulf, S., 2015. The 1.35-Ma-long terrestrial climate archive of Tenaghi Philippon, northeastern Greece: Evolution, exploration, and perspectives for future research. *Newsletters on Stratigraphy* 48, 253-276. Doi: 10.1127/nos/2015/0063.

- Pulido-Villena, E., Reche, I., Morales-Baquero, R., 2005. Food web reliance on allochthonous carbon in two high mountain lakes with contrasting catchments: a stable isotope approach. *Canadian Journal of Fisheries and Aquatic Sciences* 62, 2640-2648. Doi: 10.1139/f05-169.
- Pulido-Villena, E., Reche, I., Morales-Baquero, R., 2006. Significance of atmospheric inputs of calcium over the southwestern Mediterranean region: High mountain lakes as tools for detection. *Global Biogeochemical Cycles* 20 Doi: 10.1029/2005gb002662.
- Ramos-Román, M.J., 2018. Holocene paleoenvironmental change, climate and human impact in Sierra Nevada, Southern Iberian Peninsula, Stratigraphy and Paleontology Department. Universidad de Granada, Granada.
- Ramos-Román, M.J., Jiménez-Moreno, G., Camuera, J., García-Alix, A., Anderson, R.S., Jiménez-Espejo, F.J., Carrión, J.S., 2018a. Holocene climate aridification trend and human impact interrupted by millennial- and centennial-scale climate fluctuations from a new sedimentary record from Padul (Sierra Nevada, southern Iberian Peninsula). *Climate of the Past* 14, 117-137. Doi: 10.5194/cp-14-117-2018.
- Ramos-Román, M.J., Jiménez-Moreno, G., Camuera, J., García-Alix, A., Scott Anderson, R., Jiménez-Espejo, F.J., Sachse, D., Toney, J.L., Carrión, J.S., Webster, C., Yanes, Y., 2018b. Millennial-scale cyclical environment and climate variability during the Holocene in the western Mediterranean region deduced from a new multi-proxy analysis from the Padul record (Sierra Nevada, Spain). *Global and Planetary Change* 168, 35-53. Doi: 10.1016/j.gloplacha.2018.06.003.
- Ramos-Román, M.J., Jiménez-Moreno, G., R.S., A., García-Alix, A., Toney, J.L., Jiménez-Espejo, F.J., Carrión, J.S., 2016. Centennial-scale vegetation and North Atlantic Oscillation changes during the Late Holocene in the southern Iberia. *Quaternary Science Reviews* 143, 84-95.
- Rampen, S.W., Willmott, V., Kim, J.-H., Uliana, E., Mollenhauer, G., Schefuß, E., Sinninghe Damsté, J.S., Schouten, S., 2012. Long chain 1,13- and 1,15-diols as a potential proxy for palaeotemperature reconstruction. *Geochimica et Cosmochimica Acta* 84, 204-216. Doi: 10.1016/j.gca.2012.01.024.
- Ramsey, C.B., 2017. Methods for summarizing radiocarbon datasets. *Radiocarbon* 59, 1809-1833. Doi: 10.1017/RDC.2017.108.
- Rasmussen, S.O., Bigler, M., Blockley, S.P., Blunier, T., Buchardt, S.L., Clausen, H.B., Cvijanovic, I., Dahl-Jensen, D., Johnsen, S.J., Fischer, H., Gkinis, V., Guillevic, M., Hoek, W.Z., Lowe, J.J., Pedro, J.B., Popp, T., Seierstad, I.K., Steffensen, J.P., Svensson, A.M., Vallelonga, P., Vinther, B.M., Walker, M.J.C., Wheatley, J.J., Winstrup, M., 2014. A stratigraphic framework for abrupt climatic changes during the Last Glacial period based on three synchronized Greenland ice-core records: refining and extending the INTIMATE event stratigraphy. *Quaternary Science Reviews* 106, 14-28. Doi: 10.1016/j.quascirev.2014.09.007.
- Rawson, D.S., 1956. Algal Indicators of Trophic Lake Types. *Limnology and Oceanography* 1, 18-25. Doi: 10.4319/lo.1956.1.1.0018.
- Raya Garrido, J., 2003. Composición isotópica del vapor de agua atmosférico en el sureste de la Península Ibérica. Editorial de la Universidad de Granada, Granada, 417.

## References

Regato, P., Salman, R., 2008. Mediterranean Mountains in a Changing World. International Union for Conservation of Nature, Gland, Switzerland and Malaga, Spain, 88.

Reimer, P.J., Baillie, M.G.L., Bard, E., Bayliss, A., Beck, J.W., Blackwell, P.G., Bronk Ramsey, C., Buck, C.E., Burr, G.S., Edwards, R.L., Friedrich, M., Grootes, P.M., Guilderson, T.P., Hajdas, I., Heaton, T.J., Hogg, A.G., Hughen, K.A., Kaiser, K.F., Kromer, B., McCormac, F.G., Manning, S.W., Reimer, R.W., Richards, D.A., Southon, J.R., Talamo, S., Turney, C.S.M., van der Plicht, J., Weyhenmeyer, C.E., 2009. IntCal09 and Marine09 Radiocarbon Age Calibration Curves, 0–50,000 Years cal BP. *Radiocarbon* 51, 1111-1150. Doi: 10.1017/S0033822200034202.

Reimer, P.J., Bard, E., Bayliss, A., Beck, J.W., Blackwell, P.G., Ramsey, C.B., Buck, C.E., Cheng, H., Edwards, R.L., Friedrich, M., 2013. IntCal13 and Marine13 radiocarbon age calibration curves 0–50,000 years cal BP. *Radiocarbon* 55, 1869-1887. Doi: 10.2458/azu\_js\_rc.55.16947.

Renssen, H., Geel, B.v., Plicht, J.v.d., Magny, M., 2000. Reduced solar activity as a trigger for the start of the Younger Dryas? *Quaternary International* 68-71, 373-383. Doi: 10.1016/S1040-6182(00)00060-4.

Repschläger, J., Weinelt, M., Kinkel, H., Andersen, N., Garbe-Schönberg, D., Schwab, C., 2015. Response of the subtropical North Atlantic surface hydrography on deglacial and Holocene AMOC changes. *Paleoceanography* 30, 456-476. Doi: 10.1002/2014pa002637.

Roberts, N., 1983. Age, palaeoenvironments, and climatic significance of late Pleistocene Konya lake, Turkey. *Quaternary Research* 19, 154-171. Doi: 10.1016/0033-5894(83)90002-9.

Roberts, N., Black, S., Boyer, P., Eastwood, W.J., Griffiths, H.I., Lamb, H.F., Leng, M.J., Parish, R., Reed, J.M., Twigg, D., Yiğitbaşıoğlu, H., 1999. Chronology and stratigraphy of Late Quaternary sediments in the Konya Basin, Turkey: Results from the KOPAL Project. *Quaternary Science Reviews* 18, 611-630. Doi: 10.1016/S0277-3791(98)00100-0.

Rodó, X., Baert, E., Comin, F.A., 1997. Variations in seasonal rainfall in Southern Europe during the present century: Relationships with the North Atlantic Oscillation and the El Niño-Southern Oscillation. *Climate Dynamics* 13, 275-284. Doi: 10.1007/s003820050165.

Rodrigo-Gámiz, M., Martínez-Ruiz, F., Chiaradia, M., Jiménez-Espejo, F.J., Ariztegui, D., 2015. Radiogenic isotopes for deciphering terrigenous input provenance in the western Mediterranean. *Chemical Geology* 410, 237-250. Doi: 10.1016/j.chemgeo.2015.06.004.

Rogerson, M., Colmenero-Hidalgo, E., Levine, R., Rohling, E., Voelker, A., Bigg, G.R., Schönfeld, J., Cacho, I., Sierro, F., Löwemark, L., 2010. Enhanced Mediterranean-Atlantic exchange during Atlantic freshening phases. *Geochemistry, Geophysics, Geosystems* 11 Doi: 10.1029/2009GC002931.

Rohling, E., Marino, G., Grant, K., 2015. Mediterranean climate and oceanography, and the periodic development of anoxic events (sapropels). *Earth-Science Reviews* 143, 62-97. Doi: 10.1016/j.earscirev.2015.01.008.

Rosman, K.J.R., Chisholm, W., Hong, S., Candelone, J.-P., Boutron, C.F., 1997. Lead from Carthaginian and Roman Spanish Mines Isotopically Identified in Greenland Ice Dated from 600 B.C. to 300 A.D. *Environmental Science & Technology* 31, 3413-3416. Doi: 10.1021/es970038k.

- Roucoux, K.H., Tzedakis, P.C., Frogley, M.R., Lawson, I.T., Preece, R.C., 2008. Vegetation history of the marine isotope stage 7 interglacial complex at Ioannina, NW Greece. *Quaternary Science Reviews* 27, 1378-1395. Doi: 10.1016/j.quascirev.2008.04.002.
- Roucoux, K.H., Tzedakis, P.C., Lawson, I.T., Margari, V., 2011. Vegetation history of the penultimate glacial period (Marine isotope stage 6) at Ioannina, north-west Greece. *Journal of Quaternary Science* 26, 616-626. Doi: 10.1002/jqs.1483.
- Ruddiman, W.F., 2001. *Earth's Climate: past and future*. Macmillan.
- Ruddiman, W.F., 2003. Orbital insolation, ice volume, and greenhouse gases. *Quaternary Science Reviews* 22, 1597-1629. Doi: 10.1016/S0277-3791(03)00087-8.
- Sachse, D., Radke, J., Gleixner, G., 2004. Hydrogen isotope ratios of recent lacustrine sedimentary n-alkanes record modern climate variability. *Geochimica et Cosmochimica Acta* 68, 4877-4889. Doi: 10.1016/j.gca.2004.06.004.
- Sadori, L., Koutsodendris, A., Panagiotopoulos, K., Masi, A., Bertini, A., Combourieu-Nebout, N., Francke, A., Kouli, K., Joannin, S., Mercuri, A.M., Peyron, O., Torri, P., Wagner, B., Zanchetta, G., Sinopoli, G., Donders, T.H., 2016. Pollen-based paleoenvironmental and paleoclimatic change at Lake Ohrid (south-eastern Europe) during the past 500 ka. *Biogeosciences* 13, 1423-1437. Doi: 10.5194/bg-13-1423-2016.
- Salgueiro, E., Naughton, F., Voelker, A.H.L., de Abreu, L., Alberto, A., Rossignol, L., Duprat, J., Magalhães, V.H., Vaqueiro, S., Turon, J.L., Abrantes, F., 2014. Past circulation along the western Iberian margin: a time slice vision from the Last Glacial to the Holocene. *Quaternary Science Reviews* 106, 316-329. Doi: 10.1016/j.quascirev.2014.09.001.
- Samartin, S., Heiri, O., Lotter, A.F., Tinner, W., 2012. Climate warming and vegetation response after Heinrich event 1 (16 700-16 000 cal yr BP) in Europe south of the Alps. *Climate of the Past* 8, 1913-1927. Doi: 10.5194/cp-8-1913-2012.
- Sánchez-Castillo, P.M., Cruz-Pizarro, L., Carrillo, P., 1989. Caracterización del fitoplancton de las lagunas de alta montaña de Sierra Nevada (Granada, Spain) en relación con las características físico-químicas del medio. *Limnetica* 5, 37-50
- Sánchez Goñi, M., Cacho, I., Turon, J., Guiot, J., Sierro, F., Peyrouquet, J., Grimalt, J., Shackleton, N., 2002. Synchronicity between marine and terrestrial responses to millennial scale climatic variability during the last glacial period in the Mediterranean region. *Climate Dynamics* 19, 95-105. Doi: 10.1007/s00382-001-0212-x.
- Sánchez Goñi, M.a.F., Turon, J.-L., Eynaud, F., Gendreau, S., 2000. European Climatic Response to Millennial-Scale Changes in the Atmosphere–Ocean System during the Last Glacial Period. *Quaternary Research* 54, 394-403. Doi: 10.1006/qres.2000.2176.
- Sánchez Goñi, M.F., Desprat, S., Fletcher, W.J., Morales-Molino, C., Naughton, F., Oliveira, D., Urrego, D.H., Zorzi, C., 2018. Pollen from the Deep-Sea: A Breakthrough in the Mystery of the Ice Ages. *Frontiers in Plant Science* 9, 38. Doi: 10.3389/fpls.2018.00038.

## References

- Sánchez Goñi, M.F., Eynaud, F., Turon, J.L., Shackleton, N.J., 1999. High resolution palynological record off the Iberian margin: direct land-sea correlation for the Last Interglacial complex. *Earth and Planetary Science Letters* 171, 123-137. Doi: 10.1016/S0012-821X(99)00141-7.
- Sánchez Goñi, M.F., Harrison, S.P., 2010. Millennial-scale climate variability and vegetation changes during the Last Glacial: Concepts and terminology. *Quaternary Science Reviews* 29, 2823-2827. Doi: 10.1016/j.quascirev.2009.11.014.
- Sánchez Goñi, M.F., Landais, A., Fletcher, W.J., Naughton, F., Desprat, S., Duprat, J., 2008. Contrasting impacts of Dansgaard–Oeschger events over a western European latitudinal transect modulated by orbital parameters. *Quaternary Science Reviews* 27, 1136-1151. Doi: 10.1016/j.quascirev.2008.03.003.
- Sánchez Goñi, M.F., Loutre, M.F., Crucifix, M., Peyron, O., Santos, L., Duprat, J., Malaizé, B., Turon, J.L., Peyrouquet, J.P., 2005. Increasing vegetation and climate gradient in Western Europe over the Last Glacial Inception (122–110 ka): data-model comparison. *Earth and Planetary Science Letters* 231, 111-130. Doi: 10.1016/j.epsl.2004.12.010.
- Santanach, P.F., Sanz de Galdeano, C., Bousquet, J.C., 1980. Neotectónica de las regiones mediterráneas de España (Cataluña y Cordilleras Béticas). *Boletín Geológico y Minero* 91, 417-440.
- Sánz de Galdeano, C., El Hamdouni, R., Chacón, J., Gómez, A., Salvador, F., Schulte, L., García, A., 1998. Neotectónica de la fosa del Padul y del Valle de Lecrín. *Itinerarios Geomorfológicos por Andalucía Oriental*. Publicacions de la Universitat de Barcelona, Barcelona, 65-81.
- Satow, C.G., 2012. *The Tephrostratigraphy of Three, Late Quaternary, Mediterranean Marine Cores*. University of London.
- Schönfeld, J., Zahn, R., de Abreu, L., 2003. Surface and deep water response to rapid climate changes at the Western Iberian Margin. *Global and Planetary Change* 36, 237-264. Doi: 10.1016/S0921-8181(02)00197-2.
- Schröder, T., van't Hoff, J., López-Sáez, J.A., Viehberg, F., Melles, M., Reicherter, K., 2018. Holocene climatic and environmental evolution on the southwestern Iberian Peninsula: A high-resolution multi-proxy study from Lake Medina (Cádiz, SW Spain). *Quaternary Science Reviews* 198, 208-225. Doi: 10.1016/j.quascirev.2018.08.030.
- Schröter, D., Cramer, W., Leemans, R., Prentice, I.C., Araújo, M.B., Arnell, N.W., Bondeau, A., Bugmann, H., Carter, T.R., Gracia, C.A., de la Vega-Leinert, A.C., Erhard, M., Ewert, F., Glendining, M., House, J.I., Kankaanpää, S., Klein, R.J.T., Lavorel, S., Lindner, M., Metzger, M.J., Meyer, J., Mitchell, T.D., Reginster, I., Rounsevell, M., Sabaté, S., Sitch, S., Smith, B., Smith, J., Smith, P., Sykes, M.T., Thonicke, K., Thuiller, W., Tuck, G., Zaehle, S., Zierl, B., 2005. Ecosystem Service Supply and Vulnerability to Global Change in Europe. *Science* 310, 1333-1337. Doi: 10.1126/science.1115233.
- Schulte, L., 2002. Climatic and human influence on river systems and glacier fluctuations in southeast Spain since the Last Glacial Maximum. *Quaternary International* 93-94, 85-100. Doi: 10.1016/S1040-6182(02)00008-3.

- Schulz, M., Mudelsee, M., 2002. REDFIT: estimating red-noise spectra directly from unevenly spaced paleoclimatic time series. *Computers & Geosciences* 28, 421-426. Doi: 10.1016/S0098-3004(01)00044-9.
- Schulz, M., Paul, A., 2002. Holocene climate variability on centennial-to-millennial time scales: 1. Climate records from the North-Atlantic realm, in: Wefer, G., Berger, W.H., Behre, K.-E., Jansen, E. (Eds.), *Climate development and history of the North Atlantic realm*. Springer, 41-54.
- Seki, O., Meyers, P.A., Yamamoto, S., Kawamura, K., Nakatsuka, T., Zhou, W., Zheng, Y., 2011. Plant-wax hydrogen isotopic evidence for postglacial variations in delivery of precipitation in the monsoon domain of China. *Geology* 39, 875-878. Doi: 10.1130/G32117.1.
- Shackleton, N.J., Opdyke, N.D., 1973. Oxygen Isotope and Palaeomagnetic Stratigraphy of Equatorial Pacific Core V28-238: Oxygen Isotope Temperatures and Ice Volumes on a 105 Year and 106 Year Scale. *Quaternary Research* 3, 39-55. Doi: 10.1016/0033-5894(73)90052-5.
- Shackleton, N.J., Pisias, N.G., 1985. Atmospheric Carbon Dioxide, Orbital Forcing, and Climate, The Carbon Cycle and Atmospheric CO<sub>2</sub>: Natural Variations Archean to Present, 303-317. Doi: 10.1029/GM032p0303.
- Shakun, J.D., Clark, P.U., He, F., Marcott, S.A., Mix, A.C., Liu, Z., Otto-Bliesner, B., Schmittner, A., Bard, E., 2012. Global warming preceded by increasing carbon dioxide concentrations during the last deglaciation. *Nature* 484, 49. Doi: 10.1038/nature10915.
- Shimokawara, M., Nishimura, M., Matsuda, T., Akiyama, N., Kawai, T., 2010. Bound forms, compositional features, major sources and diagenesis of long chain, alkyl mid-chain diols in Lake Baikal sediments over the past 28,000 years. *Organic Geochemistry* 41, 753-766. Doi: 10.1016/j.orggeochem.2010.05.013.
- Siani, G., Paterne, M., Michel, E., Sulpizio, R., Sbrana, A., Arnold, M., Haddad, G., 2001. Mediterranean Sea surface radiocarbon reservoir age changes since the last glacial maximum. *Science* 294, 1917-1920. Doi: 10.1126/science.1063649
- Sicre, M.-A., Jalali, B., Martrat, B., Schmidt, S., Bassetti, M.-A., Kallel, N., 2016. Sea surface temperature variability in the North Western Mediterranean Sea (Gulf of Lion) during the Common Era. *Earth and Planetary Science Letters* 456, 124-133. Doi: 10.1016/j.epsl.2016.09.032.
- Sicre, M.-A., Siani, G., Genty, D., Kallel, N., Essallami, L., 2013. Seemingly divergent sea surface temperature proxy records in the central Mediterranean during the last deglaciation. *Climate of the Past* 9, 1375-1383. Doi: 10.5194/cp-9-1375-2013.
- Sierralta, M., Urban, B., Linke, G., Frechen, M., 2017. Middle pleistocene interglacial peat deposits from Northern Germany investigated by 230Th/U and palynology: Case studies from wedel and schönigen. *Zeitschrift der Deutschen Gesellschaft für Geowissenschaften* 168, 373-387. Doi: 10.1127/zdgg/2017/0065.
- Sierro, F.J., Hodell, D.A., Curtis, J.H., Flores, J.A., Reguera, I., Colmenero-Hidalgo, E., Bárcena, M.A., Grimalt, J.O., Cacho, I., Frigola, J., Canals, M., 2005. Impact of iceberg melting on Mediterranean thermohaline circulation during Heinrich events. *Paleoceanography* 20, 1-13. Doi: 10.1029/2004pa001051.

## References

Singh, G., Wasson, R.J., Agrawal, D.P., 1990. Vegetational and seasonal climatic changes since the last full glacial in the Thar Desert, northwestern India. *Review of Palaeobotany and Palynology* 64, 351-358. Doi: 10.1016/0034-6667(90)90151-8.

Skinner, L., Elderfield, H., 2007. Rapid fluctuations in the deep North Atlantic heat budget during the last glacial period. *Paleoceanography* 22.

Soon, W., Connolly, R., Connolly, M., 2015. Re-evaluating the role of solar variability on Northern Hemisphere temperature trends since the 19th century. *Earth-Science Reviews* 150, 409-452. Doi: 10.1016/j.earscirev.2015.08.010.

Srokosz, M., Baringer, M., Bryden, H., Cunningham, S., Delworth, T., Lozier, S., Marotzke, J., Sutton, R., 2012. Past, present, and future changes in the Atlantic meridional overturning circulation. *Bulletin of the American Meteorological Society* 93, 1663-1676.

Stanford, J.D., Rohling, E.J., Bacon, S., Roberts, A.P., Grousset, F.E., Bolshaw, M., 2011. A new concept for the paleoceanographic evolution of Heinrich event 1 in the North Atlantic. *Quaternary Science Reviews* 30, 1047-1066. Doi: 10.1016/j.quascirev.2011.02.003.

Stern, J.V., Lisiecki, L.E., 2013. North Atlantic circulation and reservoir age changes over the past 41,000 years. *Geophysical Research Letters* 40, 3693-3697. Doi: 10.1002/grl.50679.

Stockhecke, M., Anselmetti, F.S., Meydan, A.F., Odermatt, D., Sturm, M., 2012. The annual particle cycle in Lake Van (Turkey). *Palaeogeography, Palaeoclimatology, Palaeoecology* 333-334, 148-159. Doi: 10.1016/j.palaeo.2012.03.022.

Stuiver, M., Grootes, P.M., Braziunas, T.F., 1995. The GISP2  $\delta^{18}\text{O}$  climate record of the past 16,500 years and the role of the sun, ocean, and volcanoes. *Quaternary Research* 44, 341-354. Doi: 10.1006/qres.1995.1079.

Sun, Y., An, Z., 2005. Late Pliocene-Pleistocene changes in mass accumulation rates of eolian deposits on the central Chinese Loess Plateau. *Journal of Geophysical Research* 110, 1-8. Doi: 10.1029/2005jd006064.

Swain, A.M., Kutzbach, J.E., Hastenrath, S., 1983. Estimates of holocene precipitation for Rajasthan, India, based on pollen and lake-level data. *Quaternary Research* 19, 1-17. Doi: 10.1016/0033-5894(83)90024-8.

Taylor, S.R., McClennan, S.M., 1985. *The continental crust: Its composition and evolution*. Blackwell Scientific Publications, Oxford.

Thiagarajan, N., Subhas, A.V., Southon, J.R., Eiler, J.M., Adkins, J.F., 2014. Abrupt pre-Bølling–Allerød warming and circulation changes in the deep ocean. *Nature* 511, 75. Doi: 10.1038/nature13472.

Toti, F., 2018. *A Mediterranean Perspective on the Early-middle Pleistocene Transition with Emphasis on Marine Isotope Stage 19*. University of Florence, Florence.

Toucanne, S., Soulet, G., Freslon, N., Jacinto, R.S., Dennielou, B., Zaragosi, S., Eynaud, F., Bourillet, J.-F., Bayon, G., 2015. Millennial-scale fluctuations of the European Ice Sheet at the end of the last

glacial, and their potential impact on global climate. *Quaternary Science Reviews* 123, 113-133. Doi: 10.1016/j.quascirev.2015.06.010.

Trouet, V., Esper, J., Graham, N.E., Baker, A., Scourse, J.D., Frank, D.C., 2009. Persistent Positive North Atlantic Oscillation Mode Dominated the Medieval Climate Anomaly. *Science* 324, 78-80. Doi: 10.1126/science.1166349.

Turner, C., West, R., 1968. The subdivision and zonation of interglacial periods. *Eiszeitalter und Gegenwart* 19, 101.

Turney, C., Baillie, M., Clemens, S., Brown, D., Palmer, J., Pilcher, J., Reimer, P., Leuschner, H.H., 2005. Testing solar forcing of pervasive Holocene climate cycles. *Journal of Quaternary Science: Published for the Quaternary Research Association* 20, 511-518. Doi: 10.1002/jqs.927.

Tzedakis, P.C., 2005. Towards an understanding of the response of southern European vegetation to orbital and suborbital climate variability. *Quaternary Science Reviews* 24, 1585-1599. Doi: 10.1016/j.quascirev.2004.11.012.

Tzedakis, P.C., 2007. Seven ambiguities in the Mediterranean palaeoenvironmental narrative. *Quaternary Science Reviews* 26, 2042-2066. Doi: 10.1016/j.quascirev.2007.03.014.

Tzedakis, P.C., Bennett, K.D., 1995. Interglacial vegetation succession: A view from southern Europe. *Quaternary Science Reviews* 14, 967-982. Doi: 10.1016/0277-3791(95)00042-9.

Tzedakis, P.C., Drysdale, R.N., Margari, V., Skinner, L.C., Meniel, L., Rhodes, R.H., Taschetto, A.S., Hodell, D.A., Crowhurst, S.J., Hellstrom, J.C., Fallick, A.E., Grimalt, J.O., McManus, J.F., Martrat, B., Mokeddem, Z., Parrenin, F., Regattieri, E., Roe, K., Zanchetta, G., 2018. Enhanced climate instability in the North Atlantic and southern Europe during the Last Interglacial. *Nat Commun* 9, 4235. Doi: 10.1038/s41467-018-06683-3.

Tzedakis, P.C., Frogley, M.R., Heaton, T.H.E., 2003a. Last Interglacial conditions in southern Europe: evidence from Ioannina, northwest Greece. *Global and Planetary Change* 36, 157-170. Doi: 10.1016/s0921-8181(02)00182-0.

Tzedakis, P.C., Frogley, M.R., Lawson, I.T., Preece, R.C., Cacho, I., de Abreu, L., 2004. Ecological thresholds and patterns of millennial-scale climate variability: The response of vegetation in Greece during the last glacial period. *Geology* 32, 109. Doi: 10.1130/g20118.1.

Tzedakis, P.C., Hooghiemstra, H., Pälike, H., 2006. The last 1.35 million years at Tenaghi Philippon: revised chronostratigraphy and long-term vegetation trends. *Quaternary Science Reviews* 25, 3416-3430. Doi: 10.1016/j.quascirev.2006.09.002.

Tzedakis, P.C., Lawson, I.T., Frogley, M.R., Hewitt, G.M., Preece, R.C., 2002. Buffered tree population changes in a quaternary refugium: evolutionary implications. *Science* 297, 2044-2047. Doi: 10.1126/science.1073083.

Tzedakis, P.C., McManus, J.F., Hooghiemstra, H., Oppo, D.W., Wijmstra, T.A., 2003b. Comparison of changes in vegetation in northeast Greece with records of climate variability on orbital and suborbital frequencies over the last 450,000 years. *Earth and Planetary Science Letters* 212, 197-212. Doi: 10.1016/s0012-821x(03)00233-4.



## References

Vaks, A., Bar-Matthews, M., Ayalon, A., Schilman, B., Gilmour, M., Hawkesworth, C.J., Frumkin, A., Kaufman, A., Matthews, A., 2003. Paleoclimate reconstruction based on the timing of speleothem growth and oxygen and carbon isotope composition in a cave located in the rain shadow in Israel. *Quaternary Research* 59, 182-193. Doi: 10.1016/S0033-5894(03)00013-9.

Valero-Garcés, B., Zeruoual, E., Kelts, K., 1998. Arid phases in the western Mediterranean region during the last glacial cycle reconstructed from lacustrine records. *Paleohydrology and Environmental Change*, 67-80.

Valle-Hernández, M., Rivas-Carballo, M.R., Lucini, M., Ortiz, J.E., Torres, T., 2003. Interpretación paleoecológica y paleoclimática del tramo superior de la turbera de Padul (Granada, España). *Polen*, 85-95.

Valle, F.E., 2003. Mapa de series de vegetación de Andalucía. Editorial Rueda, Madrid.

Van Geel, B., 2001. Non-pollen palynomorphs, in: Smol, J.P., Birks, H.J.B., W.M., L. (Eds.), *Tracking Environmental Change Using Lake Sediments*. Kluwer Academic Publishers, Dordrecht, The Netherlands, 99-119.

Van Geel, B., Raspopov, O.M., Renssen, H., van der Plicht, J., Dergachev, V.A., Meijer, H.A.J., 1999. The role of solar forcing upon climate change. *Quaternary Science Reviews* 18, 331-338. Doi: 10.1016/S0277-3791(98)00088-2.

Vegas, J., Ruiz-Zapata, B., Ortiz, J.E., Galán, L., Torres, T., García-Cortés, Á., Gil-García, M.J., Pérez-González, A., Gallardo-Millán, J.L., 2010. Identification of arid phases during the last 50 cal. ka BP from the Fuentillejo maar-lacustrine record (Campo de Calatrava Volcanic Field, Spain). *Journal of Quaternary Science* 25, 1051-1062. Doi: 10.1002/jqs.1262.

Vescovi, E., Ravazzi, C., Arpentini, E., Finsinger, W., Pini, R., Valsecchi, V., Wick, L., Ammann, B., Tinner, W., 2007. Interactions between climate and vegetation during the Lateglacial period as recorded by lake and mire sediment archives in Northern Italy and Southern Switzerland. *Quaternary Science Reviews* 26, 1650-1669. Doi: 10.1016/j.quascirev.2007.03.005.

Villegas Molina, F., 1967. Laguna de padul: Evolución geológico-histórica. *Estudios Geográficos* 28, 561.

Visbeck, M.H., Hurrell, J.W., Polvani, L., Cullen, H.M., 2001. The North Atlantic Oscillation: Past, present, and future. *Proceedings of the National Academy of Sciences* 98, 12876-12877. Doi: 10.1073/pnas.231391598.

Volkman, J.K., 1986. A review of sterol markers for marine and terrigenous organic matter. *Organic Geochemistry* 9, 83-99. Doi: 10.1016/0146-6380(86)90089-6.

Wagner, B., Wilke, T., Francke, A., Albrecht, C., Baumgarten, H., Bertini, A., Combourieu-Nebout, N., Cvetkoska, A., amp, apos, Addabbo, M., Donders, T.H., Föller, K., Giaccio, B., Grazhdani, A., Hauße, T., Holtvoeth, J., Joannin, S., Jovanovska, E., Just, J., Kouli, K., Koutsodendris, A., Krastel, S., Lacey, J.H., Leicher, N., Leng, M.J., Levkov, Z., Lindhorst, K., Masi, A., Mercuri, A.M., Nomade, S., Nowaczyk, N., Panagiotopoulos, K., Peyron, O., Reed, J.M., Regattieri, E., Sadori, L., Sagnotti, L., Stelbrink, B., Sulpizio, R., Tofilovska, S., Torri, P., Vogel, H., Wagner, T., Wagner-Cremer, F., Wolff, G.A., Wonik, T., Zanchetta, G., Zhang, X.S., 2017. The environmental and evolutionary

history of Lake Ohrid (FYROM/Albania): interim results from the SCOPSCO deep drilling project. *Biogeosciences* 14, 2033-2054. Doi: 10.5194/bg-14-2033-2017.

Wagner, B., Wilke, T., Krastel, S., Zanchetta, G., Sulpizio, R., Reicherter, K., Leng, M.J., Grazhdani, A., Trajanovski, S., Francke, A., Lindhorst, K., Levkov, Z., Cvetkoska, A., Reed, J.M., Zhang, X., Lacey, J.H., Wonik, T., Baumgarten, H., Vogel, H., 2014. The SCOPSCO drilling project recovers more than 1.2 million years of history from Lake Ohrid. *Scientific Drilling* 17, 19-29. Doi: 10.5194/sd-17-19-2014.

Watts, W., Allen, J., Huntley, B., 1996. Vegetation history and palaeoclimate of the last glacial period at Lago Grande di Monticchio, southern Italy. *Quaternary Science Reviews* 15, 133-153. Doi: 10.1016/0277-3791(95)00093-3.

Wei, D., González-Sampériz, P., Gil-Romera, G., Harrison, S.P., Prentice, I.C., 2019. Climate changes in interior semi-arid Spain from the last interglacial to the late Holocene. *Climate of the Past Discussions*.

Wells, N.A., 1983. Carbonate deposition, physical limnology and environmentally controlled chert formation in Paleocene-Eocene Lake Flagstaff, central Utah. *Sedimentary Geology* 35, 263-296. Doi: 10.1016/0037-0738(83)90062-3.

White, S.D., Ganf, G.G., 1998. The influence of convective flow on rhizome length in *Typha domingensis* over a water depth gradient. *Aquatic Botany* 62, 57-70. Doi: 10.1016/S0304-3770(98)00077-1.

Whiteside, M.C., 1965. On the Occurrence of *Pediastrum* in Lake Sediments. *Journal of the Arizona Academy of Science* 3, 144-146. Doi: 10.2307/40022766.

Whyte, R.S., Trexel-Kroll, D., Klarer, D.M., Shields, R., Francko, D.A., 2008. The Invasion and Spread of *Phragmites australis* during a Period of Low Water in a Lake Erie Coastal Wetland. *Journal of Coastal Research*, 111-120. Doi: 10.2112/si55-19.1.

Wijmstra, T., 1969. Palynology of the first 30 metres of a 120 m deep section in northern Greece. *Acta botanica neerlandica* 18, 511-527.

Wright, D.T., 1999. The role of sulphate-reducing bacteria and cyanobacteria in dolomite formation in distal ephemeral lakes of the Coorong region, South Australia. *Sedimentary Geology* 126, 147-157. Doi: 10.1016/S0037-0738(99)00037-8.

Yamane, M., Yokoyama, Y., Miyairi, Y., Suga, H., Matsuzaki, H., Dunbar, R.B., Ohkouchi, N., 2014. Compound-specific <sup>14</sup>C dating of IODP expedition 318 core U1357A obtained off the Wilkes Land coast, Antarctica. *Radiocarbon* 56, 1-9. Doi: 10.2458/56.17773.

Yokoyama, Y., Koizumi, M., Matsuzaki, H., Miyairi, Y., Ohkouchi, N., 2010. Developing ultra Small-scale radiocarbon sample measurement at the University of Tokyo. *Radiocarbon* 52, 310-318. Doi: 10.1017/S0033822200045355.

Zhang, Z., Metzger, P., Sachs, J.P., 2011. Co-occurrence of long chain diols, keto-ols, hydroxy acids and keto acids in recent sediments of Lake El Junco, Galápagos Islands. *Organic Geochemistry* 42, 823-837. Doi: 10.1016/j.orggeochem.2011.04.012.

## *References*

Ziegler, M., Tuenter, E., Lourens, L.J., 2010. The precession phase of the boreal summer monsoon as viewed from the eastern Mediterranean (ODP Site 968). *Quaternary Science Reviews* 29, 1481-1490. Doi: 10.1016/j.quascirev.2010.03.011.